RAFT synthesis of diblock copolymers for use as aqueous pigment dispersants

Shannon M. North

A thesis submitted in partial fulfilment of the requirements for the degree of
Doctor of Philosophy

The University of Sheffield
Faculty of Science
Department/School of Chemistry

February 2021

Declaration

The work described in this thesis was undertaken at the University of Sheffield between October 2016 and February 2021, under the supervision of Professor S. P. Armes. Unless otherwise stated, it is the work of the author and has not been submitted in whole or any other part for any other degree at this or any other institute.

Signature:

Shannon M. North

February 2021

Acknowledgements

I am extremely grateful to all the people who have supported me over the past 6 ½ years working in the Armes group. Firstly, I would like to give the biggest thanks to Professor Steven Armes FRS, who has supported me since I made the decision to stay in Sheffield for my industry year. I definitely would not have made it this far if it weren't for your encouragement. Thank you for the guidance, wealth of knowledge and ideas, painstaking proof reading and for giving me the opportunity to travel to international conferences.

I would also like to acknowledge my industrial sponsors Lubrizol, particularly Dr. Tom Annable, Dr. Elliot Coulbeck and Conor Wilkinson, not only for providing funding for my PhD project but also for supervising me during my placement at Blackley, and always being a friendly ear to ask upon. Thank you to Dr. Stuart Richards and Dr. Andy Shooter for their input into my project. Thank you to Dr. Vicky Verona for providing me with all the pigment, and support in pursuing my PhD after my industrial placement. Further thanks to everyone working at Lubrizol Hazelwood for organising great conferences and the opportunity to share work, ideas and buffets!

The Polymers, Colloids and Soft Matter CDT and the EPSRC are thanked for the partial funding of this project, and a special thanks to Dr Joe Gaunt for all the invaluable advice and encouragement to persevere through the ups and downs.

A huge thank you everyone in the chemistry department who have helped me over the past 5 years, including Dr. Sandra van Meurs for all the NMR help and running some variable temperature experiments for me, as well as Dr. Chris Hill and Dr Svet Tzokov for all their help and hours making different stains for me for TEM.

Thank you to so many members of the Armes group, past and present, as well as members of the CDT and the RyMyk group, for answering my questions, being there to try new activities in Sheffield with, and making time in the office enjoyable.

To my housemate Joe, thank you for always being there for me when I needed you.

And finally thank you to my Mum and Dad, your unwavering love, support and generosity, I couldn't have done this without you.

Publications

Primary publications resulting from work in this thesis

1. "Aqueous solution behavior of stimulus-responsive poly (methacrylic acid)-poly (2-hydroxypropyl methacrylate) diblock copolymer nanoparticles." S. M. North, & S. P. Armes, *Polymer Chemistry*, **2020**, *11*, 2147-2156.

2. "Aqueous One-Pot Synthesis of Well-defined Zwitterionic Diblock Copolymers by RAFT Polymerization: An Efficient and Environmentally-friendly Route to a Useful Dispersant for Aqueous Pigments S. M. North, & S. P. Armes, *Green Chemistry*, **2021**, https://doi.org/10/1039/D0GC04271D

Oral presentations at Conferences

1. "Adsorption of small cationic nanoparticles onto large anionic particles from aqueous solution: A model system for understanding pigment dispersion and the problem of effective particle density" S. M. North, E. R. Jones, G. N. Smith, O. O. Mykhaylyk, T. Annable, S. P. Armes, 255th ACS National Meeting & Exposition, 18th-22nd March 2018, New Orleans, LA, USA.

2. "Properties of poly(methacrylic acid)-block-poly(2-hydroxypropyl methacrylate) diblock copolymers and their use as dispersants for inkjet-grade carbon black." S. M. North, S. P. Armes, 13th International Conference on Advanced Polymers via Macromolecular Engineering, 15th – 18th April 2019, Stellenbosch, South Africa.

Poster presentations at Conferences

1. "Model Polymeric Dispersants to Stabilise Colloidal Systems" S. M. North and S. P Armes, Macro Group UK Young Researchers' Meeting 2017, 19th-20th June 2017, Edinburgh, UK

2. "Block Copolymer Stabilisers for Aqueous Pigment Dispersion" S. M. North and S. P Armes, RSC Twitter Poster Confernce, 20th March 2017, Online

Abstract

This Thesis focuses on the preparation of novel dispersants for aqueous pigments in the form of either diblock copolymer nanoparticles or molecularly-dissolved copolymer chains. The former are prepared *via* polymerisation-induced self-assembly, and both types of copolymer are synthesised using aqueous reversible addition-fragmentation chain transfer polymerisation.

Firstly, the synthesis and aqueous solution behaviour of novel poly(methacrylic acid)-poly(2-hydroxypropyl methacrylate) (PMAA-PHPMA) nanoparticles, *via* RAFT dispersion polymerisation of HPMA is reported. More specifically, $PMAA_{50}$-$PHPMA_{235}$ is investigated owing to its particularly interesting pH- and thermo-responsive behaviour. As synthesised at pH 5.5, relative large, polydisperse particles are obtained owing to the partially ionised nature of the PMAA block. At higher pH, this steric stabiliser block becomes highly anionic, leading to the formation of thermoresponsive nanoparticles. ^{1}H NMR, dynamic light scattering (DLS), and transmission electron microscopy (TEM) studies indicate molecularly-dissolved chains are formed at 5 °C that aggregate to produce spheres at 10 – 35 °C and worm-like particles at 50 °C. The latter particles form a gel-like dispersion and shear-induced polarised light imaging yields a characteristic Maltese cross, as expected for anisotropic nanoparticles.

This $PMAA_{50}$-$PHPMA_{235}$ diblock copolymer is evaluated as a dispersant for commercial-grade carbon black. Its thermoresponsive behaviour leads to more effective pigment dispersant performance at lower temperatures. Moreover, the resulting carbon black dispersions exhibit greater long-term stability compared to that prepared with a commercial copolymer dispersant.

A novel synthetic route to zwitterionic diblock copolymers *via* an atom-efficient, wholly aqueous one-pot protocol is reported. Depending on the nature of the anionic and cationic comonomers and the solution pH that is selected, this involves RAFT aqueous solution polymerisation, RAFT aqueous dispersion polymerisation or RAFT aqueous emulsion polymerisation. Some of these zwitterionic diblock copolymers exhibit macroscopic precipitation at their isoelectric points (IEP), which enables efficient trithiocarbonate end-group removal using hydrazine followed by a wholly aqueous work-up.

Zwitterionic diblock copolymers are investigated as dispersants for two commercial inorganic pigments. Poly((2-dimethylamino)ethyl methacrylate)-poly(methacrylic acid) (PDMA-PMAA) is shown to be a particularly effective dispersant for transparent yellow iron oxide, which is known to be a typically problematic nano-sized pigment. DLS studies indicate a large reduction in the apparent pigment particle size compared to no dispersant, and rheology measurements confirm a substantial reduction in dispersion viscosity after milling using a high-energy mixer. Furthermore, these zwitterionic diblock copolymer dispersants require a lower concentration based on mass of pigment than commercially available dispersants.

Finally, the synthesis of zwitterionic poly((2-diethylamino)ethyl methacrylate)-poly(2-carboxyethyl acrylate) (PDEA-PCEA) diblock copolymer nanoparticles via RAFT aqueous dispersion polymerisation is investigated. Such copolymers can also be prepared using a convenient aqueous one-pot protocol and self-assemble to form either anionic micelles above or cationic micelles below the copolymer isoelectric point. This is the most convenient synthesis route yet reported for such schizophrenic diblock copolymers. Preliminary results for their effectiveness as nanoparticle dispersants for titanium dioxide is briefly reported; nanoparticle adsorption onto this white pigment appears to occur both below and above the IEP.

Abbreviations

^{1}H NMR	Proton nuclear magnetic resonance
2VP	2-vinyl pyridine
4VP	4-vinylpyridine
AA	acrylic acid
ACVA	4,4′-Azobis(4-cyanovaleric acid)
AIBN	2,2′-Azobis(2-methylpropionitrile)
ATRP	Atom transfer radical polymerisation
BA	n-Butyl acrylate
BzMA	benzyl methacrylate
CEA	2-carboxyethyl acrylate
CGT	Critical gelation temperature
CMC	Critical micelle concentration
CPDB	4-cyanopropyl dithiobenzoate
CRP	Controlled radical polymerisation
CTA	Chain transfer agent
DEA	2-(diethylamino)ethyl methacrylate
DLS	Dynamic light scattering
DMA	2-(dimethylamino)ethyl methacrylate
DMF	Dimethylformamide
DP	Degree of polymerisation
DPA	2-(diisopropylamino)ethyl-methacrylate
EDL	Electrical double layer
FRP	Free radical polymerisation
FT-IR	Fourier-Transform Infrared
GPC	Gel permeation chromatography
GTP	Group transfer polymerisation
HBMA	hydroxybutyl methacrylate
HPLC	High performance liquid chromatography
HPMA	2-hydroxypropyl methacrylate
IEP	Isoelectric point
LAP	Living anionic polymerisation

LCST	Lower critical solution temperature
MAA	methacrylic acid
MEMA	2-(N-morpholino)ethyl methacrylate
METAC	2-(trimethylammonium chloride) ethyl methacrylate
MMA	methyl methacrylate
M_n	Number-average molecular weight
MPC	2-(methacryloyloxy)ethyl phosphorylcholine
M_w	Weight-average molecular weight
MWD	Molecular weight distribution
NaAA	sodium acrylate
N_{agg}	Aggregation number
NaMAA	sodium methacrylate
NIPAm	N-isopropylacrylamide
NMP	Nitroxide-mediated polymerisation
ODT	Order-disorder transition
PDI	Polydispersity index
PEO	Poly(ethylene oxide)
PETTC	4-Cyano-4-(2-phenylethanesulfanylthiocarbonyl)sulfanylpentanoic acid)
PISA	Polymerisation-induced self-assembly
PPO	Poly(propylene oxide)
PS	Polystyrene
RAFT	Reversible addition-fragmentation chain transfer polymerisation
RDRP	Reversible deactivation radical polymerisation
SAXS	Small-angle X-ray scattering
SEM	Scanning electron microscopy
SIPLI	Shear-induced polarised light imaging
TEM	Transmission electron microscopy
TGA	Thermogravimetric analysis
THF	Tetrahydrofuran
TiO_2	Titania
UV/Vis	Ultraviolet/visible
VA-044	2,2'-azobis[2-(2-imidazolin-2-yl)propane] dihydrochloride
VBA	4-vinylbenzoic acid

Contents

Chapter 1

Introduction

1.1 Polymer Science

Polymers or macromolecules comprise long chains made up of individual repeat units known as monomers. These chains are constructed *via* polymerisation, whereby monomers are covalently bonded together. Synthetic polymers are used for an enormous range of applications in the modern world, e.g. in coatings, packaging, drug delivery, electrical insulation, home and personal care products, energy storage and protective equipment.[1–5]

1.1.1 Polymer Architectures

Polymer chains can either be linear or non-linear (**Figure 1.1**). Linear polymers include homopolymers, block copolymers, statistical copolymers and alternating copolymers. Non-linear polymers can be separated into three categories: branched polymers, graft copolymers and star polymers.
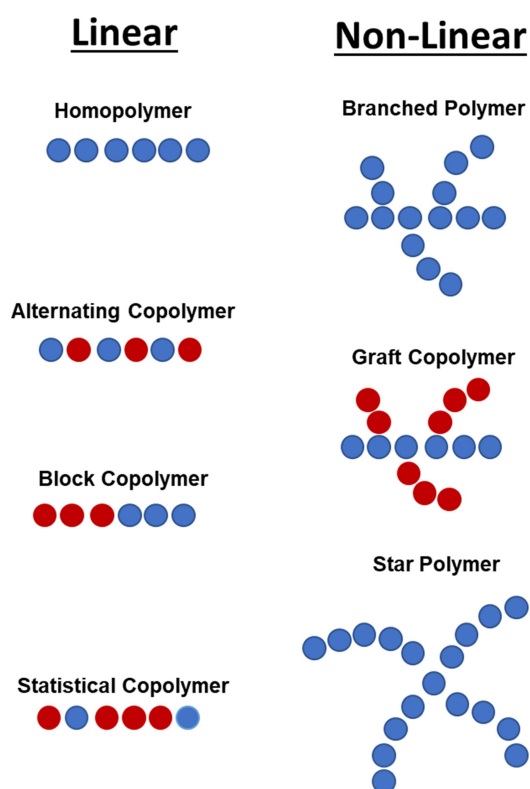

Figure 1.1 Pictorial representation of various copolymer architectures.

1.1.2 Polymer Characterisation

The mean number of monomer repeat units per polymer chain is known as the degree of polymerisation (DP). Ideally, polymers should possess a single unique molecular weight and hence comprise chains of identical length (or DP). However, synthetic polymers are invariably polydisperse and hence exhibit a molecular weight distribution (MWD). The width of the MWD typically depends on the method of polymerisation. The three most important averages used to describe the MWD curve correspond to the number-average (M_n), weight-average (M_w) and z-average (M_z) molecular weight, see **Figure 1.2** and **Equations 1.1-1.3**. The peak molecular weight (M_p) is also sometimes reported: this is the molecular weight of the highest peak, or the mode of the MWD.[6]

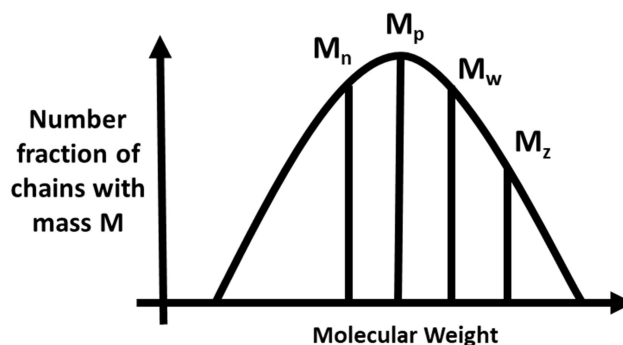**Figure 1.2** Schematic representation of the moments of the molecular weight distribution: number-average (M_n), weight-average (M_w) and z-average (M_z) molecular weight.

$$M_n = \frac{\sum n_i M_i}{\sum n_i} \text{ (Equation 1.1)}$$

$$M_w = \frac{\sum w_i M_i}{\sum w_i} = \frac{\sum n_i M_i^2}{\sum n_i M_i} \text{ (Equation 1.2)}$$

$$M_z = \frac{\sum n_i M_i^3}{\sum n_i M_i^2} \text{ (Equation 1.3)}$$

For equations 1.1-1.3, n_i is the number of chains of molecular weight M_i, for i monomer units (i = 0, 1, 2, ...). M_n is biased towards low molecular weight species, while M_w is biased towards higher molecular weight species. In practice, M_z is rarely used. By definition, $M_n <$ $M_w < M_z$ for all polymers that have an MWD of finite width. M_p is often cited for near-monodisperse polymers, such as those used for calibration standards.

The most convenient method for analysing polymer MWDs is gel permeation chromatography (GPC). A dilute polymer solution is pumped at a constant flow rate through a column packed with microporous gel beads exhibiting a range of porosity: shorter polymer chains can diffuse into a larger number of pores and hence are retained within the gel beads for a longer time period. This leads to fractionation of the chains according to their hydrodynamic volume. Instrument calibration requires the use of near-monodisperse standards, which are often not available for the polymer of interest. Thus, in many cases only *relative* molecular weights are reported, rather than *absolute* molecular weights.

A polydispersity index (PDI), or dispersity, can be calculated for a specific molecular weight distribution, where PDI = M_w/M_n. The DP can also be defined according to **Equation 1.4**.

$$DP = \frac{M_n}{Molecular\ weight\ of\ monomer} \quad \textbf{(Equation 1.4)}$$

If the DP is less than 10, this corresponds to oligomers rather than polymers.[7] Chemical methods for the determination of M_n rely on end-group analysis. Depending on the nature of the polymer, suitable techniques may include acid titration, UV-visible spectroscopy, Fourier transform infrared (FT-IR) spectroscopy and nuclear magnetic resonance (NMR) spectroscopy, using **Equation 1.5**.

$$M_n = \frac{Polymer\ concentration}{End-group\ concentration} \quad \textbf{(Equation 1.5)}$$

1.2 Methods of Polymerisation

Carothers was the first to classify polymers as either addition or condensation, with such assignments being based on their chemical structure.[8] However, this could sometimes lead to discrepancies. For example, it was quickly recognised that there were certain 'condensation' polymers (e.g. polyurethanes) whose synthesis did not involve the elimination of small molecules as condensates. Subsequently, Flory introduced the terms 'step' and 'chain' to classify polymers according to the chemical mechanism involved in their formation.[9] In step polymerisation, all molecules present are capable of reacting with each other, including monomers, dimers, trimers, oligomers and polymers. In contrast, chain polymerisations involve repeated addition of monomer units *via* active centres located at the end of the growing chains.

1.2.1 Free Radical Polymerisation

Free radical polymerisation (FRP) is the most widely used form of chain polymerisation. The FRP mechanism involves four distinct steps (**Figure 1.3**).

$$\text{INITIATION} \begin{cases} I-I \xrightarrow{k_d} 2I\cdot \\[6pt] I\cdot + M \xrightarrow{k_i} P\cdot \end{cases}$$

$$\text{PROPAGATION} \begin{cases} P_n\cdot + M \xrightarrow{k_p} P_{n+1}\cdot \end{cases}$$

$$\text{TERMINATION} \begin{cases} P_n\cdot + P_m\cdot \xrightarrow{k_{tc}} P_{n+m} \\[6pt] P_n\cdot + P_m\cdot \xrightarrow{k_{td}} P_n + P_m \end{cases}$$

$$\text{TRANSFER} \begin{cases} P_n\cdot + I-I \xrightarrow{k_{trI}} P_n-I + I\cdot \\[6pt] P_n\cdot + M-I \xrightarrow{k_{trM}} P_n + M\cdot \\[6pt] P_n\cdot + P_x \xrightarrow{k_{trPol}} P_n + P_y\cdot \\[6pt] P_n\cdot + S \xrightarrow{k_{trS}} P_n + S\cdot \end{cases}$$
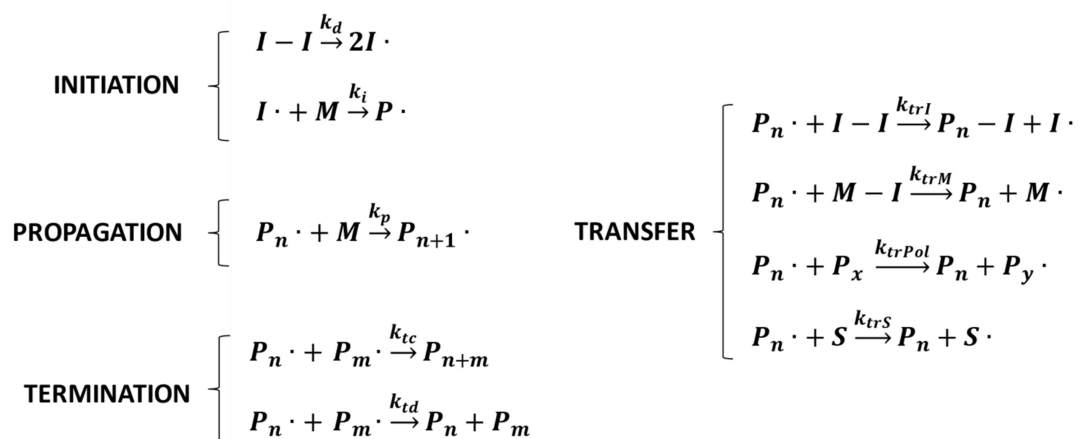
Figure 1.3 The three fundamental steps and chain transfer side-reactions involved in free radical polymerisation.

Firstly, in the initiation step, primary free radicals ($I^\bullet$) are generated by *in situ* decomposition of an initiator (*I*) *via* heat, redox chemistry, or UV irradiation. This typically involves homolytic fission and generates two radicals at a relatively slow rate constant k_d, which is usually rate-limiting. Initiation occurs when a monomer unit reacts with a free radical, thus forming a chain-initiating radical ($P^\bullet$), where k_i is the rate constant for initiation. Propagation then proceeds *via* rapid sequential addition of multiple monomer units at a rate constant k_p. Termination is the final step, whereby radicals are eliminated by either combination (with rate constant k_{tc}) or disproportionation (with rate constant k_{td}). The latter mode of termination is favoured for methacrylic monomers, whereas combination is much more likely for styrene and acrylate monomers, examples of these are given in **Scheme 1.1**.

Methacrylic monomer **Acrylic monomer** **Styrene**
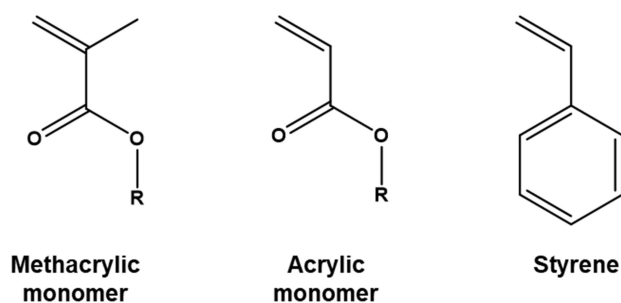
Scheme 1.1 Chemical structures for (meth)acrylic monomers and styrene.

Combining the rate laws for initiation, propagation and termination enables derivation of an expression for the rate of polymerisation (R_{polym}), see **Equation 1.6**.

$$R_{polym} = k_p[M]\sqrt{\frac{f k_d[I]}{k_t}} \quad \textbf{(Equation 1.6)}$$

Here [M] is the monomer concentration, f is the initiator efficiency, k_d is the rate constant for decomposition, [I] is the initiator concentration and k_t is the rate of termination. Derivation of **Equation 1.6** is based on two assumptions. First, the rate of initiation is equal to the rate of termination (the so-called 'steady-state' approximation). Second, the number of monomer

units consumed during initiation is negligible compared to the number consumed during propagation.[10] Inspection of **Equation 1.6** indicates that increasing [M] and [I] lead to faster rates of polymerisation in each case. The dependence of R_{polym} on k_d is also important. This is because it ultimately determines the rate of initiation (R_i), which is known to be around three orders of magnitude slower than the rate of propagation (R_p). A slow rate of initiation and chain termination are the two main causes of the broad MWD that invariably characterises polymers prepared by FRP. This is because new radicals are continuously generated over the course of the reaction, which results in the production of polymer chains of many different lengths.

The kinetic chain length, D_k, can be defined as R_p/R_i, the ratio of propagating species to initiating species. Because R_i = rate of termination (or R_t), then $[P^\bullet] = (fk_d[I]/k_t)^{0.5}$. These rate laws can be combined to give D_k, see **Equation 1.7**.

$$D_k = \frac{k_p[M]}{2(fk_dk_t[I])^{0.5}} \text{ (Equation 1.7)}$$

Hence molecular weight is proportional to [M], but also to $[I]^{-0.5}$. This explains the intrinsic difficulty in obtaining fast rates of polymerisation when targeting high molecular weight polymers. The DP is related to the dominant mode of termination: $DP = 2D_k$ for termination solely by combination and $DP = D_k$ for termination solely by disproportionation. However, in either case chain termination means that the average lifetime of a propagating chain is relatively short (<< 1 second). Therefore, it is impossible to produce well-defined block copolymers by sequential monomer addition because the first block will be deactivated once all of monomer A is consumed.

Various side reactions can also occur during FRP, which are known as chain transfer reactions (see **Figure 1.3**). For example, $P^\bullet$ can react with initiator, *I*, monomer, *M*, polymer, P_x, or solvent, *S*, to produce a dead polymer chain P_n and a new radical species $R^\bullet$. These

transfer reactions do not affect the overall polymerisation kinetics, because there is no net loss of radicals. Instead, $R^\bullet$ can reinitiate and create new $P_n^\bullet$ species.
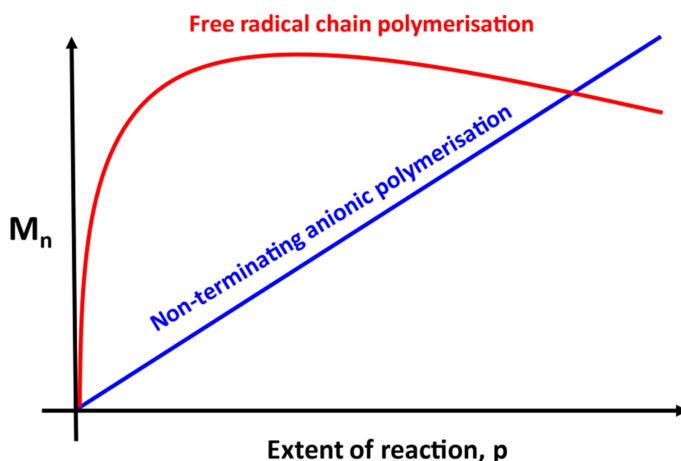

Figure 1.4 Variation of number-average molecular weight, M_n, with extent of reaction, p, for free radical polymerisation (FRP) and for living anionic polymerisation (LAP).

1.2.2 Living Anionic Polymerisation (LAP)

Anionic polymerisation was the first type of polymerisation to exhibit so-called 'living' character. In contrast to FRP, living anionic polymerisation (LAP) has no intrinsic termination step since the anionic chain-ends cannot react with one another. Moreover, the rate of initiation is much faster than the rate of propagation. Rapid simultaneous initiation of all chains gives them an equal probability to grow. Szwarc *et al.*[11] demonstrated that the anionic polymerisation of styrene in THF led to living polymers that showed little or no tendency to undergo termination. Living polymers exhibit a linear evolution of molecular weight with monomer conversion (**Figure 1.4**), and low dispersities ($M_w/M_n < 1.10$). Once the polymerisation is complete, the living character of the chains is retained, enabling the synthesis of well-defined block copolymers *via* sequential monomer addition.[12] The rate of polymerisation, R_p, is given by **Equation 1.8**.

$$R_p = k_p[M^-][M] \text{ (Equation 1.8)}$$

In this equation, k_p is the propagation constant, [M⁻] is the concentration of living anionic propagating centres in the system, and [M] is the monomer concentration. The detailed kinetics depend on the type of solvent and initiator used, as well as the chosen vinyl monomer. LAP is very sensitive to reaction conditions: for example, protic solvents and other electrophiles will react rapidly with the anionic active centre. LAP syntheses require rigorous purification of the monomer, solvent and glassware to remove water. Moreover, it is only applicable to a small sub-set of vinyl monomers that contain electron-withdrawing substituents to stabilise the anionic chain-ends, making its scope rather limited.

1.3 Reversible Deactivation Radical Polymerisation

Reversible deactivation radical polymerisation (RDRP) is a term used to describe polymerisations that have 'pseudo-living' character. It has been suggested as an alternative, more accurate description compared to older terms such as Living Radical Polymerisation (LRP) and Controlled Radical Polymerisation (CRP).[13] However, the latter terms are still widely used in the literature. RDRP combines many of the advantages of FRP and LAP and eliminates some of their inherent disadvantages. RDRP does not require rigorous purification of the reagents or glassware and is tolerant of a range of solvents, including protic solvents such as water and alcohols. RDRP is much more tolerant of monomer functionality than anionic polymerisation, which significantly expands the monomer palette and reduces the need for atom-inefficient protecting group chemistry. However, RDRP usually results in a slightly higher polydispersity, and the pseudo-living character is typically reduced under monomer-starved conditions towards the end of the reaction.[14] Furthermore, the required reagents can introduce problems such as colour, malodour or toxicity.

Nitroxide-mediated polymerisation (NMP),[15] atom transfer radical polymerisation (ATRP),[16] and reversible addition-fragmentation chain transfer (RAFT) polymerisation[17,18] are the most commonly used RDRP techniques. The common feature of such processes is a dynamic (and rapid) equilibrium between the propagating radicals and a 'dormant' or deactivated species during the polymerisation.[19] Radicals are either reversibly capped in a deactivation/activation process (**Figure 1.5**), or they can undergo 'reversible transfer' degenerative exchange (**Figure 1.6**).
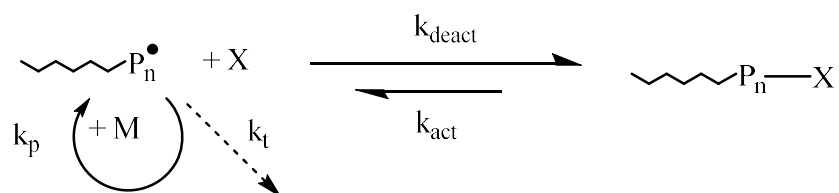

Figure 1.5 Radical participation in deactivation/activation process.

The first strategy is based on the persistent radical effect (PRE), which provides a self-regulating effect in certain CRP formulations. In **Figure 1.5**, the propagating radical $P_n^{\bullet}$ is capped in a deactivation process with a rate constant k_{deact} by species X. As a result of this reaction, the dormant species P_n-X is formed. This dormant species can be subsequently reactivated and then participate in propagation or irreversible termination. Persistent radicals cannot terminate with each other and can only reversibly cross-couple with the growing species (k_{deact}). X can be a nitroxide radical, such as 2,2,6,6,-tetramethyl-1-piperidinyloxy (TEMPO) or a derivative thereof.[20]
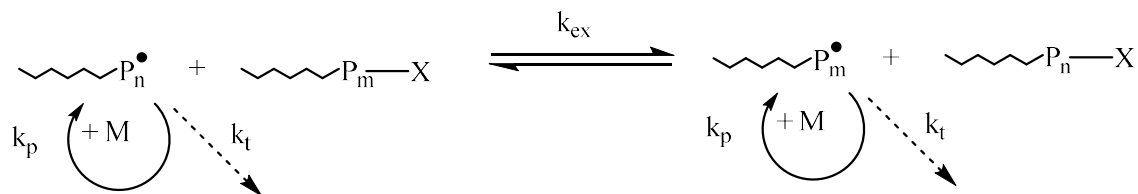

Figure 1.6 Radical participation in reversible transfer/degenerative exchange process.

In the reversible activation-deactivation reaction, the equilibrium favours the dormant species, as the rate constant for its formation is higher than that for the propagating radical and persistent radical. Thus, the concentration of the stable counter-radical is higher than that of the growing radical. This provides some degree of control over the polymerisation although termination is only suppressed relative to propagation, rather than being eliminated.[21]

1.3.1 Reversible Addition-Fragmentation chain Transfer (RAFT) Polymerisation

RAFT polymerisation was first reported in 1998 by a team of Australian scientists working at the Commonwealth Scientific & Industrial Research Organization (CSIRO).[18,22] Since then, it has grown into one of the most versatile and powerful polymerisation techniques for the synthesis of complex copolymer architectures.[23] The RAFT polymerisation mechanism is shown in **Figure 1.7**.
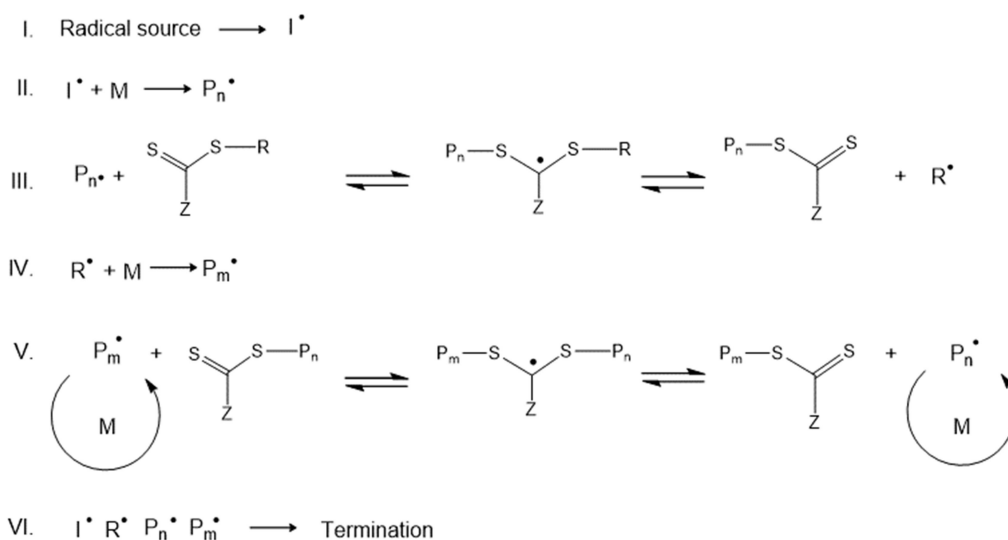

Figure 1.7 Proposed mechanism of RAFT polymerisation according to Rizzardo et al.[23]

Following activation (step I), radicals can react with monomer to produce a propagating polymer radical (step II). This enters an equilibrium between active and dormant species (steps III and V). This is a degenerative transfer process as it involves rapid reversible

transfer of the organosulfur chain ends (typically a thiocarbonylthio group) between dormant chains and the propagating radicals.

The rate of addition/fragmentation should be higher than the rate of propagation, since this ensures that all chains should grow at a similar rate.[23] A key requirement of RAFT polymerisation is the use of a radical initiator. This allows the rate of polymerisation to be tuned and influences the fraction of living chains according to the choice of polymerisation conditions.[24] Unlike ATRP and NMP (which are based on reversible deactivation), bimolecular termination does not lead to the loss of 'living' chain ends, so the number of living chains can be predicted.[23] The number of polymer chains corresponds to the sum of primary radicals (I•) and fragment radicals (R•) that have added monomer units.[25] The theoretical M_n can be approximated using **Equation 1.9**.[26]

$$M_n = \frac{[M_0]xM_0}{[CTA]} \text{ (Equation 1.9)}$$

Where M_0 is the molar mass of the monomer, and x is the fractional conversion. While the mechanism shown in **Figure 1.7** is widely accepted, it only describes the ideal behaviour of a RAFT polymerisation. There is still some dispute over the relative rates of individual equilibria, as well as the precise reasons for deviations from ideal living behaviour, e.g. side reactions and retardation effects.[17] For effective control over the MWD in a RAFT polymerisation, several criteria must be fulfilled. Firstly, it is necessary to initiate all the chains within a short period of time. Secondly, the number of monomer units added while the polymer chains are active should be relatively low prior to chain transfer to ensure a similar growth rate for all chains. Thirdly, any side reactions leading to dead chains should be minimised. Thus, RAFT control is strongly dependent on the chemical structure of the RAFT agent (i.e. its Z and R substituents) since this determines both its selectivity and efficiency for a given monomer class (**Figure 1.8**).[19,25]
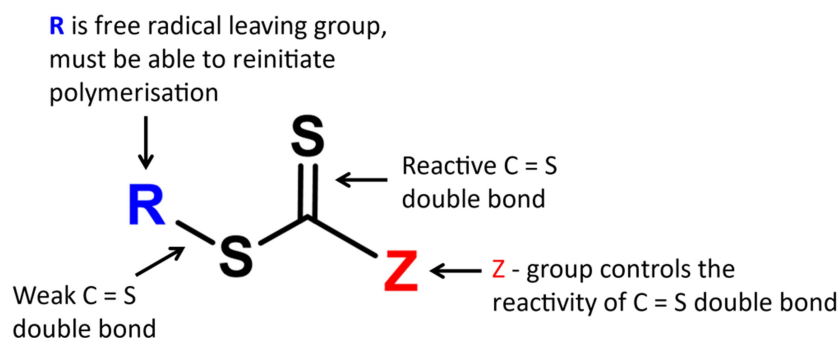
Figure 1.8 General chemical structure of a RAFT agent, whereby the R and Z groups determine its reactivity.[27,28]

By determining the relative rates of addition and fragmentation, the efficiency of chain transfer and probability of inhibition can be controlled.[27] The R group must be a good radical leaving group and thus be capable of reinitiating the polymerisation. Steric effects are much more important than for ATRP. For example, the reactivity of *t*-butyl halides is higher than that of benzyl derivatives in RAFT, whereas the opposite trend is reported for ATRP.[29]

The Z group is involved in stabilising the transition states in steps III and V, see **Figure 1.7**. There are also important structure-activity relationships. For example, a phenyl Z group stabilises styrene and methacrylate polymerisations, but retards the polymerisation of acrylates and inhibits vinyl ester polymerisations.[19] According to the RAFT literature, dithioesters, dithiocarbamates, trithiocarbonates and xanthates can each be used to control molecular weight, MWDs and molecular architecture for a given monomer class.[18,22,30]

A key feature of RAFT polymerisation is that the organosulfur end-groups are retained in the final polymer chains, rendering the process suitable for synthesising block copolymers.[31] However, RAFT CTAs are intrinsically coloured (e.g. dithiobenzoates are red and trithiocarbonates are yellow) and extremely malodorous. Removal of end groups can be achieved by thermolysis, oxidation, treatment with base or radical-induced transformation.[32–35] When polymerisation conditions are optimised, high conversions can be achieved and

RAFT is often considered the best RDRP technique for producing high molecular weight *functional* polymers with low dispersities ($M_w/M_n < 1.20$-1.30). It is arguably also more industrially applicable, as it can be conducted in a similar fashion to thermally-initiated FRP, thus minimising the need for major changes to current commercial processes.[36] RAFT polymerisations can be conducted in the bulk, in solution or using several types of heterogeneous polymerisation (see below).

1.4.1 Aqueous Emulsion Polymerisation

In an aqueous emulsion polymerisation, both the monomer and the resulting polymer are insoluble in the polymerisation solvent (water). This formulation also requires a water-soluble initiator and a surfactant or polymeric stabiliser, which can be either added at the beginning or generated *in situ*.[37] When using FRP, the main locus of polymerisation is within the monomer-swollen micelles/latex particles which are formed at the start of the polymerisation. Alternatively, a seed latex can be used, as in the case of seeded emulsion polymerisation.[38] One of the main advantages of emulsion polymerisation is that it enables the rapid production of high molecular weight polymers, achieving high monomer conversions while maintaining a low solution viscosity.[39] Aqueous emulsion polymerisation is widely used in industry owing to its wide applicability and environmentally-friendly nature, especially for the multi-tonne production of waterborne paints and coatings.[40]

The mechanism for conventional emulsion polymerisation in the presence of added surfactant is shown in **Figure 1.9**. There are three distinct stages: intervals I, II and III. Interval I involves particle formation *via* surfactant micelles (if the surfactant concentration is above the critical micelle concentration, CMC). Micrometre-sized monomer droplets are created by the shear forces induced *via* mechanical stirring. Particle nucleation depends on several factors, including monomer and initiator type, their respective solubilities in water and the

reaction conditions (e.g. temperature, pH). However, it is generally accepted that nucleation takes place by either homogeneous nucleation or micellar nucleation, or both.[37]
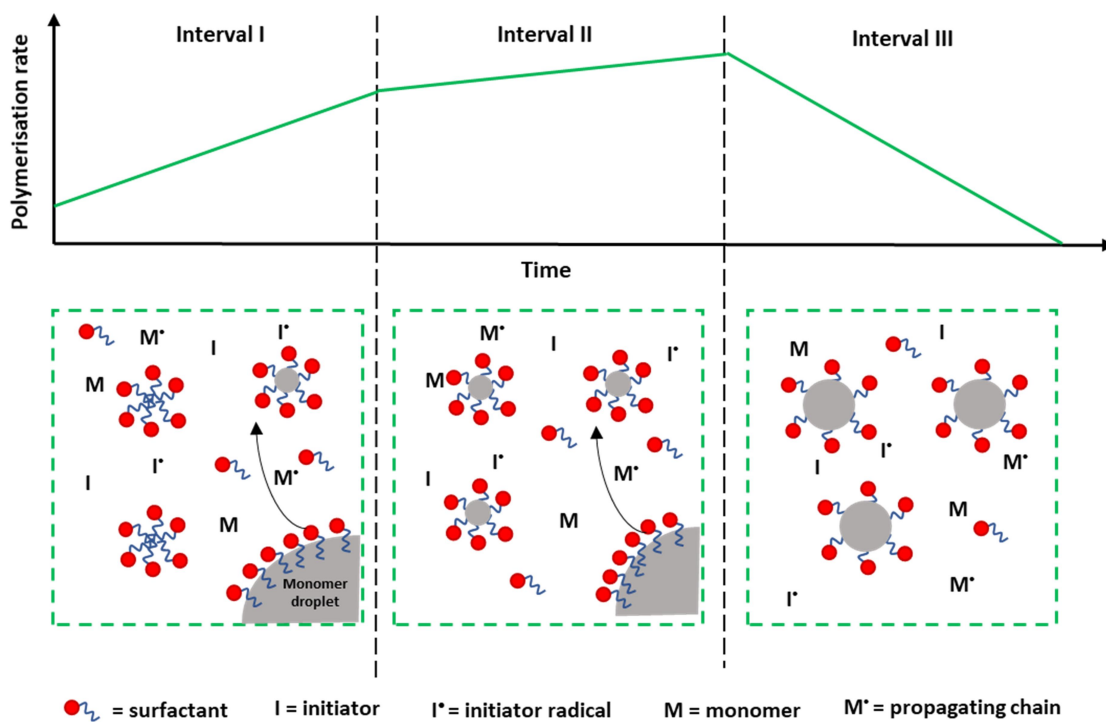

Figure 1.9 Schematic representation of the main events of an emulsion polymerisation and the accompanying rate of polymerisation during intervals I to III. The time intervals shown are not necessarily to scale.[41]

The water-soluble initiator decomposes to produce radicals that enter the monomer-swollen micelles (10 – 50 nm diameter). Radicals preferentially enter such micelles rather than monomer droplets (1 – 10 μm), as the former species are far more numerous and hence present a much larger surface area than the latter. Therefore, polymerisation occurs almost exclusively within the micelles. However, radicals can also react with the relatively small proportion of monomer that is dissolved in the solvent. This is known as homogeneous nucleation, which results in the formation of oligomers. These oligomers can enter existing micelles while they remain water-soluble. However, once they reach a critical length, they undergo precipitation, and form new nano-sized particles. Once these particles reach a certain

critical size, monomer swelling occurs, and the particles grow at an enhanced rate owing to the relatively high local monomer concentration within them. Once particle nucleation has ceased, interval I is complete. This is usually attributed to the surfactant concentration falling below the CMC so that new micelles cannot be formed. In interval II, the polymerisation rate remains essentially constant as no new particles are formed, allowing the remaining monomer droplets to act as reservoirs and provide each particle with a continuous supply of monomer through the aqueous phase. A rate enhancement is sometimes observed owing to an increase in viscosity – this is known as the Trommsdorff-Norrish effect.[42] As the supply of monomer is gradually depleted, the rate of polymerisation is reduced, which marks the start of interval III. During this final stage, the rate of polymerisation is gradually lowered until all monomer is consumed. The final product is a colloidal dispersion of latex particles, whose stability arises from a surface layer of adsorbed surfactant molecules or polymer chains.[43]

1.4.2 Aqueous Dispersion Polymerisation

For dispersion polymerisations, the reaction solution comprises monomer, initiator and a polymeric stabiliser, which are all initially soluble in the chosen solvent.[44] As the monomer is converted into insoluble polymer, macroscopic precipitation is prevented by the stabiliser, which adsorbs onto the growing particles to confer steric stabilisation (**Figure 1.10**).[45,46] This technology has been extensively used in the manufacture of solvent-borne film-forming latex paints over the past six decades.[14,47] The size of latex particles produced are usually in the range of 50 - 300 nm, however this is strongly dependent on the nature of the polymerisation mixture.[48] If nucleation is confined to a relatively short period of time at the start of the reaction, then near-monodisperse latex particles can be prepared.[49] FRP-mediated dispersion polymerisation is believed to proceed via the mechanism shown in **Figure 1.10**.
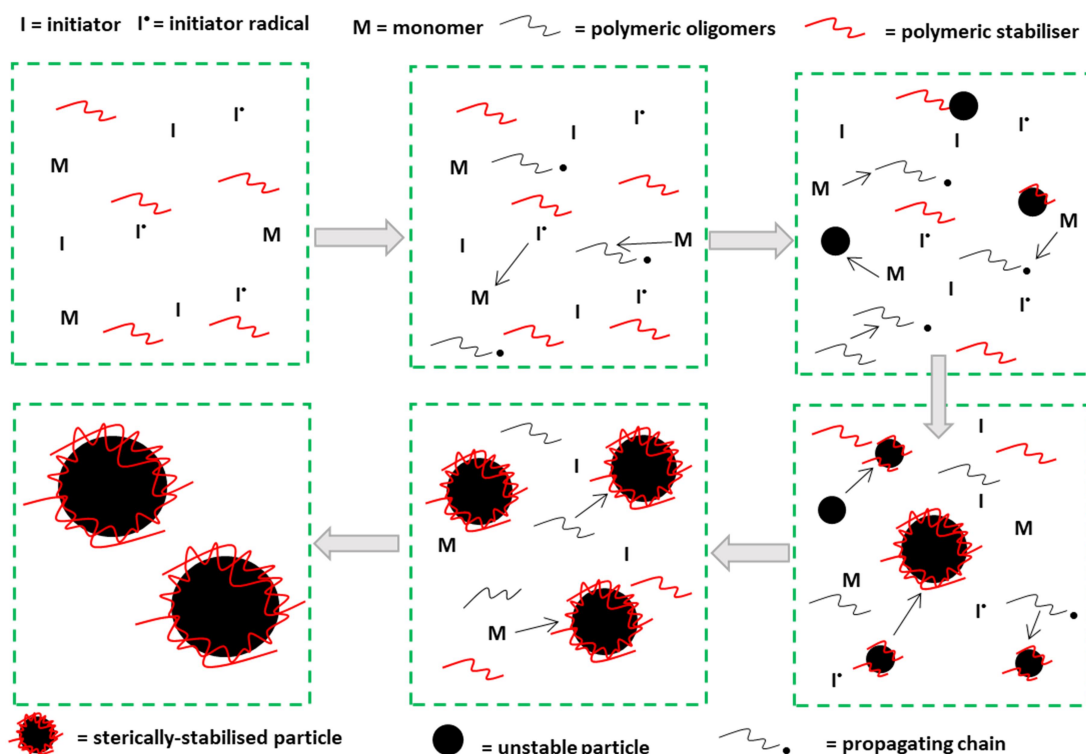

Figure 1.10 Schematic representation of the main components of a dispersion polymerisation.[50]

Prior to polymerisation, all components are dissolved in the reaction mixture. When the polymerisation begins, radicals are created by decomposition of the initiator. These species react with the soluble monomer to form oligomers, whose solubility in the reaction mixture depends on their molecular weight (and various other parameters). At some critical DP, they begin to precipitate and coagulate to form nuclei. These nascent particles begin to aggregate, and the soluble stabiliser chains either physically adsorb or become chemically grafted onto the colloidally unstable particles. Once all particles acquire sufficient stabiliser to ensure colloidal stability, no new nuclei are formed, and no further particle aggregation occurs. Instead, the monomer-swollen particles grow by diffusive capture of oligomers and small nuclei precursors. This growth continues until all the monomer is consumed.[51,52] Polymerisation can occur both within the particles and also in solution. Thus, a higher number density of small particles can more efficiently capture growing polymer chains in solution, leading to higher molecular weights. Conversely, larger particles are more likely to capture chains that have already terminated in solution, which leads to a lower overall molecular weight.

Various non-aqueous dispersion polymerisation formulations have also been developed. For example, Vanderhoff *et al*. reported the synthesis of micron-sized latex particles in 1984 *via* polymerisation of styrene in methanol using AIBN initiator and PNVP as a steric stabiliser.[53] Ober *et al.* also synthesised latex particles in 1985 by dispersion polymerisation of styrene in ethanol using non-ionic cellulosic derivatives as the steric stabiliser.[54]

In the specific case of aqueous dispersion polymerisation, as the water-soluble monomer is converted into a water-insoluble polymer, precipitation is prevented by the water-soluble polymeric stabiliser, which ensures colloidal stability. However, there are relatively few water-soluble vinyl monomers that yield water-insoluble polymers when polymerised, due to

increasing hydrophobicity of long chain macromolecules.[45] Some examples of such vinyl monomers are shown in **Figure 1.11**.
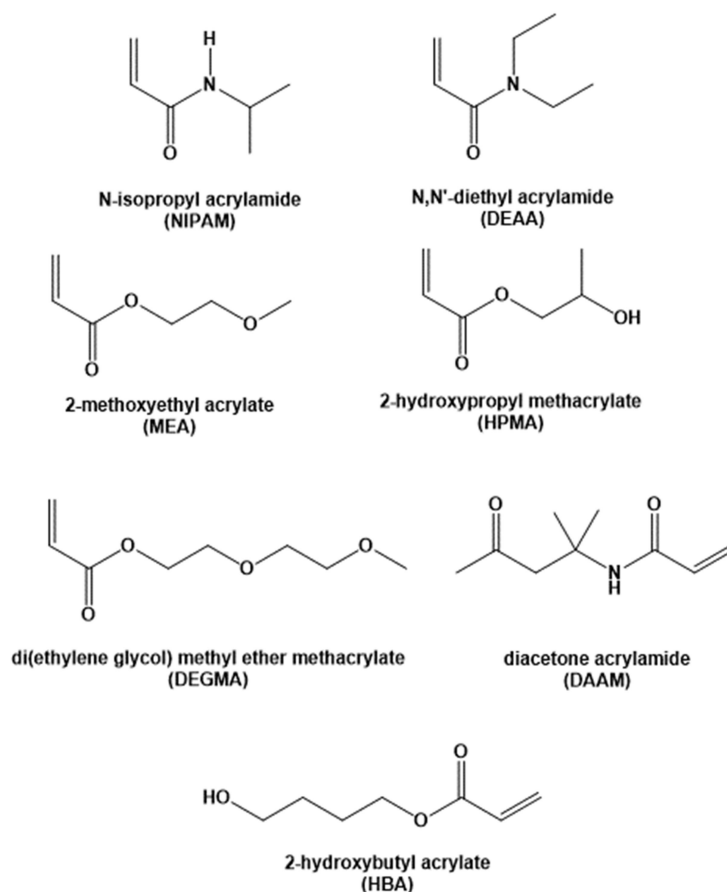

Figure 1.11 Chemical structures of seven water-miscible vinyl monomers for which each corresponding homopolymer is water-insoluble.[45,55,56]

The most widely examined monomer is 2-hydropropyl methacrylate (HPMA), which has been used for both FRP-mediated[44] and RAFT-mediated aqueous dispersion polymerisation.[57–66]

1.5 Principles of Self-Assembly

Self-assembly is a process by which (macro)molecules spontaneously form ordered aggregates.[67] Self-assembly is essential for the formation of important biological structures such as cell membranes. Moreover, it enables the synthesis of many complex nanostructured materials. For amorphous materials, the main non-covalent forces that drive self-assembly are hydrogen bonding, hydrophobic effects, electrostatic interaction, and Van der Waals forces.

1.5.1 Self-Assembly of Surfactants

All surfactant molecules are amphiphilic, meaning that they possess both hydrophilic and hydrophobic components. In aqueous solution, the polar head group interacts with the water molecules while the non-polar lipophilic chains migrate to the air-water and solid-water interface. If the surfactant concentration exceeds the critical micelle concentration (CMC), once such interfaces become saturated with adsorbed surfactant monolayers, surfactant micelles are formed in the bulk solution.[68,69]

The driving force for self-assembly originates from the hydrophobic attraction of the molecule to the hydrophilic-hydrophobic (water-carbon) interface.

The size and shape of a micelle depends on both the molecular structure of the surfactant and the solution conditions, e.g. the surfactant concentration, temperature, pH, and ionic strength. Israelachvili *et al.*[70] defined the packing parameter p to determine the micelle morphology adopted as a result of lipid self-assembly (**Equation 1.10**).

$$p = \frac{v}{a_o l_c} \text{ (Equation 1.10)}$$

Here v is the volume occupied by the hydrophobic chain, a_o is the optimal surface area occupied by the head-group at the hydrophilic-hydrophobic interface and l_c is the maximum

effective length for the hydrophobic chain. In principle, the numerical fractional value of *p* governs the micelle morphology as shown in **Figure 1.12**.

The traditional thermodynamic interpretation of surfactant micelle formation based on the Gibbs equation (**Equation 1.11**) is characterised by a small positive enthalpy, but a large positive entropy. Thus, micelle formation is entropy driven, which is surprising as the surfactants are molecules are forming ordered aggregates. This has been explained by accounting for the ordering of water molecules as self-assembly occurs. Water forms clathrates (cage structures)[71] around hydrophobic solute molecules to reduce the disruption of hydrogen bonding interactions (the hydrophobic effect).[72] This increases the structuring of water molecules, hence decreasing the solvent entropy. Thus, the release of water molecules from their confinement can act as a powerful driving force for surfactant aggregation, as it results in a large overall entropy gain in the system.

critical chain length, l_c

p < ⅓ = spherical micelles

⅓ < *p* < ½ = non-spherical micelles

½ < *p* < 1 = vesicles or bilayers

p > 1

volume, *v*

area, a_0
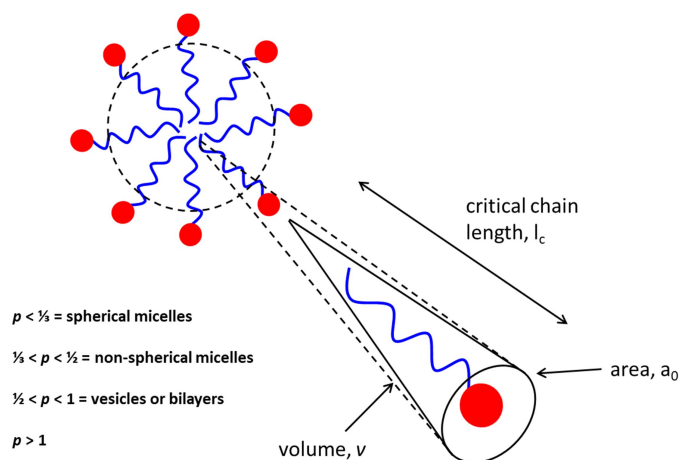
Figure 1.12 Schematic representation of the packing of surfactant amphiphiles within a spherical micelle with some common fractional values for the packing parameter, *p*, for other micelle morphologies, as outlined by Israelachvili.[73]

1.5.2 Block Copolymer Self-Assembly

The assembly of AB diblock copolymers has been extensively researched, both in the bulk and in solution.[74–76] In the former case, micro-phase separation is typically observed owing to

enthalpic incompatibility between the two blocks. The resulting copolymer morphology depends on three parameters: the relative volume fractions of the two blocks, the overall degree of polymerisation (*N*), and the Flory-Huggins parameter (which is a measure of the enthalpic incompatibility between the two blocks). Micro-phase separation can be related to the master equation for the thermodynamics of mixing for small molecules (**Equation 1.11**).

$$\Delta G_{mix} = \Delta H_{mix} - T\Delta S_{mix} \qquad \textbf{(Equation 1.11)}$$

where ΔH_{mix} is the enthalpy of mixing and ΔS_{mix} is the entropy of mixing at a given absolute temperature. Flory[77] and Huggins[78] independently developed a lattice model to calculate ΔG_{mix} when mixing two chemically distinct polymers. This assumes that the lattice solely consists of polymer segments and solvent molecules, the size of the segments is the same as that of the solvent molecules, and that the mixing of these two components is random. This theory takes account of the great dissimilarity in molecular sizes to adapt the usual expression for Gibbs free energy of mixing. The enthalpic contribution is contained within the Flory-Huggins interaction parameter χ_{AB}, which considers energy change due to different monomer interactions, and interaction with nearest monomer neighbours. The degree of incompatibility between A and B blocks is given by **Equation 1.12**.

$$\chi_{AB} = \left(\frac{z}{k_B T}\right)\left[\varepsilon_{AB} - \frac{1}{2}\left(\varepsilon_{AA} + \varepsilon_{BB}\right)\right] \qquad \textbf{(Equation 1.12)}$$

Here *z* is the number of nearest neighbours per polymer repeat unit, k_B is the Boltzmann constant, $k_B T$ is the thermal energy, and ε_{AB}, ε_{AA} and ε_{BB} are the interaction energies per repeat unit for A-B, A-A and B-B interactions, respectively. A positive χ_{AB} indicates net repulsion between species A and B, a negative value indicates a free-energy drive towards mixing. ΔG_{mix} can be calculated by considering the *additional* configurational entropy associated with copolymer chains, see **Equation 1.13**.

$$\frac{\Delta G_{mix}}{k_B T} = \left(\frac{\varphi_1 \ln \varphi_1}{N_1}\right) + \left(\frac{\varphi_2 \ln \varphi_2}{N_2}\right) + \varphi_1 \varphi_2 \chi \qquad \textbf{(Equation 1.13)}$$

Where $\boldsymbol{\varphi_1}$ and $\boldsymbol{\varphi_2}$ are the volume fractions of components 1 and 2 respectively, and N_1 and N_2 are the mean number of monomer units per copolymer chain. Thus, **Equation 1.13** shows that a negative value of χ is required for the spontaneous mixing of two species, whereas a positive value results in demixing. For interactions between non-polar molecules, a positive value is usually favoured as ε_{AB} tends to be less negative than the combination of ε_{AA} and ε_{BB} energies. Moreover, χ varies inversely with temperature, meaning that elevated temperatures are often required for mixing to occur *via* an order-disorder transition (ODT). Furthermore, as N tends to infinity, the number of moles of copolymer chains tends to zero, as does the entropy term. For larger values of N, there is an additional reduction in the diffusional and configurational entropy of the copolymer chains, which also reduces A-B contacts and results in local ordering.[79]

The product of the interaction parameter and the mean degree of polymerisation, χN, is important for determining the micro-phase separation behaviour for diblock copolymers. Thus, the ODT depends on both the composition, f, and χN. Importantly, the inability of two chemically different blocks to completely escape one another prevents macrophase separation and microphase separation occurs instead (**Figure 1.13**).
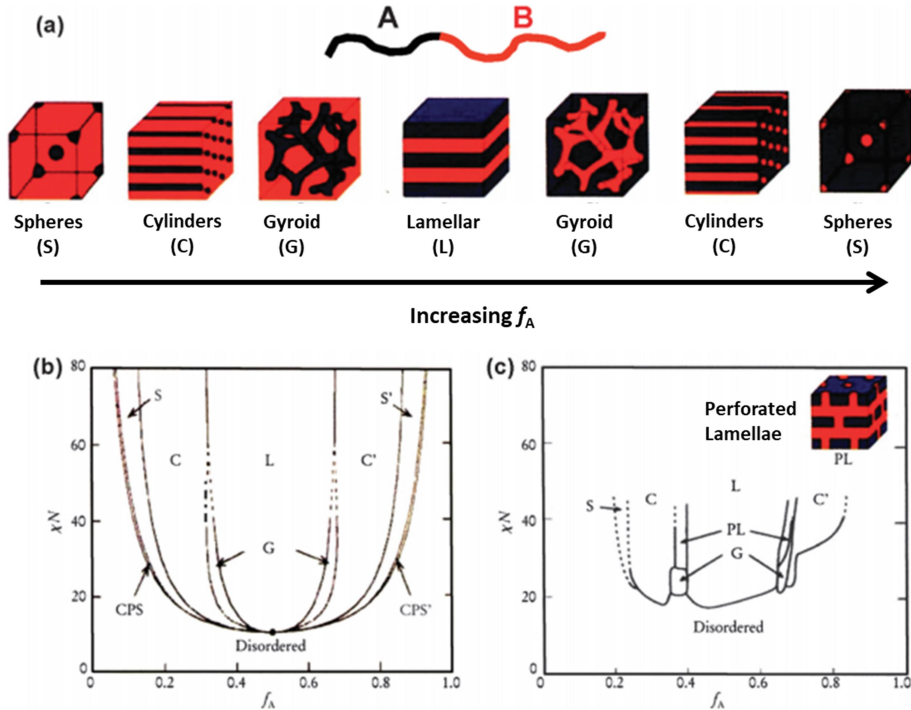
Figure 1.13 (a) Bulk morphologies obtained for an AB diblock copolymer below its ODT, dependent on the relative volume fraction, *f*, of block A. **(b)** Theoretical phase diagram of an AB diblock copolymer depending on *f* and *xN* (the product of the interaction parameter and the mean degree of polymerisation respectively) as predicted by self-consistent mean-field theory.[80] CPS = close-packed spheres. **(c)** Experimental phase diagram constructed by Bates and co-workers[81] for polyisoprene-polystyrene diblock copolymers where f_A is the relative volume fraction of polyisoprene. Reproduced from reference 80.

There are three distinct χN regimes for an AB diblock copolymer where $f = 0.5$.[82] These regimes correspond to weak ($\chi N = 0 – 12$), intermediate ($\chi N = 12 – 100$), and strong segregation limits ($\chi N > 100$). These relate to the relative sharpness (or fuzziness) of the block junction interface and the conformation (stretching/freedom) of the individual copolymer chains.[82] Flory defines displacement length as the distance between one end of the polymer chain and the other for a coiled polymer. The contour length is defined as the distance between one end of the polymer chain and the other when the polymer is stretched out (maximum displacement length). Segregation regimes (and periodicity of microstructures) can be related to the radius of gyration (R_g) of the polymer chains. For a

Gaussian coil (random walk), $R_g = (Nl)^{1/2}/6^{1/2}$, where N is the number of Kuhn segments, and l is the statistical segment length (which is often used to quantify polymer stiffness).

In the weak segregation limit, the periodicity of microstructures, d, is expected to scale as $N^{1/2}$ above the ODT as chains prefer to adopt a random coil conformation. However, this scaling relationship becomes $d \sim N^{2/3}$ for stronger segregation. Controlling the composition and architecture of block copolymers provides access to a wide range of structures that are suitable for various applications such as elastomers, dispersants, adhesives and coatings.[14,29,81,83]

In the presence of a solvent that is selective for one block, the block copolymer chains self-assemble to form aggregates that resemble the micelles formed by low molecular weight amphiphilic surfactants in aqueous solution (**Figure 1.14**). For example, an AB diblock copolymer in a solvent that is selective for block B will form micelles consisting of a core region comprising A blocks and a surrounding shell composed of B blocks.[75] However, block copolymer micelles have much slower exchange kinetics than surfactant micelles. Depending on the nature of the insoluble block, the former structures are often frozen whereas the latter are invariably in rapid dynamic equilibrium.[84,85]
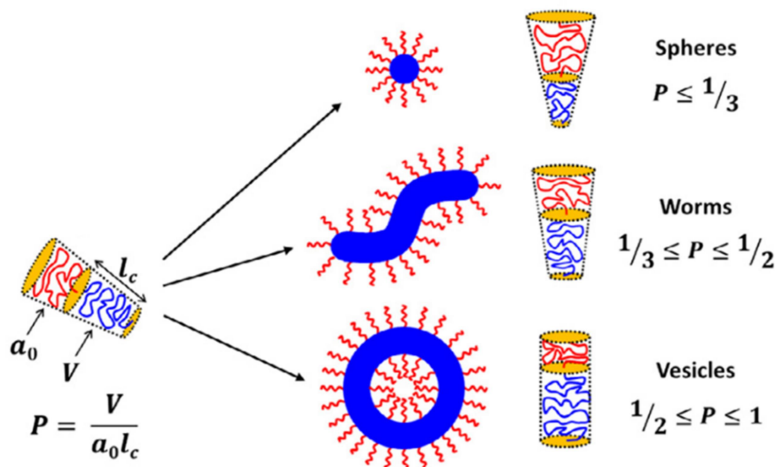
Figure 1.14 Self-assembled structures formed by an AB diblock copolymer in a selective solvent. The packing parameter, P, for the individual block copolymer chains is defined in terms of V, the volume of the core-forming blue chain, a_0, the optimal head-group area occupied by the red stabiliser chain, and l_c, the length of the blue core-forming chain. The preferred copolymer morphology (i.e., spheres, worms or vesicles) is dictated by the numerical value of P.[86] Reproduced from reference 85.

Self-assembly of amphiphilic diblock copolymers to form micelles in water has been known for many decades.[85,87] This field was substantially developed in the 1990s by Eisenberg *et al*.,[88] who used the solvent displacement method to prepare a wide range of copolymer morphologies for a series of well-defined diblock copolymers prepared *via* anionic polymerisation. For example, the self-assembly of polystyrene-poly(acrylic acid) (PS-PAA) has been studied in DMF-water mixtures, as well as various other binary mixtures of good and bad solvents.[89,90] It was found that the morphology could be controlled by varying the copolymer composition, copolymer concentration, nature of the water-miscible co-solvent and the presence of added salt. Transmission electron microscopy (TEM) images of the various morphologies formed by a series of PS-PAA diblock copolymers with varying block compositions are shown in **Figure 1.15**. Such micellar systems can enhance the solubility of hydrophobic compounds that otherwise display very low aqueous solubility.
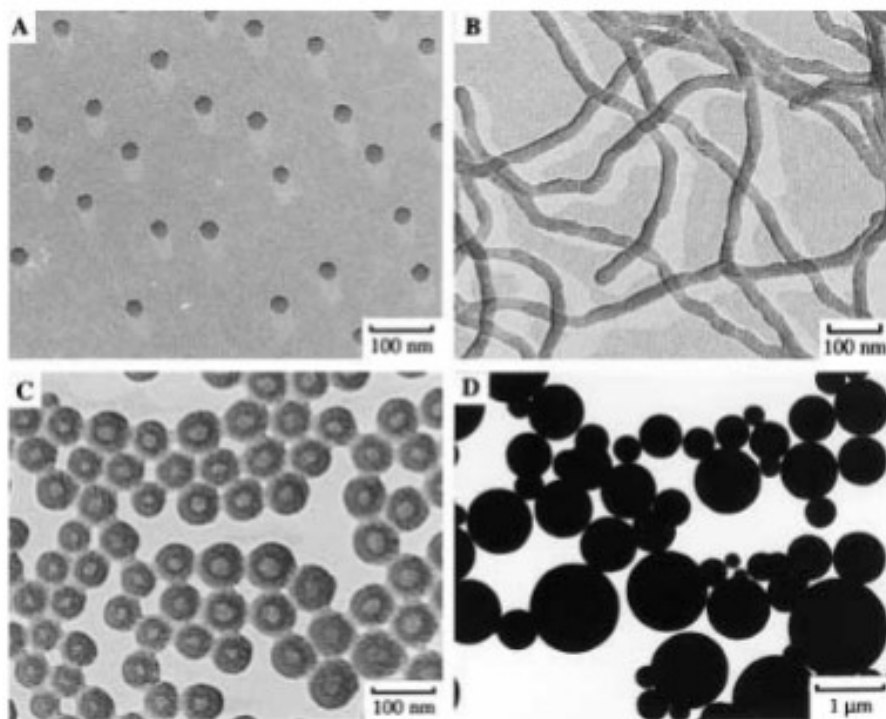
Figure 1.15 Typical copolymer morphologies formed by asymmetric amphiphilic diblock copolymers using the solvent displacement method: (A) PS_{500}-PAA_{58} spheres; (B) worm-like PS_{190}-PAA_{20} micelles; (C) PS_{410}-PAA_{20} vesicles and (D) large compound micelles comprising PS_{200}-PAA_4.[91] Reproduced from reference 90.

One advantage of block copolymers over surfactants is that they exhibit much lower CMCs. A typical CMC for a PS-PAA diblock copolymer in water is around six orders of magnitude lower than that of sodium dodecylsulfate.[92]

1.5.3 Polymerisation-Induced Self-Assembly (PISA)

Over the past decade or so, many academic research groups have focused on using RDRP techniques for the *in situ* synthesis of amphiphilic diblock copolymer nanoparticles *via* polymerisation-induced self-assembly (PISA).[45,93] PISA does not require the presence of low molecular weight surfactants or block copolymers to confer colloidal stability. In addition, PISA does not involve time-consuming post-polymerisation processes such as solvent[88] or pH-switching,[94] or thin film rehydration,[95] which are invariably conducted in dilute solution (< 1% w/w copolymer). Aqueous PISA syntheses can be conducted using a wide range of

functional monomers *via* either RAFT aqueous emulsion polymerisation or RAFT aqueous dispersion polymerisation.

1.5.3.1 PISA *via* RAFT Aqueous Emulsion Polymerisation

RAFT aqueous emulsion polymerisation has provided access to a range of block copolymer nanoparticles. Early research by Hawkett and co-workers focused on using water-immiscible monomers such as methyl methacrylate, *n*-butyl acrylate or styrene.[38,96] However, these initial formulations utilised 'seed' micelles that were synthesised in 1,4-dioxane prior to chain extension in water. In contrast, the Charleux group[97] used PEO-based macro-RAFT agents to conduct the *ab initio* RAFT emulsion polymerisation of styrene in a batch process. Spherical,[98,99] worm-like,[100] and vesicular particles[101] have been prepared using methacrylic,[101] acrylic,[102] or PEO-based stabilisers.[50,100] Other hydrophobic monomers such as *n*-butyl acrylate (BA)[103], methyl methacrylate (MMA)[104] and benzyl methacrylate (BzMA)[98] have also provided suitable core-forming blocks.
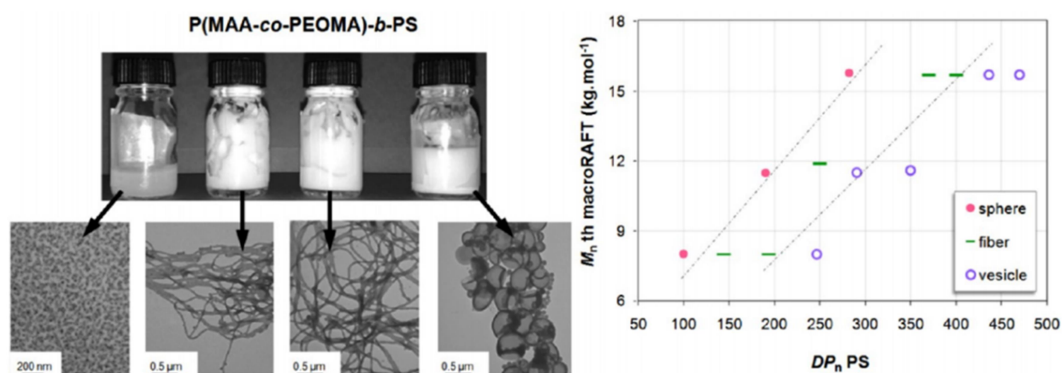

Figure 1.16 Digital photographs, corresponding TEM images and phase diagram obtained for P(MAA-*co*-PEOMA)-*b*-PS diblock copolymers prepared via RAFT aqueous emulsion polymerisation of styrene at pH 5 as reported by Zhang *et al*.[101,105] Systematic variation of the DP of the polystyrene block and the mass of the hydrophilic stabiliser block has a predictable effect on the final copolymer morphology, with spheres worms or vesicles being obtained. Reproduced from reference 100.

The use of water-soluble macro-RAFT agents for the RAFT emulsion polymerisation of styrene (**Figure 1.16**) has enabled fast polymerisations and high final conversions to be

achieved along with the formation of well-defined amphiphilic block copolymer nano-objects, where the morphology can be tuned by various parameters. This method is efficient, does not require any organic co-solvent and produces block copolymer nanoparticles in the form of concentrated dispersions.[101]

1.5.3.2 PISA *via* RAFT Aqueous Dispersion Polymerisation

Initially, an aqueous dispersion polymerisation formulation is a homogeneous solution because the monomer, initiator, and steric stabiliser (macro-CTA) are all water-soluble. At a certain critical DP for the growing hydrophobic block, the copolymer chains self-assemble to form nanoparticles, which remain colloidally stable owing to steric stabilisation conferred by the water-soluble precursor block (**Figure 1.17**).
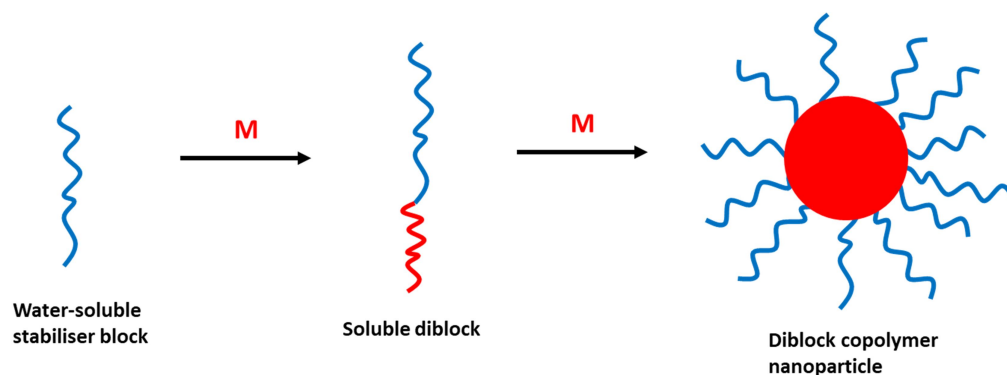

Figure 1.17 Schematic representation of polymerisation-induced self-assembly (PISA) *via* RAFT aqueous dispersion polymerisation (if the monomer **M** is water-miscible).

The first example of PISA *via* RAFT dispersion polymerisation was reported in 2007 by Houillot *et al.*,[106] who polymerised methyl acrylate in *iso*-decane using a soluble poly(2-ethylhexyl acrylate) macro-CTA. There are many examples of RAFT dispersion polymerisation formulations being conducted in alcohol/mixed aqueous media,[107–109] supercritical carbon dioxide[110] and other organic solvents.[86,111] As noted earlier, only a limited number of monomers are suitable for use in aqueous dispersion polymerisation.[76] Many examples concern the formation of thermosensitive particles, with hydrophobic blocks

such as poly(N-isopropylacrylamide) (PNIPAm), and thus possess lower critical solution temperature (LCST) behaviour. For example, An *et al.*[112] described an early example of the RAFT aqueous dispersion polymerisation of NIPAm using a water-soluble poly(*N,N'*-dimethylacrylamide) (PDAAm) macro-CTA. Introducing a suitable bisacrylamide cross-linker into this aqueous PISA formulation produced multiresponsive nanogel particles that become swollen with water on cooling to ambient temperature. Yan and Tao also employed aqueous dispersion polymerisation conditions for nanogel syntheses using a PEO-based macro-CTA and poly((2-dimethylamino)ethyl methacrylate) (PDMA) as the core-forming block.[113]

The Armes group were the first to report the RAFT aqueous dispersion polymerisation of a commodity monomer, 2-hydroxypropyl methacrylate (HPMA), using poly(glycerol monomethacrylate) as a steric stabiliser.[114] This formulation could be used to produce well-defined spheres with tunable mean diameter (**Figure 1.18**) and also worms and vesicles.[65,115]
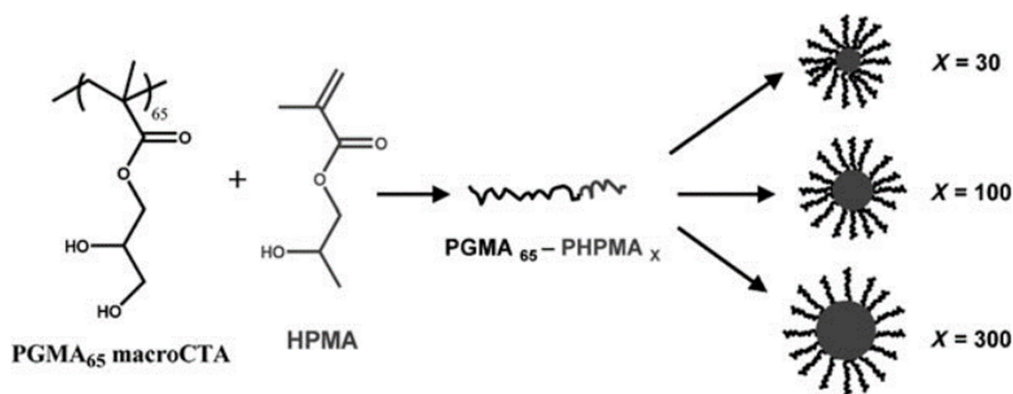

Figure 1.18 Synthesis of sterically-stabilised methacrylic nanoparticles by RAFT aqueous dispersion polymerisation.[114] Reproduced from reference 113.

It was found that the rate of polymerisation increased significantly after the onset of particle formation, which was attributed to compartmentalisation of monomer within the micelle

cores.[115] Periodic sampling of the polymerising solution gave an insight into the mechanism of morphological evolution (**Figure 1.19**).[115]
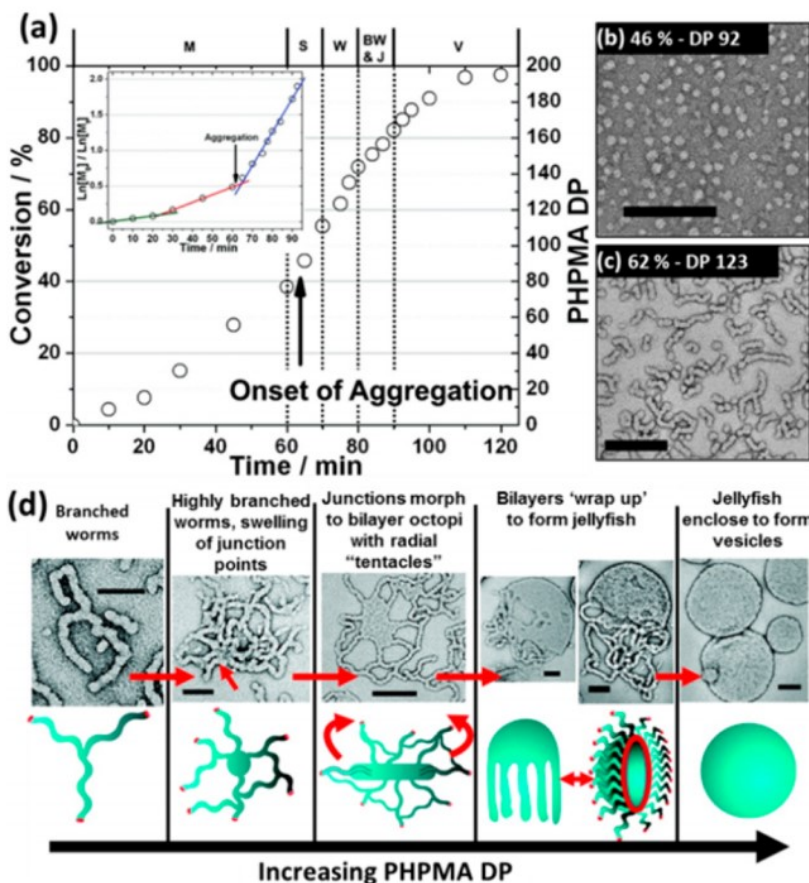

Figure 1.19 (a) HPMA polymerisation kinetics obtained using ^{1}H NMR spectroscopy when targeting PGMA$_{47}$-PHPMA$_{200}$ at 70 °C and 10% w/w solids. According to TEM studies, the five morphological regimes are: molecularly-dissolved polymer chains (M), spherical micelles (S), worms (W), branched worms (BW), jellyfish (J) and vesicles (V). The inset shows a semi-logarithmic plot for a subset of the data, indicating the five-fold rate enhancement observed after micellar nucleation. **(b)** Spherical micelles at 46% HPMA conversion. **(c)** Worms at 62% HPMA conversion (scale bar = 100 nm). **(d)** Suggested mechanism for the worm-to-vesicle transformation during the synthesis of PGMA$_{47}$-PHPMA$_{200}$ vesicles by RAFT aqueous dispersion polymerisation.[45,115] Reproduced from reference 114.

The final copolymer morphology depends on the DP of both the core-forming block and the stabiliser block, as well as other synthesis parameters such as the copolymer concentration. These can be predicted by constructing a pseudo-phase diagram, as shown in **Figure 1.20**. In this case, sterically-stabilised nanoparticles can be obtained at up to 25% w/w solids.[65]
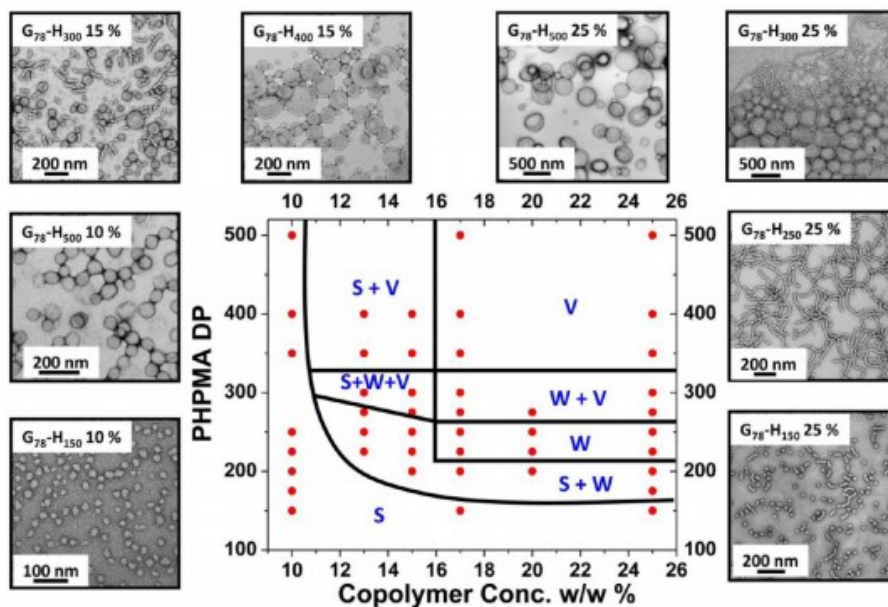
Figure 1.20 Representative TEM images and the corresponding pseudo-phase diagram for a series of PGMA$_{78}$-PHPMA$_x$ diblock copolymer nano-objects prepared by RAFT aqueous dispersion polymerisation at 10 – 25% w/w solids (S = spherical micelles, W = worms and V = vesicles).[65] Reproduced from reference 65.

Various other hydrophilic blocks have been utilised for the RAFT aqueous dispersion polymerisation of HPMA, including zwitterionic or polyelectrolytic stabilisers such as poly(2-(methacryloyloxy)ethyl phosphorylcholine) (PMPC),[57,116,117] poly(2-(trimethylammonium chloride) ethyl methacrylate) (PMETAC)[118] and poly(methacrylic acid) (PMAA).[119] PMAA has also been used for the RAFT dispersion polymerisation of other monomers such as MMA and BzMA in alcoholic media,[120] hydroxybutyl methacrylate (HBMA)[121] and LMA.[122] MAA has also been statistically copolymerised with BzMA to produce so-called 'schizophrenic' diblock copolymers with poly(2-(diethylamino)ethyl methacrylate) (PDEA) being used as a steric stabiliser (**Figure 1.21**).[123] These cationic PDEA-stabilised spherical nanoparticles were initially prepared in acidic solution, with nanoparticle inversion occurring to form PDEA-core nanoparticles on switching the solution pH from 2 to 10, because this led to deprotonation of the PDEA chains.
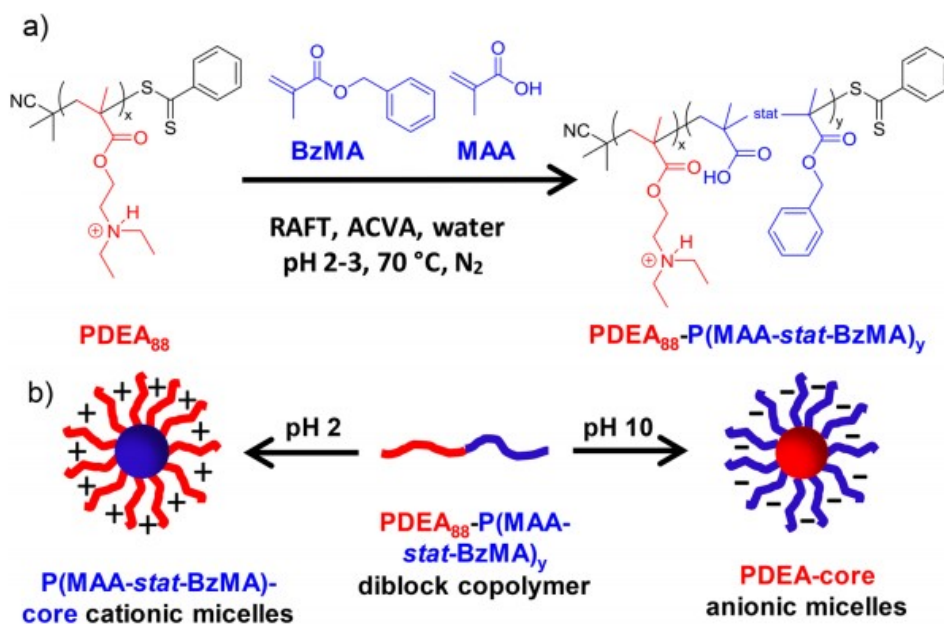
Figure 1.21 (a) Schematic representation of the RAFT aqueous copolymerisation of methacrylic acid and benzyl methacrylate using a PDEA$_{88}$ macro-CTA. **(b)** Schizophrenic micellization behaviour exhibited by PDEA$_{88}$-P(MAA-*stat*-BzMA)$_y$ diblock copolymers in aqueous solution.[123] Reproduced from reference 122.

In summary, RAFT aqueous dispersion polymerisation enables the rational design of bespoke block copolymer nano-objects for various potential commercial applications.[45]

1.6 Pigment Dispersion in Aqueous Media

Many industrial products such as paints,[83] pesticides,[124] printing inks,[125] ceramics,[126] and pharmaceutics[127] require the dispersion of polymeric particles within a continuous fluid phase Such formulations typically require concentrated colloidal dispersions. Polymeric dispersants can improve wetting, control foaming and prevent film defects, as well as enable optimisation of the rheological properties.[128] These dispersants enable the introduction of repulsive forces that offset the ever-present attractive van der Waals forces and hence prevent particle aggregation.[46]

1.6.1 Characteristics of common pigments

A pigment is any type of solid particle – coloured, black, white or fluorescent – that alters the appearance of any object by the selective absorption and/or scattering of light. The pigment is the most important component for a water-based paint or ink formulation.[129,130] The smallest possible form of a pigment is known as the primary particle, typically having a diameter of 0.01 – 10 μm. These are generally clustered into aggregates or agglomerates. In aggregates, the primary particles are bound strongly through chemical interactions, whereas agglomerates are loosely packed through weak bonds. Dispersion of pigments in aqueous media requires wetting, dispersion and stabilisation. Using water as a solvent for pigment dispersion can introduce certain problems owing to its high surface tension and highly polar nature. Pigments must be well-dispersed to optimise important end-use properties such as gloss potential, colour strength, opacity and long-term storage stability.

1.6.1.1 Inorganic Pigments

Inorganic pigments (e.g. TiO_2 and iron oxides) are generally chemically inert and insoluble. They also have highly polar surfaces, so they are readily wetted by water. Pigments are often surface treated, which can have important implications for their colloidal stability. For example, an ultrathin layer of alumina (or silica) is added to TiO_2 to improve the dispersibility of this important pigment.[131] Such surface layers can also reduce photocatalytic activity and enhance the adsorption of polymeric dispersants. The specific surface area of a typical untreated paint-grade titania pigment is 6-9 m^2 g^{-1}.[132] However, alumina or silica surface coatings can double the specific surface area owing to the greater surface roughness.[133] In some cases, surface treatments can reduce the TiO_2 content by as much as 25% by mass.

For any combination of pigment, polymeric dispersant and water, there is usually a pH at which the net surface charge is zero: this is known as the isoelectric point (IEP). colloidal

instability is typically observed under these conditions. Above the IEP, the particles become anionic and below the IEP the particles acquire net cationic charge. In each case this aids particle redispersion.

1.6.1.2 Organic Pigments

Most inorganic pigments comprise transition metal compounds, which are usually highly coloured. However, growing concerns regarding their toxicity has led to the replacement of many inorganic pigments (e.g. molybdenum orange or cadmium red) with organic pigments, which exhibit enhanced long-term light stability and reduced toxicity.[134] Moreover, organic pigments such as carbon black tend to be much smaller in size than inorganic pigments, which leads to improved colour properties. Carbon black has a structural morphology which is composed of multiple hierarchies of aggregates, ranging in size from 10 – 1000 nm.[135] Primary particles fuse to form mass fractal aggregates of various shapes,[136] which have been studied primarily through small angle scattering.[137,138]

1.6.2   Colloidal stabilisation mechanisms for pigment dispersions

The effect of inter-particle interactions determines the colloidal stability of a system. Particle aggregates are much more difficult to break up than agglomerates. Either charge or steric stabilisation can be used to prevent particle aggregation. In each case, the ever-present attractive Van der Waals forces operating between colloidal particles are offset by introducing a suitable repulsive force.

1.6.2.1 Charge Stabilisation

Charge stabilisation occurs as a result of the accumulation of surface charge on the pigment particles. Surface charge can arise from ionised groups attached/adsorbed to the particle surface, or by the adsorption of oppositely-charged ions from solution. This leads to the formation of an electrical double layer (EDL) surrounding each particle, and it is the

energetically unfavourable overlap of such EDLs during inter-particle collisions that leads to the short-range inter-particle repulsive force that offsets the long-range attractive van der Waals forces (**Figure 1.22**). This mechanism is well described by the Derjaguin, Verwey, Landau and Overbeek (DVLO) theory.[139]
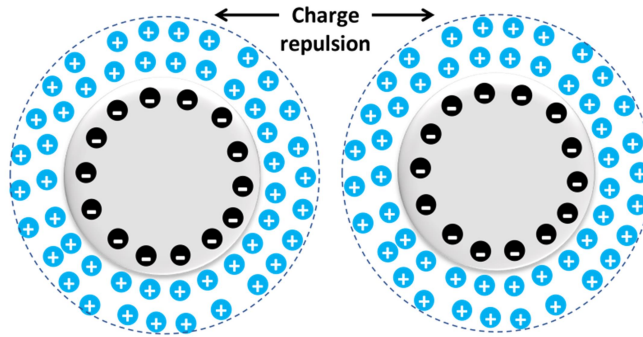

Figure 1.22 Charge stabilisation mechanism depicting the repulsive force generated by the energetically unfavourable overlap of the electrical double layers that surround negatively-charged particles.[140]

DVLO theory assumes additivity for the attractive and repulsive forces operating between particles to calculate the total interaction energy for a pair of particles on close approach. The condition for colloidal stability is that the mean kinetic energy (E_{max}) of the particles is significantly greater than kT (i.e., $E_{max} \gg k$T) (**Figure 1.23**). Charge stabilisation can only produce a *kinetically* stable system and heating such dispersions (i.e. increasing kT) will favour particle aggregation. The addition of salt also induces colloidal instability because this causes the EDLs to shrink in size. This in turn lowers the kinetic energy barrier E_{max}, so the ever-present attractive van der Waals forces can cause flocculation. Moreover, charge stabilisation is restricted to polar solvents such as water or lower alcohols in which the particles can acquire surface charge, and becomes ineffective at relatively high particle concentration.
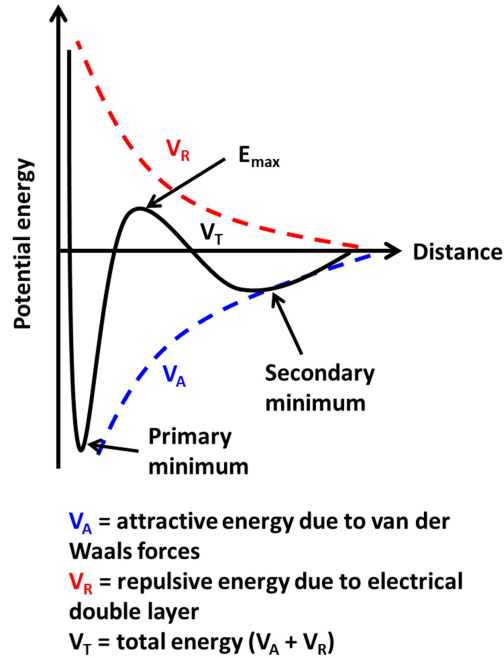
V_A = attractive energy due to van der Waals forces
V_R = repulsive energy due to electrical double layer
V_T = total energy (V_A + V_R)

Figure 1.23 Potential energy curve for charge stabilisation.[141]

Van der Waals forces dominate at low distances, as V_T increases due to the occurrence of Born repulsive forces. These are short range and only come into play when the atoms on the surface come into contact. This leads to the primary minimum, which represents strong attractive force. At high distances, the van der Waals forces can overcome repulsive forces to form a secondary minimum. In practice, an energy barrier significantly higher than kT is required to ensure colloidal stability. The kinetic energy needed for particles to overcome this barrier derives from Brownian motion, which results from random bombardment of the particle surface by molecules in the solvent.[142]

1.6.2.2 Steric Stabilisation

Steric stabilisation relies on the adsorption of polymer chains at the particle surface. The solvent is a good solvent for these polymer chains, so the adsorbed layer is well-solvated and relatively thick. When two particles coated with adsorbed polymer layers approach each

other, these layers start to interpenetrate. This intermingling of the polymer chains is clearly entropically unfavourable because fewer conformations can be adopted by the compressed chains. Moreover, it is also enthalpically unfavourable because the polymer chains would rather interact with solvents molecules. Thus, solvent diffuses into this local region of overlapping polymer layers, leading to interparticle repulsion (**Figure 1.24**).[46]
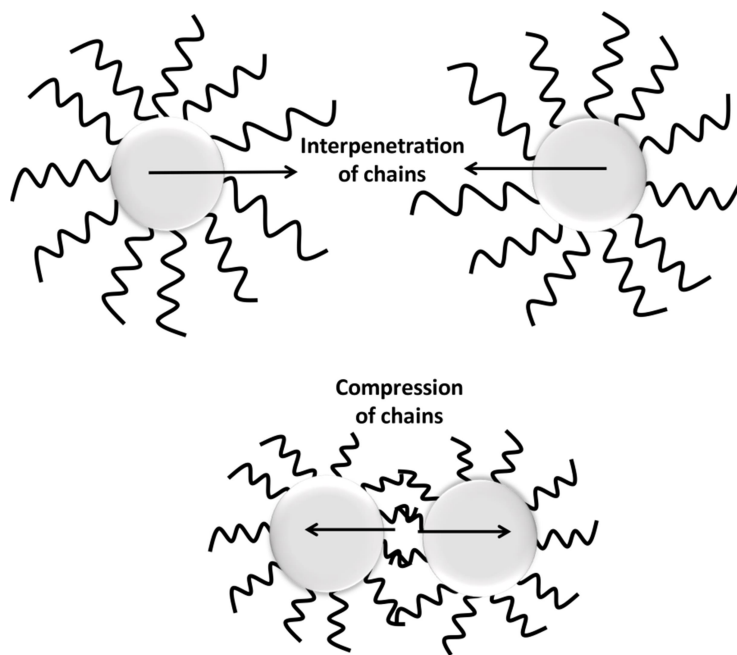
Figure 1.24 Mechanism of steric stabilisation according to Napper.[46]

The resulting colloidal stability depends on the surface coverage and thickness of the adsorbed polymer layer, and the strength of the polymer-surface interaction. Unlike charge stabilisation, steric stabilisation results in *thermodynamic* stability, and is relatively insensitive to added salt and continues to be effective even at high particle concentration.
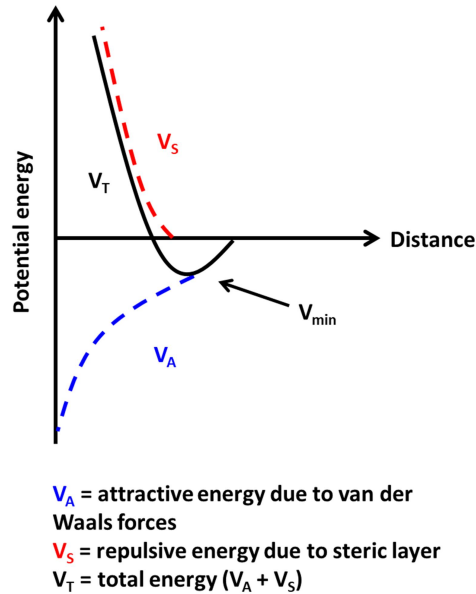
V_A = attractive energy due to van der Waals forces
V_S = repulsive energy due to steric layer
V_T = total energy ($V_A + V_S$)

Figure 1.25 Potential energy curve for the steric stabilisation of colloidal particles.[143]

As depicted in **Figure 1.25**, the stability of the system is governed by the repulsive potential (V_S) and the attractive one V_A. The minimum energy V_{min} is always present, as the range of V_S is smaller than V_A. This minimum occurs at an inter-particle separation distance equal to twice the mean thickness of the adsorbed polymer layers. A thinner stabilising layer will decrease the magnitude of this minimum, so good solvation is required for a stable dispersion.[144]

1.6.2.3 Electrosteric Stabilisation

A third type of colloidal stability mechanism is electrosteric stabilisation.[145] In this case, the adsorbed polymer has polyelectrolytic character. Polyelectrolytes, or charged polymers, tend to adsorb electrostatically onto oppositely charged surfaces, leading to surface charge reversal.[146] This maintains (opposite) surface charge and confers an additional steric barrier. Electrosterically-stabilised particles are much more tolerant of added salt and/or changes in the solution pH than charge-stabilised particles because of the additional steric stabilisation

component. If a weak polyelectrolyte is used, then the particle surface charge is likely to vary with solution pH. This may lead to an isoelectric point (IEP) where there is no net surface charge. At this critical pH (or pH range), the particles may become aggregated, with redispersion being observed on adjusting the solution pH either above or below the IEP.

1.6.2.4 Effect of added polymer on colloidal stability

The dispersion of a pigment in a liquid involves three key steps. First, the surface of the pigment particles is wetted by the liquid. Second, pigment agglomerates are broken up using mechanical agitation to achieve full wetting of the particles. The third step involves colloidal stabilisation of the individual pigment particles using a polymeric dispersant. This is required in order to overcome the ever-present attractive van der Waals forces operating between colloidal particles which would otherwise cause them to flocculate.[139] An adsorbed layer on the particle surface introduces repulsive forces through either steric and/or electrosteric stabilisation.[130]

The colloidal stability of a dispersion can be greatly influenced by addition of a suitable polymer. At relatively low polymer concentrations, bridging flocculation may occur. As shown in **Figure 1.26a**, this typically occurs with high molecular weight polymers in the presence of relatively small particles, where the chains can adsorb onto two or more particles and bring them into close proximity.[147] At higher polymer concentrations, steric stabilisation occurs as a result of repulsive forces between polymer-coated particles (**Figure 1.26b**). This mechanism requires high surface coverage and good solvency for the polymer chains, as discussed above.

In the case of a relatively high concentration of a non-adsorbing polymer, the effective osmotic pressure, or activity of the solvent between two approaching particles is affected. Polymer chains are excluded from the region between neighbouring particles. The osmotic pressure difference in the bulk solution also excludes solvent from this region, introducing an

attractive force that causes particle aggregation. This phenomenon is known as depletion flocculation (**Figure 1.26c**) and was first reported by Asakura and Oosawa in 1958.[148] At higher concentrations of non-adsorbing polymer, depletion stabilisation can occur (**Figure 1.26d**). This is a kinetic stability mechanism that is solely imparted by free (rather than adsorbed) polymer chains.[149]
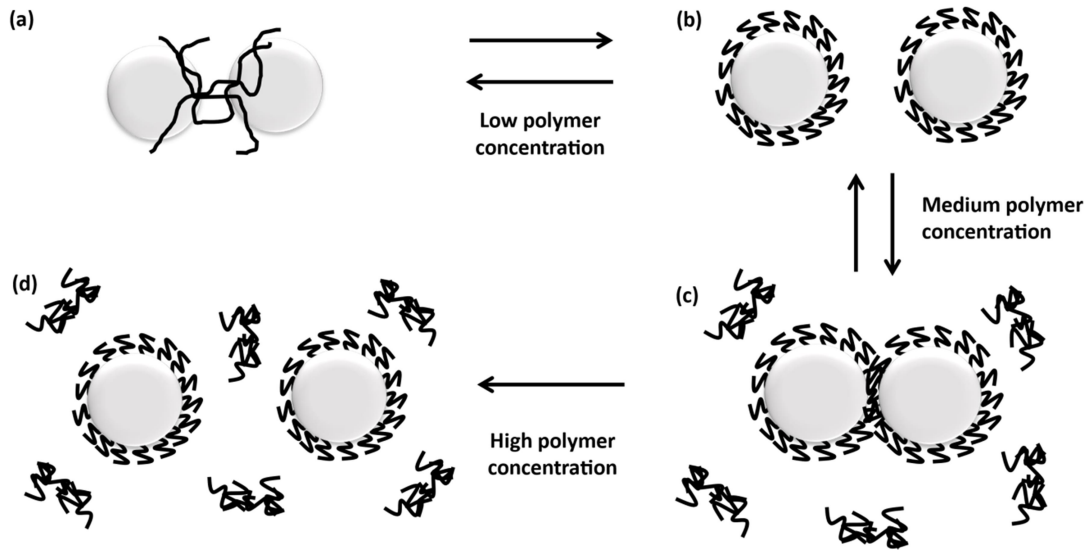

Figure 1.26 - Schematic representation of the effect of added polymer on the colloidal stability of particles: **(a)** bridging flocculation at low polymer concentration, **(b)** steric stabilisation at intermediate polymer concentration, **(c)** depletion flocculation at high polymer concentration and **(d)** depletion stabilisation at even higher polymer concentration. The first two instances involve adsorbed polymer chains whereas the latter two instances involve non-adsorbing polymer chains.

1.6.3 Pigment Dispersants

Polymeric dispersants can be differentiated from typical inorganic dispersants or surfactants by virtue of their relatively high molecular weight. This enables simultaneous binding to multiple surface sites, forming stable adsorbed layers at the pigment surface.[131,150] Polymeric dispersants confer (electro)steric stabilisation and may also enable cost-savings by enabling higher pigment loadings during grinding processes. For high solids coatings, high molecular weight additives are essential to ensure long-term colloidal stability.

1.6.3.1 Homopolymers

The adsorption of homopolymers has been studied since 1930 owing to its importance in numerous applications.[151] The mean-field theory developed by Scheutjens and Fleer[152] enables the distribution of tails, trains and loops to be calculated for adsorbed chains. This theory has also been extended to include the adsorption of block and random copolymers.[153]

Various homopolymers have been studied in the context of pigment dispersion. For example, Hoogeveen *et al.* examined the behaviour of several cationic polyelectrolytes, such as poly(2-(dimethylamino)ethyl methacrylate (PDMA) or poly(2-vinylpyridine)[154,155]. Variation of the ionic strength or solution pH influenced the rate of adsorption. At low salt concentration/pH, diffusion of such polyelectrolytes to the surface is slow, because the chains are highly expanded owing to repulsion between charged segments. This problem can be reduced by raising the solution pH. Boisvert *et al*. reported using poly(sodium acrylate) (PNaAA) for the stabilisation of alumina-coated TiO_2.[156] Such anionic polymers are well known for their excellent dispersion performance; both poly(sodium methacrylate) (PNaMAA) and PNaAA have been evaluated for the formulation of aqueous pigment dispersions.[157,158] These polyelectrolytes typically confer electrosteric stabilisation by adsorbing in a loop-train-tail conformation.[159] However, such dispersants interact strongly with the pigment surface and hence usually cannot prevent some degree of flocculation, even when the particles are fully covered. It is generally accepted that block copolymers are more effective dispersants because one block can be designed to adsorb at the pigment surface while the second block can confer steric stabilisation.[160–162] However, a wide range of *functional* block copolymers have only recently become accessible as a result of the development of RAFT polymerisation (and similar radical-based chemistries).

1.6.3.2 Amphiphilic Block Copolymer Dispersants

Amphiphilic block copolymers are of particular interest for pigment dispersion because they can improve both wetting and stabilisation of pigment dispersions. In contrast, random (statistical) copolymers are known to adsorb inefficiently at a pigment surface.[125] The extent and rate of unimer-micelle exchange can be an important factor for the application of block copolymers as pigment dispersants. In the presence of pigment, molecularly-dissolved copolymer chains (unimers) may adsorb at the pigment surface *via* the more hydrophobic block, whereas the micelles may not adsorb at all. On the other hand, there is some evidence to suggest that some types of micelles may adsorb onto the surface of certain pigments, e.g. PDMA-PMMA micelles onto the surface of silica particles.[163] Tuzar and co-workers reported that polystyrene-PNaMAA diblock copolymers formed highly stable micelles in water, with no micelle-unimer exchange being detected at all at room temperature.[164] However, recent studies by Jones *et al*. showed that cationic PDMA-PBzMA diblock copolymer micelles could be adsorbed electrostatically onto the surface of anionic silica particles, with some subsequent perturbation of the micelles suggesting affinity of the core-forming block for the silica surface.[109]

Statistical copolymers comprising NaMAA and amine-based comonomers were also assessed as putative pigment dispersants by Creutz and co-workers.[158] However, only poor dispersion stability was invariably obtained. For example, a 4VP/NaMAA random copolymer exhibited the same dispersion performance as a homopolymer of PNaMAA. On the other hand, the dispersion performance of a 'tapered' diblock copolymer was comparable to that of a pure diblock copolymer. This highlights the importance of 'blockiness' in a copolymer dispersant, which suggests the need for a controlled/living polymerisation to ensure a reproducible comonomer distribution.[161,165]

However, it is perhaps worth emphasising that the synthetic strategy employed by Creutz and co-workers for the preparation of such diblock copolymer dispersants involved anionic polymerisation and hence required protecting group chemistry for the acidic block. In contrast, Auschra and co-workers reported the synthesis of diblock copolymers for pigment dispersion using either NMP or ATRP.[162] Similarly, RAFT polymerisation has been used for *in situ* pigment encapsulation[166] to create a core-shell morphology comprising pigment cores and thick polymer shells. This process was highly efficient and involved adsorption of a macro-RAFT precursor onto the pigment surface in order to prevent secondary particle nucleation. More recently, Jagtap *et al.*[167] synthesised block copolymers *via* aqueous RAFT polymerisation for use in aqueous pigment dispersions as an eco-friendly approach to large scale manufacturing.

1.6.4 Measuring pigment dispersion

1.6.4.1 Adsorption isotherms

Adsorption isotherms enable the adsorbed amount of polymer on a surface to be quantified. Such isotherms involve plotting the adsorbed amount of polymer (Γ) versus the equilibrium concentration of polymer remaining in solution after adsorption (C_{eq}). The point at which a typical adsorption isotherm reaches a plateau value depends on various parameters. The available substrate surface area, polymer molecular weight, solvent type and copolymer architecture must all be considered. If adsorption is confined to a single monolayer - which is generally the case for polymers - then a Langmuir isotherm model can be used. In this case, the adsorbed amount can be calculated using **Equation 1.14**.

$$\Gamma = \frac{q_m K_a C_{eq}}{1 + K_a C_{eq}} \quad \textbf{(Equation 1.14)}$$

Here Γ is the adsorbed amount (mg m^{-2}), q_m is the monolayer capacity, K_a is the equilibrium constant, and C_{eq} is the equilibrium adsorbate concentration.[168] The specific surface area of

the substrate must be known in order to calculate q_m. Langmuir (L) isotherms typically exhibit a plateau region, which indicates monolayer formation. For adsorption from solution, Giles *et al.* also classified three other types of adsorption isotherms:[169] S-shaped (S), high affinity (H), and constant partition (C), see **Figure 1.28**.
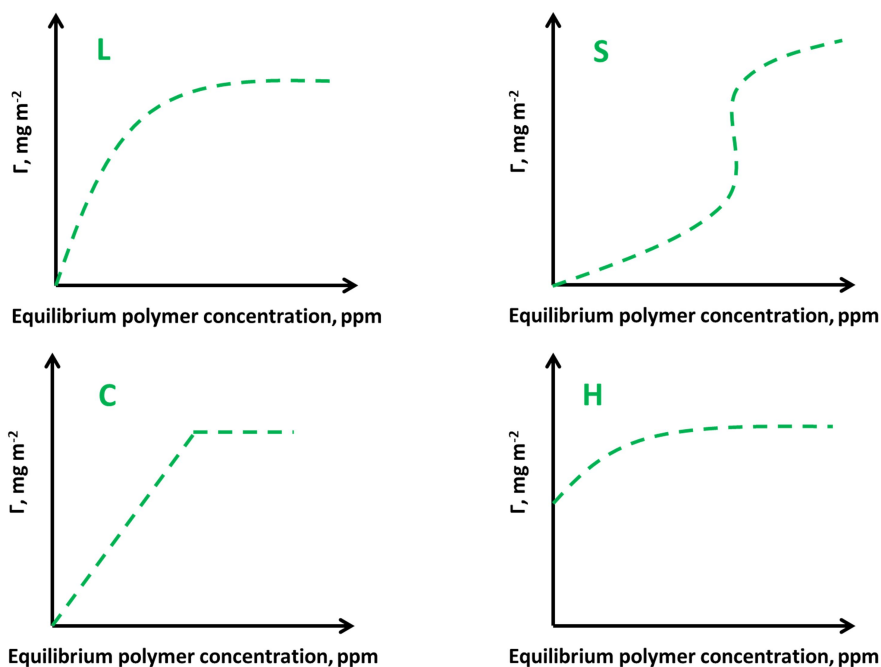

Figure 1.28 - Four types of adsorption isotherms for adsorption from solution onto a solid substrate according to Giles et al.[169]: Langmuir (L), S-shaped (S), high affinity (H), and constant partition (C).

Langmuir-type adsorption implies that it becomes increasingly difficult to adsorb more polymer chains as the surface coverage increases. H-type isotherms are obtained when the affinity for the substrate is very high even at low polymer concentrations, e.g. for the adsorption of poly(acrylic acid) on titania.[170]

The adsorbed amount of polymer is commonly determined using an indirect approach. This involves determining the polymer concentration in the continuous phase before and after adsorption. Centrifugation can be used to separate the colloidal substrate (e.g. polymer-coated pigment particles) from any excess non-adsorbed polymer and the adsorbed amount can then

be calculated by difference. This approach is sometimes known as a supernatant assay. If there is a convenient spectroscopic chromophore, the polymer concentration can be determined *via* UV spectroscopy.[171] Alternatively, a physical method such as densitometry or differential refractometry can be used. [172] In certain cases, it may be possible to determine the adsorbed amount more directly. For example, Growney *et al*. estimated the extent of adsorption of block copolymer micelles on carbon black particles using thermogravimetric analysis.[173–175]

1.6.4.2 Particle size distribution

Particle size distribution is another key parameter for assessing pigment dispersion performance.[176] For a given pigment, maximum colour strength is achieved once that pigment is dispersed below a minimum size. Therefore, the opacity/transparency and the colour strength and shade of a pigment can give an indication of its degree of dispersion. Although scattering theory was originally derived for spheres, Brockes and Chromey later modified it to include pigments of arbitrary shape.[177,178]

One useful method for sizing pigment particles is electron microscopy.[179] An electron beam is either scanned across the sample (SEM) or passed through the sample (TEM). This produces high resolution images that can be analysed using software to obtain statistically meaningful particle size distributions. However, such measurements are conducted under high vacuum and can be susceptible to drying artifacts.

In contrast, dynamic light scattering (DLS) can be used to assess particle size distributions for dilute pigment dispersions. The particles undergo Brownian motion, which causes the incident laser light to be scattered and measurement of the correlation function enables the mean diffusion coefficient of the particles to be determined. This parameter enables calculation of the mean particle diameter through the Stokes-Einstein relationship if the

solution viscosity and temperature are known.[180] DLS reports an intensity-average (or z-average) diameter that is strongly biased towards the presence of larger particles because the intensity of the scattered light scales with the sixth power of the particle radius. In principle, volume-average and number-average particle size distributions can also be calculated, but this requires an assumption to be made regarding the shape of the size distribution.

1.6.4.3 Rheology

Rheology can also be used to assess the degree of dispersion of pigment particles. The rheology of a dispersed system is sensitive to the particle size distribution: as the effective particle size becomes smaller, the overall pigment surface area increases, which requires more dispersant to be added. This normally causes the yield value, viscosity and dynamic elasticity of a dispersion to increase, resulting in a dispersion that is unsuitable for mechanical milling.[181] It is commonly found that the viscosity of a pigment dispersion passes through a minimum value as the dispersant concentration is gradually increased. At relatively low dispersant concentrations, there is insufficient dispersant to fully disperse the pigment particles.   At relatively high dispersant concentrations, there is excess non-adsorbed dispersant remaining in the supernatant. However, at some intermediate dispersant concentration there will be just sufficient dispersant to fully coat the pigment particles, which leads to a minimum in the viscosity of the pigment dispersion. This dispersant concentration corresponds to that required for monolayer coverage of the pigment particles, or the 'knee' of the Langmuir adsorption isotherm.

1.7   Thesis Aims and Outline

In this thesis RAFT polymerisation is used to prepare several new classes of novel amphiphilic diblock copolymers based on (meth)acrylic monomers using RAFT aqueous solution polymerisation, RAFT aqueous dispersion polymerisation or RAFT aqueous emulsion polymerisation. The resulting copolymers were subsequently evaluated as dispersants for pigments in aqueous media, which is relevant to the formulation of high-quality inkjet inks. A comparison between dispersants in the form of nanoparticles, or molecularly dissolved chains is attempted by various methods.

In Chapter 2, the synthesis of a new stimulus-responsive PMAA-PHPMA diblock copolymer is reported. On adjusting the solution temperature and/or pH, this copolymer forms various types of nanoparticles in aqueous solution. In Chapter 3, these PMAA-PHPMA diblock copolymers are evaluated as dispersants for inkjet-grade carbon black. Its thermoresponsive nature means that molecularly dissolved chains and nanoparticles can be directly compared. In Chapter 4, a highly convenient and generic synthetic route to zwitterionic diblock copolymers is reported, including the direct, atom-efficient, one-pot synthesis of PDMA-PMAA diblock copolymers in aqueous media. Other zwitterionic diblock copolymers include those where the cationic block can be poly(2-(dimethylamino)ethyl methacrylate) [PDMA], poly(2-(diethylamino)ethyl methacrylate) [PDEA], poly(2-(*N*-morpholino)ethyl methacrylate) [PMEMA] or poly(2-(methacryloyloxy)ethyl trimethylammonium chloride) [PMETAC], and the anionic block comprises either PMAA or poly(2-carboxyethyl acrylate) [PCEA]. These doubly-hydrophilic diblock copolymers have interesting aqueous solution behaviour. For example, depending on their precise diblock composition, they can exhibit an isoelectric point within a relatively narrow pH range; insolubility under such conditions enables facile removal of trithicarbonate-based RAFT end-groups using hydrazine utilising a wholly aqueous protocol. In Chapter 5, selected examples of these zwitterionic diblock

copolymers are evaluated for the stabilisation of colloidal dispersions of titania and yellow iron oxide pigments, respectively. One particularly interesting class of zwitterionic diblock copolymers is the PDEA-PCEA system. In this case, each block is water-insoluble in its neutral (uncharged) form, hence so-called 'schizophrenic' micellization behaviour is anticipated. Thus, such copolymers should form cationic PCEA-core micelles at low pH and anionic PDEA-core micelles at high pH. In principle, this may enable the performance of anionic (or cationic) nanoparticles as pigment dispersants to be compared to that of molecularly-dissolved PDMA-PMAA zwitterionic diblock copolymers. This possibility is explored in Chapter 6.

1.8 References

1. Schofield, J. D. Extending the boundaries of dispersant technology. *Prog. Org. Coatings* **45**, 249–257 (2002).

2. Silvestre, C., Duraccio, D. & Cimmino, S. Food packaging based on polymer nanomaterials. *Progress in Polymer Science (Oxford)* **36**, 1766–1782 (2011).

3. Galaev, I. Y. & Mattiasson, B. 'Smart' polymers and what they could do in biotechnology and medicine. *Trends in Biotechnology* **17**, 335–340 (1999).

4. Nyholm, L., Nyström, G., Mihranyan, A. & Strømme, M. Toward flexible polymer and paper-based energy storage devices. *Advanced Materials* **23**, 3751–3769 (2011).

5. Richards, R. W. *Emerging Themes in Polymer Science*. *Emerging Themes in Polymer Science* **263**, (The Royal Society of Chemistry, 2001).

6. Agilent Technologies. *Polymer Molecular Weight Distribution and Definitions of MW Averages*. *Technical Overview* (2015).

7. Poole, C. F., Cooke, M. & Wilson, I. D. Encyclopedia of separation science. **38**, 38-5919-38–5919 (2000).

8. Carothers, W. H. Studies on polymerization and ring formation. I. An introduction to the general theory of condensation polymers. *J. Am. Chem. Soc.* **51**, 2548–2559 (1929).

9. Kennedy, J. W. Principles of Polymer Chemistry. *J. Am. Chem. Soc.* **76**, 2854 (1954).

10. Flory, P. J. *Principles of Polymer Chemistry*. (Cornell University Press, 1953).

11. Szwarc, M., Levy, M. & Milkovich, R. Polymerization initiated by electron transfer to monomer. A new method of formation of block polymers. *Journal of the American Chemical Society* **78**, 2656–2657 (1956).

12. Hadjichristidis, N., Pitsikalis, M., Pispas, S. & Iatrou, H. Polymers with complex architecture by living anionic polymerization. *Chemical Reviews* **101**, 3747–3792 (2001).

13. Jenkins, A. D., Jones, R. G. & Moad, G. Terminology for reversible-deactivation radical polymerization previously called 'controlled' radical or 'living' radical polymerization (IUPAC recommendations 2010). *Pure Appl. Chem.* **82**, 483–491 (2010).

14. Asua, J. M. *Polymeric Dispersions: Principles and Applications*. *Polymeric Dispersions: Principles and Applications* (Springer Netherlands, 1997). doi:10.1007/978-94-011-5512-0

15. Couvreur, L. *et al.* First nitroxide-mediated controlled free-radical polymerization of acrylic acid. *Macromolecules* **36**, 8260–8267 (2003).

16. Matyjaszewski, K. & Xia, J. Atom transfer radical polymerization. *Chem. Rev.* **101**, 2921–2990 (2001).

17. Moad, G., Rizzardo, E. & Thang, S. H. Living radical polymerization by the RAFT process - A first update. *Aust. J. Chem.* **59**, 669–692 (2006).

18. Chiefari, J. *et al.* Living free-radical polymerization by reversible addition - Fragmentation chain transfer: The RAFT process. *Macromolecules* **31**, 5559–5562 (1998).

19. Braunecker, W. A. & Matyjaszewski, K. Controlled/living radical polymerization: Features, developments, and perspectives. *Progress in Polymer Science (Oxford)* **32**, 93–146 (2007).

20. Fischer, H. The Persistent Radical Effect In 'Living' Radical Polymerization. *Macromolecules* **30**, 5666–5672 (1997).

21. B, V., Bohme, F. & Adler, H.-J. *Synthesis of Defined Polymer Architectures*. (Wiley-VCH, 2002).

22. Moad, G., Rizzardo, E. & Thang, S. H. Living radical polymerization by the RAFT process. *Aust. J. Chem.* **58**, 379–410 (2005).

23. Perrier, S. 50th Anniversary Perspective: RAFT Polymerization - A User Guide. *Macromolecules* **50**, 7433–7447 (2017).

24. Keddie, D. J. A guide to the synthesis of block copolymers using reversible-addition fragmentation chain transfer (RAFT) polymerization. *Chem. Soc. Rev.* **43**, 496–505 (2014).

25. Favier, A. & Charreyre, M. T. Experimental requirements for an efficient control of free-radical polymerizations via the reversible addition-fragmentation chain transfer (RAFT) process. *Macromolecular Rapid Communications* **27**, 653–692 (2006).

26. Monteiro, M. J., Hodgson, M. & De Brouwer, H. Influence of RAFT on the rates and molecular weight distributions of styrene in seeded emulsion polymerizations. *J. Polym. Sci. Part A Polym. Chem.* **38**, 3864–3874 (2000).

27. Keddie, D. J., Moad, G., Rizzardo, E. & Thang, S. H. RAFT agent design and synthesis. *Macromolecules* **45**, 5321–5342 (2012).

28. Grajales, S. Controlled radical polymerization guide: ATRP, RAFT, NMP. *Aldrich Mater. Sci.* 12–14 (2012).

29. Parthiban, A. *Synthesis and Applications of Copolymers*. *Synthesis and Applications of Copolymers* **9781118057**, (John Wiley & Sons, 2014).

30. Destarac, M., Taton, D., Zard, S. Z., Saleh, T. & Six, Y. On the importance of xanthate substituents in the MADIX process. in *ACS Symposium Series* **854**, 536–550 (2003).

31. Moad, G., Rizzardo, E. & Thang, S. H. Toward living radical polymerization. *Acc. Chem. Res.* **41**, 1133–1142 (2008).

32. Moad, G., Rizzardo, E. & Thang, S. H. End-functional polymers, thiocarbonylthio group removal/transformation and reversible addition-fragmentation-chain transfer (RAFT) polymerization. *Polymer International* **60**, 9–25 (2011).

33. Jesson, C. P. *et al.* H$_2$O$_2$ enables convenient removal of RAFT end-groups from block copolymer nano-objects prepared via polymerization-induced self- assembly in water. *Macromolecules* **50**, 182–191 (2017).

34. Postma, A., Davis, T. P., Moad, G. & O'shea, M. S. Thermolysis of RAFT-Synthesized Polymers. A Convenient Method for Trithiocarbonate Group Elimination. *Macromolecules* **38**, 5371–5374 (2005).

35. Willcock, H. & O'Reilly, R. K. End group removal and modification of RAFT polymers. *Polymer Chemistry* **1**, 149–157 (2010).

36. Barner-Kowollik, C. & Perrier, S. The future of reversible addition fragmentation chain transfer polymerization. *J. Polym. Sci. Part A Polym. Chem.* **46**, 5715–5723 (2008).

37. van Herk, A. M. *Chemistry and Technology of Emulsion Polymerisation: Second Edition*. *Chemistry and Technology of Emulsion Polymerisation: Second Edition* (John Wiley & Sons, 2013). doi:10.1002/9781118638521

38. Ferguson, C. J. *et al.* Effective ab Initio Emulsion Polymerization under RAFT Control. *Macromolecules* **35**, 9243–9245 (2002).

39. Brooks, B. W. Interfacial and diffusion phenomena in emulsion polymerisation. *Br. Polym. J.* **3**, 269–273 (1971).

40. Asua, J. M. Emulsion Polymerization: From Fundamental Mechanisms to Process Developments. *Journal of Polymer Science, Part A: Polymer Chemistry* **42**, 1025–1041 (2004).

41. Sherrington, D. C. *Emulsion polymerization and emulsion polymers*. *Reactive and Functional*

Polymers **36**, (J. Wiley, 1998).

42. Tulig, T. J. & Tirrell, M. Toward a Molecular Theory of the Trommsdorff Effect. *Macromolecules* **14**, 1501–1511 (1981).

43. Goodall, A. R., Wilkinson, M. C. & Hearn, J. *J Polym Sci Polym Chem Ed* **15**, 2193–2218 (1977).

44. Ali, A. M. I. *et al.* Synthesis of poly(2-hydroxypropyl methacrylate) latex particles via aqueous dispersion polymerization. *Soft Matter* **3**, 1003–1013 (2007).

45. Warren, N. J. & Armes, S. P. Polymerization-induced self-assembly of block copolymer nano-objects via RAFT aqueous dispersion polymerization. *J. Am. Chem. Soc.* **136**, 10174–10185 (2014).

46. Napper, D. H. Steric stabilization. *J. Colloid Interface Sci.* **58**, 390–407 (1977).

47. Bosma, G. *et al.* Preparation of monodisperse, fluorescent PMMA-latex colloids by dispersion polymerization. *J. Colloid Interface Sci.* **245**, 292–300 (2002).

48. Arshady, R. Suspension, emulsion, and dispersion polymerization: A methodological survey. *Colloid Polym. Sci.* **270**, 717–732 (1992).

49. Ober, C. K. & Lok, K. P. Formation of Large Monodisperse Copolymer Particles by Dispersion Polymerization. *Macromolecules* **20**, 268–273 (1987).

50. Kawaguchi, S. & Ito, K. Dispersion polymerization. *Adv. Polym. Sci.* **175**, 299–328 (2005).

51. Paine, A. J. Dispersion Polymerization of Styrene in Polar Solvents. 7. A Simple Mechanistic Model to Predict Particle Size. *Macromolecules* **23**, 3109–3117 (1990).

52. Kawaguchi, S. & Ito, K. Dispersion polymerization. *Adv. Polym. Sci.* **175**, 299–328 (2005).

53. Vanderhoff, J. W. *et al.* Preparation of Large-Particle-Size Monodisperse Latexes in Space: Polymerization Kinetics and Process Development. *J. Dispers. Sci. Technol.* **5**, 231–246 (1984).

54. Ober, C. K., Lok, K. P. & Hair, M. L. Monodispersed, micron-sized polystyrene particles by dispersion polymerization. *J. Polym. Sci. Polym. Lett. Ed.* **23**, 103–108 (1985).

55. Byard, S. J. *et al.* Unique aqueous self-assembly behavior of a thermoresponsive diblock copolymer. *Chem. Sci.* **11**, 396–402 (2020).

56. Byard, S. J., Williams, M., McKenzie, B. E., Blanazs, A. & Armes, S. P. Preparation and Cross-Linking of All-Acrylamide Diblock Copolymer Nano-Objects via Polymerization-Induced Self-Assembly in Aqueous Solution. *Macromolecules* **50**, 1482–1493 (2017).

57. Sugihara, S., Blanazs, A., Armes, S. P., Ryan, A. J. & Lewis, A. L. Aqueous dispersion polymerization: a new paradigm for in situ block copolymer self-assembly in concentrated solution. *J. Am. Chem. Soc.* **133**, 15707–13 (2011).

58. Tan, J. *et al.* Room Temperature Synthesis of Self-Assembled AB/B and ABC/BC Blends by Photoinitiated Polymerization-Induced Self-Assembly (Photo-PISA) in Water. *Macromolecules* **51**, 7396–7406 (2018).

59. Blackman, L. D., Doncom, K. E. B., Gibson, M. I. & O'Reilly, R. K. Comparison of photo- and thermally initiated polymerization-induced self-assembly: A lack of end group fidelity drives the formation of higher order morphologies. *Polym. Chem.* **8**, 2860–2871 (2017).

60. Ren, K. & Perez-Mercader, J. Thermoresponsive gels directly obtained via visible light-mediated polymerization-induced self-assembly with oxygen tolerance. *Polym. Chem.* **8**, 3548–3552 (2017).

61. Wang, X. & An, Z. New Insights into RAFT Dispersion Polymerization-Induced Self-Assembly: From Monomer Library, Morphological Control, and Stability to Driving Forces.

Macromol. Rapid Commun. **40**, 1800325 (2019).

62.   Valade, D., Boyer, C., Davis, T. P. & Bulmus, V. Synthesis of siRNA Polyplexes Adopting a Combination of RAFT Polymerization and Thiol-ene Chemistry. *Aust. J. Chem.* **62**, 1344 (2009).

63.   Ratcliffe, L. P. D., Ryan, A. J. & Armes, S. P. From a water-immiscible monomer to block copolymer nano-objects via a one-pot RAFT aqueous dispersion polymerization formulation. *Macromolecules* **46**, 769–777 (2013).

64.   Penfold, N. J. W., Whatley, J. R. & Armes, S. P. Thermoreversible Block Copolymer Worm Gels Using Binary Mixtures of PEG Stabilizer Blocks. *Macromolecules* **52**, 1653–1662 (2019).

65.   Blanazs, A., Ryan, A. J. & Armes, S. P. Predictive phase diagrams for RAFT aqueous dispersion polymerization: Effect of block copolymer composition, molecular weight, and copolymer concentration. *Macromolecules* **45**, 5099–5107 (2012).

66.   Lovett, J. R., Warren, N. J., Ratcliffe, L. P. D., Kocik, M. K. & Armes, S. P. pH-responsive non-ionic diblock copolymers: Ionization of carboxylic acid end-groups induces an order-order morphological transition. *Angew. Chemie - Int. Ed.* **54**, 1279–1283 (2015).

67.   Whitesides, G. M. & Boncheva, M. Beyond molecules: Self-assembly of mesoscopic and macroscopic components. *Proc. Natl. Acad. Sci. U. S. A.* **99**, 4769–4774 (2002).

68.   Adamson, A. W. & Gast, A. P. *Physical Chemistry of Surfaces Sixth Edition*. (John Wiley and Sons Inc.).

69.   Lombardo, D., Kiselev, M. A., Magazù, S. & Calandra, P. Amphiphiles self-assembly: Basic concepts and future perspectives of supramolecular approaches. *Advances in Condensed Matter Physics* **2015**, 1–22 (2015).

70.   Israelachvili, J. N., Mitchell, D. J. & Ninham, B. W. Theory of self-assembly of hydrocarbon amphiphiles into micelles and bilayers. *Journal of the Chemical Society, Faraday Transactions 2: Molecular and Chemical Physics* **72**, 1525–1568 (1976).

71.   Frank, H. S. & Evans, M. W. Free volume and entropy in condensed systems III. Entropy in binary liquid mixtures; Partial molal entropy in dilute solutions; Structure and thermodynamics in aqueous electrolytes. *J. Chem. Phys.* **13**, 507–532 (1945).

72.   Tanford, C. The hydrophobic effect and the organization of living matter. *Science* **200**, 1012–1018 (1978).

73.   Israelachvili, J. *Intermolecular and Surface Forces*. *Intermolecular and Surface Forces* (Elsevier, 2011). doi:10.1016/C2009-0-21560-1

74.   Mai, Y. & Eisenberg, A. Self-assembly of block copolymers. *Chem. Soc. Rev* **41**, 5969–5985 (2012).

75.   Nagarajan, R. & Ganesh, K. Block Copolymer Self-Assembly in Selective Solvents: Theory of Solubilization in Spherical Micelles. *Macromolecules* **22**, 4312–4325 (1989).

76.   Charleux, B., Delaittre, G., Rieger, J. & D'Agosto, F. Polymerization-induced self-assembly: From soluble macromolecules to block copolymer nano-objects in one step. *Macromolecules* **45**, 6753–6765 (2012).

77.   Flory, P. J. Thermodynamics of high polymer solutions. *J. Chem. Phys.* **10**, 51–61 (1942).

78.   Huggins, M. L. Theory of Solutions of High Polymers. *J. Am. Chem. Soc.* **64**, 1712–1719 (1942).

79.   Muthukumar, M. & Edwards, S. Chain Statistics and Scaling Concepts. in *Comprehensive Polymer Science and Supplements* **2**, 1–47 (1989).

80.   Matsen, M. W. Self-consistent field theory and its applications. *Soft Matter* **1**, 87–178 (2006).

81. Bates, F. S. & Fredrickson, G. H. Block copolymers-designer soft materials. *Phys. Today* **52**, 32–38 (1999).

82. Fredrickson, G. H. & Bates, F. S. *Dynamics of Block Copolymers: Theory and Experiment*. *Annu. Rev. Muter. Sci* **26**, (1996).

83. Reuter, E., Silber, S. & Psiorz, C. Use of new blockcopolymeric dispersing agents for waterborne paints - theoretical and practical aspects. *Prog. Org. Coatings* **37**, 161–167 (1999).

84. Dormidontova, E. E. Micellization kinetics in block copolymer solutions: scaling model. *Macromolecules* **32**, 7630–7644 (1999).

85. Leibler, L. Theory of Microphase Separation in Block Copolymers. *Macromolecules* **13**, 1602–1617 (1980).

86. Derry, M. J., Fielding, L. A. & Armes, S. P. Polymerization-induced self-assembly of block copolymer nanoparticles via RAFT non-aqueous dispersion polymerization. *Prog. Polym. Sci.* **52**, 1–18 (2016).

87. Ohta, T. & Kawasaki, K. Equilibrium Morphology of Block Copolymer Melts. *Macromolecules* **19**, 2621–2632 (1986).

88. Zhang, L. & Eisenberg, A. Multiple morphologies of 'crew-cut' aggregates of polystyrene-b-poly(acrylic acid) block copolymers. *Science (80-.).* **268**, 1728–1731 (1995).

89. Zhang, L. & Eisenberg, A. Formation of crew-cut aggregates of various morphologies from amphiphilic block copolymers in solution. *Polym. Adv. Technol.* **9**, 677–699 (1998).

90. Zhang, L. & Eisenberg, A. Multiple morphologies and characteristics of 'crew-cut' micelle-like aggregates of polystyrene-b-poly(acrylic acid) diblock copolymers in aqueous solutions. *J. Am. Chem. Soc.* **118**, 3168–3181 (1996).

91. Eisenberg, A. & Zhang, L. Formation of crew-cut aggregates of various morphologies from amphiphilic block copolymers in solution. *Polym. Adv. Technol.* **9**, 677–699 (1998).

92. Matyjaszewski, K., Gnanou, Y. & Leibler, L. *Macromolecular engineering: Precise synthesis, materials properties, applications*. **Vol. 3**, (Wiley-VCH Verlag GmbH & Co. KGaA, 2008).

93. Blanazs, A., Armes, S. P. & Ryan, A. J. Self-assembled block copolymer aggregates: From micelles to vesicles and their biological applications. *Macromolecular Rapid Communications* **30**, 267–277 (2009).

94. Bütün, V., Armes, S. P. & Billingham, N. C. Synthesis and aqueous solution properties of near-monodisperse tertiary amine methacrylate homopolymers and diblock copolymers. *Polymer* **42**, 5993–6008 (2001).

95. Howse, J. R. *et al.* Templated formation of giant polymer vesicles with controlled size distributions. *Nat. Mater.* **8**, 507–511 (2009).

96. Ferguson, C. J. *et al.* Ab initio emulsion polymerization by RAFT-controlled self-assembly. *Macromolecules* **38**, 2191–2204 (2005).

97. Rieger, J. *et al.* Amphiphilic poly(ethylene oxide) macromolecular RAFT agent as a stabilizer and control agent in ab initio batch emulsion polymerization. *Macromolecules* **41**, 4065–4068 (2008).

98. Cunningham, V. J. *et al.* Poly(glycerol monomethacrylate)-poly(benzyl methacrylate) diblock copolymer nanoparticles via RAFT emulsion polymerization: Synthesis, characterization, and interfacial activity. *Macromolecules* **47**, 5613–5623 (2014).

99. Akpinar, B. *et al.* Determining the Effective Density and Stabilizer Layer Thickness of Sterically Stabilized Nanoparticles. *Macromolecules* **49**, 5160–5171 (2016).

100. Zhang, W., D'Agosto, F., Boyron, O., Rieger, J. & Charleux, B. Toward a better understanding of the parameters that lead to the formation of nonspherical polystyrene

particles via RAFT-mediated one-pot aqueous emulsion polymerization. *Macromolecules* **45**, 4075–4084 (2012).

101. Zhang, X. *et al.* Well-defined amphiphilic block copolymers and nano-objects formed in situ via RAFT-mediated aqueous emulsion polymerization. *Macromolecules* **44**, 4149–4158 (2011).

102. Chaduc, I. *et al.* Effect of the ph on the raft polymerization of acrylic acid in water. Application to the synthesis of poly(acrylic acid)-stabilized polystyrene particles by RAFT emulsion polymerization. *Macromolecules* **46**, 6013–6023 (2013).

103. Rieger, J., Zhang, W., Stoffelbach, F. & Charleux, B. Surfactant-free RAFT emulsion polymerization using poly(N,N -dimethylacrylamide) trithiocarbonate macromolecular chain transfer agents. *Macromolecules* **43**, 6302–6310 (2010).

104. Zhang, W., D'Agosto, F., Dugas, P. Y., Rieger, J. & Charleux, B. RAFT-mediated one-pot aqueous emulsion polymerization of methyl methacrylate in presence of poly(methacrylic acid-co-poly(ethylene oxide) methacrylate) trithiocarbonate macromolecular chain transfer agent. *Polymer* **54**, 2011–2019 (2013).

105. Charleux, B., Delaittre, G., Rieger, J. & D'Agosto, F. Polymerization-induced self-assembly: From soluble macromolecules to block copolymer nano-objects in one step. *Macromolecules* **45**, 6753–6765 (2012).

106. Houillot, L. *et al.* Synthesis of well-defined polyacrylate particle dispersions in organic medium using simultaneous RAFT polymerization and self-assembly of block copolymers. A strong influence of the selected thiocarbonylthio chain transfer agent. *Macromolecules* **40**, 6500–6509 (2007).

107. Semsarilar, M., Ladmiral, V., Blanazs, A. & Armes, S. P. Poly(methacrylic acid)-based AB and ABC block copolymer nano-objects prepared via RAFT alcoholic dispersion polymerization. *Polym. Chem.* **5**, 3466–3475 (2014).

108. Jones, E. R., Semsarilar, M., Wyman, P., Boerakker, M. & Armes, S. P. Addition of water to an alcoholic RAFT PISA formulation leads to faster kinetics but limits the evolution of copolymer morphology. *Polym. Chem.* **7**, 851–859 (2016).

109. North, S. M. *et al.* Adsorption of Small Cationic Nanoparticles onto Large Anionic Particles from Aqueous Solution: A Model System for Understanding Pigment Dispersion and the Problem of Effective Particle Density. *Langmuir* **33**, 1275–1284 (2017).

110. Zong, M., Thurecht, K. J. & Howdle, S. M. Dispersion polymerisation in supercritical CO2 using macro-RAFT agents. *Chem. Commun.* **0**, 5942–5944 (2008).

111. Ji, W., Yan, J., Chen, E., Li, Z. & Liang, D. In situ and onliner monitoring polymerization-induced micellization. *Macromolecules* **41**, 4914–4919 (2008).

112. An, Z. *et al.* Facile RAFT precipitation polymerization for the microwave-assisted synthesis of well-defined, double hydrophilic block copolymers and nanostructured hydrogels. *J. Am. Chem. Soc.* **129**, 14493–14499 (2007).

113. Yan, L. & Tao, W. One-step synthesis of pegylated cationic nanogels of poly(N,N′-dimethylaminoethyl methacrylate) in aqueous solution via self-stabilizing micelles using an amphiphilic macroRAFT agent. *Polymer* **51**, 2161–2167 (2010).

114. Li, Y. & Armes, S. P. RAFT Synthesis of sterically stabilized methacrylic nanolatexes and vesicles by aqueous dispersion polymerization. *Angew. Chemie - Int. Ed.* **49**, 4042–4046 (2010).

115. Blanazs, A., Madsen, J., Battaglia, G., Ryan, A. J. & Armes, S. P. Mechanistic insights for block copolymer morphologies: how do worms form vesicles? *J. Am. Chem. Soc.* **133**, 16581–7 (2011).

116. Madsen, J., Armes, S. P. & Lewis, A. L. Preparation and Aqueous Solution Properties of New Thermoresponsive Biocompatible ABA Triblock Copolymer Gelators. *Macromolecules* **39**, 7455–7457 (2006).

117. Madsen, J. *et al.* Biocompatible wound dressings based on chemically degradable triblock copolymer hydrogels. *Biomacromolecules* **9**, 2265–2275 (2008).

118. Penfold, N. J. W., Ning, Y., Verstraete, P., Smets, J. & Armes, S. P. Cross-linked cationic diblock copolymer worms are superflocculants for micrometer-sized silica particles. *Chem. Sci.* **7**, 6894–6904 (2016).

119. North, S. M. & Armes, S. P. Aqueous solution behavior of stimulus-responsive poly(methacrylic acid)-poly(2-hydroxypropyl methacrylate) diblock copolymer nanoparticles. *Polym. Chem.* **11**, 2147–2156 (2020).

120. Semsarilar, M., Ladmiral, V., Blanazs, A. & Armes, S. P. Anionic polyelectrolyte-stabilized nanoparticles via RAFT aqueous dispersion polymerization. *Langmuir* **28**, 914–922 (2012).

121. Cockram, A. A. *et al.* Effect of monomer solubility on the evolution of copolymer morphology during Polymerization-Induced Self-Assembly in aqueous solution. *Macromolecules* **50**, 796–802 (2017).

122. Ning, Y., Meldrum, F. C. & Armes, S. P. Efficient occlusion of oil droplets within calcite crystals. *Chem. Sci.* **10**, 8964–8972 (2019).

123. Canning, S. L., Neal, T. J. & Armes, S. P. pH-Responsive Schizophrenic Diblock Copolymers Prepared by Polymerization-Induced Self-Assembly. *Macromolecules* **50**, 6108–6116 (2017).

124. Perlatti, B., Souza Bergo, P. L. de, Fernandes da Silva, M. F. das G., Batista, J. & Rossi, M. Polymeric Nanoparticle-Based Insecticides: A Controlled Release Purpose for Agrochemicals. in *Insecticides - Development of Safer and More Effective Technologies* (InTech, 2013). doi:10.5772/53355

125. Spinelli, H. J. Polymeric Dispersants in Ink Jet Technology. *Adv. Mater.* **10**, 1215–1218 (1998).

126. Cesarano, J., Aksay, I. A. & Bleier, A. Stability of Aqueous α-Al$_2$O$_3$ Suspensions with Poly(methacrylic acid) Polyelectrolyte. *J. Am. Ceram. Soc.* **71**, 250–255 (1988).

127. de las Heras Alarcón, C., Pennadam, S. & Alexander, C. Stimuli-Responsive Polymers: Biomedical Applications. *Chem. Soc. Rev.* **34**, 276–285 (2005).

128. Hellgren, A. C., Weissenborn, P. & Holmberg, K. Surfactants in water-borne paints. *Prog. Org. Coatings* **35**, 79–87 (1999).

129. Buxbaum, G. *Industrial inorganic pigments*. *Additives for Polymers* (John Wiley & Sons, 2008). doi:10.1016/0306-3747(94)90036-1

130. Agbo, C., Jakpa, W., Sarkodie, B., Boakye, A. & Fu, S. A Review on the Mechanism of Pigment Dispersion. *J. Dispers. Sci. Technol.* **39**, 874–889 (2018).

131. Farrokhpay, S. A review of polymeric dispersant stabilisation of titania pigment. *Adv. Colloid Interface Sci.* **151**, 24–32 (2009).

132. Day, R. E. The characterisation of the surface of titanium dioxide pigments. *Prog. Org. Coatings* **2**, 269–288 (1974).

133. Braun, J. H. Titanium dioxide - A review. *Journal of Coatings Technology* **69**, 59–72 (1997).

134. Herbst, W. & Hunger, K. *Industrial Organic Pigments: Production, Properties, Applications*. (John Wiley & Sons, 2006).

135. Lahaye, J. & Ehrburger-Dolle, F. Mechanisms of carbon black formation. Correlation with the morphology of aggregates. *Carbon N. Y.* **32**, 1319–1324 (1994).

136. Herd, C. R., McDonald, G. C. & Hess, W. M. Morphology of carbon-black aggregates. Fractal versus Euclidean geometry. *Rubber Chem. Technol.* **65**, 107–129 (1992).

137. Rieker, T. P., Misono, S. & Ehrburger-Dolle, F. Small-angle X-ray scattering from carbon blacks: Crossover between the fractal and porod regimes. *Langmuir* **15**, 914–917 (1999).

138. Medalia, A. I. & Heckman, F. A. Morphology of aggregates-II. Size and shape factors of carbon black aggregates from electron microscopy. *Carbon N. Y.* **7**, 567–582 (1969).

139. Derjaguin, B. V. *et al.* The Derjaguin—Landau—Verwey—Overbeek (DLVO) Theory of Stability of Lyophobic Colloids. in *Surface Forces* 293–310 (Springer US, 1987). doi:10.1007/978-1-4757-6639-4_8

140. Morgan, L. J. *Polymeric stabilization of colloidal dispersions*. *Colloids and Surfaces* **15**, (Academic Press: London, 1985).

141. Mendoza, C., González, Z., Castro, Y., Gordo, E. & Ferrari, B. Improvement of TiN nanoparticles EPD inducing steric stabilization in non-aqueous suspensions. *J. Eur. Ceram. Soc.* **36**, 307–317 (2016).

142. Everett, D. H. Basic Principles of Colloid Science. in *Basic Principles of Colloid Science* 26–260 (The Royal Society of Chemistry, 2007). doi:10.1039/9781847550200-00026

143. Ottewill, R. H. Stability and instability in disperse systems. *J. Colloid Interface Sci.* **58**, 357–373 (1977).

144. Araki, J. Electrostatic or steric?-preparations and characterizations of well-dispersed systems containing rod-like nanowhiskers of crystalline polysaccharides. *Soft Matter* **9**, 4125–4141 (2013).

145. Fritz, G., Schädler, V., Willenbacher, N. & Wagner, N. J. Electrosteric stabilization of colloidal dispersions. *Langmuir* **18**, 6381–6390 (2002).

146. Napper, D. H. & Netschey, A. Studies of the steric stabilization of colloidal particles. *J. Colloid Interface Sci.* **37**, 528–535 (1971).

147. Ruehrwein, R. A. & Ward, D. W. Mechanism of clay aggregation by polyelectrolytes. *Soil Sci.* **73**, 485–492 (1952).

148. Asakura, S. & Oosawa, F. Interaction between particles suspended in solutions of macromolecules. *J. Polym. Sci.* **33**, 183–192 (1958).

149. Feigin, R. I. & Napper, D. H. Depletion stabilization and depletion flocculation. *J. Colloid Interface Sci.* **75**, 525–541 (1980).

150. Zheng, S. & Zhang, Q. Surface-modification of fine red iron oxide pigment. *China Particuology* **1**, 176–180 (2003).

151. Wang, Y. & Mattice, W. L. Adsorption of Homopolymers on a Solid Surface: A Comparison between Monte Carlo Simulation and the Scheutjens–Fleer Mean-Field Lattice Theory. *Langmuir* **10**, 2281–2288 (1994).

152. Scheutjens, J. & Fleer, G. Statistical theory of the adsorption of interacting chain molecules. 2. Train, loop, and tail size distribution. *J. Phys. Chem.* **84**, 178–190 (1980).

153. Joanny, J. F. & Johner, A. Adsorption of polymers with various architectures: Mean field theory. *J. Phys. II* **6**, 511–527 (1996).

154. Hoogeveen, N. G., Cohen Stuart, M. A. & Fleer, G. J. Polyelectrolyte adsorption on oxides. I. Kinetics and adsorbed amounts. *J. Colloid Interface Sci.* **182**, 133–145 (1996).

155. Hoogeveen, N. G., Cohen Stuart, M. A. & Fleer, G. J. Can charged (block co)polymers act as stabilisers and flocculants of oxides? *Colloids Surfaces A Physicochem. Eng. Asp.* **117**, 77–88 (1996).

156. Boisvert, J. P., Persello, J., Castaing, J. C. & Cabane, B. Dispersion of alumina-coated TiO2 particles by adsorption of sodium polyacrylate. *Colloids Surfaces A Physicochem. Eng. Asp.* **178**, 187–198 (2001).

157. Boisvert, J.-P., Persello, J., Foissy, A., Castaing, J.-C. & Cabane, B. Effect of surface charge on the adsorption mode of sodium poly(acrylate) on alumina-coated TiO2 used as coating pigment. *Colloids Surfaces A Physicochem. Eng. Asp.* **168**, 287–296 (2000).

158. Creutz, S. & Jérôme, R. Effectiveness of poly(vinylpyridine) block copolymers as stabilizers of aqueous titanium dioxide dispersions of a high solid content. *Langmuir* **15**, 7145–7156 (1999).

159. Chibowski, S. & Wiśniewska, M. Study of the adsorption mechanism and the structure of adsorbed layers of polyelectrolytes at the metal oxide/solution interface. *Adsorpt. Sci. Technol.* **19**, 409–421 (2001).

160. Duivenvoorde, F. L., Van Nostrum, C. F. & Van Der Linde, R. The pigmentation of powder coatings with the use of block copolymer dispersants. *Prog. Org. Coatings* **36**, 225–230 (1999).

161. Creutz, S. & Jérôme, R. Effectiveness of block copolymers as stabilizers for aqueous titanium dioxide dispersions of a high solid content. *Prog. Org. Coatings* **40**, 21–29 (2000).

162. Auschra, C., Eckstein, E., Mühlebach, A., Zink, M. O. & Rime, F. Design of new pigment dispersants by controlled radical polymerization. *Prog. Org. Coatings* **45**, 83–93 (2002).

163. An, S. W. *et al.* Structure of a Diblock Copolymer Adsorbed at the Hydrophobic Solid/Aqueous Interface: Effects of Charge Density on a Weak Polyelectrolyte Brush. *Macromolecules* **32**, 2731–2738 (1999).

164. Tian, M. *et al.* Hybridization of Block Copolymer Micelles. *Langmuir* **9**, 1741–1748 (1993).

165. Creutz, S., Jérôme, R., Kaptijn, G. M. P., Van Der Werf, A. W. & Akkerman, J. M. Design of polymeric dispersants for waterborne coatings. *J. Coatings Technol.* **70**, 41–46 (1998).

166. Nguyen, D. *et al.* Pigment encapsulation by emulsion polymerization using macro-RAFT copolymers. *Langmuir* **24**, 2140–2150 (2008).

167. Saindane, P. & Jagtap, R. N. RAFT copolymerization of amphiphilic poly (ethyl acrylate-b-acrylicacid) as wetting and dispersing agents for water borne coating. *Prog. Org. Coatings* **79**, 106–114 (2015).

168. Langmuir, I. The constitution and fundamental properties of solids and liquids. Part I. Solids. *J. Am. Chem. Soc.* **38**, 2221–2295 (1916).

169. Giles, C. H., Smith, D. & Huitson, A. A general treatment and classification of the solute adsorption isotherm. I. Theoretical. *J. Colloid Interface Sci.* **47**, 755–765 (1974).

170. Chibowski, S. Effect of functional groups of polyacrylamide and polyacrylic acid on their adsorption onto TiO_2 surface. *J. Colloid Interface Sci.* **140**, 444–449 (1990).

171. McGuire, M. J., Addai-Mensah, J. & Bremmell, K. E. Spectroscopic investigation of the adsorption mechanisms of polyacrylamide polymers onto iron oxide particles. *J. Colloid Interface Sci.* **299**, 547–555 (2006).

172. Foissy, A., El Attar, A. & Lamarche, J. M. Adsorption of polyacrylic acid on titanium dioxide. *J. Colloid Interface Sci.* **96**, 275–287 (1983).

173. Growney, D. J., Mykhaylyk, O. O. & Armes, S. P. Micellization and adsorption behavior of a near-monodisperse polystyrene-based diblock copolymer in nonpolar media. *Langmuir* **30**, 6047–6056 (2014).

174. Growney, D. J. *et al.* Is Carbon Black a Suitable Model Colloidal Substrate for Diesel Soot? *Langmuir* **31**, 10358–69 (2015).

175. Growney, D. J. *et al.* Star Diblock Copolymer Concentration Dictates the Degree of Dispersion of Carbon Black Particles in Nonpolar Media: Bridging Flocculation versus Steric Stabilization. *Macromolecules* **48**, 3691–3704 (2015).

176. Van Sang, T., Velamakanni, B. V & Adkins, R. R. Comparison of methods to assess pigment dispersion. *J. Coatings Technol.* **73**, 61–70 (2001).

177. Brockes, A. Der Zusammenhang von Farbstaerke und Teilchengroesse von Buntpigmenten nach der Mie-Theorie. *Optik (Stuttg).* **21**, 550 (1964).

178. Chromey, F. C. Evaluation of Mie Equations for Colored Spheres. *J. Opt. Soc. Am.* **50**, 730 (1960).

179. Delgado, A. & Matijević, E. Particle Size Distribution of Inorganic Colloidal Dispersions: A comparison of different techniques. *Part. Part. Syst. Charact.* **8**, 128–135 (1991).

180. International Organization for Standardization. Particle Size Analysis – Dynamic Light Scattering (DLS). in *ISO 22412:2017*

181. Schröder, J. Aspekte zum Fließverhalten von Pigmentdispersionen / Some comments on the flow properties of pigment dispersions. *Appl. Rheol.* **2**, 40–50 (2019).

Chapter 2

Aqueous solution behaviour of stimulus-responsive poly(methacrylic acid)-poly(2-hydroxypropyl methacrylate) diblock copolymer nanoparticles

2.1 Introduction

It is well-known that stimulus-responsive polymers are sensitive to changes in their external environment, such as pH,[1] temperature,[2] salt[3] or light,[4] which in turn affects their chain conformation and/or solubility.[5–9] In principle, such stimulus-responsive polymers offer potential applications in stabilisation and flocculation of colloidal dispersions, e.g. for catalysis,[10] water treatment,[11] water-borne coatings,[12,13] solid-liquid separation[14] and drug delivery.[15–18] One of the most studied thermoresponsive synthetic polymers is poly(*N*-isopropylacrylamide) (PNIPAM).[19,20,29,21–28] This non-ionic water-soluble polymer undergoes a coil-to-globule transition in aqueous solution and becomes insoluble when heated above its lower critical solution temperature (LCST) of approximately 32°C. Incorporation of ionisable comonomers such as (meth)acrylic acid confers pH-responsive character.[30,31] This approach has been used to design a range of dual-responsive copolymer microgels that undergo reversible swelling on varying the solution pH and temperature.[32,33] However, the incorporation of polymers that exhibit LCST behaviour as the hydrophobic structure-directing block for aqueous PISA formulations is not trivial. The reaction temperature must be judiciously chosen to ensure particle formation during the reaction while covalent cross-linking is typically required to retain the copolymer morphology (if desired) on cooling the reaction temperature below the LCST of the polymer.

To avoid this drawback, recent research has focused on hydrophobic thermoresponsive polymers that possess *LCST-like* behaviour such as poly(2-hydroxypropyl methacrylate) (PHPMA).[34–36] HPMA is a water-miscible monomer but the corresponding PHPMA homopolymer is water-insoluble over a wide range of temperature. Thus, this commodity monomer offers a useful model system for understanding latex syntheses *via* aqueous dispersion polymerisation.[37]

PHPMA has been used as a core-forming block for RAFT aqueous dispersion polymerisation synthesis utilising non-ionic steric stabilisers such as poly(glycerol monomethacrylate) or poly(ethylene glycol).[36,38–41] For such PISA syntheses, the PHPMA block can confer thermoresponsive character. Unusually, this block always remains hydrophobic but a subtle increase in its (partial) degree of hydration on lowering the solution temperature leads to a change in the relative volume fractions of the stabiliser and core-forming blocks, which can be sufficient to induce a worm-to-sphere transition.[42] Thus this can be considered to be an LCST-like transition. In contrast to traditional LCST behaviour, the PHPMA block never becomes truly water-soluble on lowering the solution temperature. Instead, the HPMA repeat units near the block junction point become more solvated, which leads to an effective increase in the volume fraction of the stabiliser block. This causes a subtle increase in the fractional packing parameter, which is sufficient to induce a worm-to-sphere transition. This phenomenon has been described as 'surface plasticisation' by Armes and co-workers.[43–45] It is perhaps worth emphasising here that if 'uniform plasticisation' occurred, it would instead lead to a worm-to-vesicle transition, which is not observed. Moreover, Warren et al. recently reported that such LCST-like behaviour is only observed over a relatively narrow range of PHPMA DPs – if this block is too long it becomes sufficiently hydrophobic that thermoresponsive behaviour is no longer observed.[36]

There are many examples of pH-responsive polymers based on either weak polyacids such as poly(methacrylic acid) (PMAA)[46,47] and poly(acrylic acid)[48] or weak polybases such as poly(2-vinylpyridine) (P2VP)[49] or poly(2-(dimethylamino)ethyl methacrylate) (PDMA).[50,51] The former class is particularly relevant to the present study. Ionisation of carboxylic acid groups confers polyelectrolytic character which causes PMAA to expand at high pH; this results in a conformational switch from compact (hyper-coiled) to highly extended chains.[52]

Such anionic PMAA chains can act as an effective electrosteric stabiliser for colloidal particles.[53]

Both PAA and PMAA have been evaluated as polyelectrolytic stabilisers for aqueous PISA formulations. For example, Chaduc and co-workers reported various RAFT aqueous emulsion polymerisation formulations using such electrosteric stabilisers to stabilise *n*-butyl acrylate, methyl methacrylate or styrene latexes to form spherical particles at pH 3.5, and other morphologies at pH 5.[54,55] Similarly, Cockram *et al.* used PMAA as a stabiliser block for the polymerisation of butyl methacrylate and benzyl methacrylate to form well-defined spheres at pH 5.[57] The increased aqueous solubility of 2-hydroxybutyl methacrylate was also utilised to form anisotropic particles at pH 5.[58] PMAA and PAA have been also been used as steric stabiliser blocks for the synthesis of diblock copolymer spheres, worms and vesicles *via* RAFT alcoholic dispersion polymerisation.[58–60]

In the present study, we examine a new PISA formulation based on the chain extension of a PMAA precursor *via* RAFT aqueous dispersion polymerisation of HPMA. This particular composition of $PMAA_{50}-PHPMA_{237}$ nanoparticles exhibits interesting pH-responsive and thermoresponsive behaviour in aqueous solution. This hypothesis is explored using a range of analytical techniques. Knowledge of the stimulus responsive behaviour of $PMAA_x-PHPMA_y$ nanoparticles is utilised to assess its pigment dispersion ability in Chapter 3.

2.2 Experimental

Materials

Methacrylic acid (MAA; 99%) and 4-cyanopropyl dithiobenzoate (CPDB) were purchased from Sigma-Aldrich (UK) and used without further purification. 4,4′-Azobis(4-cyanovaleric acid) (ACVA; 98%) was purchased from Alfa Aesar (UK) and used as received. HPMA was

donated by GEO Specialty Chemicals. CD_3OD and dimethyl sulfoxide-d_6 were purchased from Goss Scientific Ltd (Cheshire, UK). Deuterium oxide (D_2O), sodium deuteroxide (NaOD) and deuterium chloride (DCl) were purchased from Sigma-Aldrich (Dorset, UK). All other solvents were purchased from Fisher Scientific (Loughborough, UK) and used as received. Deionised water was used for all experiments.

Synthesis of the poly(methacrylic acid) (PMAA) steric stabiliser

In a typical synthesis of the $PMAA_{50}$ precursor, a round-bottomed flask was charged with MAA (10.0 g, 116 mmol), 4-cyanopropyl dithiobenzoate (CPDB) (514 mg, 2.30 mmol), ACVA (130 mg, 0.46 mmol; CTA/initiator molar ratio = 5.0) and ethanol (16.0 g, 40% w/w). The sealed reaction vessel was purged with nitrogen gas and place in a pre-heated oil bath at 70 °C for 3 h. The resulting PMAA precursor (MAA conversion = 68%; M_n = 5 600 g mol^{-1}, M_w = 7 000 g mol^{-1}, M_w/M_n = 1.26) was purified by precipitation into a ten-fold excess of diethyl ether (twice) and then isolated by lyophilisation. A mean DP of 49 was estimated for this PMAA precursor using ^{1}H NMR spectroscopy by end-group analysis. Similarly, a mean DP of 50 was determined *via* UV spectroscopy using the 302 nm absorption band assigned to the dithiobenzoate RAFT chain-end for quantification using a Beer-Lambert calibration plot.

Synthesis of linear poly(methacrylic acid)-poly(2-hydroxypropyl methacrylate) diblock copolymer nanoparticles *via* RAFT aqueous dispersion polymerisation

This RAFT aqueous dispersion polymerisation synthesis was conducted at 20% w/w solids targeting $PMAA_{50}$-$PHPMA_{200}$. HPMA (0.60 g, 4.1 mmol), ACVA (1.45 mg, 5.2 μmol, CTA/initiator molar ratio = 4.0), and $PMAA_{50}$ macro-CTA (79.8 mg, 20.1 μmol) were dissolved in water (3.0 g). The solution pH was adjusted to 5.5 using an aqueous solution of 1 M NaOH. The pink reaction mixture was sealed in a round-bottomed flask, purged with nitrogen for 30 min, and then placed in a pre-heated oil bath at 70°C for 2 h.

^{1}H NMR spectroscopy

All ^{1}H NMR spectra were recorded using a 400 MHz Bruker Avance-400 spectrometer using CD_3OD, D_2O, or dimethyl sulfoxide-d^6. Typically, 64 scans were averaged per spectrum. NMR spectra were used to determine monomer conversions and to estimate mean degrees of polymerisation (DP) *via* end-group analysis.

UV spectroscopy

Absorption spectra were recorded using a Shimadzu UV-1800 spectrophotometer at 25 °C. A linear Beer-Lambert calibration plot was constructed using a series of solutions of CPDB (λ_{max} = 302 nm) dissolved in methanol at concentrations ranging between 1.59 and 14.8 g dm^{-3}. The PMAA$_{50}$ precursor was dissolved in methanol (0.122 g dm^{-3}) and its absorption maximum was recorded at 302 nm in order to calculate its mean degree of polymerisation *via* end-group analysis. The same approach was used to determine the mean DP for the PMAA$_{50}$-PHPMA$_{237}$ nanoparticles, which were dried by lyophilisation and then dissolved in methanol (26.4 mg copolymer in 10 ml) prior to analysis.

Variable temperature ^{1}H NMR studies of an aqueous dispersion of PMAA$_{50}$-PHPMA$_{237}$ nanoparticles

Nanoparticles were diluted to 1.0% w/w in NaOD/D_2O (pD 10). The dispersion was cooled to 5 °C, equilibrated for 5 min and a spectrum was recorded. The temperature was then gradually increased to 50 °C and further spectra were recorded at 5°C intervals, with 5 min being allowed for thermal equilibration in each case. A final spectrum was recorded after returning to 25 °C. A capillary tube containing 0.1 mol dm^{-3} pyridine dissolved in 1,1,2,2-tetrachloroethane-d^2 (lock solvent) was used as an external standard.

Exhaustive methylation protocol

$PMAA_{50}$ homopolymer was modified *via* exhaustive methylation of its carboxylic acid groups to form poly(methyl methacrylate). Excess trimethylsilyldiazomethane was added dropwise to a solution of $PMAA_{50}$ (20 mg) in THF (2.0 mL), until the yellow colour persisted. This reaction solution was then stirred overnight until all THF had evaporated. The degree of methylation was determined to be 100% by ^{1}H NMR spectroscopy. This was determined by comparing the integrated backbone signal (0 – 2.5 ppm) to that of the new methoxy signal at 3.34 ppm.

Gel Permeation Chromatography (GPC)

The molecular weight distributions of the $PMAA_{50}$ precursor (after exhaustive methylation) and $PMAA_{50}$-$PHPMA_{237}$ diblock copolymer (without modification) were assessed using an Agilent Technologies PL GPC-50 system. The mobile phase was HPLC-grade THF containing 4.0% v/v glacial acetic acid at a flow rate of 1.0 ml min^{-1}. Molecular weights were calculated using a series of near-monodisperse poly(methyl methacrylate) calibration standards.

Dynamic Light Scattering (DLS)

0.10% w/w aqueous copolymer dispersions were analysed in glass cuvettes at 25°C using a Malvern Zetasizer NanoZS instrument. Scattered light was detected at 173° and the hydrodynamic diameters were calculated by cumulants analysis of the experimental correlation function, which uses the Stokes-Einstein equation. Data were averaged over three consecutive measurements comprising eleven runs per measurement.

Aqueous Electrophoresis

Measurements were performed using the same Malvern Zetasizer NanoZS instrument on a 0.10% w/w aqueous dispersion of nanoparticles in the presence of 1 mM KCl as background

salt. The solution pH was adjusted using NaOH or HCl. The zeta potential was calculated from the electrophoretic mobility (μ) *via* the Henry equation using the Smoluchowsky approximation, which is valid for the electrophoretic determination of zeta potentials in aqueous media at moderate electrolyte concentrations.

Rheology Measurements

An AR-G2 rheometer equipped with a variable temperature Peltier plate and a 40 mm 2° aluminium cone was used for all experiments. An oscillatory mode was used to measure loss modulus (G''), and storage modulus (G') as a function of percentage strain amplitude, angular frequency, and temperature to assess critical gelation temperatures and gel strengths using a cone and plate geometry. Temperature sweeps were conducted using the same applied strain amplitude and at angular frequencies of 1 rad s^{-1}. Measurements were recorded at 1 °C intervals, allowing 5 min for thermal equilibration in each case.

Shear-Induced Polarised Light Imaging (SIPLI) studies of PMAA$_{50}$-PHPMA$_{237}$

The instrument design and general experimental set-up has been previously reported by Mykhaylyk and co-workers.[61] SIPLI experiments were conducted using a mechano-optical rheometer (Anton Paar Physica MCR301 with SIPLI attachment). Measurements were performed using a plate−plate geometry composed of a 25 mm polished steel plate and a fused quartz plate connected to a variable temperature Peltier system. Sample illumination was achieved using an Edmund Optics 150 W MI-150 high-intensity fibre-optic white light source with a constant light intensity maintained for all measurements. The polariser and analyser axes were crossed at 90° to obtain polarised light images (PLIs), which were recorded using a colour CCD camera (Lumenera Lu165c). SIPLI experiments were conducted on a 20% w/w aqueous dispersion of PMAA$_{50}$-PHPMA$_{237}$ nano-objects at an

applied shear rate of 250 s^{-1} during temperature ramp experiments conducted at a heating/cooling rate of 1.0 °C min^{-1}.

Transmission electron microscopy (TEM)

A 0.2 µL droplet of a 0.10 % w/w aqueous copolymer dispersion at the desired solution pH was deposited onto a glow discharge-treated carbon-coated copper/palladium TEM grid (Agar Scientific, UK) for 30 seconds. Each grid was stained with 10 µL of an aqueous uranyl formate solution (0.75 % w/w) for 30 seconds and then carefully dried using a vacuum hose.

TEM images were recorded using a Philips CM100 instrument operating at 100 kV and equipped with a Gatan 1 k CCD camera. ImageJ software was used to manually measure nanoparticle diameters and hence estimate averages and standard deviations from TEM images (at least 100 nanoparticles were analysed per sample).

2.3 Results and Discussion

Initially, a PMAA homopolymer precursor was prepared at 40% w/w *via* RAFT solution polymerisation of MAA at 70 °C in ethanol using 2-cyanopropyl dithiobenzoate (CPDB) as a chain transfer agent (CTA). A DP of 50 was targeted and the polymerisation was terminated after 3 h (65% conversion) to preserve RAFT chain-end functionality. After purification to remove excess monomer and other low molecular weight components, end-group analysis *via* ^{1}H NMR spectroscopy suggested a mean DP of 49. A calibration plot of absorbance against CPDB concentration was produced using CPDB dissolved in methanol. The molar extinction coefficient for the absorption maximum at 302 nm, assigned to its dithiobenzoate end-group, was determined to be 12600 ± 200 mol^{-1} dm^3 cm^{-1}.[62] Using this value, the mean DP of the PMAA homopolymer precursor was determined to be 50. The latter value was used because UV spectroscopy is considered to be much more sensitive than ^{1}H NMR spectroscopy for

such measurements. These data indicate a RAFT agent efficiency of around 67% for CPDB.

This PMAA$_{50}$ precursor was then chain-extended *via* RAFT aqueous dispersion polymerisation of HPMA, targeting a PHPMA block DP of 200 (**Figure 2.1**).
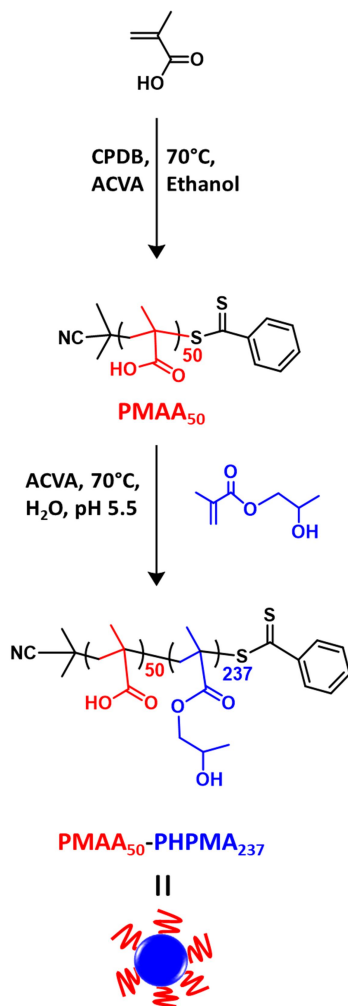

Figure 2.1 RAFT solution polymerisation of methacrylic acid (MAA) in ethanol using CPDB as a RAFT agent and 4,4'-azobis(4-cyanovaleric acid) (ACVA) as a free radical initiator to produce poly(methacrylic acid) (PMAA). This water-soluble precursor is then used for the RAFT aqueous dispersion polymerisation of 2-hydroxypropyl methacrylate (HPMA) at 70 °C to produce spherical PMAA$_{50}$-PHPMA$_{237}$ diblock copolymer nanoparticles. The optimum solution pH for this PISA synthesis is pH 5.5.

The diblock copolymer was analysed by GPC using THF eluent containing 4% acetic acid, with the latter being added to the mobile phase to suppress ionisation of the methacrylic acid groups.[56] The PMAA$_{50}$ macro-CTA required exhaustive methylation of its carboxylic acid

groups to ensure THF solubility prior to GPC analysis. The M_n of this methylated precursor was determined to be 5 600 g mol^{-1}. Given that GPC calibration involved the use of a series of poly(methyl methacrylate) standards, this value is close to that expected (5 000 g mol^{-1}). Moreover, its M_w/M_n was determined to be 1.26, which indicates a reasonably well-controlled RAFT polymerisation. This PMAA$_{50}$ precursor was used to prepare PMAA$_{50}$-PHPMA$_{237}$ nanoparticles directly *via* RAFT aqueous dispersion polymerisation of HPMA at 70 °C. Periodic sampling of the reaction mixture (with quenching achieved by dilution with concomitant cooling to 20 °C) enabled the kinetics of polymerisation to be assessed by ^{1}H NMR spectroscopy. This was achieved by monitoring the disappearance of the vinyl proton signals at ~ 6 ppm relative to the methacrylic backbone signals at 0 – 2.5 ppm (**Figure 2.2 (a-c)**). This approach indicated that the HPMA polymerisation was essentially complete within 2 h at 70 °C (**Figure 2.2d**). The final DP for the PHPMA block can be calculated by comparing the integrated oxymethylene PHPMA signal at ~ 4 ppm to that of the methacrylic backbone signals at 0 – 2.5 ppm. The complex PHPMA signals owe their existence to two HPMA isomers, which are present in a 75:25 ratio.[63]

The evolution in molecular weight over the course of the HPMA polymerisation was followed by THF GPC (**Figure 2.3**). PMAA-PHPMA diblock copolymers did not require methylation as the level of acetic acid was enough to stop copolymers from interacting with the GPC column. PMAA homopolymer could not be analysed without methylation as it was not soluble in the THF eluent, despite the addition of acetic acid. The molecular weight increased linearly with monomer conversion, as expected for a RAFT polymerisation. M_w/M_n values remain below 1.20 throughout the polymerisation, and all chromatograms were unimodal, indicating a well-controlled RAFT polymerisation. The final PMAA$_{50}$-PHPMA$_{237}$ diblock copolymer obtained at full monomer conversion had an apparent M_n of 36 000 g mol^{-1} and its M_w/M_n was 1.15.
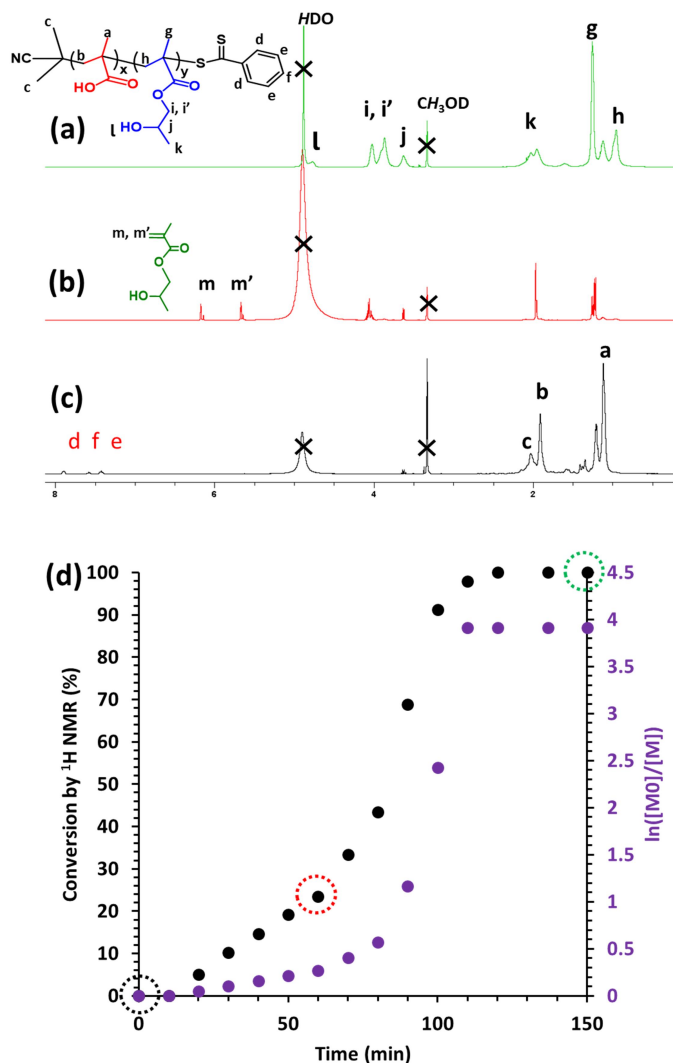
Figure 2.2 ^{1}H NMR spectra illustrating the gradual disappearance in the vinyl monomer signals at ~6 ppm and progressive appearance of methacrylic backbone signals (0–2.5 ppm). **(a)** Full conversion of HPMA to afford PMAA$_{50}$-PHPMA$_{237}$ after 150 min, **(b)** 23% HPMA conversion after 60 min, **(c)** original PMAA precursor, **(d)** conversion vs. time curve and corresponding semi-logarithmic plot indicating that the HPMA polymerisation is complete within 2 h at 70 °C.

The mean degree of polymerisation for the PHPMA block was also determined using UV spectroscopy. This end-group analysis assumes that the λ_{max} and molar absorption coefficient (ε) remain unchanged during the course of the reaction (**Figure 2.4**).[64] The mean DP for the PHPMA block was calculated to be 237, whereas its target DP was 200. This suggests a

RAFT agent efficiency of 84% for the RAFT aqueous dispersion polymerisation step, which is comparable to that reported for other RAFT aqueous polymerisations.[65,66]
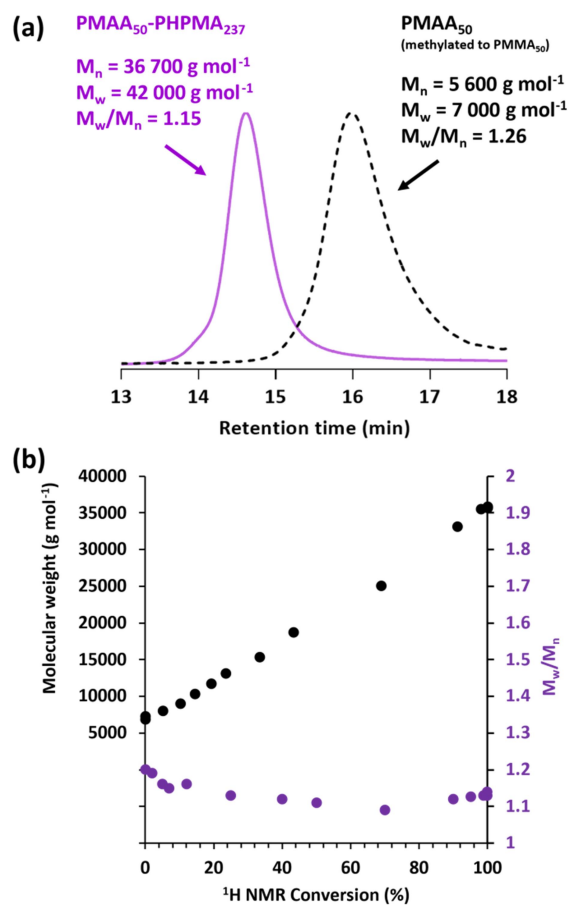
Figure 2.3 THF GPC curves recorded for a $PMAA_{50}$-$PHPMA_{237}$ diblock copolymer (and its corresponding $PMAA_{50}$ precursor, after exhaustive methylation to form $PMMA_{50}$) prepared at 20% w/w solids via RAFT aqueous dispersion polymerisation of PHPMA at 70 °C. M_n values are expressed relative to a series of near-monodisperse poly(methyl methacrylate) calibration standards. Evolution of M_n and M_w/M_n with HPMA monomer conversion observed for this PISA synthesis.
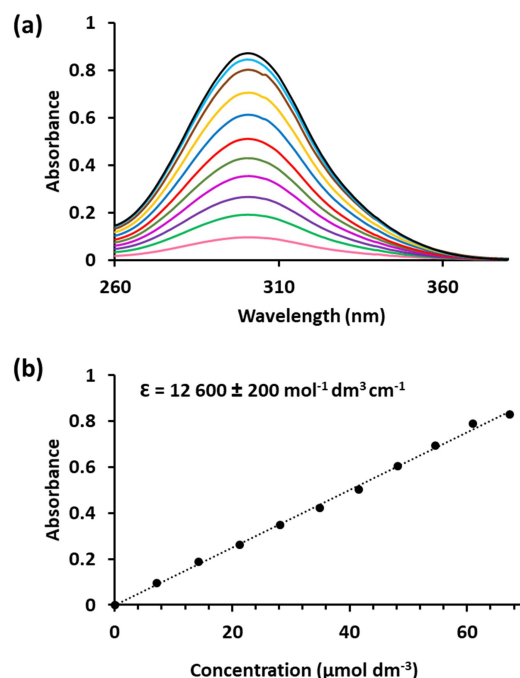
Figure 2.4 (a) UV spectra recorded for CPDB dissolved in methanol for concentrations ranging from 7.2 µmol dm^{-3} (light pink spectrum) to 67.0 µmol dm^{-3} (black spectrum). **(b)** Determination of the molar absorption coefficient for CPDB using the Beer–Lambert law.

Aqueous electrophoresis measurements show that the nanoparticles become highly anionic above pH 6.3, exhibiting zeta potentials of approximately -45 mV owing to a high degree of ionisation for the PMAA stabiliser chains (**Figure 2.5**). According to potentiometric acid titration studies (**Figure 2.6**), this pH corresponds to the pK$_a$ for the PMAA$_{50}$-PHPMA$_{237}$ block of 6.27, which is slightly higher than the pK$_a$ for the PMAA$_{50}$ precursor of 5.82; these experimental data lie close to the literature values reported for PMAA homopolymer and for diblock copolymer nanoparticles comprising PMAA coronas.[67,68] Below pH 6.3, the nanoparticles become progressively less anionic, exhibiting an isoelectric point (IEP) at approximately pH 2.3. Under such conditions, the neutral PMAA chains undergo a so-called 'hypercoiling' transition as a result of intramolecular hydrogen bonding interactions.[69]
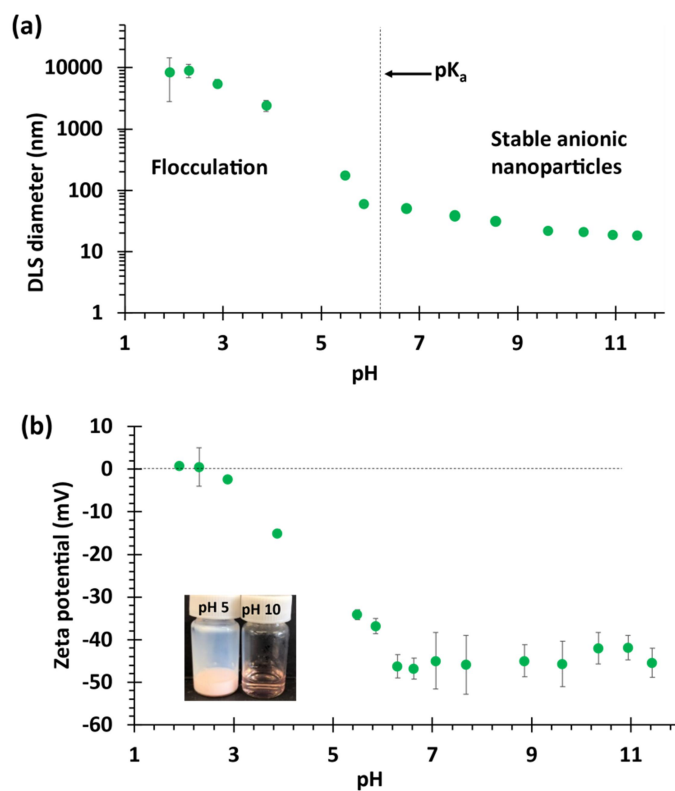
Figure 2.5 (a) Dynamic light scattering (DLS) studies of a 0.10 % aqueous dispersion of $PMAA_{50}$-$PHPMA_{237}$ nanoparticles at 25 °C. The large increase in hydrodynamic diameter observed below pH 6.3 is consistent with the onset of turbidity and observation of macroscopic precipitation below pH 6.3. **(b)** Zeta potential vs. pH curve obtained for a 0.10% aqueous dispersion of $PMAA_{50}$-$PHPMA_{237}$ nanoparticles. Inset digital photograph shows (left) the turbid dispersion obtained below the pK_a for the $PMAA_{50}$-$PHPMA_{237}$ diblock copolymer and (right) the relatively transparent dispersion formed above this pK_a. In both sets of experiments, the solution pH was adjusted using dilute aqueous solutions of either NaOH or HCl.
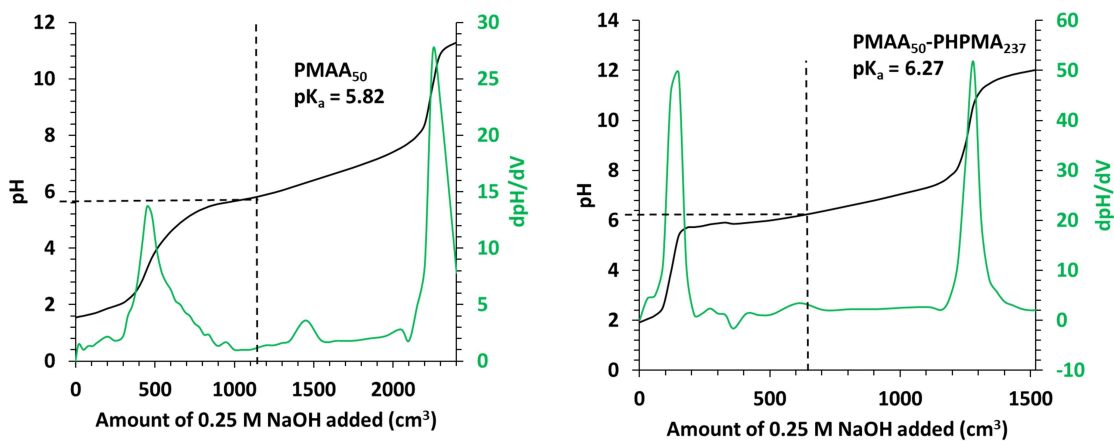
Figure 2.6 Potentiometric acid titration studies on the $PMAA_{50}$ precursor and the $PMAA_{50}$-$PHPMA_{237}$ diblock copolymer to determine their pK_a values.

DLS studies of a 0.10% w/w aqueous dispersion of these $PMAA_{50}$-$PHPMA_{237}$ nanoparticles indicate a significant increase in the scattered light intensity on lowering the solution pH (from ~1 000 kcps at pH 6.3 to ~ 20 000 kcps at pH 5.9). Visual inspection confirms that a substantial increase in turbidity occurs under such conditions, which is confirmed by turbidimetry studies (see **Figure 2.7**).
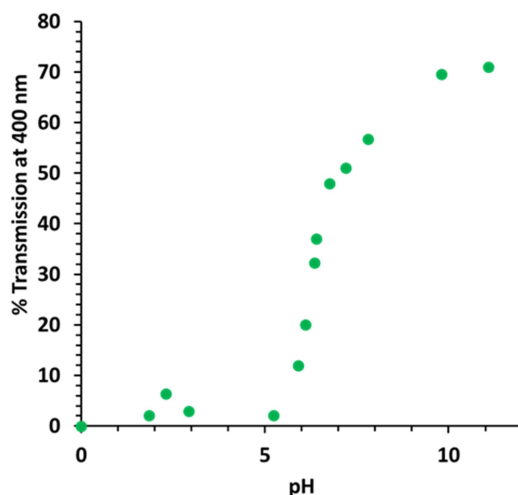

Figure 2.7 Turbidimetry studies using visible absorption spectroscopy to measure the light transmittance at 400 nm. The large increase in turbidity at approximately pH 6 indicates the onset of macroscopic precipitation.

As the solution pH is reduced further, the nanoparticles become colloidally unstable: the marked increase in apparent particle size observed at low pH indicates flocculation, because the nanoparticles no longer bear sufficient anionic surface charge to ensure their stabilisation. On the other hand, relatively transparent nanoparticle dispersions are obtained above pH 6.3. The degree of ionisation of the PMAA stabiliser chains exceeds 50% under such conditions, which is sufficient to ensure effective charge stabilisation. According to the DLS data shown in **Figure 2.5a**, somewhat smaller nanoparticles are formed at higher pH. This size reduction is corroborated by TEM studies, which can only reveal the hydrophobic PHPMA cores (**Figure 2.8**). For example, the mean number-average diameter is 90 ± 33 nm at pH 5.5 but

only 25 ± 5 nm at pH 10.5. This corresponds to a reduction in the mean aggregation number
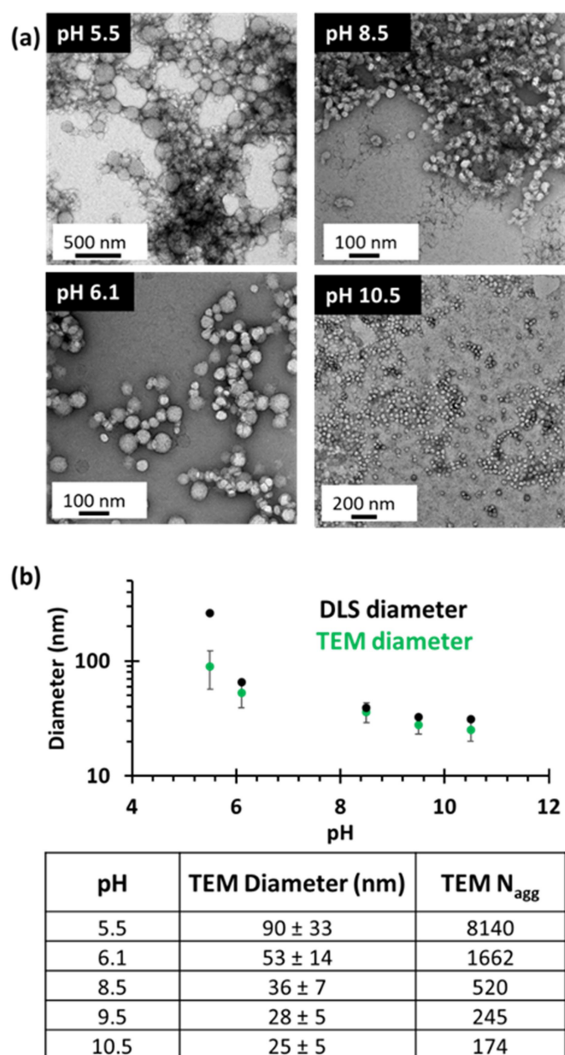
from 8140 to 174 (**see Equations 2.1-2.3**).

pH	TEM Diameter (nm)	TEM N_{agg}
5.5	90 ± 33	8140
6.1	53 ± 14	1662
8.5	36 ± 7	520
9.5	28 ± 5	245
10.5	25 ± 5	174

Figure 2.8 (a) Transmission electron microscopy images of PMAA$_{50}$-PHPMA$_{237}$ nanoparticles dried from 0.10 % aqueous solution between pH 5.5 and pH 10.5. **(b)** Variation of the mean particle diameter for these PMAA$_{50}$-PHPMA$_{237}$ nanoparticles as a function of pH as determined by TEM and DLS, respectively.

The volume (V) of the core-forming PHPMA block was calculated using the equation:

$$V_{PHPMA} = \frac{DP.M_{(HPMA)}}{N_A.\rho} \quad \textbf{(Equation 2.1)}$$

Where *DP* is the mean degree of polymerisation of the PHPMA block determined by UV spectroscopy, *M* is the molecular weight of the repeat unit (HPMA), N_A is Avogadro's constant, and ρ is the density of the PHPMA block.

The mean aggregation number (N_{agg}) is calculated in **Equation 2.2** using the volume of the core-forming block from **Equation 2.1**, as follows.

$$N_{agg} = \frac{\frac{4}{3}.\pi.r^3}{V_{PHPMA}} \text{ (Equation 2.2)}$$

Here *r* is the mean radius of the PMAA$_{50}$-PHPMA$_{237}$ spheres as determined from TEM studies.

Equation 2.3 was used to estimate the mean aggregation number for the worm-like nanoparticles, using the volume of the core-forming PHPMA block from **Equation 2.1.**

$$N_{agg} = \frac{\pi.r^2.L}{V_{PHPMA}} \text{ (Equation 2.3)}$$

Here *r* is the mean core radius (or half of the mean worm width) and *L* is the mean worm length.

A comparison of the reduction in nanoparticle diameter with increasing pH observed by TEM and DLS is shown in **Figure 2.8b**. The latter technique oversizes relative to the former because it reports the intensity-average diameter, which always exceeds the number-average diameter for particle size distributions of finite width. This pH-dependent particle size is owed to the repulsion of PMAA chains when they become charged. Previously, this has been reported for the ionisation of carboxylic end-groups, where the introduction of a single anionic charge was sufficient to change the packing parameter and induce a change in copolymer morphology. [70] In the present case, the introduction of multiple ionised acid

groups on the PMAA stabiliser chains is expected to induce a significant reduction in the
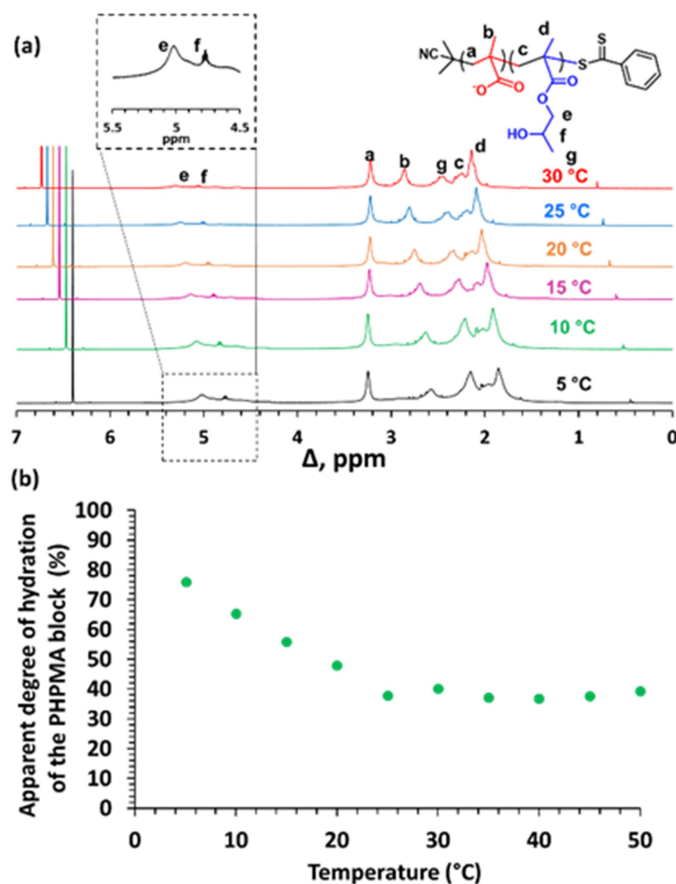
mean aggregation number and hence particle size.

Figure 2.9 (a) ^{1}H NMR spectra recorded for PMAA$_{50}$-PHPMA$_{237}$ nanoparticles dispersed in NaOD/D$_2$O (pD 10) between 5 °C and 30 °C using an external standard to monitor the systematic reduction in PHPMA signal intensity that occurs on heating (see signals e and f at 5.0 and 4.57 ppm). **(b)** Relative degree of hydration for the PHPMA block calculated from 5 °C to 50 °C.

According to our previous studies, PHPMA only exhibits thermoresponsive character when

conjugated to a suitably hydrophilic block.[71] For this reason, thermosensitive behaviour is

only observed for these sterically-stabilised nanoparticles when the PMAA stabiliser chains

become highly ionised in alkaline solution. Thus, variable temperature ^{1}H NMR spectroscopy

studies were conducted at pD 10 using NaOD/D$_2$O. These experiments confirm that the

integrated signal for the two oxymethylene protons assigned to the core-forming PHPMA

block at around 5 ppm become attenuated at elevated temperature (**Figure 2.9**). This indicates that the weakly hydrophobic PHPMA block becomes progressively dehydrated on heating, as expected.[37] Since the intensity of the methacrylic backbone signals vary with temperature for both blocks, an external standard (pyridine dissolved in 1,1,2,2-tetrachloroethane-d_2) was used to monitor the extent of dehydration of this oxymethylene signal. The degree of hydration of the PHPMA chains is estimated to be approximately 75% at 5 °C.[72] However, gradual dehydration to around 37% is observed on heating to 25 °C, with this value remaining more or less constant up to 50 °C. These observations are consistent with prior reports for diblock copolymer nanoparticles comprising thermoresponsive PHPMA core-forming chains.[42,45,73]
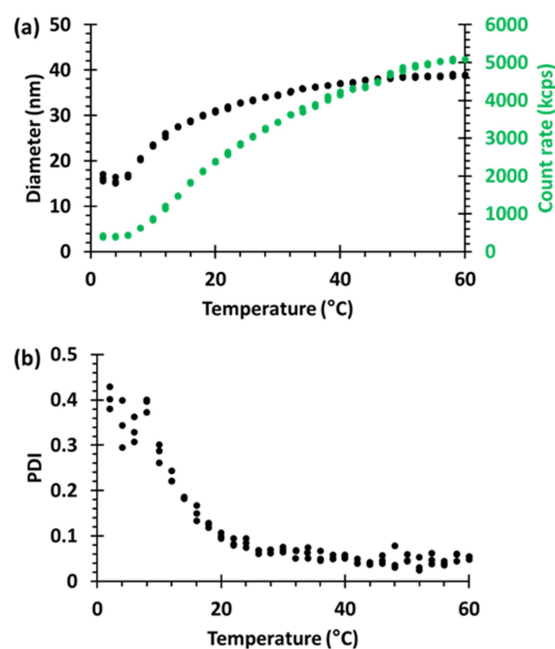
Figure 2.10 Variation in **(a)** intensity-average diameter and count rate and **(b)** polydispersity index (PDI) with temperature as determined by DLS studies of a 0.10% w/w aqueous dispersion of $PMAA_{50}$-$PHPMA_{237}$ nanoparticles at pH 10.

These variable temperature ^{1}H NMR spectroscopy experiments are consistent with DLS studies (**Figure 2.10**). A very low count rate (or scattered light intensity) is observed for this

aqueous copolymer dispersion at 2 °C and the apparent mean diameter is only 15 nm under such conditions. As the solution temperature is increased, the core-forming PHPMA block becomes progressively more hydrophobic. This leads to a gradual increase in nanoparticle size, with an intensity-average diameter of 41 nm being observed at 50 °C.
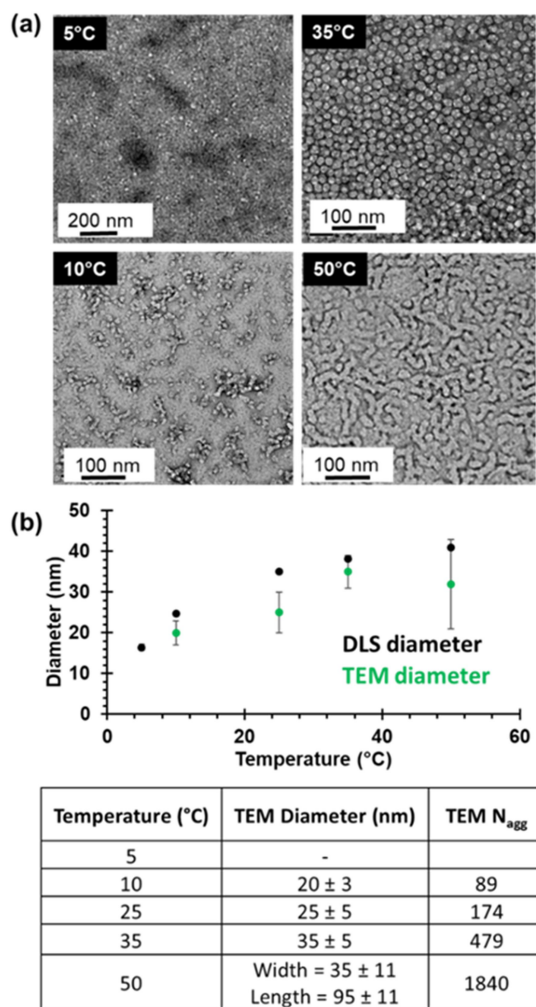

Temperature (°C)	TEM Diameter (nm)	TEM N_{agg}
5	-	
10	20 ± 3	89
25	25 ± 5	174
35	35 ± 5	479
50	Width = 35 ± 11 Length = 95 ± 11	1840

Figure 2.11 (a) Transmission electron microscopy images recorded after drying 0.10% aqueous dispersions of PMAA$_{50}$-PHPMA$_{237}$ nanoparticles at pH 10 at temperatures ranging from 2 °C to 50 °C. **(b)** Effect of varying the solution temperature on mean particle diameter as determined by TEM (green data set) and DLS (black data set) studies.

TEM studies confirm this increase in particle size (**Figure 2.11**). The copolymer chains are close to molecular dissolution at 5 °C, so no nanoparticles are observed at this temperature.[74]

The nanoparticle core diameter is 20 ± 3 nm at 10 °C and 35 ± 5 nm at 50 °C. This indicates a significant increase in mean aggregation number from 89 to 1840. These number-average diameters are consistent with the (larger) intensity-average diameters reported by DLS. The TEM image obtained when drying this aqueous copolymer dispersion at 50 °C indicates the formation of short worms.
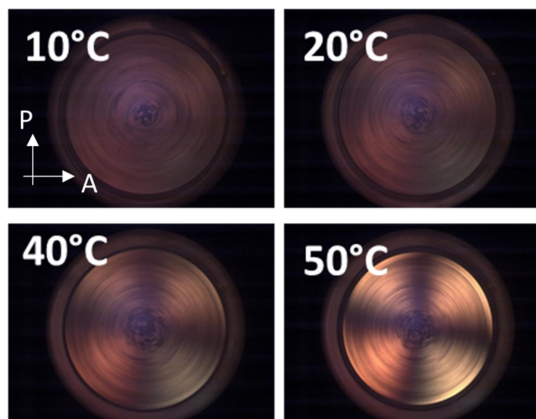

Figure 2.12 SIPLI images obtained from a 20% w/w dispersion of $PMAA_{50}$-$PHPMA_{237}$ nanoparticles at pH 10 at 10 °C, 20 °C, 40 °C and 50 °C during a temperature ramp experiment (heating cycle). The featureless images recorded at 10 °C and 20 °C are consistent with the presence of isotropic spheres and/or dissolved copolymer chains. A characteristic Maltese cross is formed at 50 °C, owing to the birefringence caused by the alignment of anisotropic worm-like nanoparticles in the direction of shear flow.

This thermally-induced sphere-to-worm transition is supported by shear-induced polar light imaging (SIPLI) experiments: birefringence is observed at 50 °C which indicates alignment of these weakly anisotropic nanoparticles at pH 10 (**see Figure 2.12**).[57,61] Finally, temperature-dependent rheology measurements were performed as a function of temperature on the 20 % w/w aqueous copolymer dispersion, which forms a free-standing gel (G' ~ 1 000 Pa) above 25 °C at pH 10. The critical gelation temperature (CGT) is estimated to be 10 °C for this copolymer dispersion (see **Figure 2.13**) at 20% w/w. This is thought to be due to the formation of a 'sphere gel' due to the high anionic charge forming a network structure. The rheology plot suggests an increase in the gel strength (possibly a sphere-gel to worm-gel

transition) at approximately 25 °C. This does not correspond to the formation of worms by TEM at 50 °C, however it is thought that there is a large difference in the temperature responsive behaviour at 0.1% w/w compared to 20% w/w. Further studies would be required to deduce this. Complex pH and thermoresponsive behaviour exhibited by $PMAA_{50}$-$PHPMA_{237}$ nanoparticles in aqueous solution is summarised in **Figure 2.14.**
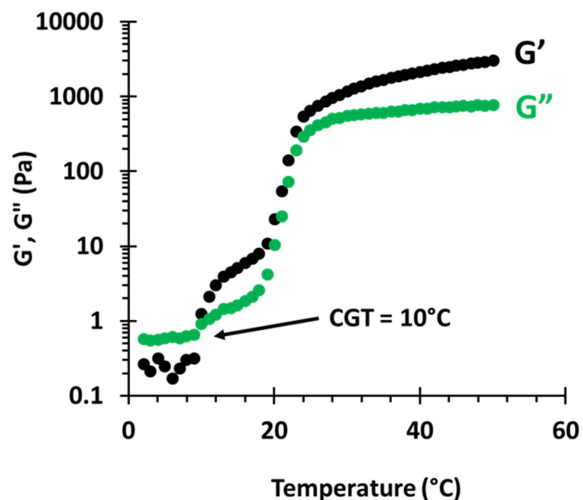

Figure 2.13 Temperature-dependent oscillatory rheology studies obtained on heating a 20% w/w aqueous copolymer dispersion of $PMAA_{50}$-$PHPMA_{237}$ nanoparticles at pH 10 from 2 ° C to 50 ° C. Measurements were conducted at an angular frequency of 1.0 rad s^{-1} and a strain amplitude of 1.0%, with an equilibration time of 5 min being allowed at each temperature. A critical gelation temperature was observed at around 10 ° C, as judged by the cross-over point for the G' and G" curves.

The schematic representation in **Figure 2.14** is presented as a summary of the pH and temperature responsive behaviour of this copolymer composition. These particles are not thermoresponsive at pH 5.5, as synthesised, but as the pH is increased to 10, the large polydisperse spheres become small spherical particles. These small particles dissolve to form chains on cooling and become larger and anisotropic at higher temperatures.
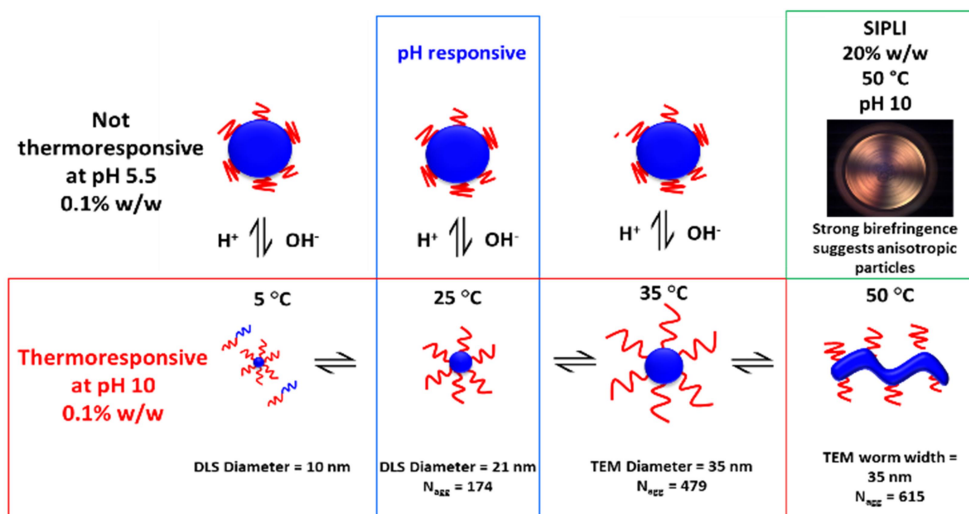
Figure 2.14 Schematic representation of the stimulus-responsive behaviour of PMAA$_{50}$-PHPMA$_{237}$ nanoparticles in aqueous solution. Relatively large, polydisperse spheres are formed at pH 5.5, which is the solution pH used for the RAFT aqueous dispersion polymerisation of HPMA. At pH 10, the PMAA$_{50}$ stabiliser block becomes much more anionic, which leads to the formation of relatively small spherical nanoparticles at 5 °C. On increasing the solution temperature, these spheres grow in size and weakly anisotropic worms are formed at 50 °C, confirmed by SIPLI measurements (see **Figure 2.12**).

2.4 Conclusions

A new amphiphilic PMAA$_{50}$-PHPMA$_{237}$ diblock copolymer has been prepared by RAFT dispersion polymerisation of HPMA at pH 5.5. In dilute aqueous solution, the as-synthesised sterically-stabilised particles are relatively large and polydisperse because the mean degree of ionisation of the PMAA block (pK$_a$ ~ 6.3) is relatively low under such conditions. Lowering the solution pH leads to macroscopic precipitation owing to loss of their anionic surface charge. However, in alkaline solution the PMAA chains become highly anionic, which leads to the formation of relatively small thermoresponsive nanoparticles. Thus, molecularly-dissolved diblock copolymer chains are formed at 5 °C, rather than nanoparticles. At higher temperatures (10 - 35 °C), DLS, TEM and ^{1}H NMR spectroscopy studies indicate that the weakly hydrophobic PHPMA chains become progressively more dehydrated, which drives the formation of relatively small nanoparticles of gradually increasing aggregation number

and size. At 50 °C, TEM studies indicate the formation of weakly anisotropic worm-like nanoparticles. At higher copolymer concentration (20% w/w), rheological studies indicate the formation of a free-standing transparent gel above 10 °C when the solution pH exceeds 6.3.

2.5 References

1. Kocak, G., Tuncer, C. & Bütün, V. pH-Responsive polymers. *Polym. Chem.* **8**, 144–176 (2017).

2. Roy, D., Brooks, W. L. A. & Sumerlin, B. S. New directions in thermoresponsive polymers. *Chem. Soc. Rev.* **42**, 7214–7243 (2013).

3. Kozlovskaya, V., Kharlampieva, E., Mansfield, M. L. & Sukhishvili, S. A. Poly(methacrylie acid) hydrogel films and capsules: Response to pH and ionic strength, and encapsulation of macromolecules. *Chem. Mater.* **18**, 328–336 (2006).

4. Bertrand, O. & Gohy, J. F. Photo-responsive polymers: Synthesis and applications. *Polym. Chem.* **8**, 52–73 (2017).

5. Du, J., Tang, Y., Lewis, A. L. & Armes, S. P. pH-sensitive vesicles based on a biocompatible zwitterionic diblock copolymer. *J. Am. Chem. Soc.* **127**, 17982–17983 (2005).

6. Schild, H. G. Poly(N-Isopropylacrylamide): Experiment, Theory & Application. *Prog. Polym. Sci.* **17**, 163–249 (1992).

7. Stuart, M. A. C. *et al.* Emerging applications of stimuli-responsive polymer materials. *Nat. Mater.* **9**, 101–113 (2010).

8. Gohy, J. F. & Zhao, Y. Photo-responsive block copolymer micelles: Design and behavior. *Chem. Soc. Rev.* **42**, 7117–7129 (2013).

9. Arotçaréna, M., Heise, B., Ishaya, S. & Laschewsky, A. Switching the inside and the outside of aggregates of water-soluble block copolymers with double thermoresponsivity. *J. Am. Chem. Soc.* **124**, 3787–3793 (2002).

10. Chen, T. *et al.* Temperature responsive polymer-supported TEMPO: An efficient and recoverable catalyst for the selective oxidation of alcohols. *Tetrahedron Lett.* **60**, 419–422 (2019).

11. Wei, R. *et al.* Bidirectionally pH-responsive zwitterionic polymer hydrogels with switchable selective adsorption capacities for anionic and cationic dyes. *Ind. Eng. Chem. Res.* **57**, 8209–8219 (2018).

12. Tso, C. P. *et al.* Stability of metal oxide nanoparticles in aqueous solutions. *Water Sci. Technol.* **61**, 127–133 (2010).

13. Cesarano, J., Aksay, I. A. & Bleier, A. Stability of Aqueous α-Al$_2$O$_3$ Suspensions with Poly(methacrylic acid) Polyelectrolyte. *J. Am. Ceram. Soc.* **71**, 250–255 (1988).

14. Ng, J. *et al.* Stimuli-Responsive Hybrid Polymer for Enhanced Solid-Liquid Separation of

Industrial Effluents. *Environ. Sci. Technol.* **53**, 6436–6443 (2019).

15. Mura, S., Nicolas, J. & Couvreur, P. Stimuli-responsive nanocarriers for drug delivery. *Nat. Mater.* **12**, 991–1003 (2013).

16. Guragain, S., Bastakoti, B. P., Malgras, V., Nakashima, K. & Yamauchi, Y. Multi-Stimuli-Responsive Polymeric Materials. *Chem. - A Eur. J.* **21**, 13164–13174 (2015).

17. Hoffman, A. S. Stimuli-responsive polymers: Biomedical applications and challenges for clinical translation. *Adv. Drug Deliv. Rev.* **65**, 10–16 (2013).

18. Bae, Y., Fukushima, S., Harada, A. & Kataoka, K. Design of environment-sensitive supramolecular assemblies for intracellular drug delivery: Polymeric micelles that are responsive to intracellular pH change. *Angew. Chemie - Int. Ed.* **42**, 4640–4643 (2003).

19. Halperin, A., Kröger, M. & Winnik, F. M. Poly(N-isopropylacrylamide) Phase Diagrams: Fifty Years of Research. *Angew. Chemie - Int. Ed.* **54**, 15342–15367 (2015).

20. Pelton, R. Temperature-sensitive aqueous microgels. *Advances in Colloid and Interface Science* **85**, 1–33 (2000).

21. Heskins, M. & Guillet, J. E. Solution Properties of Poly(N-isopropylacrylamide). *J. Macromol. Sci. Part A - Chem.* **2**, 1441–1455 (1968).

22. de las Heras Alarcón, C., Pennadam, S. & Alexander, C. Stimuli-Responsive Polymers: Biomedical Applications. *Chem. Soc. Rev.* **34**, 276–285 (2005).

23. Senff, H. & Richtering, W. Temperature sensitive microgel suspensions: Colloidal phase behavior and rheology of soft spheres. *J. Chem. Phys.* **111**, 1705–1711 (1999).

24. Liu, R., Fraylich, M. & Saunders, B. R. Thermoresponsive copolymers: From fundamental studies to applications. *Colloid Polym. Sci.* **287**, 627–643 (2009).

25. Stieger, M., Richtering, W., Pedersen, J. S. & Lindner, P. Small-angle neutron scattering study of structural changes in temperature sensitive microgel colloids. *J. Chem. Phys.* **120**, 6197–6206 (2004).

26. Steinschulte, A. A. *et al.* Stimulated Transitions of directed nonequilibrium self-assemblies. *Adv. Mater.* **29**, 1–8 (2017).

27. Figg, C. A. *et al.* Polymerization-induced thermal self-assembly (PITSA). *Chem. Sci.* **6**, 1230–1236 (2015).

28. Bobrin, V. A. & Monteiro, M. J. Temperature-directed self-assembly of multifunctional polymeric tadpoles. *J. Am. Chem. Soc.* **137**, 15652–15655 (2015).

29. Zhang, Y., Furyk, S., Bergbreiter, D. E. & Cremer, P. S. Specific ion effects on the water solubility of macromolecules: PNIPAM and the Hofmeister series. *J. Am. Chem. Soc.* **127**, 14505–14510 (2005).

30. Bergbreiter, D. E., Case, B. L., Liu, Y.-S. & Caraway, J. W. Poly(N -isopropylacrylamide) soluble polymer supports in catalysis and synthesis. *Macromolecules* **31**, 6053–6062 (1998).

31. Hoare, T. & Pelton, R. Highly pH and Temperature Responsive Microgels Functionalized with Vinylacetic Acid. *Macromolecules* **37**, 2544–2550 (2004).

32. Saunders, B. R., Crowther, H. M. & Vincent, B. Poly[(methyl methacrylate)-co-(methacrylic acid)] microgel particles: swelling control using pH, cononsolvency, and osmotic deswelling.

Macromolecules **30**, 482–487 (2002).

33. Saunders, B. R. On the structure of poly(N-isopropylacrylamide) microgel particles. *Langmuir* **20**, 3925–3932 (2004).

34. Cunningham, V. J. *et al.* Tuning the critical gelation temperature of thermo-responsive diblock copolymer worm gels. *Polym. Chem.* **5**, 6307–6317 (2014).

35. Lovett, J. R., Warren, N. J., Armes, S. P., Smallridge, M. J. & Cracknell, R. B. Order-Order Morphological Transitions for Dual Stimulus Responsive Diblock Copolymer Vesicles. *Macromolecules* **49**, 1016–1025 (2016).

36. Warren, N. J. *et al.* Critical Dependence of Molecular Weight on Thermoresponsive Behavior of Diblock Copolymer Worm Gels in Aqueous Solution. *Macromolecules* **51**, 8357–8371 (2018).

37. Ali, A. M. I. *et al.* Synthesis of poly(2-hydroxypropyl methacrylate) latex particles via aqueous dispersion polymerization. *Soft Matter* **3**, 1003–1013 (2007).

38. Blackman, L. D., Doncom, K. E. B., Gibson, M. I. & O'Reilly, R. K. Comparison of photo- and thermally initiated polymerization-induced self-assembly: A lack of end group fidelity drives the formation of higher order morphologies. *Polym. Chem.* **8**, 2860–2871 (2017).

39. Williams, M. *et al.* Bespoke cationic nano-objects: Via RAFT aqueous dispersion polymerisation. *Polym. Chem.* **7**, 3864–3873 (2016).

40. Tan, J. *et al.* Room Temperature Synthesis of Self-Assembled AB/B and ABC/BC Blends by Photoinitiated Polymerization-Induced Self-Assembly (Photo-PISA) in Water. *Macromolecules* **51**, 7396–7406 (2018).

41. Ren, K. & Perez-Mercader, J. Thermoresponsive gels directly obtained: Via visible light-mediated polymerization-induced self-assembly with oxygen tolerance. *Polym. Chem.* **8**, 3548–3552 (2017).

42. Blanazs, A. *et al.* Sterilizable Gels from Thermoresponsive Block Copolymer Worms. *J. Am. Chem. Soc.* **134**, 9741–9748 (2012).

43. Thompson, K. L. *et al.* Vermicious thermo-responsive Pickering emulsifiers. *Chem. Sci.* **6**, 4207–4214 (2015).

44. Warren, N. J. & Armes, S. P. Polymerization-induced self-assembly of block copolymer nano-objects via RAFT aqueous dispersion polymerization. *J. Am. Chem. Soc.* **136**, 10174–10185 (2014).

45. Ratcliffe, L. P. D., Derry, M. J., Ianiro, A., Tuinier, R. & Armes, S. P. A Single Thermoresponsive Diblock Copolymer Can Form Spheres, Worms or Vesicles in Aqueous Solution. *Angew. Chemie - Int. Ed.* **58**, 18964–18970 (2019).

46. Liu, X. *et al.* A dual responsive targeted drug delivery system based on smart polymer coated mesoporous silica for laryngeal carcinoma treatment. *New J. Chem.* **38**, 4830–4836 (2014).

47. Fernyhough, C., Ryan, A. J. & Battaglia, G. pH controlled assembly of a polybutadiene-poly(methacrylic acid) copolymer in water: Packing considerations and kinetic limitations. *Soft Matter* **5**, 1674–1682 (2009).

48. Canning, S. L. *et al.* Highly-ordered onion micelles made from amphiphilic highly-branched copolymers. *Polym. Chem.* **9**, 5617–5629 (2018).

49. Yin, J., Dupin, D., Li, J., Armes, S. P. & Liu, S. pH-induced deswelling kinetics of sterically stabilized poly(2-vinylpyridine) microgels probed by stopped-flow light scattering. *Langmuir* **24**, 9334–9340 (2008).

50. Sakai, K. *et al.* pH-responsive behavior of selectively quaternized diblock copolymers adsorbed at the silica/aqueous solution interface. *J. Colloid Interface Sci.* **314**, 381–388 (2007).

51. Falireas, P. G. & Vamvakaki, M. Triple-Responsive Block Copolymer Micelles with Synergistic pH and Temperature Response. *Macromolecules* **51**, 6848–6858 (2018).

52. Ruiz-Pérez, L. *et al.* Conformation of poiy(methacrylic acid) chains in dilute aqueous solution. *Macromolecules* **41**, 2203–2211 (2008).

53. Qu, Z., Xu, H. & Gu, H. Synthesis and biomedical applications of poly((meth)acrylic acid) brushes. *ACS Appl. Mater. Interfaces* **7**, 14537–14551 (2015).

54. Chaduc, I. *et al.* Batch emulsion polymerization mediated by poly(methacrylic acid) macroRAFT agents: One-pot synthesis of self-stabilized particles. *Macromolecules* **45**, 5881–5893 (2012).

55. Chaduc, I. *et al.* Effect of the ph on the raft polymerization of acrylic acid in water. Application to the synthesis of poly(acrylic acid)-stabilized polystyrene particles by RAFT emulsion polymerization. *Macromolecules* **46**, 6013–6023 (2013).

56. Cockram, A. A. *et al.* Optimization of the high-throughput synthesis of multiblock copolymer nanoparticles in aqueous media: Via polymerization-induced self-assembly. *React. Chem. Eng.* **3**, 645–657 (2018).

57. Cockram, A. A. *et al.* Effect of monomer solubility on the evolution of copolymer morphology during Polymerization-Induced Self-Assembly in aqueous solution. *Macromolecules* **50**, 796–802 (2017).

58. Upadhyaya, L. *et al.* Nanostructured mixed matrix membranes from supramolecular assembly of block copolymer nanoparticles and iron oxide nanoparticles. *Macromolecules* **49**, 7908–7916 (2016).

59. Semsarilar, M., Ladmiral, V., Blanazs, A. & Armes, S. P. Poly(methacrylic acid)-based AB and ABC block copolymer nano-objects prepared via RAFT alcoholic dispersion polymerization. *Polym. Chem.* **5**, 3466–3475 (2014).

60. Canning, S. L., Cunningham, V. J., Ratcliffe, L. P. D. & Armes, S. P. Phenyl acrylate is a versatile monomer for the synthesis of acrylic diblock copolymer nano-objects: Via polymerization-induced self-assembly. *Polym. Chem.* **8**, 4811–4821 (2017).

61. Mykhaylyk, O. O., Warren, N. J., Parnell, A. J., Pfeifer, G. & Laeuger, J. Applications of shear-induced polarized light imaging (SIPLI) technique for mechano-optical rheology of polymers and soft matter materials. *J. Polym. Sci. Part B Polym. Phys.* **54**, 2151–2170 (2016).

62. Laga, R. *et al.* Thermoresponsive Polymer Micelles as Potential Nanosized Cancerostatics. *Biomacromolecules* **16**, 2493–2505 (2015).

63. Save, M., Weaver, J. V. M., Armes, S. P. & McKenna, P. Atom transfer radical polymerization of hydroxy-functional methacrylates at ambient temperature: Comparison of glycerol monomethacrylate with 2-hydroxypropyl methacrylate. *Macromolecules* **35**, 1152–1159 (2002).

64. Skrabania, K., Miasnikova, A., Bivigou-Koumba, A. M., Zehm, D. & Laschewsky, A. Examining the UV-vis absorption of RAFT chain transfer agents and their use for polymer analysis. *Polym. Chem.* **2**, 2074–2083 (2011).

65. Rosselgong, J., Armes, S. P., Barton, W. & Price, D. Synthesis of highly branched methacrylic copolymers: Observation of near-ideal behavior using RAFT polymerization. *Macromolecules* **42**, 5919–5924 (2009).

66. Ratcliffe, L. P. D., Ryan, A. J. & Armes, S. P. From a water-immiscible monomer to block copolymer nano-objects via a one-pot RAFT aqueous dispersion polymerization formulation. *Macromolecules* **46**, 769–777 (2013).

67. Cockram, A. A. Novel Block Copolymer Nanoparticles via RAFT Aqueous Emulsion Polymerization. (University of Sheffield, 2018).

68. Spencer, H. G. A Note on Dissociation Constants of Polycarboxylic Acids. *J. Polym. Sci.* **56**, S25–S28 (1962).

69. Morawetz, H. Nature of the 'hypercoiled' form of poly(methacrylic acid) in water at low pH. *Macromolecules* **29**, 2689–2690 (1996).

70. Lovett, J. R., Warren, N. J., Ratcliffe, L. P. D., Kocik, M. K. & Armes, S. P. pH-responsive non-ionic diblock copolymers: Ionization of carboxylic acid end-groups induces an order-order morphological transition. *Angew. Chemie - Int. Ed.* **54**, 1279–1283 (2015).

71. Madsen, J., Armes, S. P. & Lewis, A. L. Preparation and Aqueous Solution Properties of New Thermoresponsive Biocompatible ABA Triblock Copolymer Gelators. *Macromolecules* **39**, 7455–7457 (2006).

72. Madsen, J., Armes, S. P., Bertal, K., MacNeil, S. & Lewis, A. L. Preparation and aqueous solution properties of thermoresponsive biocompatible AB diblock copolymers. *Biomacromolecules* **10**, 1875–1887 (2009).

73. Penfold, N. J. W., Whatley, J. R. & Armes, S. P. Thermoreversible Block Copolymer Worm Gels Using Binary Mixtures of PEG Stabilizer Blocks. *Macromolecules* **52**, 1653–1662 (2019).

74. Madsen, J. *et al.* Biocompatible wound dressings based on chemically degradable triblock copolymer hydrogels. *Biomacromolecules* **9**, 2265–2275 (2008).

Chapter 3

Is poly(methacrylic acid)-poly(2-hydroxypropyl methacrylate) an effective block copolymer dispersant for carbon black particles?

3.1 Introduction

Manufacture of printing inks is a highly specialised process and research in this field is essential for a wide range of technologies.[1,2] The development of pigment-based inkjet compositions is becoming more widespread, as they result in better image permanence than dye-based inks. Moreover, dyes are more susceptible to blotting and spreading owing to their solubility.[3]

Preparation of pigmented inks involves two steps. First, the pigment is milled in the presence of a polymeric dispersant to break up the aggregates into primary particles. Second, the resulting dispersion of primary particles is diluted and formulated to afford the final ink composition. The choice of polymeric dispersant in the milling step is important because it facilitates wetting, breaks up agglomerates, and ultimately determines the primary pigment size. The dispersant also ensures stability for the final ink composition.[4] Dispersed primary particles are thermodynamically unstable with respect to aggregation, so repulsive forces must be introduced to offset the ever-present van der Waals attractive forces. This is achieved *via* steric stabilisation, which is conferred by adsorption of the polymeric dispersant at the pigment surface.[5] Therefore, the primary function of a good dispersant is to extend shelf life by preventing the aggregation of pigment particles and their ensuing sedimentation.

It is well known within the coatings industry that an effective polymeric dispersant for colloidal particles requires both a strong anchoring group and a highly repulsive, soluble component to confer steric stabilisation.[1,6,7] Various copolymer architectures can be used, e.g. homopolymers, random or statistical copolymers, tapered/gradient copolymers, comb copolymers or block copolymers.[8–11] It is also known that polyelectrolytes can act as suitable steric stabilisers.[12,13] More specifically, anionic polymeric dispersants are particularly useful for inkjet printing owing to their strong interaction with surface-treated paper substrates.[14,15]

Amphiphilic block copolymers bearing an anionic stabiliser block can provide strong anchoring at the surface of various pigments.[16]

Low molecular weight polymeric dispersants can be prone to desorption from the pigment surface at high temperatures, resulting in poor long-term stability.[17,18] High molecular weight polymers are preferable, especially those which enable the formulation of low-viscosity pigment dispersions. Example here include hyperbranched structures and self-assembled nanoparticles.[19,20] Such dispersants form relatively thick adsorbed stabiliser layers around the pigment particles, resulting in more effective steric stabilisation.

Dispersant efficiency can be determined using several analytical techniques. The most useful technique is particle size analysis by either analytical centrifugation or dynamic light scattering. The particle size distribution enables the degree of dispersion of the primary pigment particles to be assessed. In general, the industry requirement for inkjet applications is that the mean particle diameter must be below 500 nm to enable the formulation to pass through a printer nozzle head without blocking it. Dispersant performance can also be assessed by viscosity measurements: a minimum in dispersion viscosity at a fixed pigment concentration is known as the 'surfactant demand' of the pigment.[21] This is where the system is assumed to be fully dispersed. Excess dispersant can cause depletion flocculation, which increases the dispersion viscosity.[21] This is because the dispersant is located in the continuous phase, as well as adsorbed at the surface of the pigment particles.[22] Optical and electron microscopy can be used to assess the pigment morphology and determine the relative proportion of primary particles and aggregates.[23] Other important characterisation techniques include evaluating colour quality by transmission, reflectivity and opacity measurements.[24]

The chemistry of carbon black has been a topic of scientific interest for many years.[25–29] It is widely used as a reinforcing agent, for semiconductive materials, for UV-resistant composites, as well as for coatings, inks and toner applications.[30,31] It usually comprises a

fine powder composed mainly of elemental carbon and with a relatively high surface area per unit mass.[32] For use in paints, coatings or inks, carbon black must be formulated as a colloidally stable dispersion.[25]

Carbon black has a complex fractal morphology with characteristic length scales ranging from nanometres to microns (see **Figure 3.1**).[33–35]
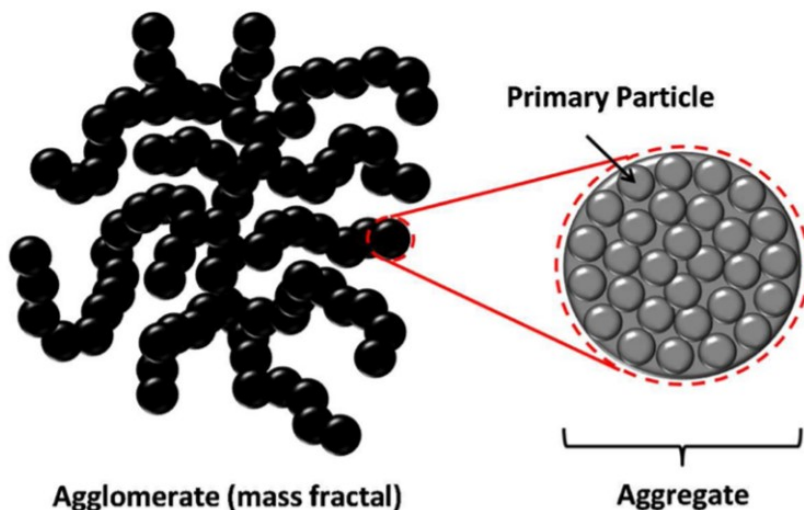

Figure 3.1 Schematic cartoon illustrating the three structural morphologies identified for carbon black and diesel soot *via* SAXS analysis. The rough surface fractal nature of the primary particles (and aggregates) is not shown in this cartoon.[34] Reproduced from Reference 34.

The carbon black used in this chapter was produced *via* the furnace process, accounting for 98% of carbon black consumed worldwide.[36] It forms carbon black by blowing petroleum oil as a feedstock into high temperature gases to partially combust them. This method allows for control over morphology.[37,38]

When used as a pigment, carbon black is more effective at absorbing light than any other material on a weight or cost basis.[32] This is determined by the size of the aggregates: a higher degree of dispersion leads to greater colour strength.[39] Colour properties are usually treated

empirically, because aggregate and primary particle size of carbon black cannot be controlled independently.[40]

Inkjet-grade carbon black is typically surface-treated using oxidising agents to introduce hydroxyl or carboxylic acid groups. Incorporating such hydrophilic groups aids the formation of aqueous carbon black dispersions and improves the degree of dispersion and flow characteristics in pigment vehicle systems.[32] Organic pigments are generally harder to disperse than inorganic pigments because their finer size makes effective wetting more difficult to achieve.[41]

The carbon black grade evaluated in this Thesis is Printex L6. This has been studied for various applications, including use as an electrocatalyst for oxygen reduction,[30,42] and in water-based inkjet dispersions.[43] As noted above, carbon black has a complex fractal morphology rather than a spherical morphology. Nevertheless, it can sometimes be useful to consider the sphere-equivalent diameter when calculating the amount of polymeric dispersant required.[31]

In principle, $PMAA_x$-$PHPMA_y$ copolymers of any composition exhibit similar pH and temperature responsive behaviour as shown in Chapter 2, with the exact transition values depending on the precise length of each block. In this Chapter, $PMAA_x$-$PHPMA_y$ diblock copolymers of varying compositions are evaluated as a new dispersant for Printex L6 carbon black particles in aqueous media. These are compared to systems such as PMAA-*stat*-PHPMA, PMAA-*b*-PBzMA and PMAA-*stat*-PBzMA, to compare anchoring blocks of varying hydrophobicity.

3.2 Experimental

Materials

Methacrylic acid (MAA; 99%) and 4-cyanopropyl dithiobenzoate (CPDB) were purchased from Sigma-Aldrich (UK) and used without further purification. 4,4′-Azobis(4-cyanovaleric acid) (ACVA; 98%) was purchased from Alfa Aesar (UK) and used as received. HPMA was donated by GEO Specialty Chemicals. Methanol-d_4 and dimethyl sulfoxide-d_6 was purchased from Goss Scientific Ltd (Cheshire, UK). Deuterium oxide (D_2O), sodium deuteroxide (NaOD) and deuterium chloride (DCl) were purchased from Sigma-Aldrich (Dorset, UK). All other solvents were purchased from Fisher Scientific (Loughborough, UK) and used as received. Deionized water was used for all experiments. Inkjet-grade Printex L6 carbon black was kindly supplied by Lubrizol (Blackley, Manchester).

Synthesis of the poly(methacrylic acid) (PMAA) steric stabilizer

See **Chapter 2, Section 2.2.**

Synthesis of linear poly(methacrylic acid)-poly(2-hydroxypropyl methacrylate) diblock copolymer nanoparticles *via* RAFT aqueous dispersion polymerization of HPMA

This RAFT aqueous dispersion polymerization synthesis was conducted at 20% w/w solids targeting PMAA$_{50}$-PHPMA$_{100}$. HPMA (0.350 g, 2.4 mmol), ACVA (1.70 mg, 6.06 μmol, CTA/initiator molar ratio = 4.0), and a PMAA$_{50}$ macro-CTA (109 mg, 24.3 μmol) were dissolved in water (4.15 g). The solution pH was adjusted to 5.5 using an aqueous solution of 1 M NaOH. The pink reaction mixture was sealed in a round-bottomed flask, purged with nitrogen for 30 min, and then placed in a pre-heated oil bath at 70 °C for 2 h.

Synthesis of linear poly(methacrylic acid)-poly(benzyl methacrylate) diblock copolymer nanoparticles *via* RAFT aqueous emulsion polymerisation of BzMA

This RAFT aqueous emulsion polymerization synthesis was conducted at 20% w/w solids targeting PMAA$_{50}$-PBzMA$_{100}$. BzMA (0.700 g, 3.97 mmol), ACVA (1.79 mg, 3.97 μmol, CTA/initiator molar ratio = 4), and a dithiobenzoate-functionalised PMAA$_{50}$ macro-CTA (180 mg, 39.7 μmol) were dissolved in water (3.53 g). The solution pH was adjusted to 5.5 using an aqueous solution of 1 M NaOH. The pink reaction mixture was sealed in a round-bottomed flask, purged with nitrogen for 30 min, and then placed in a pre-heated oil bath at 70 °C for 6 h.

Synthesis of poly(methacrylic acid-*stat*-2-hydroxypropyl methacrylate) copolymer *via* RAFT alcoholic solution copolymerisation of MAA and HPMA

This RAFT alcoholic solution copolymerisation synthesis was conducted at 20% w/w solids targeting P(MAA$_{50}$-*stat*-HPMA$_{100}$). MAA (0.500 g, 5.81 mmol), HPMA (1.67 g, 11.6 mmol), CPDB (25.7 mg, 116 μmol), ACVA (6.51 mg, 0.23 μmol, CTA/initiator molar ratio = 5), were dissolved in anhydrous ethanol (5.14 g). The pink reaction mixture was sealed in a round-bottomed flask, purged with nitrogen for 30 min, and then placed in a pre-heated oil bath at 70 °C for 16 h. The resulting copolymer was purified by precipitation into diethyl ether, then isolated *via* lyophilisation.

Synthesis of poly(methacrylic acid)-*stat*-poly(benzyl methacrylate) copolymer *via* RAFT solution polymerisation in ethanol

This RAFT aqueous solution polymerisation synthesis was conducted at 20% w/w solids targeting P(MAA$_{50}$-*stat*-BzMA$_{100}$). MAA (0.500 g, 5.81 mmol), BzMA (2.04 g, 11.6 mmol), CPDB (25.7 g, 116 μmol) and ACVA (6.51 mg, 0.23 μmol, CTA/initiator molar ratio = 5), were dissolved in ethanol (6.02 g). The pink reaction mixture was sealed in a round-bottomed

flask, purged with nitrogen for 30 min, and then placed in a pre-heated oil bath at 70°C for 16 h. The resulting copolymer was purified by precipitation into diethyl ether, then isolated *via* lyophilisation.

Preparation of polymer-stabilised carbon black dispersions – Trident vial

A typical dispersion protocol was conducted as follows: 3.50 g glass beads were added to a Trident vial (20 ml capacity). Dry pigment (1.00 g) was added to the vial, then varying amounts of copolymer were added, e.g. for 50% unit mass of copolymer per unit mass of pigment using a 20% w/w copolymer dispersion, 2.5 g of the copolymer dispersion was added. The vials were then made up to 10 g with deionised water and placed on a high energy mechanical shaker for 16 h prior to analysis.

Dynamic Light Scattering (DLS)

Carbon black dispersions were diluted to 0.1% w/w using deionised water. Hydrodynamic diameters were measured at 25 °C using a Malvern Zetasizer NanoZS model ZEN 3600 instrument equipped with a 4 mW He−Ne solid-state laser operating at 633 nm. Back-scattered light was detected at 173°, and the mean particle diameter was calculated from the quadratic fitting of the correlation function over ten runs of 10 seconds duration. All measurements were performed three times using disposable 1 cm plastic cuvettes and data were analysed using cumulants analysis of the experimental correlation function using Dispersion Technology Software version 6.20.

Aqueous electrophoresis

Zeta potentials were determined for dilute aqueous carbon black dispersions and copolymer dispersions using the same Malvern Zetasizer Nano ZS instrument described above. The solution pH was initially adjusted to pH 11 in the presence of 1 mM KCl background

electrolyte using 0.5 M NaOH. The solution pH was then manually lowered using either 0.1 M or 0.01 M HCl as required.

Transmission Electron Microscopy (TEM)

Studies were conducted using a Philips CM100 microscope operating at 100 kV on unstained samples prepared by drying a single droplet of a ~ 0.01% w/w aqueous dispersion on a carbon-coated copper grid.

^{1}H NMR Spectroscopy

^{1}H NMR spectra were recorded for diblock copolymers dissolved in CD_3OD using a Bruker 400 MHz NMR spectrometer (64 scans per spectrum). Mean degrees of polymerisation were determined by end-group analysis.[44]

Analytical Centrifugation

The mean diameters of carbon black aggregates were determined using a LUMiSizer® analytical photocentrifuge (LUM GmbH, Berlin, Germany) at 25 °C. Measurements were conducted on 0.5% w/w carbon black dispersions in water at 3500 rpm using 2 mm pathlength polyamide cells. The LUMiSizer® employs STEP™ Technology (Space- and Time-resolved Extinction Profiles) that allows the measurement of the intensity of transmitted light as a function of time and position over the entire cell length simultaneously. The progression of these transmission profiles contains information on the rate of sedimentation. This sedimentation velocity is used to calculate a particle size distribution, if the particle density is accurately known.

Thermogravimetric Analysis

Analyses were conducted on polymeric dispersants, carbon black alone and dispersant-coated carbon black particles. Each sample was heated under air up to 800 °C at a heating rate of 10 °C min^{-1} using a Q500 TGA instrument (TA Instruments). The mass loss observed between

300 and 500 °C was attributed to complete pyrolysis of the diblock copolymer, and mass loss above 700 °C was attributed to complete combustion of carbon black.

Solution Densitometry

Densitometry measurements were conducted at 20 °C on aqueous copolymer solutions using an Anton Paar DMA 5000 M density meter. A linear calibration curve was constructed using copolymer dispersions with concentrations ranging between 0 and 10 g dm^{-3}. This calibration curve was then used to calculate the copolymer concentration in supernatant solutions (obtained after centrifugation of the pigment particles) after determining the corresponding solution density in each case.

Viscosity Measurements

These studies were conducted using an Ostwald viscometer immersed in a water bath at 20 °C. Each measurement was repeated five times and the date were averaged. The solution viscosity was calculated from the viscosity of a known solvent i.e. water at 20 °C has a viscosity of 0.001 Pa.s.

Optical Microscopy

0.10 % w/w carbon black dispersions were placed on a microscope slide and covered with a coverslip. Digital images were recorded using a Motic DMBA300 digital biological microscope equipped with a built-in camera and Motic Images Plus 2.0 ML software.

Helium pycnometry

The solid-state density of the Printex L6 carbon black was measured to be 1.95 g cm^{-3} using a Micrometrics AccuPyc 1330 helium pycnometer at 20 °C.

Specific surface area analysis

BET surface area measurements were performed using a Quantachrome Nova 1000e instrument with dinitrogen gas (mean area per molecule = 16.2 Å^2) as an adsorbate at 77 K. Samples were degassed under vacuum at 100 °C for at least 16 h prior to analysis. The particle diameter, d, was calculated using the formula $d = 6/(\rho.A_s)$, where A_s is the BET specific surface area in $m^2\,g^{-1}$ and ρ is the carbon black density in $g\,m^{-3}$ obtained from helium pycnometry.

Surface tension

Surface tension was determined by the platinum ring method using a Lauda Tensiometer TDI (Lauda-Konigshofen, Germany) at 25.0 ± 0.5 °C. Ten measurements were taken at each concentration and averaged for CMC measurements.

3.3 Results and Discussion

3.3.1 Dispersion Characterisation

The inkjet-grade Printex L6 carbon black was characterised by aqueous electrophoresis, optical microscopy, BET surface area analysis, helium pycnometry, and dynamic light scattering **(Figures 3.1 and 3.2)**. Firstly, the zeta potential vs. pH curve obtained by aqueous electrophoresis analysis shows that the carbon black aggregates are cationic below pH 9, which corresponds to the pH range that is relevant to pigment dispersion applications. This was not unexpected because this carbon black is known to have alkaline character. This should make it well suited to an anionic dispersant.
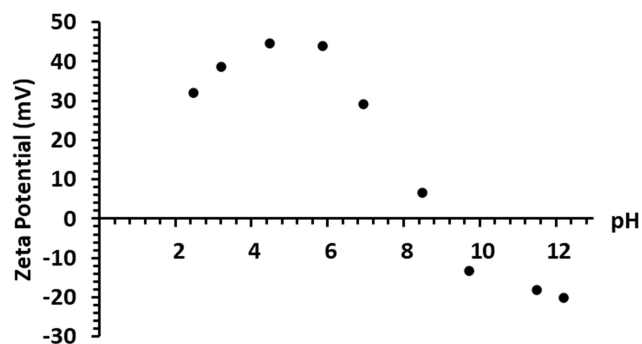
Figure 3.1 Zeta potential vs. pH curve obtained for Printex L6 carbon black aggregates (0.1% w/w in 1mM KCl), indicating cationic character below pH 9.
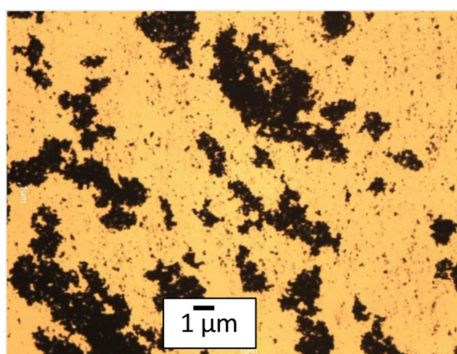
Figure 3.2 Optical microscopy image recorded for micron-sized carbon black aggregates dispersed in water in the absence of any dispersant.

If dispersion in deionised water is attempted with no additives, these carbon black particles are poorly dispersed, with optical microscopy analysis indicating the formation of relatively large, micron-sized aggregates (**Figure 3.2**). DLS measurements suggested that the hydrodynamic diameter of these 'primary aggregates' was approximately 166 nm. This is in agreement with the accepted hierarchical structural model for carbon black. However, substantial sedimentation was observed in the cuvette during such experiments, so the reported value substantially underestimates the true aggregate size.

The specific surface area of this carbon black indicated by BET measurements using N_2 at 77 K is 226 m^2 g^{-1}. Its density was determined to be 1.95 g cm^{-3} using helium pycnometry

(averaged over ten measurements). These two values can be used to calculate the primary grain size using **Equation 3.1**.[45]

$$A_S = \frac{3}{\rho . R} \ (\mathbf{3.1})$$

Here A_s is the specific surface area, ρ is the solid-state density, and R is the primary grain radius. This results in a primary grain diameter of approximately 14 nm. This is in very good agreement with SAXS measurements of carbon black primary particles.[46]

3.3.2 Initial Dispersant Screening Studies

Initial screening experiments were undertaken to identify an effective copolymer dispersant for this carbon black. These preliminary studies involved a 1.0% w/w aqueous dispersion of carbon black particles prepared using 1.0% w/w copolymer. Two block copolymers were prepared containing PMAA as the steric stabiliser component because anionic polyelectrolytes are often effective in this context.[46–48] PBzMA and PHPMA were compared as adsorbing anchor blocks, with the former block known to be significantly more hydrophobic than the latter. The corresponding statistical copolymers were also investigated (**Scheme 3.1**). These four putative copolymer dispersants are summarised in **Table 3.1**.
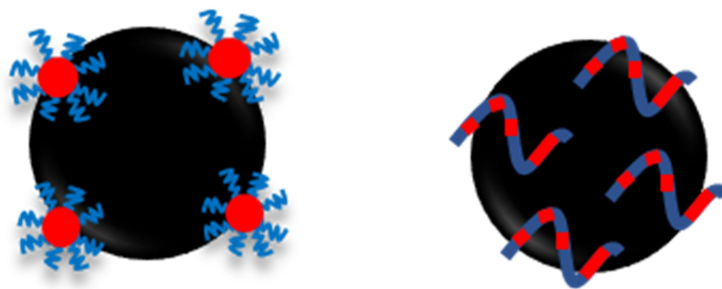
Scheme 3.1 Schematic representation of dispersion of a carbon black aggregate with nanoparticles (left) where PBzMA or PHPMA form the red core-forming block, versus a statistical copolymer dispersant (right).

Table 3.1 Summary of initial polymer compositions and structures screened for their effectiveness as dispersants for Printex L6.

Sample	Composition	Copolymer Structure
A	PMAA$_{50}$-b-PHPMA$_{100}$	Block
B	PMAA$_{50}$-b-PBzMA$_{100}$	Block
C	PMAA$_{50}$-$stat$-PBzMA$_{100}$	Statistical
D	PMAA$_{50}$-$stat$-PHPMA$_{100}$	Statistical

These copolymer-stabilised carbon black dispersions were allowed to stand in sample vials at 20 °C over the course of one month. Sample **C** sedimented after just 10 min, but the other three dispersions remained colloidally stable (no visible sedimentation) after 30 days. These dispersions were then evaluated by analytical centrifugation using a LUMiSizer instrument (**Figure 3.3**). Sedimentation velocity is a raw measurement from the LUMiSizer, which enables a particle size distribution to be calculated with knowledge of particle density. The cumulative sedimentation velocity can be used to determine the timescale on which a dispersion will sediment due to colloidal instability.

As expected, the PMAA$_{50}$-$stat$-PBzMA$_{100}$ stabilised carbon black particles sedimented much faster than the other dispersions, which have similar sedimentation profiles. However, it appears that carbon black dispersions prepared using the two diblock copolymer dispersants have slightly slower sedimentation velocities, indicating greater colloidal stability and/or smaller aggregates. This confirms the importance of having a well-defined anchoring block, rather than anchoring groups randomly distributed along the copolymer chains. The PMAA$_{50}$-b-PHPMA$_{100}$ diblock copolymer is the most effective dispersant in this case, as it has the smallest sedimentation velocity. PHPMA is less hydrophobic than PBzMA, which could affect its extent of adsorption at the surface of the pigment particles.
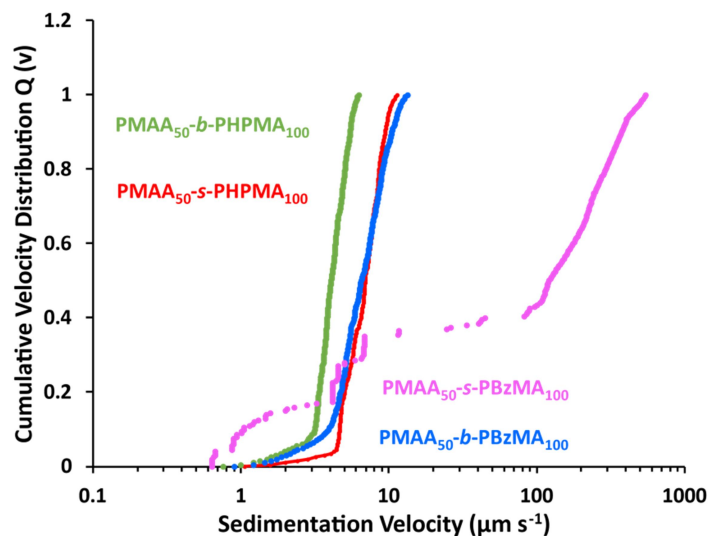
Figure 3.3 Sedimentation velocity profiles obtained using analytical centrifugation (LUMiSizer instrument) for aqueous carbon black dispersions prepared using PMAA$_{50}$-s-PBzMA$_{100}$ (pink trace), PMAA$_{50}$-b-PBzMA$_{100}$ (blue trace), PMAA$_{50}$-s-PHPMA$_{100}$ (red trace), PMAA$_{50}$-b-PHPMA$_{100}$ (green trace).
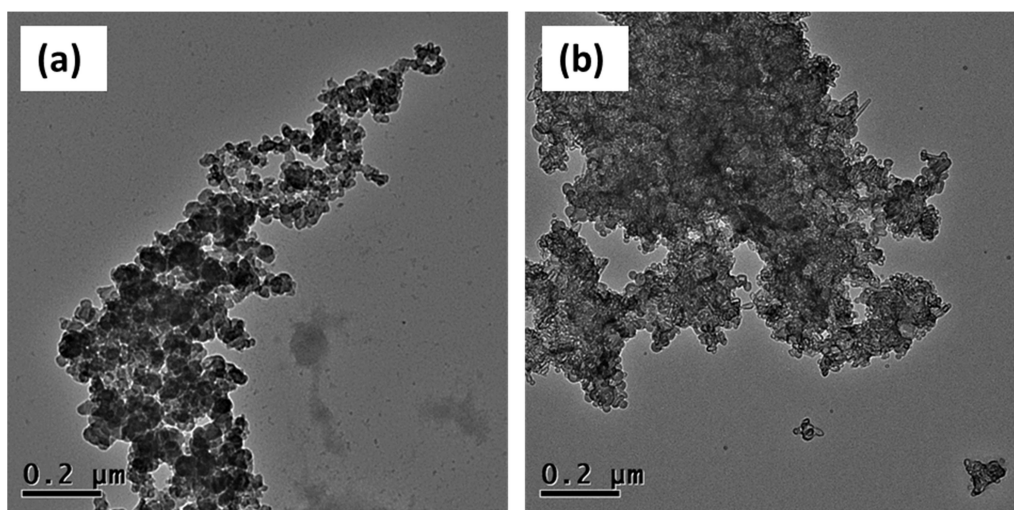
Figure 3.4 TEM images recorded for (a) carbon black particles dispersed using PMAA$_{50}$-b-PHPMA$_{100}$ and (b) carbon black particles dispersed with PMAA$_{50}$-b-PBzMA$_{100}$. The former appear to be somewhat less flocculated than the latter.

The TEM images shown in **Figure 3.4** suggest a difference in the degree of dispersion of the carbon black particles depending on the type of copolymer dispersant. More specifically, a somewhat higher degree of dispersion seems to be achieved when using PMAA$_{50}$-b-

PHPMA$_{100}$ compared to PMAA$_{50}$-b-PBzMA$_{100}$. This is consistent with the significant difference in colloidal stability indicated by the corresponding analytical centrifugation experiments. However, in both cases the aggregates are much larger than the primary grain size indicated by BET measurements.

Some pigment dispersions were then prepared on a larger scale to investigate their effectiveness at higher solids. These formulations utilised 10% w/w carbon black and 20% w/w copolymer dispersant. Particle size distributions were again assessed using dynamic light scattering. In **Table 3.2** the block structures of PMAA$_{50}$-PBzMA$_{100}$ and PMAA$_{50}$-PHPMA$_{100}$ are compared to a non-ionic commercial dispersant used for carbon black by Lubrizol.

According to Lubrizol scientists, the minimum acceptable particle size for this type of test is 400 nm. Therefore, all three dispersants pass this initial requirement. Interestingly, the PMAA$_{50}$-PHPMA$_{100}$ copolymer outperforms the non-ionic commercial dispersant in the longer-term stability test, which involved placing each dispersion in a 70 °C oven for 7 days **(Table 3.2)**.

Table 3.2 Summary of hydrodynamic diameters obtained for dilute aqueous dispersions of carbon black aggregates prepared using three different dispersants. Intensity-average particle diameters were determined for initial dispersions (24 h after their preparation) and again after storage of these dispersions in a 70°C oven for 7 days.

Dispersant	Average Particle Diameter after 24 h (nm)	Average Particle Diameter after 7 days at 70 °C (nm)
PMAA$_{50}$-b-PBzMA$_{100}$	398	2000
PMAA$_{50}$-b-PHPMA$_{100}$	189	182
Non-ionic Commercial Dispersant	156	218

In view of this promising finding, several stimulus-responsive compositions of PMAA$_{x}$-PHPMA$_{y}$ diblock copolymers were identified based on the findings presented in Chapter 2 were compared to assess their dispersant performance for carbon black. The sedimentation

velocities obtained for $PMAA_{43}$-$PHPMA_{235}$, $PMAA_{43}$-$PHPMA_{250}$ and $PMAA_{43}$-$PHPMA_{275}$ are compared in **Figure 3.5**. These copolymers were chosen from a small-scale screening experiment which indicated better dispersant performance than that achieved with $PMAA_{50}$-$PHPMA_{100}$. DLS studies show that these copolymer compositions are thermoresponsive, they form molecularly dissolved chains on cooling, however they do not form higher order morphologies on heating.
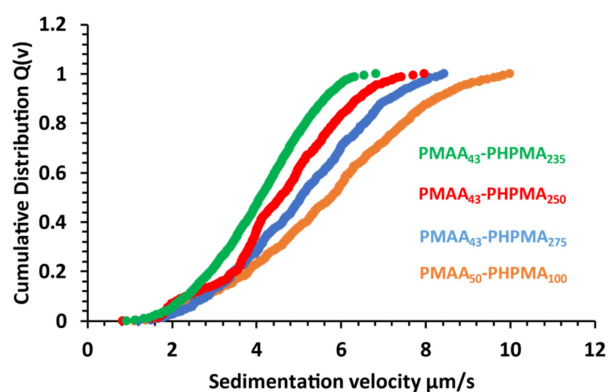

Figure 3.5 Sedimentation velocity profiles recorded for aqueous dispersions of carbon black particles prepared with three $PMAA_{43}$-$PHPMA_y$ diblock copolymer dispersants, where y = 235 (green), 250 (red) or 275 (blue). $PMAA_{43}$-$PHPMA_{235}$ provides the smallest sedimentation velocity, indicating the most effective colloidal stability. These are compared to the sedimentation profile of $PMAA_{50}$-$PHPMA_{100}$, indicating a clear increase in stability with these longer PHPMA blocks.

Figure 3.5 confirms that $PMAA_{43}$-$PHPMA_{235}$ is the most effective copolymer dispersant as the corresponding carbon black dispersion has the greatest colloidal stability (i.e., is least prone to sedimentation). According to Warren *et al.*, shorter PHPMA blocks are somewhat less hydrophobic than longer PHPMA blocks.[49] This means that the $PMAA_{43}$-$PHPMA_{235}$ nanoparticles are least likely to be kinetically frozen, which means that a higher proportion of free copolymer chains should be available for adsorption onto the surface of the pigment particles.

3.3.3 Evaluating the Dispersant Performance of PMAA$_{43}$-PHPMA$_{235}$ for Carbon Black

The chemical structure of the preferred dispersant is shown in **Figure 3.6a**. THF GPC was used to assess the molecular weight distributions of these diblock copolymer chains, see **Figure 3.6b**. This analysis could only be conducted after exhaustive methylation of the carboxylic acid groups on the PMAA block using trimethylsilyldiazomethane to ensure sufficient solubility to avoid column adsorption. After methylation, a relatively high blocking efficiency was confirmed for this diblock copolymer as there is little or no evidence for any PMAA precursor. The high molecular weight component in the diblock copolymer is likely due to crosslinking that occurred during the methylation process. Nonetheless, its M_n was 27 800 g mol^{-1} and its M_w/M_n was 1.37, suggesting that reasonably good RAFT control was achieved.
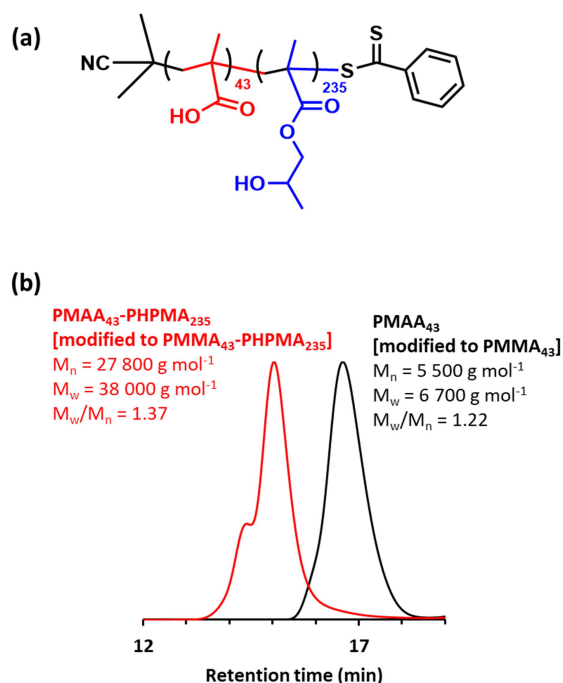
Figure 3.6 (a) Chemical structure for PMAA$_{43}$-PHPMA$_{235}$ and **(b)** THF GPC traces recorded for the PMAA$_{43}$ macro-CTA (black) and corresponding PMAA$_{43}$-PHPMA$_{235}$ diblock copolymer (after exhaustive methylation of their carboxylic acid residues) and their respective M_n, M_w and M_w/M_n data (expressed relative to a series of PMMA calibration standards).

This composition forms pH-responsive nanoparticles during HPMA polymerisation *via* PISA (**Figure 3.7**). Well-defined spheres are formed with a number-average diameter of 18 nm (calculated by TEM analysis of approximately 100 particles). This is consistent with the hydrodynamic *z*-average diameter of 24 nm reported by DLS at pH 7 (see Figure **3.7b**). The apparent particle size increases significantly below approximately pH 6.3 (see **Chapter 2, Figure 2.5**). This is because the PMAA block becomes protonated so it can no longer provide steric stabilisation, which leads to the formation of micron-sized aggregates. This reduction in colloidal stability coincides with the pK_a of the PMAA chains (i.e. the point at which 50% of the MAA units are ionised). This acid-induced flocculation is fully reversible: on returning to neutral pH the aggregates break up to form the original individual nanoparticles.
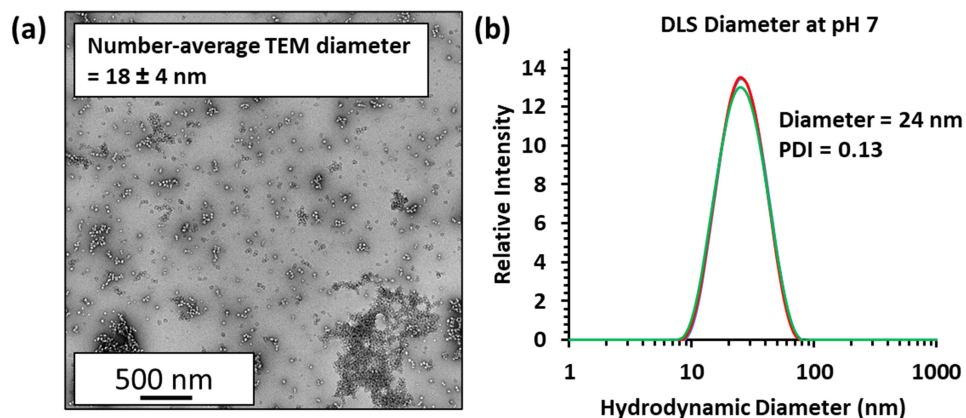
Figure 3.7 Particle size data obtained for $PMAA_{43}$-$PHPMA_{235}$ nanoparticles: (a) TEM image of 0.1% w/w solution of nanoparticles with number-average diameter = 18 nm (based on the analysis of 100 particles); (b) DLS particle size distribution of 0.1% w/w $PMAA_{43}$-$PHPMA_{235}$ diblock copolymer nanoparticles with an average hydrodynamic z-average diameter of 24 nm (PDI = 0.13) at pH 7.

The optimum copolymer concentration was identified for $PMAA_{43}$-$PHPMA_{235}$ by determining the dispersion viscosity and mean pigment diameter at a fixed pigment concentration (10 % w/w). It is well-known that the minimum viscosity and particle size correspond to monolayer coverage of the pigment particles.[50,51] This is because addition of too little copolymer to the pigment particles leads to submonolayer coverage and hence

bridging flocculation,[50] whereas too much copolymer leads to excess non-adsorbed chains that increase the dispersion viscosity and can lead to depletion flocculation.[52]
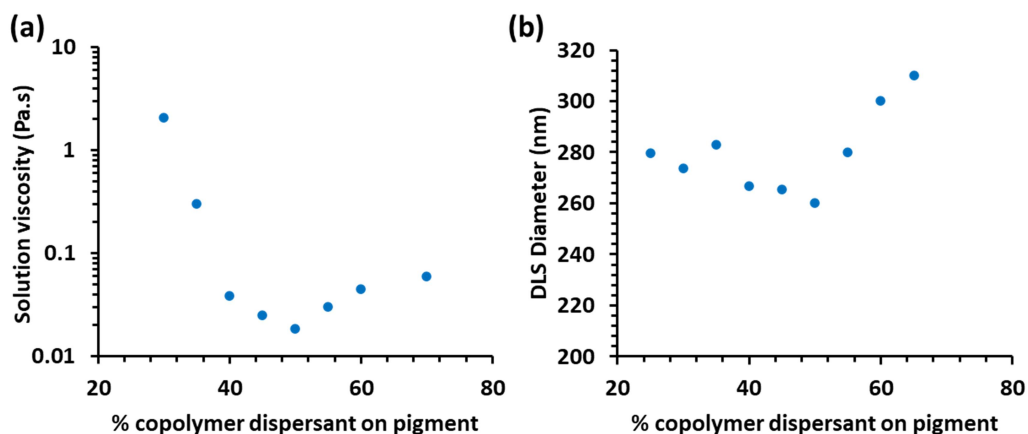

Figure 3.8 Dosage ladder determined for $PMAA_{43}$-$PHPMA_{235}$-stabilised carbon black particles by systematically varying the copolymer concentration at a fixed pigment concentration of 10% w/w. (a) The concentration dependence of the dispersion viscosity indicates that 50% dispersant mass based on pigment corresponds to monolayer coverage. (b) Similarly, DLS analysis of 0.1% pigment dispersions indicate a minimum in apparent particle size under the same conditions.

The results obtained for the so-called 'dosage ladder' experiment to determine optimal copolymer concentration for a given amount of pigment are shown in **Figure 3.8**. The minimum dispersion viscosity and particle size both occur at 50% copolymer dispersant based on the mass of pigment (5% w/w of total dispersion), indicating that this is the condition required for the highest degree of dispersion. This corresponds to an adsorbed amount of 0.18 mg m^{-2} for the copolymer dispersant chains at the surface of the pigment particles. According to Lubrizol scientists, a similar adsorbed amount is typically required when using the non-ionic commercial dispersant for commercial pigment dispersions.

Another important parameter that can affect dispersant performance is the aqueous surface tension. A lower surface tension enables the liquid to adhere to the pigment particles, in the first step of the dispersion process: the wetting stage.[53] A parameter known as the adhesion tension, calculated from the surface tension, gives a direct measure of the degree of

wettability of a solid by a liquid.[54] Flocculation and sedimentation can be caused by an undesirable interfacial tension relationship.[54]
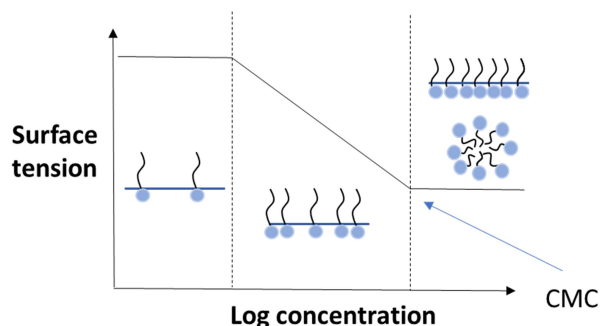

Figure 3.9 Schematic representation showing the how critical micelle concentration (CMC) can be identified from surface tension measurements at varying concentration.
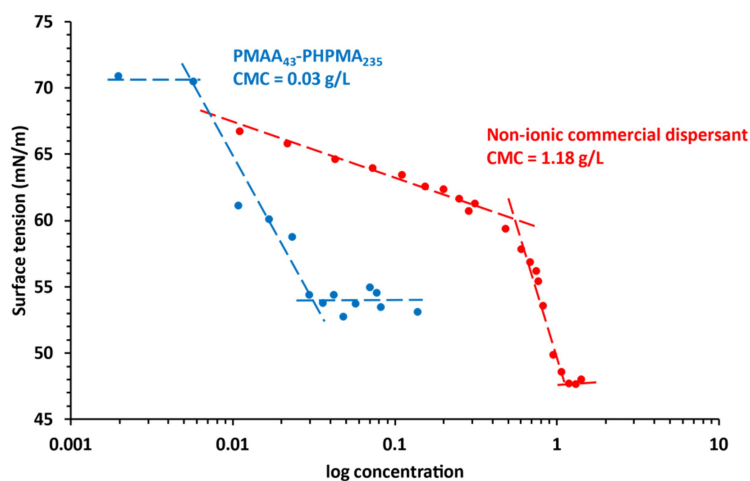

Figure 3.10 Surface tension vs. copolymer concentration plots for aqueous copolymer solutions at pH 7. The PMAA$_{43}$-PHPMA$_{235}$ copolymer dispersant (blue data set) has a CMC of 0.03 g gm^{-3} and the non-ionic commercial dispersant (red data set) has a CMC of 1.18 g dm^{-3}.

The CMC determined for the PMAA$_{43}$-PHPMA$_{235}$ copolymer dispersant is approximately 0.03 g dm^{-3} while the CMC for the non-ionic commercial dispersant is 1.18 g dm^{-3} (**Figure 3.10**). This corresponds to the point at which the copolymer concentration exceeds monolayer coverage at the interface. At higher copolymer concentration, micelles are formed in the bulk aqueous solution.[55] The lower CMC for PMAA$_{43}$-PHPMA$_{235}$ indicates that it is significantly

more effective at lowering the surface tension of the aqueous continuous phase, leading to more efficient wetting of the dry pigment particles. Generally, the minimal amount of wetting agent (typically a small molecule surfactant) should be used when formulating pigment dispersions to avoid interference with the dispersant.[1] Given its relatively high CMC, an additional wetting agent may be required for the non-ionic commercial dispersant. In contrast, the $PMAA_{43}$-$PHPMA_{235}$ copolymer can act as both a wetting agent and a dispersant, which reduces the complexity of the formulation.
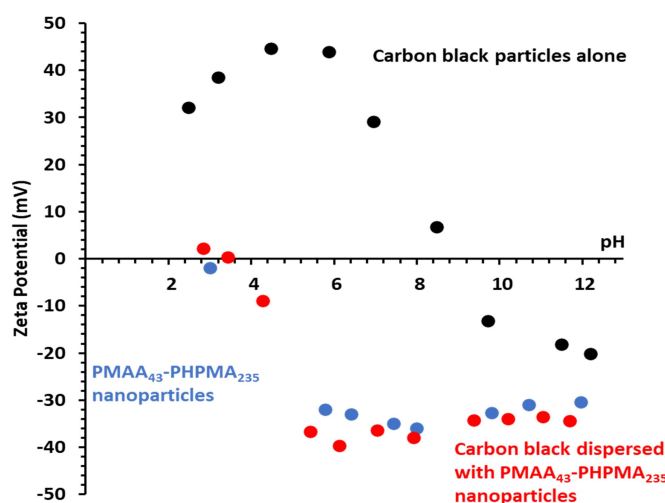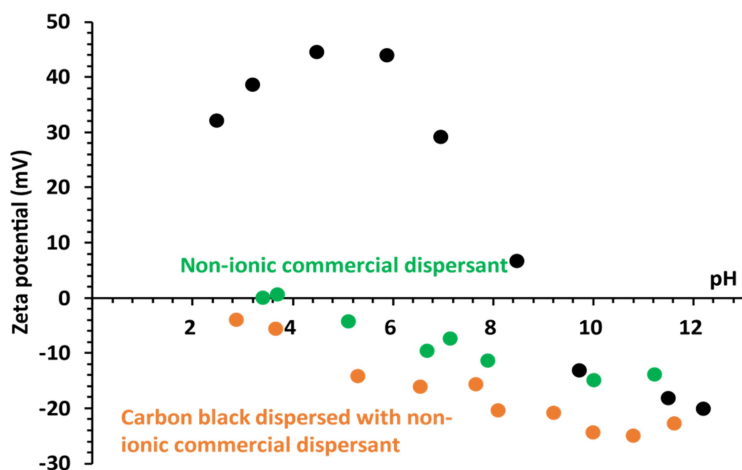

Figure 3.11 Zeta potential vs. pH curves determined in the presence of 1mM KCl for aqueous carbon black (Printex L6) particles alone (black data set), $PMAA_{43}$-$PHPMA_{235}$ nanoparticles (blue data set), and $PMAA_{43}$-$PHPMA_{235}$-stabilised carbon black particles (red data set). The similarity of the data sets for the latter two samples suggests that the carbon black particles are coated with $PMAA_{43}$-$PHPMA_{235}$, which confers steric stabilisation.

As shown in **Figure 3.11**, the carbon black particles (Printex L6) exhibit significant cationic character below pH 7 (black data; IEP ~ 8.7), whereas the $PMAA_{43}$-$PHPMA_{235}$ copolymer particles have strongly anionic character above pH 5 (blue data; IEP ~ 3.5). The zeta potential vs. pH curve recorded for $PMAA_{43}$-$PHPMA_{235}$-stabilised carbon black particles (red data) is strikingly similar to that obtained for the $PMAA_{43}$-$PHPMA_{235}$ nanoparticles alone over a wide pH range. This suggests essentially full coverage of the cationic pigment particles by the anionic nanoparticles. Maximum electrostatic attraction corresponds to around pH 5-6

because the carbon black pigment particles are highly cationic and the $PMAA_{43}$-$PHPMA_{235}$ nanoparticles are highly anionic under such conditions.

Figure 3.12 Zeta potential vs. pH curves determined in the presence of 1mM KCl for aqueous carbon black (Printex L6) particles alone (black data set), the non-ionic commercial dispersant (green data set), and the non-ionic commercial dispersant -stabilised carbon black particles (orange data set).

The non-ionic commercial dispersant is a neutral molecule, so its weakly anionic character may indicate adsorption of hydroxide ions.[56–58] Again, the cationic character of the carbon black particles is masked by surface adsorption of the non-ionic commercial dispersant, which confers weakly anionic character (**Figure 3.12**). Thus, these electrophoretic data are consistent with monolayer coverage of the pigment particles by the non-ionic commercial dispersant.

The effect of pH on the colloidal stability of both sterically-stabilised carbon black dispersions was studied in more detail (**Figure 3.13**). As discussed above, lower sedimentation velocities indicate a higher degree of dispersion for the pigment particles. In each case, the lowest sedimentation velocity of occurs at pH 7. For the $PMAA_{43}$-$PHPMA_{235}$-stabilised carbon black particles, there is a well-defined minimum sedimentation velocity at around ~ 3.8 μm s^{-1}, whereas there is much less scatter in the data obtained for the the non-ionic commercial dispersant -stabilised carbon black particles (note the log vs. linear scales).

However, the latter dispersion is much less sensitive to the precise dispersion pH, with sedimentation velocities remaining below 8.5 μm s^{-1} from pH 3.2 to pH 7.8. In contrast, relatively unstable dispersions are obtained when using the PMAA$_{43}$-PHPMA$_{235}$ nanoparticles below pH 4, with sedimentation velocities exceeding 100 μm s^{-1} under such conditions. However, sedimentation velocities remain at or below 9 μm s^{-1} from pH 7 to pH 10 (**Figure 3.13**). This pH-sensitivity can be explained by protonation of the PMAA block. At low pH (below the pK$_a$ of PMAA) these chains are protonated, have little or no anionic character and perform poorly as a steric stabiliser block.
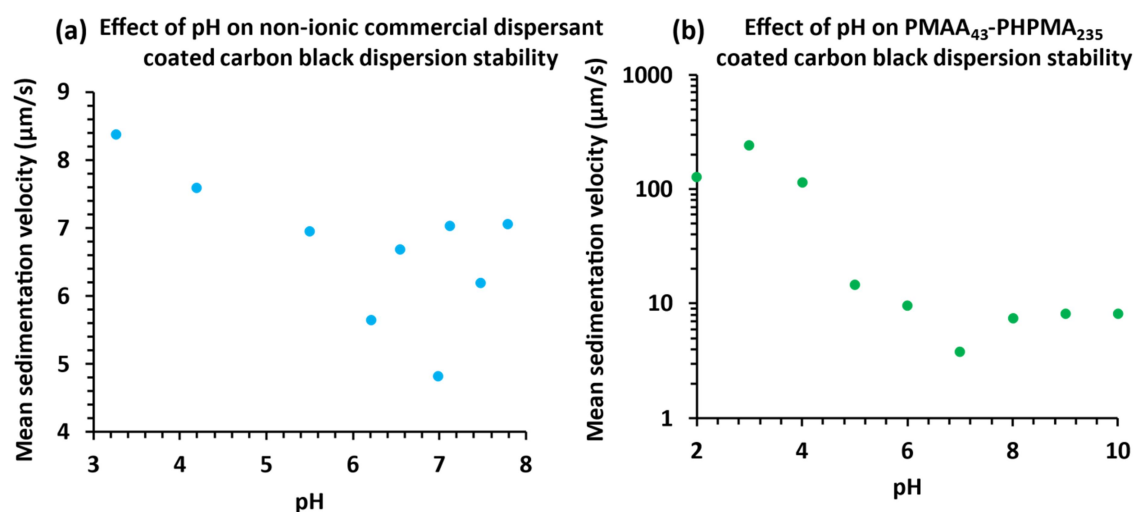
Figure 3.13 Sedimentation velocities obtained using a LUMiSizer instrument for **(a)** Non-ionic commercial dispersant-stabilised carbon black (Printex L6) particles and **(b)** PMAA$_{43}$-PHPMA$_{235}$-stabilised carbon black as a function of dispersion pH. In both cases, the smallest sedimentation velocity is observed at pH 7, which corresponds to the highest degree of dispersion for the pigment particles.

However, at higher pH (i.e. above the PMAA pK$_a$ of 6.3) this block acquires substantial anionic charge and confers electrosteric stabilisation to the pigment particles. Optimal colloidal stability is observed at pH 7, which corresponds to maximum electrostatic attraction between the anionic PMAA$_{43}$-PHPMA$_{235}$ nanoparticles and the cationic pigment particles (see **Figure 3.12**).

To measure the extent of polymer adsorption onto the carbon black pigment particles, an adsorption isotherm was constructed for both dispersants. In principle, thermogravimetric analysis can be used to measure adsorption directly,[31,34] while solution densitometry should be sufficiently sensitive to determine adsorbed amounts indirectly by supernatant assay. Adsorbed amounts were determined for pigment dispersions prepared using either the non-ionic commercial dispersant or $PMAA_{43}$-$PHPMA_{235}$ via centrifugation at 10,000 rpm for 30 min. Adsorption isotherms were constructed from the thermogravimetric curves shown in **Figures 3.14 and 3.15**. Carbon black undergoes complete combustion when heated up to 700 °C in air. However, both $PMAA_{43}$-$PHPMA_{235}$ and the non-ionic commercial dispersant undergo complete pyrolysis at 500 °C (see insets for **Figures 3.14 and 3.15**, respectively). In principle, this should enable the adsorbed amounts of copolymer to be determined. As expected, higher mass losses are observed at 500 °C in each case as the initial copolymer concentration is gradually increased.
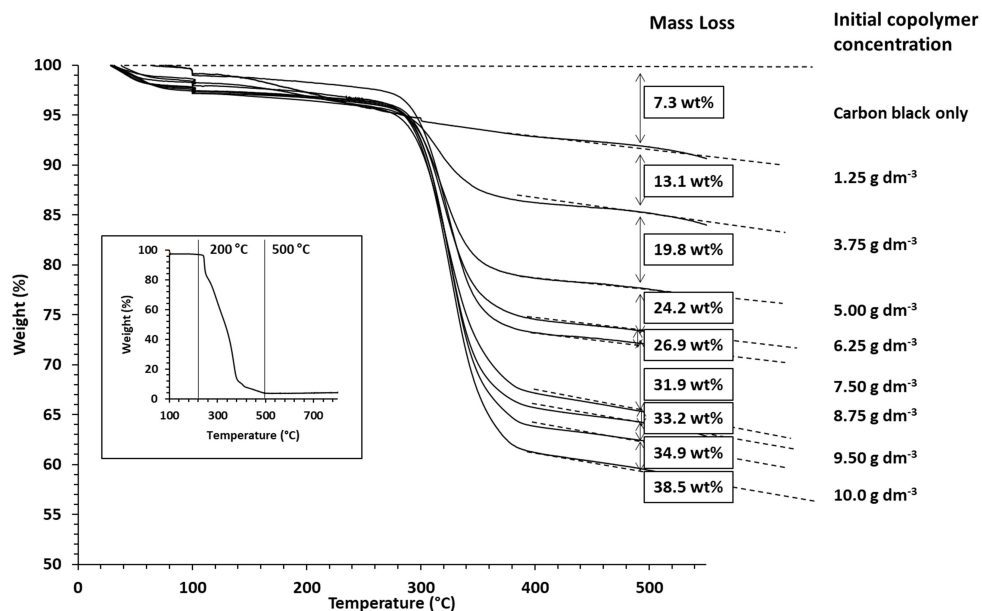

Figure 3.14 Thermogravimetric curves recorded for $PMAA_{43}$-$PHPMA_{235}$ nanoparticles adsorbed onto carbon black (Printex L6) particles at 10% w/w, pH 7. Analyses were performed in air at a heating rate of 10 °C per min. Under these conditions, the diblock copolymer (see inset) is completely pyrolysed at 500 °C. In contrast, carbon black does not undergo complete combustion until 700 °C. Arrows indicate successive mass loss at increasing copolymer concentrations.
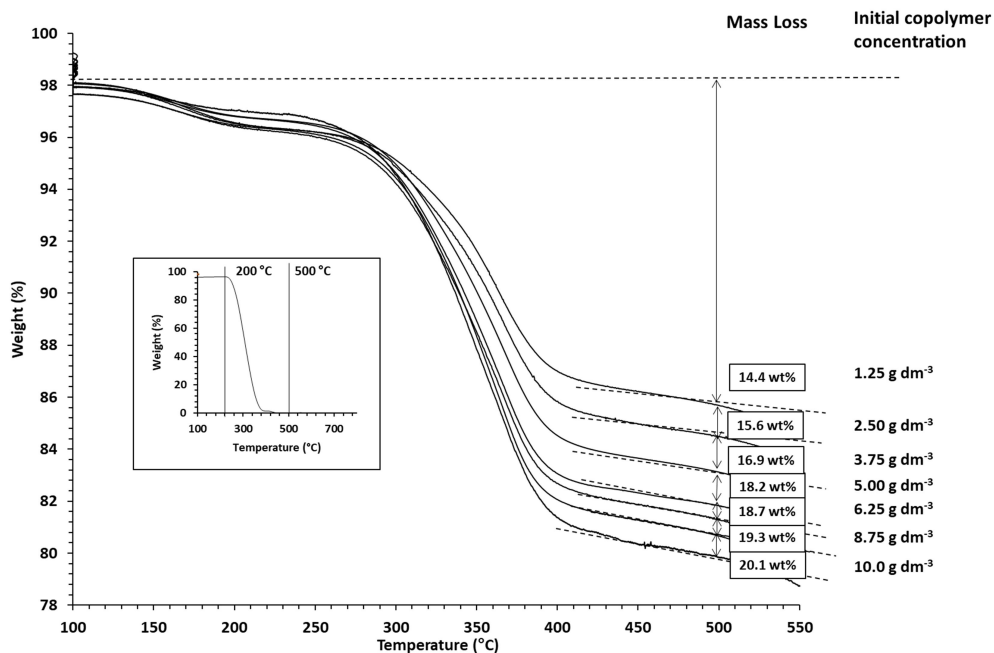
Figure 3.15 Thermogravimetric curves recorded for the non-ionic commercial dispersant adsorbed onto carbon black (Printex L6) pigment particles at 10% w/w pH 7. These analyses were performed in air at a heating rate of 10 °C per min. Under such conditions, the non-ionic commercial dispersant is completely pyrolysed at 500 °C (see inset). In contrast, carbon black does not undergo complete combustion until 700 °C. Arrows indicate successive mass loss at increasing copolymer concentrations.

For solution densitometry experiments, a calibration curve was constructed for each dispersant (**Figure 3.16**) to determine its concentration within a series of supernatants after centrifugation of the pigment particles.
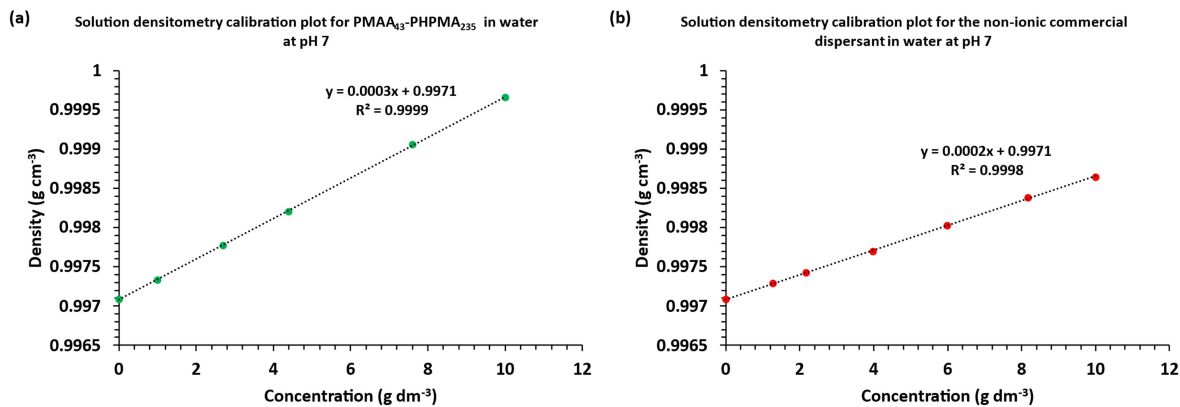
Figure 3.16 Linear calibration plots constructed at 25 °C using solution densitometry for (a) $PMAA_{43}$-$PHPMA_{235}$ and (b) the non-ionic commercial dispersant in aqueous solution at pH 7 between 0 and 10 g dm^{-3}.

The concentration of carbon black particles was fixed at 10 g dm^{-3} for all adsorption measurements. The adsorption behaviour of the non-ionic commercial dispersant follows a typical Langmuir isotherm (**Figure 3.17a**), with a well-defined plateau at an adsorbed amount of approximately 0.13 mg m^{-2} (measured by densitometry). This corresponds to monolayer coverage and is achieved at an equilibrium polymer concentration of approximately 4 g dm^{-3}. However, such supernatant assays can sometimes underestimate the adsorbed amount if centrifugation of the pigment particles also causes partial sedimentation of the excess non-adsorbed dispersant.[34] Centrifugation had to be conducted at 10 000 rpm for 30 min to achieve full sedimentation of the well-dispersed carbon black pigment particles. Even under such relatively harsh conditions, trace amounts of highly absorbing carbon black particles remained in the supernatant. Unfortunately, this was sufficient to prevent determination of the concentration of excess dispersant by UV-visible absorption spectroscopy. Thus, the concentration of non-adsorbed copolymer dispersant was instead determined by solution densitometry.[34,59,60]
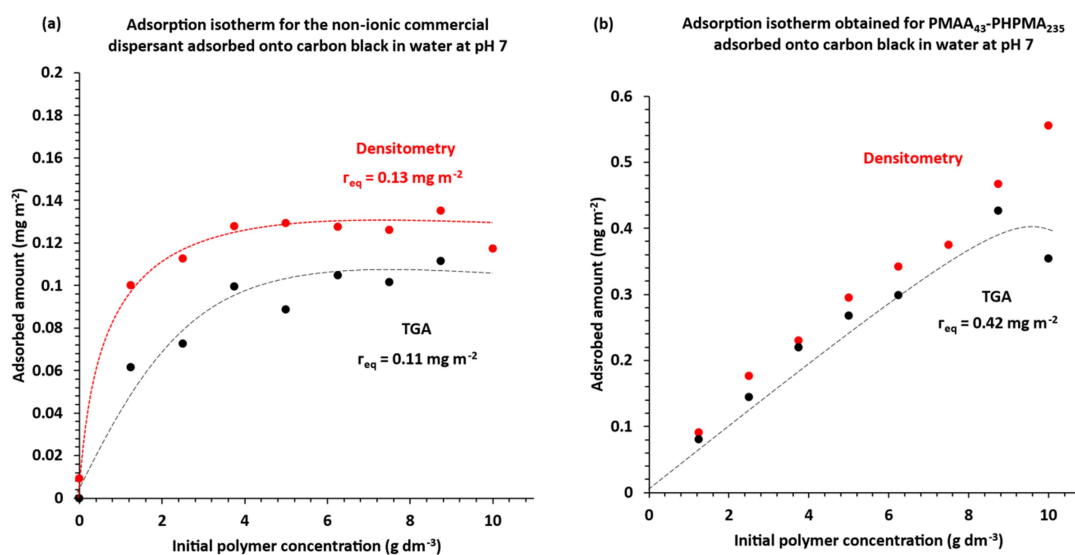

Figure 3.17 Adsorption isotherms constructed at pH 7 for **(a)** Non-ionic commercial dispersant adsorbed onto carbon black (Printex L6) particles and **(b)** PMAA$_{43}$-PHPMA$_{235}$ nanoparticles adsorbed onto the same carbon black particles, as determined directly *via* TGA (black), and indirectly using a supernatant depletion assay based on solution densitometry. The two isotherms shown in **(a)** are physically reasonable, whereas the two isotherms shown in **(b)** not, which suggests an invalid experimental protocol (see main text for further details).

According to TGA studies, the adsorbed amount of the non-ionic commercial dispersant is determined to be 0.11 mg m^{-2} (**Figure 3.17a**). This is in reasonably close agreement with the adsorbed amount of 0.13 mg m^{-2} determined by solution densitometry. Moreover, this corresponds to an equilibrium polymer concentration of 5 g dm^{-3}, which is consistent with the optimum concentration indicated by dispersion viscosity measurements. Both techniques indicate a Langmuir-type adsorption isotherm, as expected for the physical adsorption of a monolayer of steric stabiliser chains at the surface of the pigment particles.[31,34]

For the PMAA$_{43}$-PHPMA$_{235}$ copolymer dispersant (**Figure 3.17b**), TGA analysis indicated an apparent adsorbed amount of 0.42 mg m^{-2}. However, this is almost double that indicated by dispersion viscosity measurements (0.18 mg m^{-2}) when using 50% polymer per unit mass of carbon black. Moreover, the adsorption isotherms constructed for the adsorption of PMAA$_{43}$-PHPMA$_{235}$ using either solution densitometry or TGA did not exhibit the expected plateau region corresponding to monolayer coverage, therefore an adsorbed amount could not be determined.

The apparent optimal dispersant concentrations observed for a 10 g dm^{-3} aqueous dispersion of carbon black pigment are summarised in **Table 3.3**.

Table 3.3 Apparent optimum dispersant concentration based on a 10 g dm^{-3} aqueous dispersion of Printex L6 carbon black particles at pH 7 as calculated by: **(i)** dispersion viscosity measurements, **(ii)** supernatant assays using solution densitometry (following centrifugation of the pigment particles) and **(iii)** directly via TGA (following centrifugation of the pigment particles).

Dispersant	Non-ionic commercial dispersant	PMAA$_{43}$-PHPMA$_{235}$
(i) Dispersion viscosity	5.0 g dm^{-3}	5.0 g dm^{-3}
(ii) Solution densitometry	4.0 g dm^{-3}	n/a
(iii) TGA	5.0 g dm^{-3}	10.0 g dm^{-3}

For the non-ionic commercial dispersant, which requires an optimal concentration of 50% polymer per unit mass of pigment (which is equivalent to 5 g dm^{-3} under the stated

conditions, there is reasonably good agreement between the TGA and viscosity measurements. Solution densitometry gives a somewhat lower value, perhaps due to the slightly lower adsorbed amount calculated in the adsorption isotherm. In view of the anomalous adsorption isotherm data obtained for $PMAA_{43}$-$PHPMA_{235}$ particles, it was decided to conduct some control experiments. Thus an aqueous dispersion of $PMAA_{43}$-$PHPMA_{235}$ particles was centrifuged using the same conditions required to achieve full sedimentation of the pigment particles when constructing the adsorption isotherms. These studies revealed that the $PMAA_{43}$-$PHPMA_{235}$ particles also undergo significant sedimentation under these conditions, as judged by the reduction in the solution density observed for the 'supernatant' solution (**Figure 3.18**).
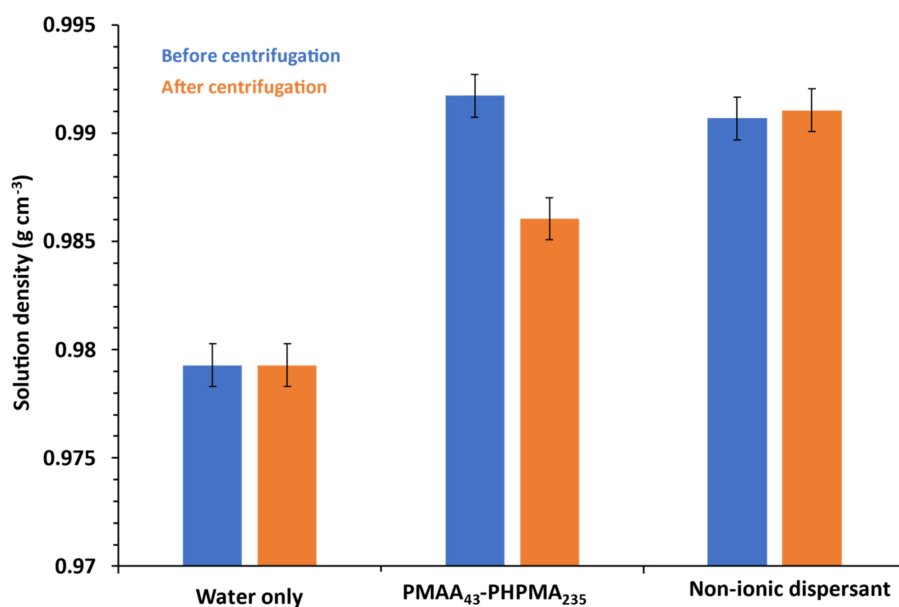

Figure 3.18 Solution densities determined at 25 °C for $PMAA_{43}$-$PHPMA_{235}$ and the non-ionic commercial dispersant at 10 g dm^{-3} before and after centrifugation to determine their extent of sedimentation during adsorption isotherm measurements. Unlike the non-ionic commercial dispersant, the $PMAA_{43}$-$PHPMA_{235}$ nanoparticles unexpectedly undergo significant sedimentation under the centrifugation conditions used to sediment the pigment particles.

However, the non-ionic commercial dispersant micelles, which are somewhat smaller than the $PMAA_{43}$-$PHPMA_{235}$ particles (5 nm vs. 24 nm diameter respectively as judged by DLS)

did not undergo any detectable sedimentation when subjected to the same centrifugal field. These unexpected observations explain the anomalous adsorption isotherms obtained for the $PMAA_{43}$-$PHPMA_{235}$ particles when using TGA and solution densitometry. The former technique is rendered unreliable by the presence of excess, non-adsorbed $PMAA_{43}$-$PHPMA_{235}$ particles within the pigment sediment, which leads to a substantial overestimate of the actual adsorbed amount. Similarly, the solution densitometry is inaccurate because the concentration of $PMAA_{43}$-$PHPMA_{235}$ particles remaining in the supernatant solution is much lower than it should be owing to their partial sedimentation. On the other hand, the adsorption isotherm data obtained for the non-sedimenting the non-ionic commercial dispersant is considered to be reliable.

Based on these results, the most reliable technique for determining the optimum copolymer concentration that corresponds to monolayer coverage appears to be the dispersion viscosity measurements. This is because this technique does not require separation of the pigment particles from the excess non-adsorbed copolymer dispersant, which is clearly problematic for this particular system.

3.3.4 Long-term Stability of Pigment Dispersions at Elevated Temperature

When ageing these aqueous carbon black dispersions at 70 °C for 7 days, preliminary studies suggested that the $PMAA_{43}$-$PHPMA_{235}$ nanoparticles were a more effective dispersant than the non-ionic commercial dispersant. This finding was further investigated using analytical centrifugation (see **Figure 3.19**). The cumulative velocity distribution profiles are quite similar for each dispersant. However, the median sedimentation velocity for the non-ionic commercial dispersant is 7.63 $\mu m\ s^{-1}$, whereas that for the diblock copolymer is slightly slower at 7.35 $\mu m\ s^{-1}$. Although this is a relatively small difference, it does suggest that the former dispersant is marginally more effective than the commercial dispersant.
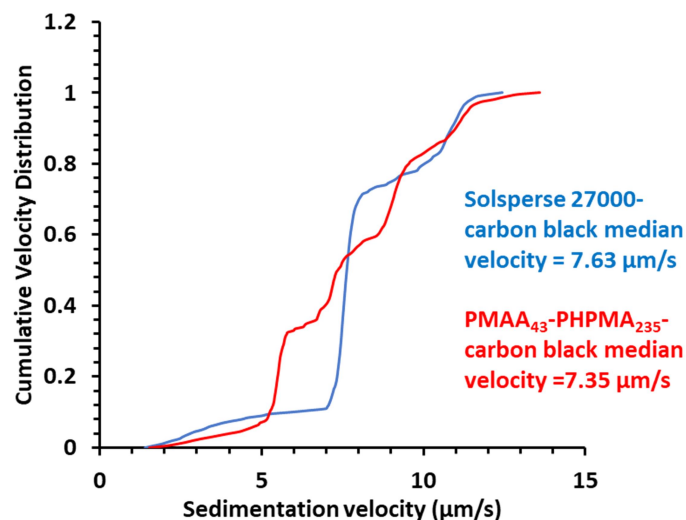
Figure 3.19 Cumulative velocity distributions recorded using a LUMiSizer instrument for the non-ionic commercial dispersant-stabilised carbon black particles (blue curve) and PMAA$_{43}$-PHPMA$_{235}$-stabilised carbon black particles (red) after storage in a 70 °C oven for 7 days (a standard accelerated ageing industry test for assessing long-term colloidal stability of aqueous pigment dispersions).

3.3.5 Stability of Pigment Dispersions at Varying Temperature

As discussed in Chapter 2, PMAA-PHPMA diblock copolymers exhibit both thermoresponsive and pH-responsive properties. The latter is conferred by the PMAA block and has already been discussed. The temperature-dependent behaviour conferred by the PHPMA block can be used to explain some observations made when employing this pigment dispersant.

Figure 3.20 shows LUMiSizer sedimentation velocities determined at various temperatures. Reduced colloidal stability is observed at 50 °C . This is because the PHPMA block becomes more hydrophobic (i.e. less hydrated) under such conditions.[61] This reduces the copolymer chain mobility, which favours kinetically-frozen micelles rather than micelles that are in equilibrium with individual copolymer chains.[62] (**red inset graphic, Figure 3.20**). However, a larger fraction of copolymer chains are expected to be molecularly dissolved at 5 °C, allowing better access for the PHPMA anchor block (depicted in **red** in **Figure 3.20**) to the

carbon black surface. It is not thought that higher order morphologies occur at higher temperatures for this composition. Thus it seems that, in this case, individual amphiphilic copolymer chains are more effective pigment dispersants than sterically-stabilised nanoparticles (micelles).
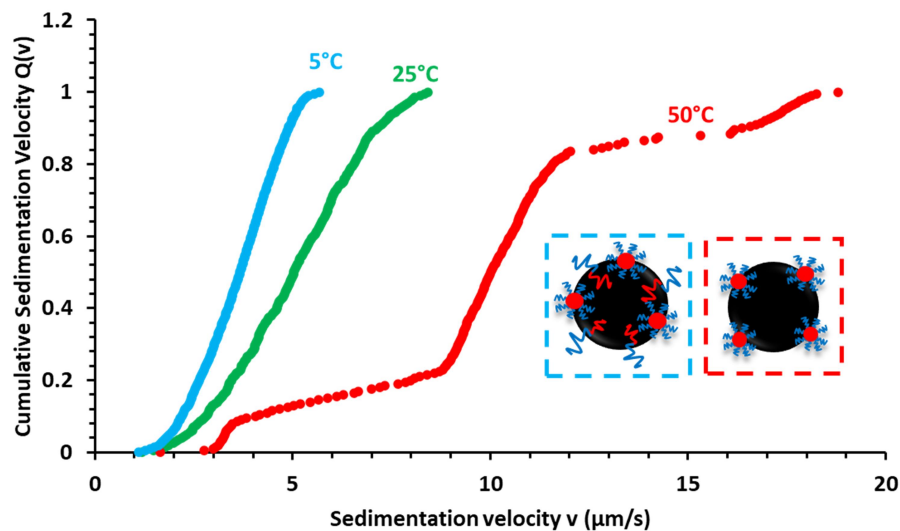

Figure 3.20 Cumulative sedimentation velocity distribution (3500 rpm, 166 min) recorded for PMAA$_{43}$-PHPMA$_{235}$ diblock copolymer-dispersed carbon black particles dispersed at pH 7, as determined by analytical centrifugation (LUMiSizer instrument) at 5 °C (blue curve), 25 °C (green curve), and 50 °C (red curve). The two inset cartoons depict either sterically-stabilised nanoparticles or a mixture of such nanoparticles with molecularly-dissolved copolymer chains adsorbed at the surface of the carbon black pigment particles.

3.4 Conclusions

PMAA$_x$-PHPMA$_y$ has been identified as an effective diblock copolymer system for the preparation of aqueous dispersions of carbon black particles. More specifically, PMAA$_{43}$-PHPMA$_{235}$ has been identified as a good dispersant for Printex L6, with the weakly hydrophobic PHPMA block acting as the anchor and the anionic PMAA block as the steric stabiliser. This diblock copolymer exhibits interesting pH-responsive behaviour, showing optimal dispersion stability at around pH 7. Here the PMAA is above its pK$_a$ and hence has

anionic character, conferring colloidal stability by an electrosteric mechanism. At pH 7, solution viscosity measurements confirmed that the optimum concentration for PMAA$_{43}$-PHPMA$_{235}$ as a dispersant is at 50% based on unit mass of pigment. However, it proved impossible to construct an adsorption isotherm for this system using either thermogravimetry (direct method) or supernatant analysis (indirect method) because appreciable sedimentation of the nanoparticles occurred when centrifuging the pigment particles. The weakly hydrophobic PHPMA block is also thermoresponsive: as it becomes more hydrated at lower temperatures, the copolymer chains are less likely to form kinetically-frozen micelles. Hence, they can adsorb more effectively onto pigment particles, leading to a more efficient dispersant under such conditions. However, mechanical milling of pigments usually involves localised heating, so it remains to be seen whether such diblock copolymer dispersants are sufficiently effective when operating above ambient temperature.

3.5 References

1.   Tadros, T. F. Formulation of Pigment and Ink Dispersions. in *Formulation of Disperse Systems* 367–396 (Wiley-VCH Verlag GmbH & Co. KGaA, 2014). doi:10.1002/9783527678297.ch18

2.   Pal, L. & Fleming, P. The Study of Ink Pigment Dispersion Parameters. *Hilltop Rev.* **2**, 61–70 (2006).

3.   Yoon, C. & Choi, J. H. Synthesising polymeric dispersants to apply to carbon black pigmented mill bases for use in ink-jet inks. *Color. Technol.* **136**, 60–74 (2020).

4.   Yossif, N. A., Kandile, N. G., Abdelaziz, M. A. & Negm, N. A. Preparation and characterization of polymeric dispersants based on vegetable oils for printing ink application. *Prog. Org. Coatings* **111**, 354–360 (2017).

5.   Makarewicz, E. & Michalik, A. Research on the influence of the type of surfactant and concentrator in aqueous dispersion of pigments. *J. Surfactants Deterg.* **17**, 773–784 (2014).

6.   Napper, D. H. & Netschey, A. Studies of the steric stabilization of colloidal particles. *J. Colloid Interface Sci.* **37**, 528–535 (1971).

7.   Napper, D. H. Steric stabilization. *J. Colloid Interface Sci.* **58**, 390–407 (1977).

8.   Klimkevicius, V., Graule, T. & Makuska, R. Effect of structure of cationic comb copolymers on their adsorption and stabilization of titania nanoparticles. *Langmuir* **31**, 2074–2083 (2015).

9.   Al-Lami, H. S., Billingham, N. C. & Calvert, P. D. Controlled Structure Methacrylic Copolymers as Dispersants for Ceramics Processing. *Chem. Mater.* **4**, 1200–1207 (1992).

10. Wang, Y. & Mattice, W. L. Adsorption of Homopolymers on a Solid Surface: A Comparison between Monte Carlo Simulation and the Scheutjens–Fleer Mean-Field Lattice Theory. *Langmuir* **10**, 2281–2288 (1994).

11. Creutz, S., Jérôme, R., Kaptijn, G. M. P., Van Der Werf, A. W. & Akkerman, J. M. Design of polymeric dispersants for waterborne coatings. *J. Coatings Technol.* **70**, 41–46 (1998).

12. Hoogeveen, N. G., Cohen Stuart, M. A. & Fleer, G. J. Can charged (block co)polymers act as stabilisers and flocculants of oxides? *Colloids Surfaces A Physicochem. Eng. Asp.* **117**, 77–88 (1996).

13. Chibowski, S. & Wiśniewska, M. Study of the adsorption mechanism and the structure of adsorbed layers of polyelectrolytes at the metal oxide/solution interface. *Adsorpt. Sci. Technol.* **19**, 409–421 (2001).

14. Zapka, W. *Handbook of Industrial Inkjet Printing: A Full System Approach*. *Handbook of Industrial Inkjet Printing: A Full System Approach* **1**–**2**, (Wiley-VCH, 2017).

15. Jankolovits, J. *et al.* Stable Aqueous Dispersions of Hydrophobically Modified Titanium Dioxide Pigments through Polyanion Adsorption: Synthesis, Characterization, and Application in Coatings. *Langmuir* **32**, 1929–1938 (2016).

16. Reuter, E., Silber, S. & Psiorz, C. Use of new blockcopolymeric dispersing agents for waterborne paints - theoretical and practical aspects. *Prog. Org. Coatings* **37**, 161–167 (1999).

17. Chen, Y. M. *et al.* Synthesis of acrylic copolymers consisting of multiple amine pendants for dispersing pigment. *J. Colloid Interface Sci.* **334**, 42–49 (2009).

18. Xu, Y., Liu, J., Du, C., Fu, S. & Liu, X. Preparation of nanoscale carbon black dispersion using hyper-branched poly(styrene-alt-maleic anhydride). *Prog. Org. Coatings* **75**, 537–542 (2012).

19. Deng, Z., Wang, L., Yu, H., Zhai, X. & Chen, Y. Non-covalent dispersion of multi-walled carbon nanotubes in aqueous solution with hyperbranched polyethylene-g-poly(methacrylic acid). *RSC Adv.* **6**, 27682–27689 (2016).

20. North, S. M. *et al.* Adsorption of Small Cationic Nanoparticles onto Large Anionic Particles from Aqueous Solution: A Model System for Understanding Pigment Dispersion and the Problem of Effective Particle Density. *Langmuir* **33**, 1275–1284 (2017).

21. Kissa, E. *Dispersions: Characterization, Testing, and Measurement - Erik Kissa - Google Books*. (Marcel Dekker Inc., 1999).

22. Kostansek, E. Controlling particle dispersion in latex paints containing associative thickeners. *J. Coatings Technol. Res.* **4**, 375–388 (2007).

23. Van Sang, T., Velamakanni, B. V & Adkins, R. R. Comparison of methods to assess pigment dispersion. *J. Coatings Technol.* **73**, 61–70 (2001).

24. Creutz, S. & Jérôme, R. Effectiveness of block copolymers as stabilizers for aqueous titanium dioxide dispersions of a high solid content. *Prog. Org. Coatings* **40**, 21–29 (2000).

25. Kuo, K. H., Peng, Y. H., Chiu, W. Y. & Don, T. M. A novel dispersant for preparation of high loading and photosensitive carbon black dispersion. *J. Polym. Sci. Part A Polym. Chem.* **46**, 6185–6197 (2008).

26. Medalia, A. I. & Heckman, F. A. Morphology of aggregates-II. Size and shape factors of carbon black aggregates from electron microscopy. *Carbon N. Y.* **7**, 567–582 (1969).

27. Smith, T. A review of carbon black pigments. *Pigment & Resin Technology* **12**, 14–16 (1983).

28. Nsib, F., Ayed, N. & Chevalier, Y. Selection of dispersants for the dispersion of carbon black in organic medium. *Prog. Org. Coatings* **55**, 303–310 (2006).

29. Lahaye, J. & Ehrburger-Dolle, F. Mechanisms of carbon black formation. Correlation with the

morphology of aggregates. *Carbon N. Y.* **32**, 1319–1324 (1994).

30. Cordeiro-Junior, P. J. M. *et al.* Oxygen reduction reaction: Semi-empirical quantum mechanical and electrochemical study of Printex L6 carbon black. *Carbon N. Y.* **156**, 1–9 (2020).

31. Growney, D. J., Mykhaylyk, O. O. & Armes, S. P. Micellization and adsorption behavior of a near-monodisperse polystyrene-based diblock copolymer in nonpolar media. *Langmuir* **30**, 6047–6056 (2014).

32. Wang, M. J., Gray, C. A., Reznek, S. A. & Mahmud, K. Carbon Black. Kirk-Othmer Encyclopedia of Chemical Technology. in *Kirk-Othmer Encyclopedia of Chemical Technology* (John Wiley & Sons, Inc., 2003). doi:10.1002/0471238961.0301180204011414.a01.pub2

33. Herd, C. R., McDonald, G. C. & Hess, W. M. Morphology of carbon-black aggregates. Fractal versus Euclidean geometry. *Rubber Chem. Technol.* **65**, 107–129 (1992).

34. Growney, D. J. *et al.* Is Carbon Black a Suitable Model Colloidal Substrate for Diesel Soot? *Langmuir* **31**, 10358–69 (2015).

35. Rieker, T. P., Misono, S. & Ehrburger-Dolle, F. Small-angle X-ray scattering from carbon blacks: Crossover between the fractal and porod regimes. *Langmuir* **15**, 914–917 (1999).

36. *Carbon Black: Science and Technology*. (Marcel Dekker Inc., 1993).

37. Krejci, J. C. Furnace carbon black process and apparatus. **865**, 717 (1958).

38. Ono, K. *et al.* Influence of furnace temperature and residence time on configurations of carbon black. *Chem. Eng. J.* **200**–**202**, 541–548 (2012).

39. Al-Sadi, J. Study on effect of dispersion and processing parameters in microscopically evaluated colour of plastic grade. in *AIP Conference Proceedings* **2139**, 110001 (2019).

40. Hess, W. M., Ban, L. L. & McDonald, G. C. Carbon Black Morphology: I. Particle Microstructure. II. Automated EM Analysis of Aggregate Size and Shape. *Rubber Chem. Technol.* **42**, 1209–1234 (1969).

41. Kiil, S. Mathematical modeling of pigment dispersion taking into account the full agglomerate particle size distribution. *J. Coatings Technol. Res.* **14**, 69–84 (2017).

42. Assumpção, M. H. M. T. *et al.* A comparative study of the electrogeneration of hydrogen peroxide using Vulcan and Printex carbon supports. *Carbon N. Y.* **49**, 2842–2851 (2011).

43. Kashiwazaki, A. *et al.* Ink set and ink-jet color recording method using the same. (1995).

44. North, S. M. & Armes, S. P. Aqueous solution behavior of stimulus-responsive poly(methacrylic acid)-poly(2-hydroxypropyl methacrylate) diblock copolymer nanoparticles. *Polym. Chem.* **11**, 2147–2156 (2020).

45. Kirillov, S. A. Surface area and pore volume of a system of particles as a function of their size and packing. *Microporous Mesoporous Mater.* **122**, 234–239 (2009).

46. Growney, D. J. *et al.* Star Diblock Copolymer Concentration Dictates the Degree of Dispersion of Carbon Black Particles in Nonpolar Media: Bridging Flocculation versus Steric Stabilization. *Macromolecules* **48**, 3691–3704 (2015).

47. Boisvert, J.-P., Persello, J., Foissy, A., Castaing, J.-C. & Cabane, B. Effect of surface charge on the adsorption mode of sodium poly(acrylate) on alumina-coated TiO2 used as coating pigment. *Colloids Surfaces A Physicochem. Eng. Asp.* **168**, 287–296 (2000).

48. Hoogeveen, N. G., Cohen Stuart, M. A. & Fleer, G. J. Polyelectrolyte adsorption on oxides. I. Kinetics and adsorbed amounts. *J. Colloid Interface Sci.* **182**, 133–145 (1996).

49. Cesarano, J., Aksay, I. A. & Bleier, A. Stability of Aqueous α-Al$_2$O$_3$ Suspensions with Poly(methacrylic acid) Polyelectrolyte. *J. Am. Ceram. Soc.* **71**, 250–255 (1988).

50. Warren, N. J. *et al.* Critical Dependence of Molecular Weight on Thermoresponsive Behavior of Diblock Copolymer Worm Gels in Aqueous Solution. *Macromolecules* **51**, 8357–8371 (2018).

51. Clayton, J. Pigment/dispersant interactions in water-based coatings. *Pigment Resin Technol.* **27**, 231–239 (1998).

52. Kosmala, A., Wright, R., Zhang, Q. & Kirby, P. Synthesis of silver nano particles and fabrication of aqueous Ag inks for inkjet printing. *Mater. Chem. Phys.* **129**, 1075–1080 (2011).

53. Mahli, D. M., Wegner, J. M. & Edward Glass, J. Waterborne Latex Coatings of Color: II. Surfactant Influences on Color Development And Viscosity. *JCT Res.* **2**, 635–647 (2005).

54. Abrahao, R. T., Postal, V., Paiva, J. L. & Guardani, R. Wettability study for pigmentary titanium dioxide. *J. Coatings Technol. Res.* **10**, 829–840 (2013).

55. Bartell, F. E. & Osterhof, H. J. Determination of the Wettability of a Solid by a Liquid: Relation of Adhesion Tension to Stability of Color Varnish and Lacquer Systems. *Ind. Eng. Chem.* **19**, 1277–1280 (1927).

56. Rewick, R. T., Gates, J. & Smith, J. H. Simple test of dispersant effectiveness based on interfacial tension measurements. *Fuel* **59**, 263–265 (1980).

57. Marinova, K. G. *et al.* Charging of oil-water interfaces due to spontaneous adsorption of hydroxyl ions. *Langmuir* **12**, 2045–2051 (1996).

58. Kudin, K. N. & Car, R. Why are water-hydrophobic interfaces charged? *J. Am. Chem. Soc.* **130**, 3915–3919 (2008).

59. Roger, K. & Cabane, B. Why are hydrophobic/water interfaces negatively charged? *Angew. Chemie - Int. Ed.* **51**, 5625–5628 (2012).

60. Malmsten, M., Linee, P. & Cosgrove, T. Adsorption of PEO-PPO-PEO Block Copolymers at Silica. *Macromolecules* **25**, 2474–2481 (1992).

61. Kalina, M., Kargerová, A. & Pekař, M. DEAE-dextran hydrochloride behaviour in aqueous solution—The effect of ionic strength and concentration. *Carbohydr. Polym.* **220**, 163–169 (2019).

62. Ratcliffe, L. P. D., Derry, M. J., Ianiro, A., Tuinier, R. & Armes, S. P. A Single Thermoresponsive Diblock Copolymer Can Form Spheres, Worms or Vesicles in Aqueous Solution. *Angew. Chemie - Int. Ed.* **58**, 18964–18970 (2019).

63. Nicolai, T., Colombani, O. & Chassenieux, C. Dynamic polymeric micelles versus frozen nanoparticles formed by block copolymers. *Soft Matter* **6**, 3111–3118 (2010).

Chapter 4

Direct Synthesis of Well-defined Zwitterionic Diblock Copolymers

in Aqueous Media without Protecting Group Chemistry

4.1 Introduction

Zwitterionic polymers, also known as polyampholytes, contain both cationic and anionic monomer repeat units.[1–7] Thus they differ from polybetaines, which possess anionic and cationic groups on the same monomer unit.[8–11] Unlike polybetaines - and indeed zwitterionic *statistical* copolymers[12] – many zwitterionic *diblock* copolymers exhibit an isoelectric point (IEP) in aqueous solution owing to charge compensation. Such copolymers are soluble in their cationic form below this IEP, become insoluble in their neutral form at around the IEP and redissolve (or redisperse) in their anionic form above the IEP. According to the literature, zwitterionic diblock copolymers offer potential applications in protein purification,[13] ion exchange,[14,15] trace metal chelation,[16] and sewage treatment.[17]

Zwitterionic diblock copolymers comprising poly(methacrylic acid) (PMAA) and poly(2-(dimethylamino)ethyl methacrylate) (PDMA) have been claimed to act as 'universal' pigment dispersants for aqueous pigment dispersions owing to their ability to confer colloidal stability *via* electrosteric stabilization.[6,18,19] More specifically, Creutz and co-workers prepared zwitterionic PMAA-PDMA diblock, random and tapered copolymers *via* sequential anionic polymerisation at -78 °C. These three copolymers were subsequently evaluated as putative dispersants for multiple pigments; this aspect is discussed further in Chapter 5.[19]

Unfortunately, the traditional synthesis of well-defined zwitterionic diblock copolymers is synthetically demanding and typically requires protecting group chemistry for the anionic block.[20] Indeed, Creutz and co-workers employed protecting group chemistry to prepare their PMAA-PDMA diblock copolymers: *t*-butyl methacrylate was used to prepare the polyacid block, with this ester group being subsequently removed *via* selective acid hydrolysis. Similarly, Kamachi *et al*. copolymerised 2-vinylpyridine with either trimethylsilyl methacrylate or *t*-butyl acrylate *via* sequential monomer addition using living anionic

polymerisation[21,22] while Lowe and co-workers prepared PDMA-PMAA diblock copolymers *via* group transfer polymerisation, with 2-tetrahydropyranyl methacrylate being used to produce the polyacid block.[23] In related work, Liu *et al*. used ATRP to prepare poly(4-vinylbenzoic acid)-poly(2-(diethylamino)ethyl methacrylate) diblock copolymers using protecting group chemistry for the polyacid block.[5] Such weak polyacid/weak polybase copolymers exhibit so-called 'schizophrenic' behaviour: they can form either cationic or anionic micelles in aqueous solution *via* micelle inversion on switching the solution pH from 2 to 10. Aside from the prohibitive cost of such multi-step syntheses, removal of protecting ester groups to generate the acidic block can lead to molecular weight distribution broadening *via* formation of intermolecular cross-links, yielding ill-defined branched architectures.[23] A more atom-efficient approach was reported by Bories-Azeau and co-workers,[24] who synthesised a series of poly(tertiary amine methacrylate)-poly(2-hydroxyethyl methacrylate) diblock copolymers using atom transfer radical polymerisation (ATRP). The hydroxyl groups on these precursors were subsequently reacted with succinic anhydride under mild conditions to introduce the desired acid functionality. Nevertheless, two steps, several organic solvents and relatively long reaction times were required for such syntheses.

In principle, controlled radical polymerisation techniques such as ATRP,[25,26] NMP[27,28] and RAFT polymerisation[29,30] should enable the direct synthesis of zwitterionic diblock copolymers without requiring any protecting group chemistry. An early example of such an approach was reported by Gabaston *et al*.,[31] who utilised NMP to prepare block copolymers of poly(sodium 4-styrenesulfonate) and poly(4-(dimethylamino)methylstyrene) in a 3:1 ethylene glycol-water mixture at 120 °C. Xin et al. also used RAFT polymerisation to prepare poly(2-(dimethylamino)ethyl methacrylate)-poly(sodium acrylate) *via* a two-step protocol, with the polybase precursor being synthesised in anisole in 84-86% yield and the zwitterionic diblock copolymers being obtained directly in a 4:3 v/v methanol-water mixture.[1] As

expected, such copolymers precipitated from aqueous solution within a relatively narrow range of solution pH either side of the IEP.

Herein we report the first *wholly aqueous, one-pot* synthesis of zwitterionic diblock copolymers using RAFT polymerisation. This convenient and highly atom-efficient synthetic route is exemplified for various classes of zwitterionic diblock copolymers. In each case, the cationic block can be poly(2-(dimethylamino)ethyl methacrylate) [PDMA], poly(2-(diethylamino)ethyl methacrylate) [PDEA], poly(2-(diisopropylamino)ethyl methacrylate) [PDPA], poly(2-(*N*-morpholino)ethyl methacrylate) [PMEMA] or poly(2-(methacryloyloxy)ethyl trimethylammonium chloride) [PMETAC], while the anionic block comprises either poly(methacrylic acid) or poly(2-carboxyethyl acrylate). The resulting zwitterionic diblock copolymers are characterised by GPC and ^{1}H NMR spectroscopy, and their aqueous solution properties are examined using DLS, TEM and aqueous electrophoresis. A highly convenient wholly aqueous protocol for removal of the trithiocarbonate end-groups is also reported that takes advantage of the insolubility exhibited by such zwitterionic diblock copolymers at around their IEP.

4.2 Experimental

Materials

4-Cyano-4-(2-phenylethanesulfanylthiocarbonyl)sulfanylpentanoic acid) (PETTC) was synthesised as previously reported.[32] 2-(Dimethylamino)ethyl methacrylate (DMA), 2-(diethylamino)ethyl methacrylate (DEA), 2-(diisopropylamino)ethyl-methacrylate (DPA), [2-(methacryloyloxy)ethyl] trimethylammonium chloride (METAC), 2-2-(*N*-morpholino)ethyl methacrylate (MEMA), 2-carboxyethyl acrylate (CEA), trimethylsilyldiazomethane (supplied as a 2.0 M solution in diethyl ether), 2,2′-Azobis(2-methylpropionitrile) (AIBN)

and hydrazine hydrate (reagent grade, 50-60% w/w aqueous solution) were purchased from Sigma-Aldrich (Dorset, UK) and were used as received. Methacrylic acid (MAA) was purchased from Merck (Germany) and was used as received. 2,2'-Azobis(2-(2-imidazolin-2-yl)propane) dihydrochloride (VA-044) was purchased from Wako Pure Chemical Industries (Japan). 4,4′-Azobis(4-cyanovaleric acid) (ACVA; 98%) and 2,2,3,3-d(4)-3-(Trimethylsilyl)propionic acid sodium salt was purchased from Alfa Aesar (Heysham, UK) and was used as received. CD_3OD and CD_2Cl_2 were purchased from Goss Scientific Instruments Ltd (Cheshire, UK). $CDCl_3$, D_2O, sodium deuteroxide (NaOD) and deuterium chloride (DCl) were purchased from Sigma-Aldrich (Dorset, UK). All other solvents were purchased from Fisher Scientific (Loughborough, UK) and were used as received. Deionised water was used for all experiments and the solution pH was adjusted using either HCl or NaOH.

Synthesis of poly(methacrylic acid) (PMAA) precursor

In a typical synthesis, a round-bottomed flask was charged with MAA (20.0 g, 232 mmol), PETTC (1.21 g, 3.57 mmol), ACVA (200 mg, 0.72 mmol; CTA/initiator molar ratio = 5.0) and ethanol (32.1 g, 40% w/w). This ethanolic solution was purged with nitrogen gas for 30 min and the sealed reaction vessel was placed in a pre-heated oil bath at 70 °C for 3 h. The resulting PMAA precursor (MAA conversion = 80%; M_n = 6 800 g mol^{-1}, M_w/M_n = 1.28 after exhaustive methylation using trimethylsilyldiazomethane) was purified by precipitation into a ten-fold excess of diethyl ether (twice) and then isolated by lyophilisation to yield a pale yellow powder. End-group analysis using ^{1}H NMR spectroscopy indicated a mean DP of 56 for this PMAA precursor.

Synthesis of poly(2-(dimethylamino)ethyl methacrylate) (PDMA) precursor

In a typical synthesis, a round-bottomed flask was charged with DMA (10.0 g, 63 mmol), PETTC (0.33 g, 0.979 mmol), AIBN (32.1 mg, 0.196 mmol; CTA/initiator molar ratio = 5.0) and THF (15.5 g, 40 w/w). The sealed reaction vessel was purged with nitrogen gas for 30 min and placed in a pre-heated oil bath at 66 °C for 8 h. The resulting PDMA precursor (DMA conversion = 70%; M_n = 5 700 g mol^{-1}, M_w/M_n = 1.24) was purified by precipitation into a ten-fold excess of petroleum ether (twice) to remove unreacted DMA monomer. The resulting yellow homopolymer was then dried under vacuum to afford a PDMA macro-CTA with a mean DP of 43, as determined by end-group analysis using ^{1}H NMR spectroscopy.

Synthesis of poly[(2-diethylamino)ethyl methacrylate) (PDEA) precursor

In a typical synthesis, a round-bottomed flask was charged with DEA (10.0 g, 53.9 mmol), PETTC (0.23 g, 0.67 mmol), ACVA (37.8 mg, 0.14 mmol; CTA/initiator molar ratio = 3.0) and THF (6.84 g, 60% w/w). The sealed reaction vessel was purged with nitrogen gas for 30 min and placed in a pre-heated oil bath at 66 °C for 5 h. The resulting PDEA precursor (DEA conversion = 67%; M_n = 8 100 g mol^{-1}, M_w/M_n = 1.17) was purified by precipitation into a ten-fold excess of mildly alkaline aqueous solution (pH 10). The neutral PDEA homopolymer was then dried under vacuum before being protonated using 2.0 M HCl. The fully protonated PDEA homopolymer was isolated in its HCl salt form by precipitation into a ten-fold excess of acetone.[33] This pale yellow homopolymer was then dried under vacuum to afford a PDEA macro-CTA with a mean DP of 67, as determined by end-group analysis using ^{1}H NMR spectroscopy.

Synthesis of poly[2-(diisopropylamino)ethyl methacrylate] (PDPA) precursor

In a typical synthesis, a round-bottomed flask was charged with DPA (10.0 g, 46.8 mmol), PETTC (0.32 g, 0.96 mmol), AIBN (41.1 mg, 0.15 mmol; CTA/initiator molar ratio = 4.0)

and 1,4-dioxane (6.83 g, 60% w/w). The sealed reaction vessel was purged with nitrogen gas for 30 min and placed in a pre-heated oil bath at 70 °C for 4 h. The resulting PDPA precursor (DPA conversion = 79%; M_n = 11 700 g mol^{-1}, M_w/M_n = 1.11) was purified by precipitation into a ten-fold excess of methanol (twice). This pale yellow homopolymer was then dried under vacuum to afford a PDPA macro-CTA with a mean DP of 75, as determined by end-group analysis using ^{1}H NMR spectroscopy. This sample was used to determine the pK$_a$ of PDPA.

Synthesis of PMAA-PDEA diblock copolymer *via* aqueous RAFT emulsion polymerisation

The protocol used for the synthesis of a PMAA$_{56}$-PDEA$_{114}$ zwitterionic diblock copolymer is representative. PMAA$_{56}$ macro-CTA (0.17 g, 33.1 µmol), DEA (0.70 g, 3.78 mmol) VA-044 (2.68 mg, 8.29 µmol, PMAA$_{56}$ macro-CTA/ACVA molar ratio = 4.0), and deionised water (3.50 g) were added to a sample vial and the solution pH was adjusted to 8.5. This vial was sealed and the aqueous solution was degassed for 20 min using a nitrogen stream. Then the vial was placed in a pre-heated oil bath at 44 °C for 16 h, yielding a viscous yellow dispersion. A final DEA conversion of 96% was indicated by ^{1}H NMR spectroscopy.

Synthesis of PMAA-PDPA diblock copolymer *via* aqueous RAFT emulsion polymerisation

The protocol used for the synthesis of a PMAA$_{56}$-PDPA$_{114}$ zwitterionic diblock copolymer is representative. PMAA$_{56}$ macro-CTA (0.13 g, 24.7 µmol), DPA (0.60 g, 2.81 mmol) ACVA (1.72 mg, 6.17 µmol, PMAA$_{56}$ macro-CTA/ACVA molar ratio = 4.0), and deionised water (2.92 g) were added to a sample vial and the solution pH was adjusted to 8.5. This vial was sealed and the aqueous solution was degassed for 20 min using a nitrogen stream. Then the

vial was placed in a pre-heated oil bath at 70 °C for 16 h, yielding a viscous yellow dispersion. A final DPA conversion of 98% was indicated by ^{1}H NMR spectroscopy.

Synthesis of PMAA-PMEMA diblock copolymer *via* RAFT aqueous solution polymerisation

A typical protocol for the synthesis of a $PMAA_{56}$-$PMEMA_{56}$ zwitterionic diblock copolymer was conducted as follows: $PMAA_{56}$ macro-CTA (0.28 g, 53.8 μmol), MEMA (0.60 g, 3.01 mmol) VA-044 (4.3 mg, 13.4 μmol, $PMAA_{56}$ macro-CTA/ACVA molar ratio = 4.0), and deionised water (3.53 g) were added to a sample vial and the solution pH was adjusted to 6.5. This vial was sealed and the aqueous solution was degassed for 20 min using a nitrogen stream. The vial was then placed in a pre-heated oil bath at 44 °C for 16 h, yielding a turbid, pale yellow solution. A final MEMA conversion of more than 99% was indicated by ^{1}H NMR spectroscopy.

Synthesis of PDMA-PCEA diblock copolymer *via* aqueous RAFT dispersion polymerisation

A typical protocol for the synthesis of a $PDMA_{43}$-$PCEA_{43}$ zwitterionic diblock copolymer is as follows. $PDMA_{43}$ macro-CTA (0.46 g, 6.45 μmol), CEA (0.40 g, 2.8 mmol) VA-044 (5.2 mg, 16.1 μmol; $PDMA_{43}$ macro-CTA/ACVA molar ratio = 4.0) and deionised water (3.45 g) were added to a sample vial. The solution pH was adjusted to 1.5. The vial was then sealed and degassed for 20 min using a nitrogen stream before being placed in a pre-heated oil bath at 44 °C for 16 h, yielding a yellow dispersion. A final CEA conversion of 99% was indicated by ^{1}H NMR spectroscopy.

Synthesis of PDEA-PMAA diblock copolymer *via* aqueous RAFT solution polymerisation

A typical protocol for the synthesis of a $PDEA_{67}$-$PMAA_{134}$ zwitterionic diblock copolymer is as follows. $PDEA_{67}$ macro-CTA (0.22 g, 17.3 μmol), MAA (0.20 g, 2.3 mmol) ACVA (1.21 mg, 4.33 μmol; $PDEA_{67}$ macro-CTA/ACVA molar ratio = 4.0) and deionised water (1.69 g) were added to a sample vial. The solution pH was adjusted to 1.5. The vial was then sealed and degassed for 20 min using a nitrogen stream before being placed in a pre-heated oil bath at 70 °C for 16 h. A final MAA conversion of 99% was achieved as determined by ^{1}H NMR spectroscopy, yielding a yellow dispersion.

Synthesis of PDEA-PCEA diblock copolymer *via* aqueous RAFT dispersion polymerisation

A typical protocol for the synthesis of a $PDEA_{67}$-$PCEA_{134}$ zwitterionic diblock copolymer is as follows. $PDEA_{67}$ macro-CTA (0.17 g, 12.9 μmol), CEA (0.25 g, 1.73 mmol) ACVA (0.91 mg, 3.24 μmol; $PDEA_{67}$ macro-CTA/ACVA molar ratio = 4.0) and deionised water (1.66 g) were added to a sample vial. The solution pH was adjusted to 1.5. The vial was then sealed and degassed for 20 min using a nitrogen stream before being placed in a pre-heated oil bath at 70 °C for 16 h. A final MAA conversion of 99% was achieved as determined by ^{1}H NMR spectroscopy, yielding a yellow dispersion.

Synthesis of PDPA-PMAA diblock copolymer *via* aqueous RAFT solution polymerisation

A typical protocol for the synthesis of a $PDPA_{75}$-$PMAA_{75}$ zwitterionic diblock copolymer is as follows. $PDPA_{75}$ macro-CTA (0.40 g, 23.2 μmol), MAA (0.15 g, 1.7 mmol) ACVA (1.63 mg, 5.81 μmol; $PDPA_{75}$ macro-CTA/ACVA molar ratio = 4.0) and deionised water (2.15 g) were added to a sample vial and the solution pH was adjusted to 1.5. The vial was then sealed

and degassed for 20 min using a nitrogen stream before being placed in a pre-heated oil bath set at 70 °C for 16 h. A final MAA conversion of 99% was achieved as determined by ^{1}H NMR spectroscopy, yielding a yellow dispersion.

Synthesis of PDPA-PCEA diblock copolymer *via* aqueous RAFT dispersion polymerisation

A typical protocol for the synthesis of a PDPA$_{75}$-PCEA$_{75}$ zwitterionic diblock copolymer is as follows. PDPA$_{75}$ macro-CTA (0.30 g, 18.5 μmol), CEA (0.20 g, 2.32 mmol) ACVA (1.30 mg, 4.63 μmol; PDPA$_{75}$ macro-CTA/ACVA molar ratio = 4.0) and deionised water (2.00 g) were added to a sample vial and the solution pH was adjusted to 1.5. The vial was then sealed and degassed for 20 min using a nitrogen stream before being placed in a pre-heated oil bath set at 70 °C for 16 h. A final CEA conversion of 99% was achieved as determined by ^{1}H NMR spectroscopy, yielding a yellow dispersion.

One-pot synthesis of poly(2-(dimethylamino)ethyl methacrylate)-poly(methacrylic acid) (PDMA-PMAA) diblock copolymer

A typical protocol for the synthesis of a PDMA$_{50}$-PMAA$_{50}$ zwitterionic diblock copolymer was conducted as follows: DMA (4.0 g, 25.4 mmol), PETTC (0.17 g, 0.51 mmol), VA-044 (32.9 mg, 0.10 mmol), and deionized water (9.81 g) were added to a 100 ml two-necked round-bottomed flask. 36% HCl (2.18 g, 25.4 mmol) was added to protonate the DMA monomer. This aqueous reaction mixture was then purged for 30 min with nitrogen and heated to 44 °C. In a separate vial, MAA (2.19 g, 25 mmol), VA-044 (55 mg, 0.51 mmol) and water (15.9 g) were purged with nitrogen for 30 min. The DMA polymerisation had reached approximately full conversion after 3 h, as determined by ^{1}H NMR spectroscopy (by sampling under nitrogen). Then the degassed aqueous solution containing MAA monomer and VA-044 initiator was added under a nitrogen atmosphere. The MAA polymerisation was

allowed to proceed for 5 h at 44 °C. A final MAA conversion of more than 99% was achieved as determined by ^{1}H NMR, yielding a low-viscosity yellow solution at pH 2.0. The amounts of DMA and/or MAA, and the PETTC concentration were adjusted accordingly when targeting other copolymer compositions. Depending on the target diblock composition, relatively viscous transparent yellow solutions can be obtained.

One-pot synthesis of poly(methacrylic acid)-poly(2-(dimethylamino)ethyl methacrylate) (PMAA-PDMA) diblock copolymer

A typical protocol for the synthesis of a PMAA$_{50}$-PDMA$_{50}$ (target DP) zwitterionic diblock copolymer was conducted as follows: MAA (1.0 g, 11.6 mmol), PETTC (78.9 mg, 0.23 mmol), ACVA (13 mg, 46.4 µmol) and deionized water (6.19 g) were added to a 50 mL two-necked round-bottomed flask. This aqueous reaction mixture was then purged for 30 min with nitrogen and heated to 70 °C. In a separate vial, DMA (1.83 g, 11.6 mmol), ACVA (25 mg, 77.4 µmol), NaOH (0.46 g, 11.6 mmol) and water (5.53 g) were purged with nitrogen for 30 min. The MAA polymerisation had reached approximately full conversion after 3 h, as determined by ^{1}H NMR spectroscopy. Then the degassed aqueous solution containing DMA monomer and ACVA initiator was added under a nitrogen atmosphere. The DMA polymerisation was allowed to proceed for 9 h at 70 °C (final solution pH = 8.5). A final DMA conversion of 95% was reached as determined by ^{1}H NMR, yielding a viscous yellow dispersion. The amounts of DMA and/or MAA, and the PETTC or CPDB concentration were adjusted accordingly when targeting other copolymer compositions.

One-pot synthesis of poly(methacrylic acid)-poly(2-(methacryloyloxy)ethyl trimethylammonium chloride) (PMAA-PMETAC) diblock copolymer

A typical protocol for the one-pot wholly aqueous synthesis of a PMAA-PMETAC zwitterionic diblock copolymer is as follows. MAA (2.60 g, 30.2 mmol) and CPDB (0.11 g,

0.50 mmol), were stirred thoroughly to ensure solvation of CPDB at 60% w/w solids content. ACVA (28 mg, 0.10 mmol) and deionised water (1.80 g) were added to a 100 ml two-necked round-bottomed flask. This aqueous solution was then purged for 30 min with nitrogen and heated up to 70 °C. In a second vial, deionised water (17.0 g) was degassed and then added to the reaction solution after 45 min to offset the increasing viscosity of the polymerising solution. After 3 h, the MAA polymerisation had reached more than 99% conversion as determined by ^{1}H NMR spectroscopy. In a separate vial, METAC (6.27 g, 30.2 mmol), ACVA (54 mg, 0.17 mmol) and deionised water (17.0 g, target solids concentration = 20% w/w) were purged with nitrogen for 30 min. This degassed aqueous solution was added under a nitrogen atmosphere and the second-stage polymerisation was allowed to continue for 6 h at 70 °C. A final METAC conversion of 96% was achieved as determined by ^{1}H NMR spectroscopy, yielding a viscous reddish-pink solution. PMAA-PMETAC diblock copolymers were modified for GPC analysis as follows: 1.0 g of a 20% w/w aqueous copolymer dispersion was diluted with 1.0 g ethylene glycol (2.1 g total volume, 10% copolymer solids) containing 0.18 g KOH (3 M). This reaction solution was then heated to 120 °C for 6 h to convert this PMAA-PMETAC precursor into PMAA homopolymer via forced ester hydrolysis. The resulting dark brown liquid was acidified using 2 M HCl (2.5 mL) and purified by precipitation (twice) into excess diethyl ether. After filtration, this PMAA homopolymer was methylated with excess trimethylsilyldiazomethane to afford off-white poly(methyl methacrylate) (PMMA), which was analysed by THF GPC.

Exhaustive methylation protocol

PMAA$_x$-based and PCEA-based diblock copolymers were modified via exhaustive methylation of their carboxylic acid groups. In a typical methylation protocol, excess trimethylsilyldiazomethane was added dropwise to PMAA$_x$-PDMA$_y$ (20 mg) dissolved in 3:2 toluene/methanol (10.0 mL) until the yellow colour persisted. This reaction solution was then

stirred at 20 °C for 72 h at the back of a fume cupboard until all the solvent had evaporated. The degree of methylation was determined by ^{1}H NMR spectroscopy by comparing the integrated oxymethylene ester protons for the PDMA block at 3.86 ppm to the integral of the new signal at 3.61 ppm assigned to the methoxy groups in the methylated block. Typically, 100% methylation was achieved under the stated conditions as judged by ^{1}H NMR spectroscopy.

DMF Gel Permeation Chromatography (GPC)

The DMF GPC instrument comprised two Agilent PL gel 5 μm Mixed-C columns and a guard column connected in series to an Agilent 1260 Infinity GPC system operating at 60 °C. The GPC eluent was HPLC-grade DMF containing 10 mM LiBr at a flow rate of 1.0 mL min^{-1} and dimethylsulfoxide was used as a flow rate marker. Calibration was achieved using a series of ten near-monodisperse poly(methyl methacrylate) standards (ranging in M_p from 625 to 618 000 g mol^{-1}).

THF Gel Permeation Chromatography (GPC)

The THF GPC set-up comprised two 5 μm (30 cm) Mixed C columns and a WellChrom K-2301 refractive index detector operating at a wavelength of 950 ± 30 nm. The mobile phase contained 2.0% v/v triethylamine and 0.05% w/v butylhydroxytoluene and the flow rate was 1.0 mL min^{-1}. A series of ten near-monodisperse poly(methyl methacrylate) standards (M_p values ranging from 645 to 2 480 000 g mol^{-1}) were used for calibration. Chromatograms were analysed using Agilent GPC/SEC software.

Aqueous Gel Permeation Chromatography (GPC)

Molecular weight distributions of diblock copolymers or homopolymers were analysed in a basic aqueous buffer (pH 10) containing 1 M NaNO$_3$ solution (adjusted to pH 10 with concentrated NaOH) at a flow rate of 1.0 mL min^{-1}. The GPC set-up comprised an Agilent

1260 Infinity series degasser and pump, an Agilent PL Aquagel-OH 30 8 μm column and an Agilent PL Aquagel-OH 40 8 μm column. Calibration was conducted using a series of near-monodisperse PEO standards ranging from 600 g mol^{-1} to 969, 000 g mol^{-1}. Chromatograms were analysed using Agilent GPC/SEC software.

Dynamic Light Scattering

Dilute (0.10% w/w) aqueous copolymer dispersions were analysed at 25 °C using a Malvern NanoZS instrument. Scattered light was detected at 173° and hydrodynamic diameters were calculated using the Stokes-Einstein equation, which assumes dilute non-interacting spheres. Data were averaged over three consecutive measurements comprising eleven runs per measurement.

Aqueous Electrophoresis

Zeta potentials were calculated from electrophoretic mobilities using a Malvern NanoZS instrument. Measurements were performed as a function of pH on dilute aqueous dispersions (0.05-0.10% w/w) in the presence of 1 mM KCl as background salt and averaged over 20 runs. In each case the solution pH was first increased by addition of 1.0 M NaOH and then gradually lowered by adding 0.1 M HCl.

^{1}H NMR spectroscopy

All ^{1}H NMR spectra were recorded using a 400 MHz Bruker Avance-400 spectrometer. The NMR solvent was CD_3OD, D_2O, $CDCl_3$ or CD_2Cl_2 and typically 64 scans were averaged per spectrum.

For in situ NMR studies during the synthesis of PDMA$_{50}$ homopolymer at 40% w/w, the reaction mixture was prepared as described above (albeit with D_2O being used as a solvent rather than H_2O) and a 0.75 mL aliquot was placed into an NMR tube equipped with a J-Young tap. The D_2O in the reaction mixture was used as the lock solvent. This NMR tube

assembly was inserted in a Bruker AVANCE III HD spectrometer operating at 500.13 MHz (^{1}H frequency) and a reference spectrum was recorded at 25 °C (no polymerization) prior to heating up to 44 °C. Spectra were recorded every 5 min for 4 h. All spectra were phase-adjusted and baseline-corrected using Bruker TopSpin 3.1 software. DMA conversions were determined by comparing integrated monomer and polymer signals relative to the aromatic signals from the PETTC RAFT agent. 2,2,3,3-d(4)-3-(Trimethylsilyl)propionic acid sodium salt (15 mg) was used as a reference signal at 0.0 ppm.

UV Spectroscopy

Absorption spectra were recorded between 200 and 800 nm at 25 °C using a PC-controlled Shimadzu UV-1800 spectrophotometer equipped with a 1 cm path length quartz cell. End-group removal was recorded at a copolymer concentration of 0.20% w/w, recording spectra at regular intervals over 3.5 h.

Removal of trithiocarbonate end-groups

Hydrazine hydrate (1.02 mL of a 50% w/w aqueous solution; 0.0159 mmol) was added to a 0.50% w/w aqueous solution of PDMA$_{50}$-PMAA$_{50}$ copolymer (40.0 mg, 0.0159 mmol; hydrazine/trithiocarbonate molar ratio = 1.0) in deionised water at pH 9 and 20 °C. The solution pH was then adjusted to the IEP (approximately pH 6.0) to induce precipitation. The aqueous supernatant was removed by careful decantation and the crude precipitate was then washed three times with deionised water (pH 6) to remove small molecule contaminants generated during the chemical degradation of the organosulfur-based chain-ends.

Transmission electron microscopy

Copper/palladium grids were surface-coated in-house to produce a thin film of amorphous carbon before being plasma glow-discharged for 40 seconds to produce a hydrophilic surface. A 1 µL droplet of a 0.1% w/w aqueous copolymer dispersion (solution pH adjusted using

either 0.1 M HCl or 0.1 M NaOH) was placed onto a grid for 45 seconds, then stained using a 0.75% w/v aqueous solution of uranyl formate or phosphotungstic acid for 45 seconds. Excess stain was removed by careful blotting and the grid was then dried using a vacuum hose. TEM images were recorded using a Philips CM100 instrument operating at 100 kV and equipped with a Gatan 1k CCCD camera. ImageJ software was used to calculate mean diameters and standard deviations from TEM images (at least 100 nanoparticles were analysed per sample).

4.3 Results and Discussion

In principle, the synthesis of zwitterionic diblock copolymers in aqueous solution can proceed *via* either solution, dispersion or emulsion polymerisation, with the precise physical nature of the polymerisation depending on the water solubility of the second monomer and its corresponding homopolymer. In this study, we explore such formulations and develop robust model one-pot aqueous formulations.

4.3.1 RAFT Aqueous Dispersion Polymerisation

The synthesis of zwitterionic diblock copolymers *via* RAFT aqueous dispersion polymerisation was investigated. Such formulations involve the polymerisation of CEA at pH 1.5: this monomer is soluble under such conditions but the corresponding polymer chains become insoluble as they grow. To synthesise the first block in these examples, the RAFT solution polymerisation of DMA, DEA or DPA was conducted in either THF or 1,4-dioxan using ACVA at 70 °C for 5 h. The resulting PDMA, PDEA or PDPA precursor was then purified, characterised, and redissolved in acidic aqueous solution for chain extension in its protonated form using CEA to form the acidic block (**Scheme 4.1).** In each case, high conversions (typically around 99%) and relatively low dispersities were obtained. On the

other hand, if the first block was synthesised in aqueous solution (as part of a wholly aqueous one-pot protocol), then the solution pH was selected to be pH 1.5 to ensure solubility of the PDEA or PDPA precursors, which are each only soluble in their protonated form. This low solution pH was maintained for the synthesis of the second block.
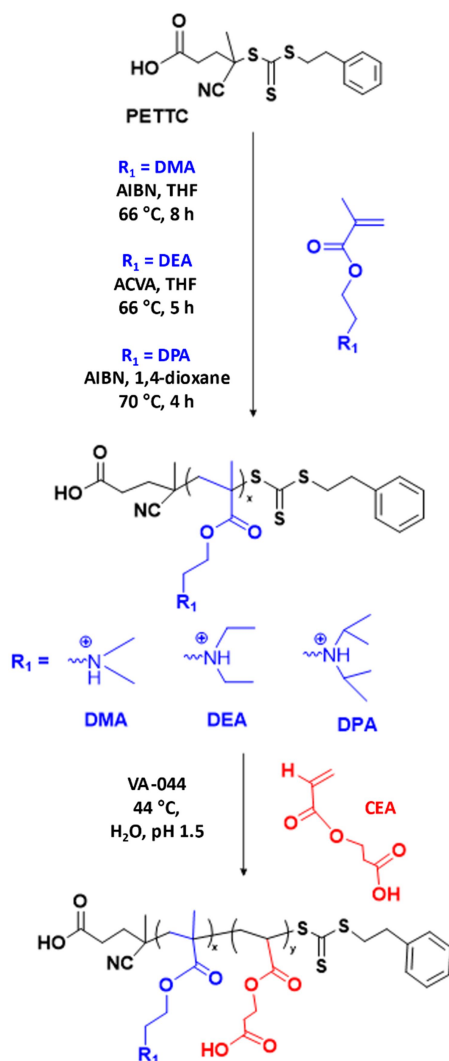
Scheme 4.1 RAFT solution polymerisation of DMA, DEA or DPA was conducted in either THF or 1,4-dioxan using PETTC with either AIBN or ACVA initiator. The resulting PDMA, PDEA or PDPA precursor was then purified, characterised and redissolved in acidic aqueous solution (pH 1.5) for subsequent chain extension using CEA to form the acidic block by aqueous dispersion polymerisation.

For PCEA syntheses, the CEA monomer is water-soluble, while PCEA homopolymer also becomes water-insoluble at low pH. Moreover, PCEA-core nanoparticles can be observed by

TEM when drying PCEA-based diblock copolymer dispersions at low pH. This indicates that such syntheses do indeed proceed *via* RAFT aqueous dispersion polymerisation, rather than RAFT aqueous solution polymerisation. A summary of the characterisation data is provided in **Table 4.1.**

Table 4.1 Summary of the characterisation data obtained for zwitterionic diblock copolymers prepared by RAFT aqueous dispersion polymerisation, for which PDMA, PDEA or PDPA is the first block and the second block comprises PCEA (with the second-stage polymerisation being conducted at pH 1.5). These PISA syntheses were conducted according to either **Scheme 4.1.**

Synthetic method	Diblock copolymer composition	^{1}H NMR conversion (%)	Theoretical M_n (g mol^{-1})	GPC (g mol^{-1})		IEP
				M_n	M_w/M_n	
Two-pot	PDMA$_{43}$-PCEA$_{100}$	> 99%	21 500	18 300[a]	1.16[a]	3.8
Two-pot	PDMA$_{43}$-PCEA$_{43}$	99	13 300	25 600[b]	1.37[b]	6.0
Two-pot	PDMA$_{87}$-PCEA$_{43}$	96	20 200	15 000[b]	1.32[b]	8.7
Two-pot	PDEA$_{67}$-PCEA$_{67}$	98	22 400	17 700[b]	1.07[b]	4.9
Two-pot	PDPA$_{75}$-PCEA$_{75}$	99	27 150	5 900[a]	1.39[a]	5.3

a. GPC analysis using DMF eluent vs. PMMA standards.

b. GPC analysis using THF eluent vs. PMMA standards.
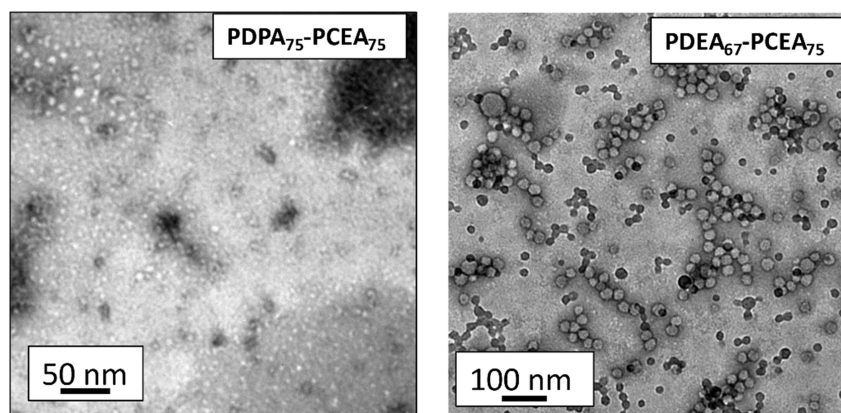
Figure 4.1 Example TEM images showing presence of nanoparticles at synthesis pH (1.5), confirming these syntheses proceed via RAFT aqueous dispersion polymerisation.

Zwitterionic diblock copolymers comprising a weak polyacid and a weak polybase usually exhibit an IEP. At the IEP, the mean number of cationic and anionic charges per copolymer chain are equal. Thus, the copolymer exhibits no net overall charge and is typically water-insoluble under such conditions.[4,23] The IEP can be determined from aqueous electrophoresis studies while DLS can be used to assess the colloid instability window, as illustrated for three examples of PDMA-PCEA copolymers in **Figure 4.2).** An increase in the IEP is observed as the proportion of DMA within the diblock copolymer is increased.
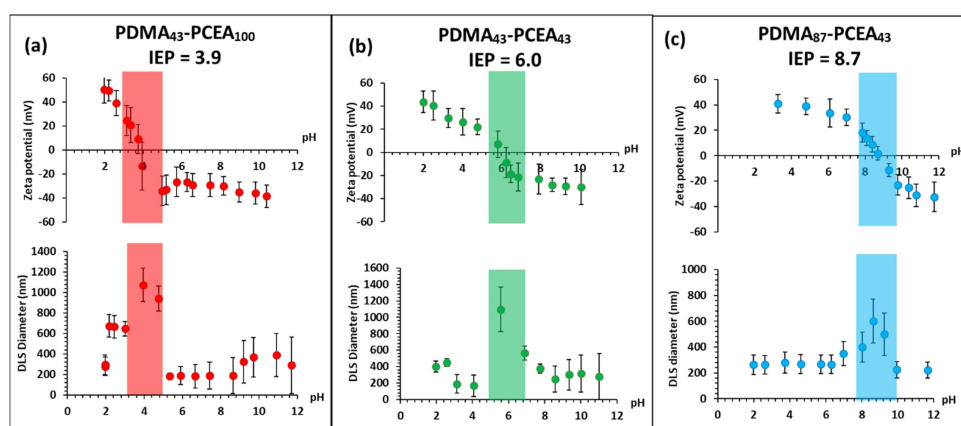
Figure 4.2 Variation in zeta potential and DLS diameter as a function of pH to determine isoelectric points and regions of colloidal instability for (a) $PDMA_{43}$-$PCEA_{100}$, (b) $PDMA_{43}$-$PCEA_{43}$ and (c) $PDMA_{87}$-$PCEA_{43}$ in the presence of 1 mM KCl as background salt. [N.B. Higher IEPs are obtained on increasing the DMA mol% in the zwitterionic diblock copolymer].

4.3.2 RAFT Aqueous Emulsion Polymerisation

The synthesis of zwitterionic diblock copolymers via RAFT aqueous emulsion polymerisation was also investigated. Such formulations involve polymerisation of a water-immiscible monomer and the growing second block is also insoluble (**Scheme 4.2**). Both DEA and DPA monomers are water-insoluble at or above pH 8.5. Following solution polymerisation of MAA in the first step, this soluble PMAA precursor will provide stabilisation to insoluble PDEA or PDPA cores. This solution pH represents an effective

upper limit for RAFT polymerisation in aqueous solution because premature hydrolysis of the

organosulfur RAFT chain-ends occurs in more alkaline media.[34–36]
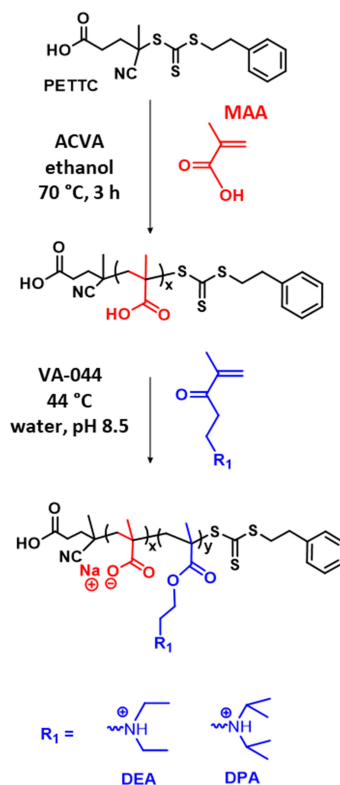
Scheme 4.2 RAFT solution polymerisation of MAA in ethanol using PETTC with ACVA initiator produced a PMAA precursor within 3 h at 70 °C, which was subsequently chain-extended via RAFT polymerisation of DEA or DPA in aqueous media at pH 8.5 using VA-044 initiator at 44 °C.

In fact, pH 8.5 proved to be the *optimal* solution pH for these polymerisations because phase

separation of the polyacid precursor occurred prior to polymerisation when attempting to use

formulations prepared below pH 8.5. At this pH, PDEA and PDPA become insoluble core-

forming blocks, leading to the formation of nanoparticles, as shown by DLS (**Figure 4.3**).

PMAA₅₆-PDPA₅₆

D_z = 88 nm (0.14)

PMAA₅₆-PDEA₅₆

D_z = 155 nm (0.10)
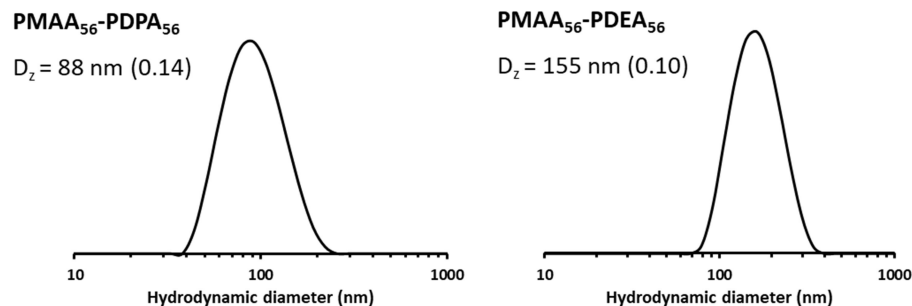
Figure 4.3 Example DLS particle size distributions showing presence of nanoparticles at synthesis pH (8.5), confirming these syntheses proceed via RAFT aqueous emulsion polymerisation.

Table 4.2 Summary of the characterisation data obtained for various types of zwitterionic diblock copolymers for which PMAA is the first block and the second block comprises PDEA or PDPA (with the second-stage polymerisation being conducted at the stated solution pH). Syntheses were conducted via a two-pot synthesis where the first step involved the RAFT solution polymerisation of MAA in ethanol and the second step was conducted via RAFT aqueous emulsion polymerisation at pH 8.5 (**Scheme 4.2**).

Synthetic method	Diblock copolymer composition	Reaction pH	^{1}H NMR conversion (%)	Theoretical M_n (g mol^{-1})	GPC (g mol^{-1})		IEP
					M_n	M_w/M_n	
Two-pot	PMAA₅₆-PDEA₁₀₈	8.5	97	23 400	11 400[b]	1.49[b]	8.1
Two-pot	PMAA₅₆-PDEA₅₆	8.5	97	14 100	12 000[a]	1.20[a]	6.5
Two-pot	PMAA₅₆-PDEA₂₈	8.5	99	8 700	7 400[a]	1.18[a]	5.1
Two-pot	PMAA₅₆-PDPA₁₁₄	8.5	> 99	29 600	21 200[b]	1.54[b]	8.5
Two-pot	PMAA₅₆-PDPA₅₆	8.5	95	17 100	36 200[b]	1.66[b]	5.6

a. GPC analysis using DMF eluent vs. PMMA standards.
b. GPC analysis using THF eluent vs. PMMA standards.

During these polymerisations, it is apparent that the M_w/M_n values become broader as longer PDEA blocks are targeted. This indicates a loss of RAFT control as higher molecular weights are targeted, a phenomenon which has been described previously in the literature.[37] The broader M_w/M_n values reported for PDPA-based copolymers compared to PDEA-based copolymers, could result from increased chain transfer to polymer, as the extra methyl group present in the tertiary amine methacrylate is more susceptible to radical abstraction.

IEP data were also determined for the three PMAA$_{56}$-PDEA$_x$ zwitterionic diblock copolymers **(see Table 4.2)** and are shown in **Figure 4.4.**
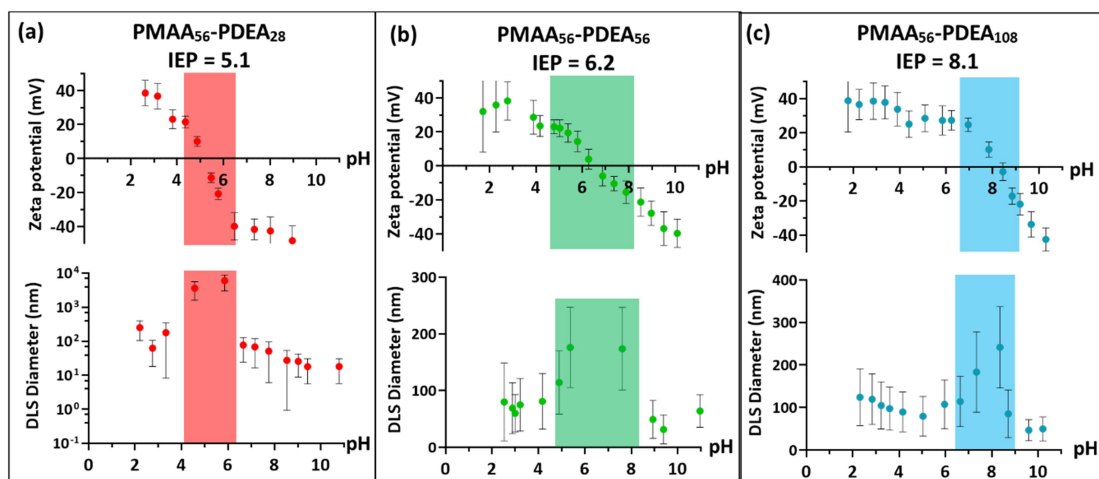
Figure 4.4 Variation in zeta potential and DLS diameter with solution pH to determine isoelectric points and regions of colloidal instability for (a) PMAA$_{134}$-PDEA$_{67}$, (b) PMAA$_{57}$-PDEA$_{57}$ and (c) PMAA$_{57}$-PDEA$_{108}$ in the presence of 1 mM KCl as background salt. N.B. Higher IEP values are observed on increasing the PDEA mol% in such zwitterionic diblock copolymers.

^{1}H NMR spectroscopy was employed to assess changes in the degree of solvation of each block for a PMAA$_{56}$-PDEA$_{56}$ zwitterionic diblock copolymer, see **Figure 4.5.** At pH 2 (0.01 M DCl in D$_2$O), signals *a*, *b*, *c*, and *d* for the protonated PDEA block are observed at 1.3, 3.2, 4.3 and 3.5 ppm, respectively. In addition, methacrylic backbone protons *e* and *f* are visible at δ 1.0 and 1.9 ppm. However, all these NMR signals disappear at pH 9 (NaOD/D$_2$O) as the PDEA block becomes deprotonated and hence insoluble under such conditions. As expected, methacrylic backbone signals *g* and *h* for the ionised PMAA block appear at 0.8 and 1.5 ppm, respectively. At the isoelectric point (pH 6), no NMR signals are observed in the absence of added salt because the charge-compensated zwitterionic diblock copolymer chains are water-insoluble under such conditions. However, addition of 4 M KCl provides sufficient charge screening to eliminate the electrostatic attractive forces and hence confer water solubility on the copolymer chains. Thus, NMR signals for both blocks can be observed under such conditions, with PDEA signals *a*, *b*, *c* and *d* being shifted to slightly higher δ values (1.4, 3.3,

3.6 and 4.4 ppm, respectively).
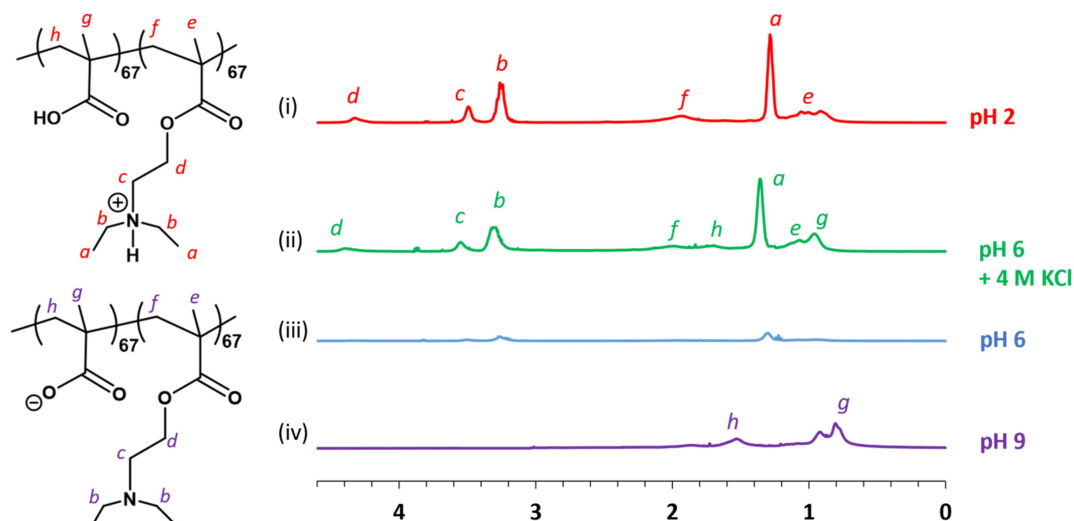
Figure 4.5 ^{1}H NMR spectra recorded for (i) a zwitterionic PDEA$_{67}$-PMAA$_{67}$ diblock copolymer in DCl/D$_2$O at pH 2 (where both blocks are fully protonated), (ii) at pH 6 in the presence of 4 M KCl (which suppresses macroscopic precipitation at this IEP), (iii) at the same pH in the absence of salt, and (iv) at pH 9 (where the PMAA block is ionised and the PDEA block is in its neutral hydrophobic form).

Provided that one of the blocks becomes sufficiently hydrophobic at a given pH, TEM studies confirm that these zwitterionic diblock copolymers can form sterically-stabilised nanoparticles. In all cases, the number-average diameter indicated by TEM is significantly smaller than the intensity-average diameter reported by DLS. For example, poly(tertiary amine methacrylate)-core nanoparticles are formed by PMAA$_{56}$-PDEA$_{108}$ diblock copolymers at pH 9, with micelle inversion to produce polyacid cores occurring at pH 2-3, see **Figure 4.6**.[3,5] The micelles produced at pH 2.0 are difficult to visualise, presumably owing to the weakly hydrophobic nature of the PMAA block under such conditions.
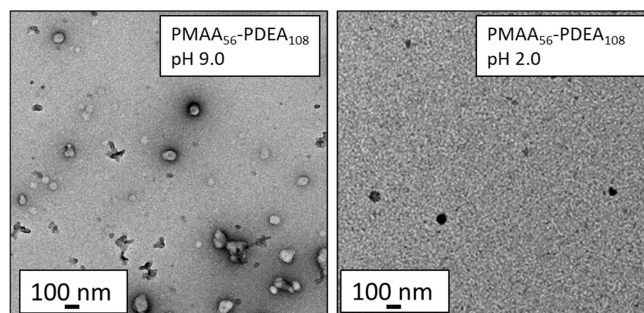
Figure 4.6 Transmission electron microscopy images recorded for a $PMAA_{56}$-$PDEA_{108}$ diblock copolymer nanoparticles at pH 9.0 and pH 2.0, respectively. In each case spherical nanoparticles can be observed.

4.3.3 Aqueous Solution Polymerisation

Finally, diblock copolymer syntheses in which both blocks remain fully solvated for the duration of the polymerisation are investigated. Such formulations include PMAA-PMEMA, PMAA-PMETAC, PMAA-PDMA and PDMA-PMAA (see **Schemes 4.3-4.6**).

The RAFT solution polymerisation of MAA in ethanol was followed by RAFT polymerisation of MEMA in aqueous media at pH 6.5 (**Scheme 4.3**). MEMA is miscible in all proportions with water, thus its RAFT polymerisation can proceed at pH 6.5, which enables significantly higher comonomer conversions and relatively narrow molecular weight distributions to be achieved than at higher solution pH, where premature hydrolysis of the RAFT chain-ends can occur (**Table 4.2**). This is owing to the relatively low pK_a for the corresponding weakly basic PMEMA homopolymer (see **Table 4.3**). This means that PMEMA has a significantly lower degree of protonation than PDMA at pH 6.5. The subtle shift in IEP observed for various $PMAA_{57}$-$PMEMA_y$ copolymer compositions is shown in **Figure 4.7**.
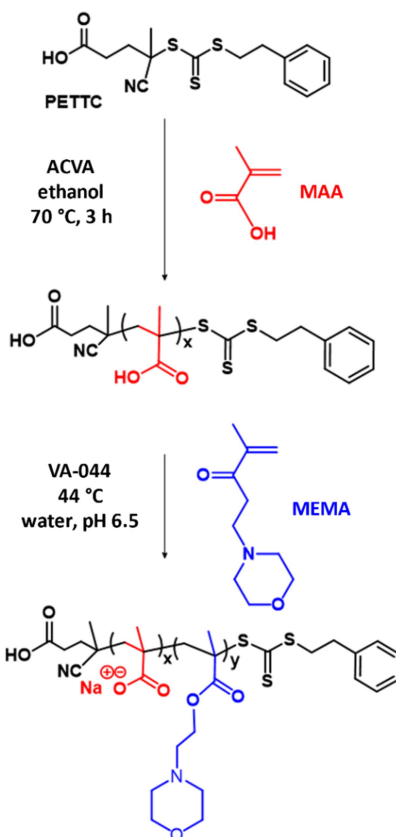
Scheme 4.3 RAFT solution polymerisation of MAA in ethanol using PETTC with ACVA initiator produced PMAA within 3 h at 70 °C. This precursor was then chain-extended via RAFT polymerisation MEMA in aqueous media using VA-044 initiator at 44 °C. See **Table 4.4** for a summary of the reaction pH in each case.

Table 4.3 Summary of pK_a values for the conjugate acid (protonated) forms of PMEMA, PDEA, PDPA, PDMA, PMAA and PCEA homopolymers taken from the literature[38–42] and those determined by acid titration.

| Homopolymer	Literature pK_a	Measured pK_a
PMEMA	4.9	5.3
PDEA	7.3	7.2
PDPA	6.0	6.0
PDMA	7.0	6.8
PCEA	5.0	5.3
PMAA	5.6	5.8
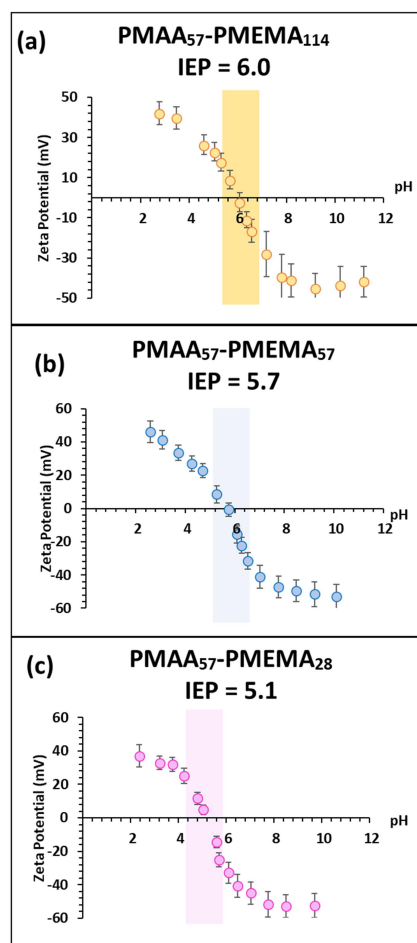
Figure 4.7 Zeta potential vs. pH curves obtained by aqueous electrophoresis studies indicate isoelectric points and regions of colloidal instability for (a) $PMAA_{57}$-$PMEMA_{114}$, (b) $PMAA_{57}$-$PMEMA_{57}$ and (c) $PMAA_{57}$-$PMEMA_{28}$ in the presence of 1 mM KCl as background salt. [N.B. A higher IEP is obtained on increasing the MEMA mol% of the zwitterionic diblock copolymer].

A wholly aqueous one-pot synthetic protocol (**Scheme 4.4**) can also be used to prepare PMAA-PMETAC diblock copolymers. Thus, a $PMAA_{67}$ precursor was synthesised in acidic aqueous solution at pH 2 using an ACVA initiator and CPDB RAFT agent (CPDB/ACVA molar ratio = 4.0). In this case, further degassed deionised water was added as the polymerisation progressed to ensure that the reaction mixture did not become too viscous. The second block can then be grown without further pH adjustment to produce a $PMAA_{67}$-$PMETAC_{116}$ diblock copolymer via RAFT aqueous solution polymerisation of METAC (99% METAC conversion; M_n = 15 000 g mol^{-1} M_w/M_n = 1.20). ^{1}H NMR conversion and GPC

molecular weight results for the polymerisations depicted in **Schemes 4.3** and **4.4** are

summarised in **Table 4.4**.
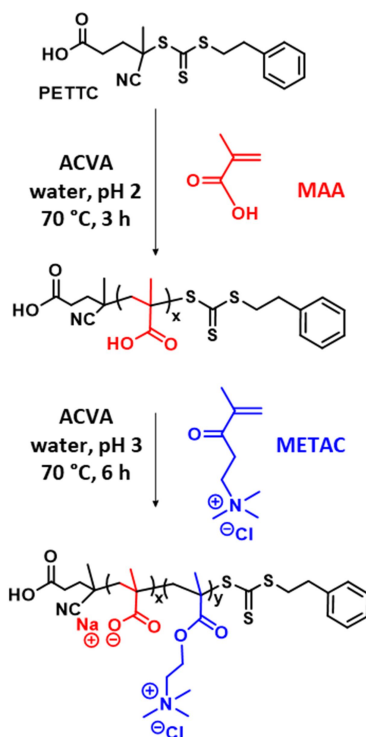
Scheme 4.4 Wholly aqueous one-pot synthesis of a zwitterionic diblock copolymer via RAFT solution polymerisation, where the first block comprises PMAA and the second block is PMETAC.

Table 4.4 Summary of the characterisation data obtained for a series of zwitterionic diblock copolymers synthesised via RAFT aqueous solution polymerisation, for which PMAA is the first block and the second block comprises PMEMA or PMETAC with the second-stage polymerisation being conducted at the stated reaction pH). These syntheses were conducted protocols described in **Scheme 4.3 and 4.4**.

Synthetic method	Diblock copolymer composition	Reaction pH	^{1}H NMR conversion (%)	Theoretical M_n (g mol^{-1})	GPC (g mol^{-1})		IEP
					M_n	M_w/M_n	
Two-pot	PMAA$_{56}$-PMEMA$_{114}$	6.5	98	26 200	31 600[a]	1.37[a]	6.1
Two-pot	PMAA$_{56}$-PMEMA$_{56}$	6.5	> 99	16 300	15 600[a]	1.28[a]	5.7
Two-pot	PMAA$_{56}$-PMEMA$_{28}$	6.5	> 99	10 700	11 000[a]	1.22[a]	5.1
One-pot	PMAA$_{67}$-PMETAC$_{116}$	3.0	> 99	16 600	15 000[a]	1.20[a]	No IEP
One-pot	PMAA$_{91}$-PMETAC$_{22}$	3.0	98	12 600	10 600[a]	1.26[a]	5.1
One-pot	PMAA$_{126}$-PMETAC$_{126}$	3.0	98	37 200	29 000[b]	1.15[b]	No IEP

a. GPC analysis using THF eluent vs. PMMA standards.

b. GPC analysis using DMF eluent vs. PMMA standards.

It is perhaps worth emphasising that certain types of zwitterionic diblock copolymers cannot exhibit an IEP. For example, PMETAC-rich copolymers for which the second block is PMAA should remain water-soluble regardless of the solution pH, because the number of anionic charges on the PMAA block can never equal the number of permanently cationic charges on the longer PMETAC block. Although the PMAA becomes more insoluble at lower pH values, it does not become sufficiently hydrophobic to form particles. On the other hand, if the number of MAA (or CEA) repeat units was equal to (or greater than) the number of METAC repeat units, then such zwitterionic diblock copolymers should exhibit an IEP. **Figure 4.8** demonstrates this phenomenon.
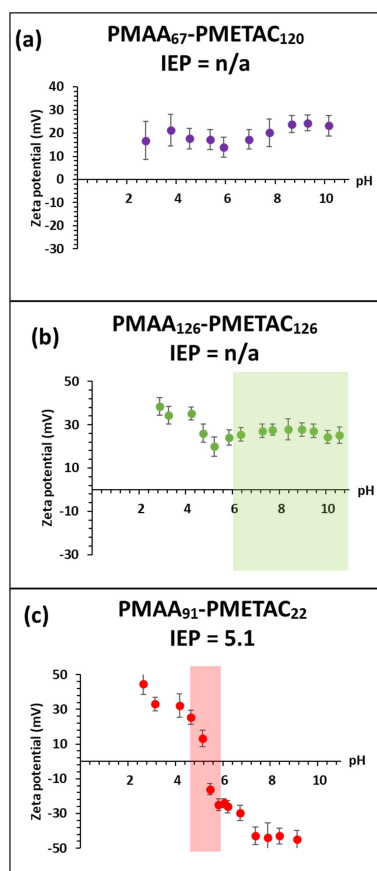
Figure 4.8 Zeta potential vs. pH curves determined by aqueous electrophoresis studies indicate isoelectric points and regions of colloidal instability for **(a)** $PMAA_{67}$-$PMETAC_{120}$, **(b)** $PMAA_{126}$-$PMETAC_{126}$ and **(c)** $PMAA_{91}$-$PMETAC_{22}$ in the presence of 1 mM KCl as background salt. Highlighted regions indicate regions of macroscopic precipitation.

As expected, $PMAA_{126}$-$PMETAC_{126}$ forms a macroscopic precipitate above pH 6. Normally, such behaviour is only observed at around the IEP. However, in this case the zeta potential actually remains positive over the entire solution pH range, so this particular zwitterionic copolymer exhibits no IEP (**Figure 4.8b**). Currently, we have no satisfactory explanation for this unexpected observation. The same analysis was performed on a $PMAA_{67}$-$PMETAC_{67}$ diblock copolymer, which yielded the same results, presenting a positive zeta potential between pH 2-11.

The feasibility of conducting the wholly aqueous synthesis of zwitterionic PDMA-PMAA diblock copolymers was also investigated (**Scheme 4.5**). A one-pot protocol utilising PDMA as the first block was optimised as follows. Firstly, a $PDMA_{50}$ precursor was prepared at 44 °C by RAFT aqueous solution polymerisation of DMA using PETTC and ACVA initiator (CTA/ACVA molar ratio = 4.0), at 40% w/w solids. Then the initial solution pH was lowered from 9.5 to 7.0 prior to polymerisation by addition of 35% HCl; this adjustment is required to suppress hydrolysis of the DMA monomer, which would otherwise afford 2-(dimethylamino)ethanol and MAA.[43] Even so, ^{1}H NMR studies indicated that this side reaction produced up to 1.5% MAA residues within the PDMA chains under these conditions, which is significantly lower than that reported by Carlsson et al.[43] who observed more than 7% hydrolysis within 2 h at 70 °C. Then MAA was added to the reaction mixture and the ensuing polymerisation proceeded to approximately 99% conversion to produce a well-defined $PDMA_{50}$-$PMAA_{50}$ diblock copolymer with a relatively narrow molecular weight distribution (M_n = 11 000 g mol^{-1}, M_w/M_n = 1.23). The conversion vs. time curves obtained from in situ NMR studies (see **Figures 4.9** and **4.10)** confirm that high conversions can be obtained for each block within 8 h at 44 °C. Similarly, in situ NMR studies conducted during the synthesis of $PDMA_{100}$ and $PDMA_{200}$ precursor blocks at 40% w/w solids indicated that

essentially full monomer conversion is achieved within 3.5 h and 4 h, respectively (**Figure 4.11**).
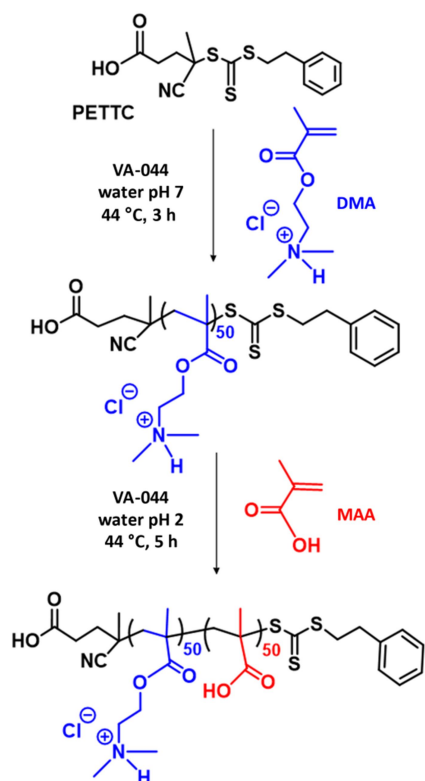
Scheme 4.5 Wholly aqueous one-pot synthetic route to zwitterionic diblock copolymers via RAFT aqueous solution polymerisation of MAA at 44 °C using a fully protonated PDMA precursor.

Aqueous GPC studies on unmodified zwitterionic diblock copolymers indicate that reasonably high blocking efficiencies (i.e. minimal contamination by the homopolymer precursor) can be achieved during their RAFT synthesis (**Table 4.5**). The PDMA precursor was necessarily analysed using THF eluent because the PDMA block is not soluble in the aqueous eluent (1.0 M NaNO$_3$, pH 10). The reported molecular weight values are based on PEO standards, and entirely dependent on how the molecules coil in the eluent, so these values are unlikely to be accurate.

Table 4.5 Summary of the characterisation data obtained for zwitterionic diblock copolymers synthesised via RAFT aqueous solution polymerisation, for which PDMA is the first block and the second block comprises PMAA with the second-stage polymerisation being conducted at pH 2. These syntheses were conducted according to protocols described in **Scheme 4.5**.

Diblock copolymer composition	PDMA ^{1}H NMR conversion (%)	PMAA ^{1}H NMR conversion (%)	THF GPC (PDMA)		Aqueous GPC (PDMA-PMAA)		IEP
			M_n (g mol^{-1})	M_w/M_n	M_n (g mol^{-1})	M_w/M_n	
PDMA$_{200}$-PMAA$_{200}$	>99	>99	45 900	1.29	41 800	1.25	6.6
PDMA$_{50}$-PMAA$_{50}$	99	>99	15 700	1.29	11 000	1.23	6.7
PDMA$_{50}$-PMAA$_{100}$	>99	>99	15 700	1.29	25 500	1.12	5.4
PDMA$_{100}$-PMAA$_{50}$	99	>99	12 400	1.12	18 700	1.32	8.6
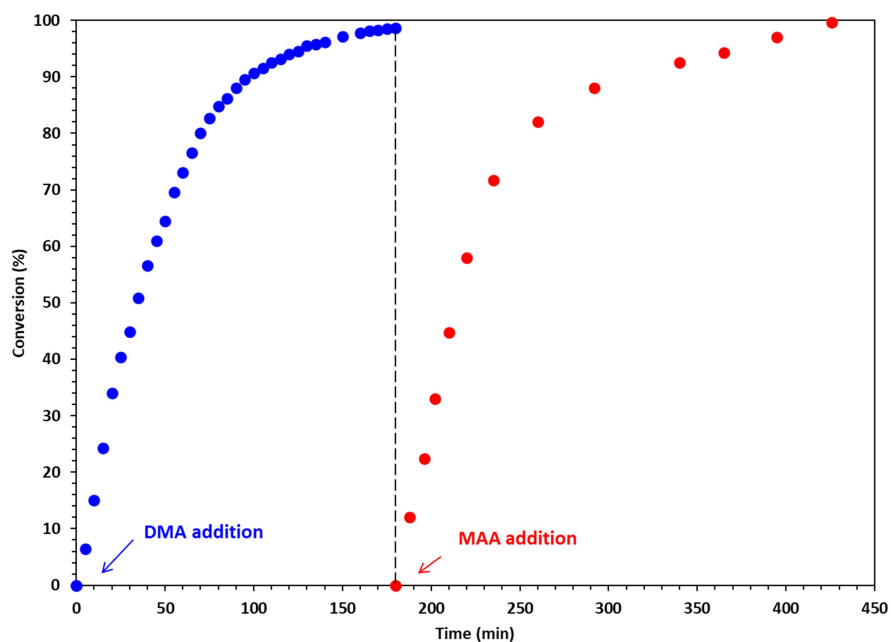
Figure 4.9 Conversion vs. time curves obtained from in situ ^{1}H NMR spectroscopy studies conducted in D$_2$O for the wholly aqueous one-pot synthesis of a PDMA$_{50}$-PMAA$_{50}$ zwitterionic diblock copolymer. Essentially full DMA conversion is achieved within 3 h at 44 °C for the first block, while the subsequent MAA polymerisation required 4.5 h at the same temperature.
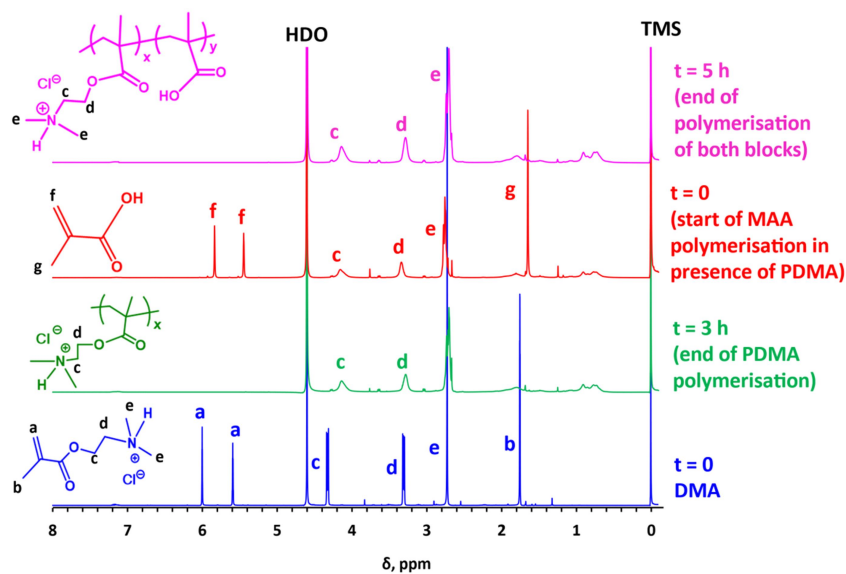
Figure 4.10 Selected ^{1}H NMR spectra recorded in D$_2$O at the start (blue) and end (green) of the RAFT aqueous solution polymerization of DMA and also at the start (red) and end (pink) of the subsequent MAA polymerisation. Note the absence of any residual monomer vinyl signals in each case. Sodium 2,2,3,3-d(4)-3-(trimethylsilyl)propionate (labelled as 'TMS') is used as a water-soluble reference compound and gives rise to a characteristic signal at 0 ppm.
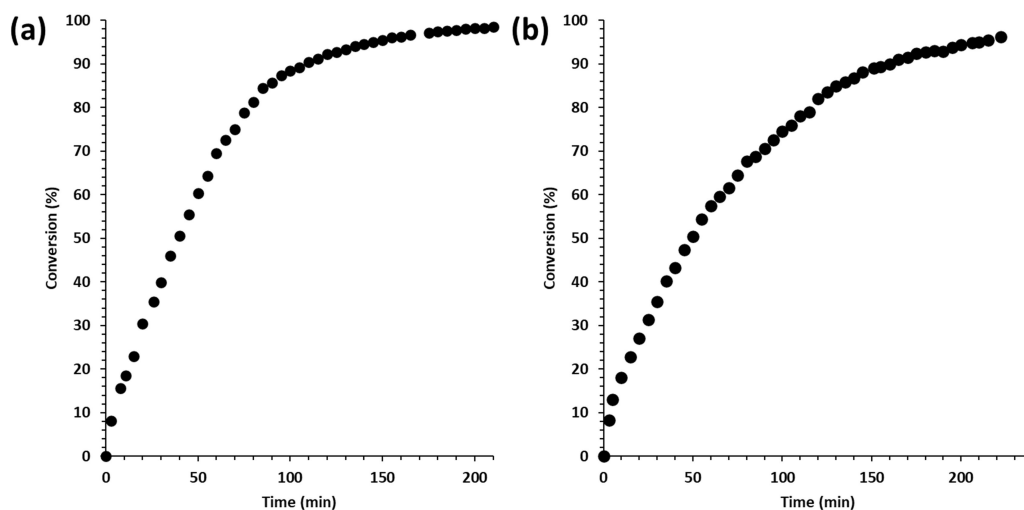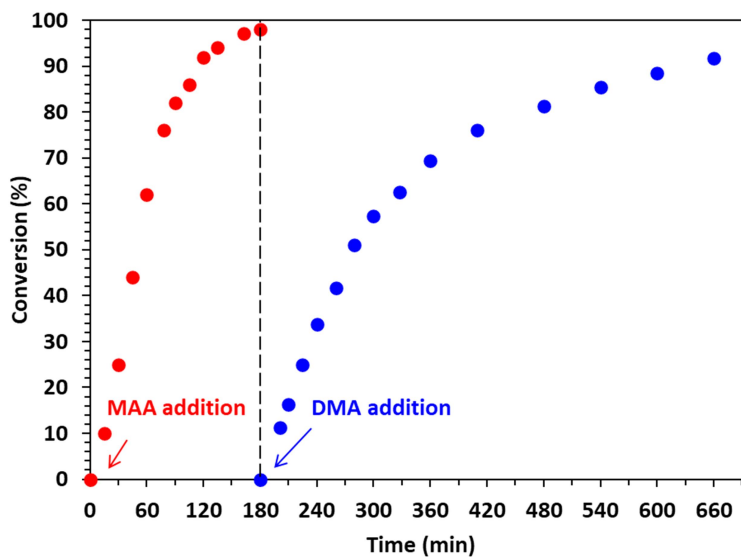

Figure 4.11 Conversion vs. time curves obtained from in situ ^{1}H NMR spectroscopy studies conducted in D$_2$O for the wholly aqueous synthesis of **(a)** a PDMA$_{100}$ precursor, where essentially full DMA conversion is achieved within 3.5 h at 44 °C and **(b)** a PDMA$_{200}$ precursor, where greater than 96% DMA conversion is achieved within 4 h at 44 °C.

A one-pot protocol was also developed for these PMAA-first syntheses (**Scheme 4.6**).

However, polymerising MAA first leads to somewhat lower comonomer conversions and

broader molecular weight distributions than those achieved when preparing the equivalent

zwitterionic diblock copolymers by polymerising DMA first (see **Table 4.6** for examples of MAA-first polymerisations). For the **MAA-first** syntheses, premature hydrolysis of the RAFT end-groups may occur in the mildly alkaline solution conditions preferred for the second-stage polymerisation of DMA.[35,44]
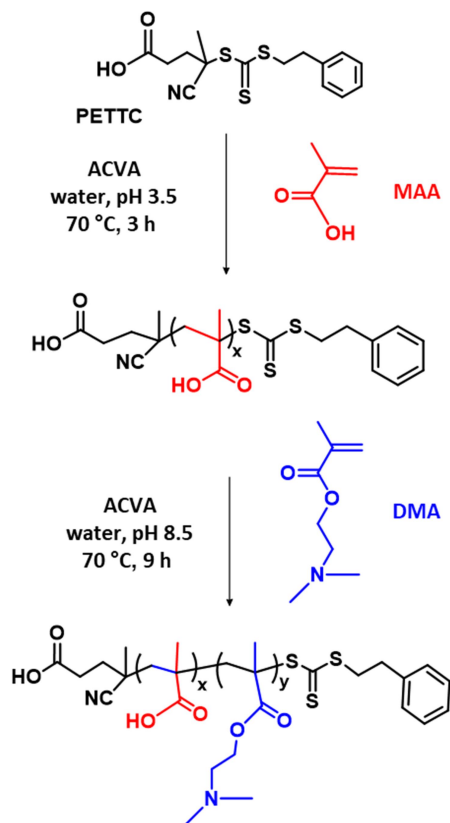
Scheme 4.6 Wholly aqueous one-pot synthetic route to zwitterionic diblock copolymers via RAFT aqueous solution polymerisation of DMA at 70 °C using a fully deprotonated PMAA precursor.

Table 4.6 Summary of the characterisation data obtained for zwitterionic diblock copolymers synthesised via RAFT aqueous solution polymerisation, for which PMAA is the first block and the second block comprises PDMA with the second-stage polymerisation being conducted at **pH 8.5.** These syntheses were conducted via the protocol described in **Scheme 4.6.**

Diblock copolymer composition	CTA	PMAA ^{1}H NMR conversion (%)	PDMA ^{1}H NMR conversion (%)	Aqueous GPC (PMAA) (g mol^{-1})		Aqueous GPC (diblock) (g mol^{-1})	
				M_n	M_w/M_n	M_n	M_w/M_n
PMAA$_{45}$-PDMA$_{48}$	PETTC	89	95	8 900	1.21	13 800	1.35
PMAA$_{47}$-PDMA$_{48}$	CPDB	93	96	7 100	1.28	14 400	1.19
PMAA$_{50}$-PDMA$_{95}$	PETTC	99	95	4 200	1.66	14 700	1.47
PMAA$_{40}$-PDMA$_{96}$	CPDB	80	96	6 100	1.30	19 700	1.21
PMAA$_{97}$-PDMA$_{49}$	PETTC	97	97	10 700	1.16	17 700	1.23
PMAA$_{84}$-PDMA$_{42}$	CPDB	84	83	14 300	1.13	17 500	1.20

IEP data for these PMAA-first syntheses is not shown, as incomplete conversion and hydrolysis led to much lower IEPs then expected.

Figure 4.12 Conversion vs. time curves obtained from in situ ^{1}H NMR spectroscopy studies conducted in D$_2$O for the wholly aqueous one-pot synthesis of a PMAA$_{50}$-PDMA$_{50}$ zwitterionic diblock copolymer. Essentially full **MAA** conversion is achieved within 3 h at 44 °C for the synthesis of the first block at pH 3.5, while the subsequent **DMA** polymerization at pH 8.5 requires 9 h at the same temperature.

The IEP is determined for three examples of PDMA$_x$-PMAA$_y$ copolymers in **Figure 4.13**. The IEP exhibited by such zwitterionic diblock copolymers can be tuned from pH 5.4 to 8.6 by systematic variation of the relative proportions of the anionic and cationic comonomers. More specifically, increasing the DMA mol% of such copolymers leads to higher IEPs.
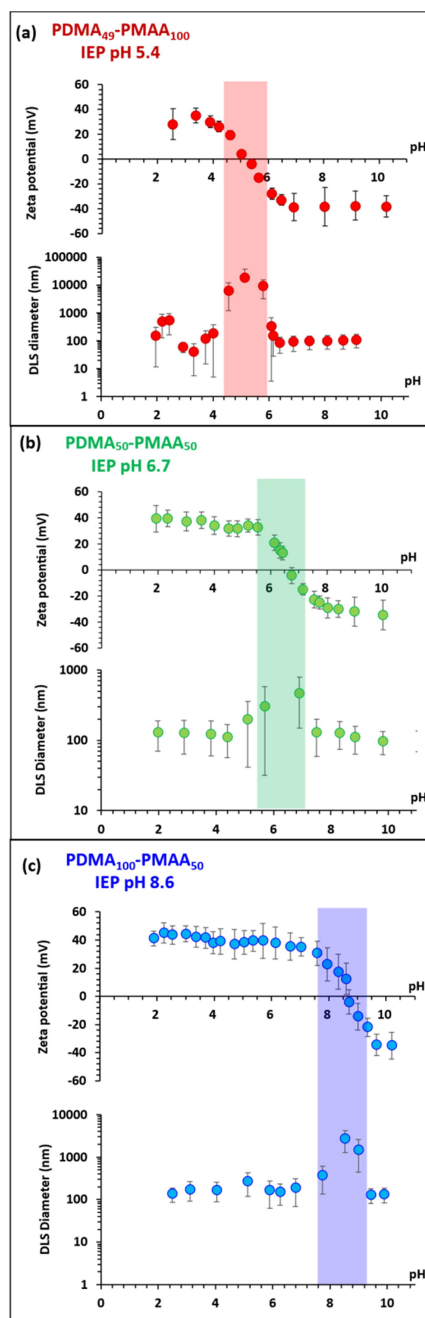
Figure 4.13 Variation in zeta potential and DLS diameter with solution pH to determine isoelectric points and regions of colloidal instability for (a) PDMA$_{49}$-PMAA$_{100}$, (b) PDMA$_{50}$-PMAA$_{50}$ and (c) PDMA$_{100}$-PMAA$_{50}$ in the presence of 1 mM KCl as background salt. [N.B. Higher IEPs are obtained on increasing the DMA mol% in the zwitterionic diblock copolymer].

^{1}H NMR spectroscopy can be used to assess changes in the degree of solvation of each block for a PDMA$_{50}$-PMAA$_{50}$ zwitterionic diblock copolymer, see **Figure 4.14**. At pH 6, almost no NMR signals can be observed for this copolymer owing to macroscopic precipitation at its IEP. However, addition of sufficient background salt at this pH enables screening of the electrostatic attractions between the cationic and anionic blocks, which in turn confers water solubility. Under such conditions, NMR signals assigned to the protonated PDMA block (see *a*, *b* and *c*) are observed. In contrast, the ionised anionic PMAA exhibits almost no unique NMR signals because its methacrylic backbone signals simply overlap with those of the PDMA block. However, there is some evidence for a weak broad signal *e* at around 1.7 ppm that is assigned to the two CH$_2$ backbone protons associated with the anionic carboxylate form of the MAA repeat units.

At pH 2 (0.01 M DCl in D$_2$O), the PDMA block is fully protonated. Hence signals *a*, *b* and *c* are observed 2.9, 3.5 and 4.3 ppm, respectively, whereas ionisation of the PMAA block is suppressed. The methacrylic backbone signals *f* and *g* assigned to the former block are also prominent at 1.0 and 1.9 ppm, respectively. However, the methacrylic backbone signals (*e* and *d*; 0 - 2.5 ppm) for the neutral PMAA block are suppressed. At pH 9 (NaOD/D$_2$O), the PMAA block becomes highly ionised and acquires highly anionic character, whereas the PDMA block becomes deprotonated (but remains at least partially solvated). As expected, some of the NMR signals assigned to the PDMA block are shifted to lower δ values: *a*, *b*, and *c* now appear at 2.0, 2.6 and 4.0 ppm. The methacrylic backbone protons *d* and *e* assigned to the anionic PMAA block are now fully solvated and appear at 0.9 and 1.6 ppm, respectively. The PDMA signals *f* and *g* remain unchanged at δ 1.0 and 1.9 ppm. The NMR shifts for these methacrylic backbone signals are less sensitive to the degree of protonation of the PDMA block than the 2-(dimethyl)amino, azamethylene and oxymethylene proton signals associated

with the pendent 2-(dimethylamino)ethyl groups (see signals *a*, *b* and *c* respectively in the purple spectrum shown in **Figure 4.14**).
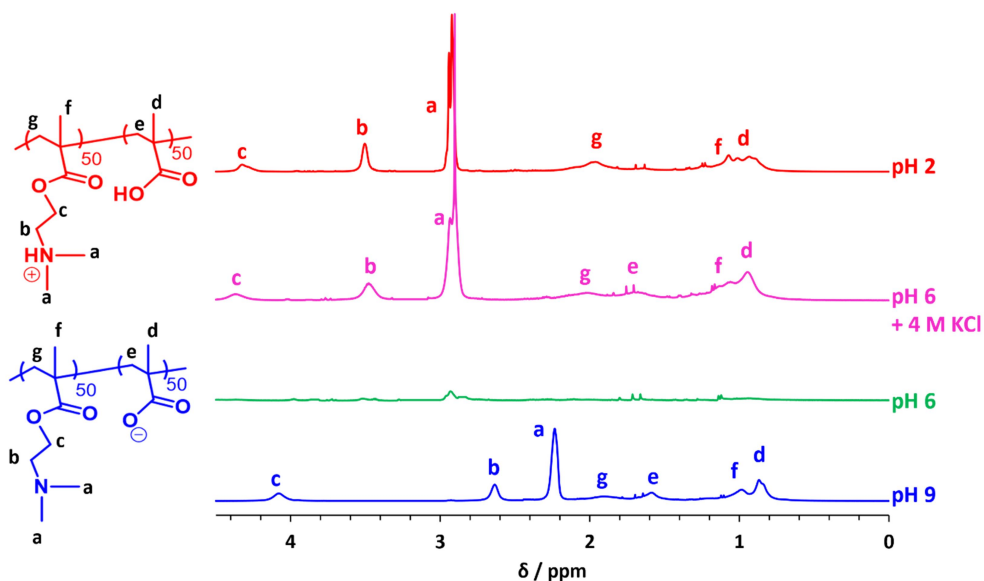

Figure 4.14 ^{1}H NMR spectra recorded for (i) a PDMA$_{50}$-PMAA$_{50}$ zwitterionic diblock copolymer in DCl/D$_2$O at pH 2 (where both blocks are fully protonated), (ii) at pH 6 in the presence of 4 M KCl (to suppress macroscopic precipitation at this IEP), (iii) at the same pH in the absence of salt, and (iv) in NaOD/D$_2$O at pH 9 (where the PMAA block is fully ionised and the PDMA block is in its near-neutral, weakly hydrophilic form).

4.3.4 Modification of zwitterionic diblock copolymers for GPC analysis

GPC analysis of some zwitterionic diblock copolymers typically requires chemical modification to ensure solubility in a suitable eluent. For PMAA-PMETAC diblock copolymers, this was achieved by forced hydrolysis of the ester groups in the PMETAC block to produce a PMAA homopolymer. This precursor was then exhaustively methylated using excess trimethylsilyldiazomethane to afford poly(methyl methacrylate) [PMMA], which is amenable to GPC analysis using THF eluent (more details for this protocol can be found in Chapter 5, see Figure 5.2).

For zwitterionic diblock copolymers comprising poly(tertiary amine methacrylate) blocks, it is important to demonstrate that methylation of the carboxylic acid groups in the PCEA block

occurs with essentially no quaternisation of the tertiary amine groups. Such selectivity can be achieved using a 3:2 toluene/methanol solvent mixture.[45,46] This was confirmed by conducting a control experiment in which a PDMA$_{50}$ homopolymer was exposed to the same methylation conditions. Compared to the other three poly(tertiary amine methacrylate) blocks examined in this study, PDMA is the least sterically-hindered and hence the most reactive towards quaternisation.[47] Thus if no quaternisation is observed when PDMA homopolymer is exposed to a ten-fold excess of trimethylsilyldiazomethane, then this potential side reaction is extremely unlikely to occur for PDEA, PDPA or PMEMA. ^{1}H NMR spectroscopy studies of a PDMA$_{50}$ homopolymer confirmed that essentially no spectral changes occurred after its exposure to typical methylation conditions (see **Figure 4.15**). Furthermore, GPC studies confirmed no significant change in its molecular weight distribution. Accordingly, selective methylation of various zwitterionic diblock copolymers was conducted using a ten-fold excess of trimethylsilyldiazomethane based on the molar concentration of tertiary amine methacrylate repeat units. However, these derivatisations were conducted in dilute solution (2.0% w/w copolymer) at 20 °C and hence required a long reaction time (72 h) to ensure the highest possible extent of reaction. In each case, the degree of methylation was determined by ^{1}H NMR spectroscopy by comparing the integral of the new methoxy proton signal at approximately 3.6 ppm to that of the methacrylic backbone signals for both blocks at 0 to 2.2 ppm. An example of the selective methylation of the MAA residues in a PDPA$_{67}$-PMAA$_{67}$ diblock copolymer to afford PDPA$_{67}$-PMMA$_{67}$ chains that are amenable to GPC analysis is shown in **Figure 4.16.**
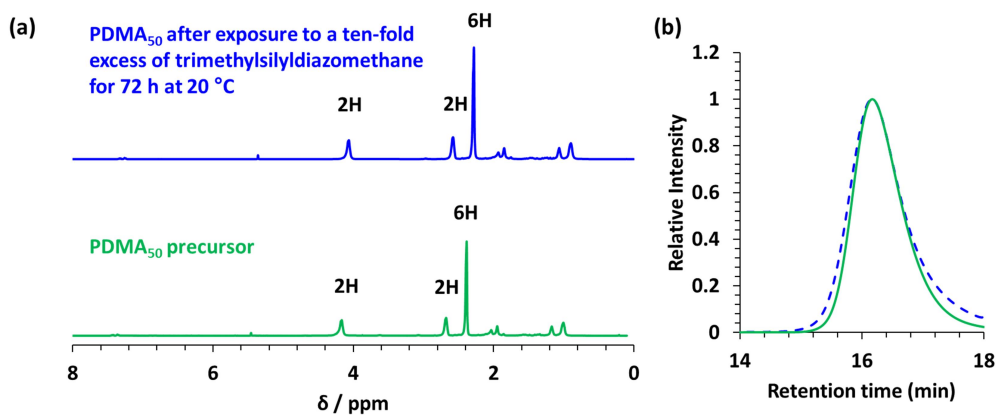
Figure 4.15 (a) ^{1}H NMR spectra recorded for a PDMA$_{50}$ homopolymer before (lower spectrum) and after (upper spectrum) exposure to a ten-fold excess of trimethylsilyldiazomethane for 72 h at 20 °C. **(b)** GPC curve recorded for PDMA$_{50}$ before (green) and after (blue) exposure to methylation conditions. This control experiment confirms no detectable quaternisation of the tertiary amine groups, thus *selective* methylation of the PMAA (or PCEA) blocks in zwitterionic diblock copolymers is anticipated under such conditions.
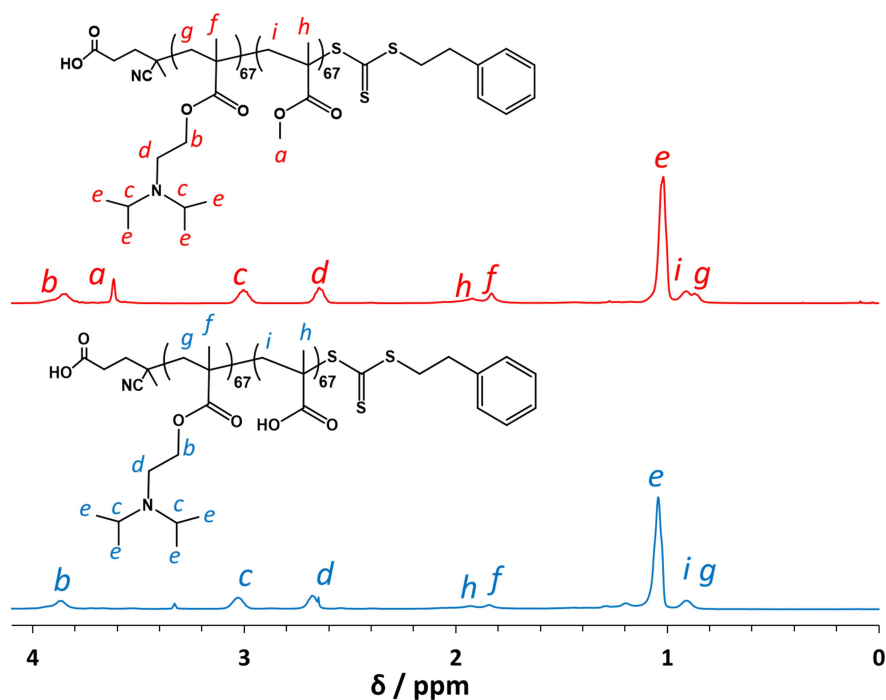
Figure 4.16 ^{1}H NMR spectra recorded for a PDPA$_{67}$-PMAA$_{67}$ diblock copolymer before (blue spectrum) and after (red spectrum) exhaustive methylation using excess trimethylsilyldiazomethane. A new signal *a* at approximately 3.6 ppm is assigned to methoxy protons, indicating successful formation of a PDPA-PMMA diblock copolymer. Such selective derivatisation is essential for reliable GPC analysis of zwitterionic diblock copolymers.

GPC analysis of methylated PDMA-PCEA diblock copolymers or PMAA homopolymer was conducted using DMF eluent. However, THF eluent was preferred for PDEA-, PMEMA- and PDPA-based diblock copolymers.

4.3.4 Aqueous end-group removal of zwitterionic diblock copolymers

Removal of the trithiocarbonate end-groups was examined using a weakly basic aqueous solution of hydrazine hydrate (pH 9) at a hydrazine/trithiocarbonate molar ratio of 2.0 at 20 °C for 3.5 h. UV spectroscopy was used to monitor the disappearance of the trithiocarbonate signal at 314 nm over 3.5 h at 20 °C. The progressive reduction in absorbance at this wavelength over time is shown in **Figure 4.17a**. However, the original band never reaches the baseline. At first sight, this suggests that end-group removal remains incomplete under such conditions. However, this is simply an artefact caused by the appearance of a new band at approximately 304 nm, which is assigned to unknown UV-active small-molecule by-products generated during chain-end removal. Similar observations have been reported by Jesson *et al.* when using UV spectroscopy to monitor the removal of dithiobenzoate end-groups using excess H_2O_2.[48] Fortunately, this technical problem can be circumvented by using UV GPC (DMF eluent; $\lambda = 314$ nm; after exhaustive methylation of the PMAA block) to monitor the extent of end-group removal, because this technique leads to fractionation of the copolymer chains from the small-molecule by-products prior to their detection. Comparison of the UV signals for the diblock copolymer chains before and after end-group removal indicates substantial loss (approximately 98%) of the original trithiocarbonate end-groups (**Figure 4.17b**). Moreover, the insolubility of such zwitterionic diblock copolymers at around their IEP enables their purification after hydrazine derivatisation using a wholly aqueous work-up. Thus, after hydrazine treatment of an initially yellow $PDMA_{50}$-$PMAA_{50}$ copolymer at pH 9 to remove its end-groups, the solution pH was lowered to the isoelectric point of the zwitterionic diblock copolymer using 0.25 M HCl to induce its macroscopic

precipitation. The insoluble crude copolymer was then washed four times using deionised water (at its IEP of pH 6) to remove the small-molecule by-products. The resulting purified white polymer was then analysed by ^{1}H NMR spectroscopy in CD$_3$OD to confirm disappearance of the aromatic signals at 7-8 ppm (data not shown).

In principle, this end-group removal method should be well-suited for industrial scale-up since it avoids the use of any organic solvents. However, it is perhaps worth emphasising that this protocol is only feasible for diblock copolymers that exhibit an IEP, For example, it is not suitable for PMETAC-rich PMAA-PMETAC diblock copolymers for which there is insufficient anionic charge to induce macroscopic precipitation even at high pH.
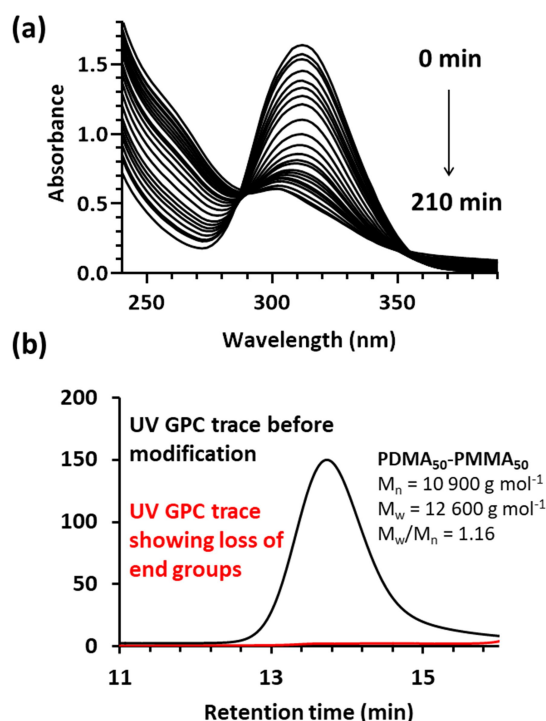
Figure 4.17 Removal of trithiocarbonate end-groups from a PDMA$_{51}$-PMAA$_{50}$ zwitterionic diblock copolymer using an aqueous solution of hydrazine at pH 9 (hydrazine/trithiocarbonate molar ratio = 1.0). (a) UV spectra showing the progressive reduction in absorbance at λ = 314 nm over 3.5 h at 20 °C. (b) After exhaustive selective methylation of the MAA residues in this PDMA$_{50}$-PMAA$_{50}$ copolymer, DMF UV GPC curves recorded at λ = 314 nm indicate a 98% reduction in the original UV signal associated with the trithiocarbonate end-groups.

4.4 Conclusions

In summary, we report a new, highly convenient and atom-efficient synthetic route to a range of well-defined zwitterionic diblock copolymers, whereby the anionic block is either poly(methacrylic acid) or poly(2-carboxyethyl acrylate), while the cationic block can be poly(2-(dimethylamino)ethyl methacrylate), poly(2-(diethylamino)ethyl methacrylate), poly(2-(*N*-morpholino)ethyl methacrylate) or poly(2-(methacryloyloxy)ethyl trimethylammonium chloride). Such wholly aqueous formulations do not require protecting group chemistry and either the cationic or the anionic monomer can be polymerised first. Varying the copolymer composition and/or the type of cationic monomer enables the isoelectric point exhibited by such zwitterionic diblock copolymers to be readily tuned and one-pot syntheses are also feasible. Treatment with hydrazine enables the trithiocarbonate RAFT end-groups to be removed and macroscopic precipitation at the isoelectric point facilitates wholly aqueous work-up after this derivatisation. According to the literature, such zwitterionic diblock copolymers should be useful pigment dispersants for aqueous formulations; this hypothesis is evaluated for two inorganic pigments in Chapter 5.

4.5 References

1. Xin, X., Wang, Y. & Liu, W. Synthesis of zwitterionic block copolymers via RAFT polymerization. *Eur. Polym. J.* **41**, 1539–1545 (2005).

2. Bütün, V. *et al.* A brief review of 'schizophrenic' block copolymers. *React. Funct. Polym.* **66**, 157–165 (2006).

3. Canning, S. L., Neal, T. J. & Armes, S. P. pH-Responsive Schizophrenic Diblock Copolymers Prepared by Polymerization-Induced Self-Assembly. *Macromolecules* **50**, 6108–6116 (2017).

4. Patrickios, C. S., Hertler, W. R., Abbott, N. L. & Hatton, T. A. Diblock, ABC Triblock, and Random Methacrylic Polyampholytes: Synthesis by Group Transfer Polymerization and Solution Behavior. *Macromolecules* **27**, 930–937 (1994).

5. Liu, S. & Armes, S. P. Polymeric surfactants for the new millennium: A pH-responsive, zwitterionic, schizophrenic diblock copolymer. *Angew. Chemie* **41**, 1413–1416 (2002).

6. Lowe, A. B. & McCormick, C. L. Synthesis and solution properties of zwitterionic polymers. *Chem. Rev.* **102**, 4177–4189 (2002).

7. Sun, T. L. *et al.* Physical hydrogels composed of polyampholytes demonstrate high toughness and viscoelasticity. *Nat. Mater.* **12**, 932–937 (2013).

8. Laschewsky, A. Structures and synthesis of zwitterionic polymers. *Polymers (Basel).* **6**, 1544–1601 (2014).

9. Doncom, K. E. B., Warren, N. J. & Armes, S. P. Polysulfobetaine-based diblock copolymer nano-objects via polymerization-induced self-assembly. *Polym. Chem.* **6**, 7264–7273 (2015).

10. McCormick, C. L. & Lowe, A. B. Aqueous RAFT polymerization: Recent developments in synthesis of functional water-soluble (Co)polymers with controlled structures. *Acc. Chem. Res.* **37**, 312–325 (2004).

11. Blackman, L. D., Gunatillake, P. A., Cass, P. & Locock, K. E. S. An introduction to zwitterionic polymer behavior and applications in solution and at surfaces. *Chem. Soc. Rev.* **48**, 757–770 (2019).

12. Ehrlich, G. & Doty, P. Macro-ions. III. The Solution Behavior of a Polymeric Ampholyte. *J. Am. Chem. Soc.* **76**, 3764–3777 (1954).

13. Chakrabarty, T., Kumar, M. & Shahi, V. K. pH responsive hybrid zwitterionomer for protein separation: Smart nanostructured adsorbent. *Ind. Eng. Chem. Res.* **51**, 3015–3022 (2012).

14. Liu, J., Ma, Y., Xu, T. & Shao, G. Preparation of zwitterionic hybrid polymer and its application for the removal of heavy metal ions from water. *J. Hazard. Mater.* **178**, 1021–1029 (2010).

15. Fultz, B. A., Terlier, T., Dunoyer De Segonzac, B., Verduzco, R. & Kennemur, J. G. Nanostructured Films of Oppositely Charged Domains from Self-Assembled Block Copolymers. *Macromolecules* **58**, 45 (2020).

16. Liu, P. *et al.* Metal-Chelating Polymers (MCPs) with Zwitterionic Pendant Groups Complexed to Trastuzumab Exhibit Decreased Liver Accumulation Compared to Polyanionic MCP Immunoconjugates. *Biomacromolecules* **16**, 3613–3623 (2015).

17. Liu, C., Lee, J., Ma, J. & Elimelech, M. Antifouling Thin-Film Composite Membranes by Controlled Architecture of Zwitterionic Polymer Brush Layer. *Environ. Sci. Technol.* **51**, 2161–2169 (2017).

18. Creutz, S. & Jérôme, R. Effectiveness of block copolymers as stabilizers for aqueous titanium dioxide dispersions of a high solid content. *Prog. Org. Coatings* **40**, 21–29 (2000).

19. Creutz, S., Jérôme, R., Kaptijn, G. M. P., Van Der Werf, A. W. & Akkerman, J. M. Design of polymeric dispersants for waterborne coatings. *J. Coatings Technol.* **70**, 41–46 (1998).

20. Lowe, A. B. & McCormick, C. L. Reversible addition-fragmentation chain transfer (RAFT) radical polymerization and the synthesis of water-soluble (co)polymers under homogeneous conditions in organic and aqueous media. *Prog. Polym. Sci.* **32**, 283–351 (2007).

21. Kamachi, M., Kurihara, M. & Stille, J. K. Synthesis of Block Polymers for Desalination Membranes. Preparation of Block Copolymers of 2-Vinylpyridine and Methacrylic Acid or

Acrylic Acid. *Macromolecules* **5**, 161–167 (1972).

22. Bütün, V., Billingham, N. C. & Armes, S. P. Unusual aggregation behavior of a novel tertiary amine methacrylate- based diblock copolymer: Formation of Micelles and reverse Micelles in aqueous solution. *J. Am. Chem. Soc.* **120**, 11818–11819 (1998).

23. Lowe, A. B., Billingham, N. C. & Armes, S. P. Synthesis and characterization of zwitterionic block copolymers. *Macromolecules* **31**, 5991–5998 (1998).

24. Bories-Azeau, X., Armes, S. P. & Van Den Haak, H. J. W. Facile Synthesis of Zwitterionic Diblock Copolymers without Protecting Group Chemistry. *Macromolecules* **37**, 2348–2352 (2004).

25. Matyjaszewski, K. & Xia, J. Atom transfer radical polymerization. *Chem. Rev.* **101**, 2921–2990 (2001).

26. Zhang, X., Ma, J., Yang, S. & Xu, J. 'Schizophrenic' micellization of poly(acrylic acid)-B poly(2-dimethylamino)ethyl methacrylate and responsive behavior of the micelles. *Soft Mater.* **11**, 394–402 (2013).

27. Nicolas, J. *et al.* Nitroxide-mediated polymerization. *Prog. Polym. Sci.* **38**, 63–235 (2013).

28. Couvreur, L. *et al.* First nitroxide-mediated controlled free-radical polymerization of acrylic acid. *Macromolecules* **36**, 8260–8267 (2003).

29. Moad, G., Rizzardo, E. & Thang, S. H. Living radical polymerization by the RAFT process. *Aust. J. Chem.* **58**, 379–410 (2005).

30. Chiefari, J. *et al.* Living free-radical polymerization by reversible addition - Fragmentation chain transfer: The RAFT process. *Macromolecules* **31**, 5559–5562 (1998).

31. Gabaston, L. I., Furlong, S. A., Jackson, R. A. & Armes, S. P. Direct synthesis of novel acidic and zwitterionic block copolymers via TEMPO-mediated living free-radical polymerization. *Polymer (Guildf).* **40**, 4505–4514 (1999).

32. Penfold, N. J. W., Whatley, J. R. & Armes, S. P. Thermoreversible Block Copolymer Worm Gels Using Binary Mixtures of PEG Stabilizer Blocks. *Macromolecules* **52**, 1653–1662 (2019).

33. Deane, O. J., Lovett, J. R., Musa, O. M., Fernyhough, A. & Armes, S. P. Synthesis of Well-Defined Pyrrolidone-Based Homopolymers and Stimulus-Responsive Diblock Copolymers via RAFT Aqueous Solution Polymerization of 2-(N-Acryloyloxy)ethylpyrrolidone. *Macromolecules* **51**, 7756–7766 (2018).

34. Chaduc, I. *et al.* Batch emulsion polymerization mediated by poly(methacrylic acid) macroRAFT agents: One-pot synthesis of self-stabilized particles. *Macromolecules* **45**, 5881–5893 (2012).

35. Thomas, D. B., Convertine, A. J., Hester, R. D., Lowe, A. B. & McCormick, C. L. Hydrolytic Susceptibility of Dithioester Chain Transfer Agents and Implications in Aqueous RAFT Polymerizations. *Macromolecules* **37**, 1735–1741 (2004).

36. Schönemann, E., Laschewsky, A. & Rosenhahn, A. Exploring the long-term hydrolytic behavior of zwitterionic polymethacrylates and polymethacrylamides. *Polymers (Basel).* **10**, (2018).

37. Jesson, C. P., Cunningham, V. J., Smallridge, M. J. & Armes, S. P. Synthesis of High

Molecular Weight Poly(glycerol monomethacrylate) via RAFT Emulsion Polymerization of Isopropylideneglycerol Methacrylate. (2018). doi:10.1021/acs.macromol.8b00294

38.   Bütün, V., Armes, S. P. & Billingham, N. C. Synthesis and aqueous solution properties of near-monodisperse tertiary amine methacrylate homopolymers and diblock copolymers. *Polymer* **42**, 5993–6008 (2001).

39.   Furukawa, Y. Polymer chemistry. in *Science in the Twentieth Century* (eds. Krige, J. & Pestre, D.) 547–563 (Royal Society of Chemistry, 2013). doi:10.4324/9781315079097-35

40.   De Luca, S., Chen, F., Seal, P., Stenzel, M. H. & Smith, S. C. Binding and Release between Polymeric Carrier and Protein Drug: PH-Mediated Interplay of Coulomb Forces, Hydrogen Bonding, van der Waals Interactions, and Entropy. *Biomacromolecules* **18**, 3665–3677 (2017).

41.   Luo, Y. L., Huang, R. J., Zhang, L. L., Xu, F. & Chen, Y. S. Dual-responsive polyacrylate copolymer micelles with PMAA and PNIPAAm graft brushes: Physicochemical properties and prednisone release. *Colloids Surfaces A Physicochem. Eng. Asp.* **436**, 1175–1185 (2013).

42.   North, S. M. & Armes, S. P. Aqueous solution behavior of stimulus-responsive poly(methacrylic acid)-poly(2-hydroxypropyl methacrylate) diblock copolymer nanoparticles. *Polym. Chem.* **11**, 2147–2156 (2020).

43.   Carlsson, L. *et al.* Modification of cellulose model surfaces by cationic polymer latexes prepared by RAFT-mediated surfactant-free emulsion polymerization. *Polym. Chem.* **5**, 6076–6086 (2014).

44.   Baussard, J. F., Habib-Jiwan, J. L., Laschewsky, A., Mertoglu, M. & Storsberg, J. New chain transfer agents for reversible addition-fragmentation chain transfer (RAFT) polymerisation in aqueous solution. *Polymer.* **45**, 3615–3626 (2004).

45.   Presser, A. & Hüfner, A. Trimethylsilyldiazomethane - A mild and efficient reagent for the methylation of carboxylic acids and alcohols in natural products. *Monatshefte fur Chemie* **135**, 1015–1022 (2004).

46.   Aldai, N., Murray, B. E., Nájera, A. I., Troy, D. J. & Osoro, K. Derivatization of fatty acids and its application for conjugated linoleic acid studies in ruminant meat lipids. *Journal of the Science of Food and Agriculture* **85**, 1073–1083 (2005).

47.   Bütün, V., Armes, S. P. & Billingham, N. C. Selective quaternization of 2-(dimethylamino)ethyl methacrylate residues in tertiary amine methacrylate diblock copolymers. *Macromolecules* **34**, 1148–1159 (2001).

48.   Jesson, C. P. *et al.* H_2O_2 enables convenient removal of RAFT end-groups from block copolymer nano-objects prepared via polymerization-induced self- assembly in water. *Macromolecules* **50**, 182–191 (2017).

Chapter 5

Zwitterionic diblock copolymers as aqueous pigment dispersants for inorganic pigments

5.1 Introduction

Aqueous formulations are becoming more widespread owing to environmental considerations and the burgeoning sustainability agenda.[1] In the context of aqueous inkjet ink formulations it is important to use appropriate polymeric dispersants, otherwise aqueous pigment dispersions can be inferior to solvent-borne dispersions in terms of gloss and colour characteristics.[2] Zwitterionic diblock copolymers, also known as polyampholytes, have been suggested to be 'universal' pigment dispersants.[3–6] This is because they possess both cationic/basic and anionic/acidic blocks, so in principle they can be used for a wide range of pigment surface chemistries.[7] When two pigment particles approach one another, the solvated adsorbed stabiliser layers interpenetrate and become compressed. In a good solvent environment, such interpenetration is unfavourable both entropically and enthalpically. This generates a strong steric repulsive interaction between particles on close approach, which ensures long-term colloidal stability. If the stabiliser chains are polyelectrolytes, this is known as *electrosteric* stabilisation (as opposed to merely *steric* stabilisation for neutral stabiliser chains).[8] Electrosteric stabilisation can tolerate much higher ionic strength than charge stabilisation, since the steric layer can compensate for any reduction in the thickness of the electrical double layer.

The solution pH can also influence colloidal stabilisation. This is because this dictates the overall surface charge on the pigment particles. In principle, this could lead to desorption of the polyelectrolyte stabiliser chains from the pigment surface but it is perhaps more likely that the pigment particles simply become unstable at their isoelectric point (IEP). The IEP is where the number of anionic surface groups match the number of cationic surface groups, leading to no net overall charge. It is well-known that various types of colloidal dispersions become unstable at their IEP, including globular proteins,[9,10] charge-stabilised latexes,[11,12] metal sols[13,14] and zwitterionic diblock copolymer nanoparticles.[15,16]

The potential use of zwitterionic diblock copolymers as pigment dispersants was first examined in detail by Creutz and co-workers.[3,4] This Belgian team employed poly(2-(dimethyamino)ethyl methacrylate) [PDMA] as an anchor block and an ammonium salt of poly(methacrylic acid) as a stabiliser block for the dispersion of an iron oxide inorganic pigment, a red organic pigment (diketopyrrolopyrrole), and a blue organic pigment (Cu-phthalocyanine). Many components in commercial paint formulations are anionic, so an anionic stabiliser block is used to ensure compatibility. Creutz and co-workers compared the dispersant performance of a block copolymer, a tapered (gradient) copolymer and a random copolymer to that of a commercial dispersant for each of the above three pigments. The block copolymer (and the tapered copolymer) proved to be superior to the random copolymer for all three pigments. This study also suggested that an effective dispersant should comprise a relatively long anionic/acidic block and a relatively short cationic/amine block.[3] Moreover, such zwitterionic diblock copolymer dispersants do not require organic cosolvents and can tolerate relatively high pigment loadings.

In 2000, the same Belgian team evaluated zwitterionic diblock copolymers for the preparation of concentrated aqueous dispersions of alumina-coated titanium dioxide particles.[5] Various AB diblock copolymers consisting of a PDMA anchor block and a poly(sodium methacrylate) [PNaMAA] stabiliser block and also the corresponding ABA and BAB triblock copolymers were evaluated alongside the corresponding tapered and random copolymers. The copolymer concentration always remained well above the CMC. Thus, the diblock copolymer micelles (a.k.a. nanoparticles) acted as reservoirs for the individual copolymer chains (unimers) that adsorb onto the pigment surface. Diblock copolymers proved to be superior to triblock copolymers, and efficient stabilisation was achieved when using just 0.3% dispersant per unit mass of pigment. Perhaps not surprisingly, triblocks containing outer anchor blocks promoted bridging flocculation, which compromised

dispersion stability. These prior studies indicate that 'blockiness' is an important criterion when designing zwitterionic copolymer dispersants, not least because this enables higher colour strength and lower viscosity to be achieved compared to a reference commercial formulation.

Two different inorganic pigments will be studied in this Chapter. The first is titanium dioxide (titania); this important pigment is well-known for its dispersibility in aqueous solution owing to the presence of surface hydroxyl groups. Furthermore, titania particles are often surface-treated with other metal oxides to improve their dispersibility. This means that typical dispersant concentrations are relatively low per unit mass of pigment (as low as 2% for some commercial dispersants). The second pigment is a transparent yellow iron oxide, which is regarded by Lubrizol as one of the most difficult pigments to disperse efficiently in aqueous solution. Such particles have a needle-like morphology, relatively high density, and exhibit hydrophobic character between pH 5 and pH 8. They are rarely surface-treated and the current standard industrial formulation requires 25% dispersant per unit mass of pigment.[17]

Titania is the most important white pigment used in paints and coatings: its annual global production was 9 million tonnes in 2014, which accounted for two-thirds of all pigment manufacture worldwide.[18] During its manufacture, partially soluble components accumulate at the surface of titania particles.[19] These components are either impurities from the ore, or additives used to control crystal structure and growth, as well as regulate agglomeration. For example, the introduction of a surface layer of alumina reduces the Hamaker constant of titania particles from 6.0×10^{-20} J to 2.75×10^{-20} J, leading to a significant reduction in the ever-present van der Waals attractive forces.[20] Although such inorganic surface treatments certainly improve pigment dispersibility, this is not always sufficient to stabilise pigment particles for practical applications.

Yellow iron oxide has long been used as a pigment but its needle-like morphology makes it rather prone to aggregation.[21,22] This particle anisotropy also leads to shear-thickening rheological behaviour, which can make effective dispersant dosing somewhat problematic prior to mechanical milling processes.[23] Dispersions must be formulated with maximum pigment loading and minimal binder; the pigment concentrate must also be compatible with further additives used to produce the final ink formulation.

Ultimately, pigments must be well-dispersed and fully coated with a relatively thick layer of strongly adsorbed copolymer stabiliser chains to achieve good long-term colloidal stability.[24] Given that such particles can become unstable at their IEP, the dispersion pH is an important parameter to consider during formulation; this aspect will be studied in detail in this Chapter. The compositions have been chosen based on preliminary small-scale studies, indicating a good affinity to the inorganic pigments.

5.2 Experimental

Materials

4-Cyano-4-(2-phenylethanesulfanylthiocarbonyl)sulfanylpentanoic acid) (PETTC) was synthesised as previously reported.[25] 2-(Dimethylamino)ethyl methacrylate (DMA), [2-(methacryloyloxy)ethyl] trimethylammonium chloride (METAC), and trimethylsilyldiazomethane (supplied as a 2.0 M solution in diethyl ether) were purchased from Sigma-Aldrich (Dorset, UK) and were used as received. Methacrylic acid (MAA) was purchased from Merck (Germany) and was used as received. 2,2'-Azobis(2- (2-imidazolin-2-yl)propane) dihydrochloride (VA-044) was purchased from Wako Pure Chemical Industries (Japan). 4,4′-Azobis(4-cyanovaleric acid) (ACVA; 98%) was purchased from Alfa Aesar (Heysham, UK) and was used as received. CD_3OD and CD_2Cl_2 were purchased from Goss

Scientific Instruments Ltd (Cheshire, UK). CDCl$_3$, D$_2$O, NaOD and DCl were purchased from Sigma-Aldrich (Dorset, UK). All other solvents were purchased from Fisher Scientific (Loughborough, UK) and were used as received. Deionised water was used for all experiments and the solution pH was adjusted using either HCl or NaOH. Samples of titanium dioxide R-960 and transparent yellow iron oxide Lanox 8916 pigments and a proprietary commercial dispersant was provided by The Lubrizol Corporation (Blackley, Manchester, UK).

Synthesis of PETTC RAFT Agent

A 1 L conical flask was charged with a magnetic stirrer bar, sodium hydride (60% in oil, 7.0 g, 175 mmol) and diethyl ether (400 mL). 2-Phenylethanethiol (21.6 g, 156 mmol) was added dropwise to the stirred grey suspension, which turned white after 2 h. Carbon disulfide (13.5 g, 177 mmol) was added dropwise and a yellow precipitate of 2-phenylethanetrithiocarbonate was formed over 2 h, collected via vacuum filtration and dried overnight in a vacuum oven set at 30 °C. Solid iodine (23.0 g, 90.6 mmol) was added to the suspension of the 2-phenylethanetrithiocarbonate (35.7 g, 151 mmol) in 400 mL diethyl ether. After 1.5 h stirring at room temperature the resulting white precipitate of sodium iodide was removed via filtration. The brown filtrate was washed with saturated sodium thiosulfate solution (4 x 150 mL), dried over magnesium sulfate and the solvent was removed under reduced pressure to afford bis-(2-phenyl ethane sulfanylthiocarbonyl)disulphide (21.0 g, 49 mmol). A 1 L two-neck round-bottom flask equipped with magnetic stirrer was charged with bis-(2-phenyl ethane sulfanylthiocarbonyl)disulphide (21.0 g, 49 mmol), ACVA (21.0 g, 103 mmol) and ethyl acetate (500 mL). This mixture was purged with nitrogen for 45 min, then refluxed under a nitrogen atmosphere overnight. The resulting orange solution was washed with water (4 x 200 mL), dried over magnesium sulfate and all volatiles were removed under reduced pressure. The crude product was purified by column chromatography using silica gel as the

stationary phase and a mobile phase comprising initially pure dichloromethane, switching to 95:5 v/v dichloromethane/ethanol after the first fraction had been removed to afford an orange oil. This oil was then recrystallized from 4 : 1 v/v ethyl acetate/hexane to yield 4-cyano4-(2-phenylethane sulfanylthiocarbonyl)sulfanylpentanoic acid (PETTC) as a yellow solid (57% yield). ^{1}H NMR (400 MHz, CD_2Cl_2, 25 °C): δ 1.91 (s, 3H, –(CN)CH$_3$), 2.40–2.62 (m, 2H, –(CH$_3$)(CN)-CH$_2$CH$_2$C(=O)OH), 2.64-2.87 m, 2H, –(CH$_3$)(CN)-CH$_2$CH$_2$C(=O)OH), 3.02–3.06 (t, 2H, –PhCH$_2$CH$_2$S(C=S)S), 3.60–3.66 (t, 2H, –PhCH$_2$CH$_2$S(C=S)S), 7.25–7.40 (m, 5H, –PhCH$_2$CH$_2$S(C=S)S). ^{13}C NMR (400 MHz, CDCl$_3$, 25 °C): δ 24.9 (CH$_3$), 29.5 (CH$_2$CH$_2$C(=O)OH), 33.5 (PhCH$_2$CH$_2$S), 34.0 (CH$_2$CH$_2$C(=O)OH), 38.0 (PhCH$_2$CH$_2$S), 46.3 (SC(CH$_3$)(CN)CH$_2$), 118.9 (SC(CH$_3$)(CN)CH$_2$), 126.9-128.6, 139.2 (PhCH$_2$), 177.1 (C=O), 216.4 (C=S). MS (ES+) m/z calcd: 339.49 Found: 339.0

Large scale one-pot synthesis of poly(2-(dimethylamino)ethyl methacrylate)-poly(methacrylic acid) (PDMA-PMAA) diblock copolymer

The large-scale protocol for the synthesis of a PDMA$_{50}$-PMAA$_{100}$ zwitterionic diblock copolymer was conducted as follows: DMA (18.0 g, 114 mmol), PETTC (0.777 g, 2.29 mmol), VA-044 (148 mg, 0.458 mmol) and deionised water (28.4 g) were added to a 500 mL two-necked round-bottomed flask. 36% HCl (9.83 g, 0.114 mol) was added to adjust the solution pH to pH 7. This aqueous reaction mixture was then purged for 30 min with nitrogen and heated to 44 °C. In a separate vial, MAA (19.7 g, 229 mmol), VA-044 (246 mg, 0.763 mmol) and water (127 g) were purged with nitrogen for 30 min. The DMA polymerisation had reached approximately full conversion after 3.5 h, as determined by ^{1}H NMR spectroscopy. Then the degassed aqueous solution containing MAA monomer and VA-044 initiator was added under a nitrogen atmosphere. The ensuing MAA polymerization was allowed to proceed for 2.5 h at 44 °C (final reaction solution was pH 2.0). A final MAA

conversion of more than 99% was achieved as determined by ^{1}H NMR spectroscopy studies, yielding a yellow dispersion.

Large scale one-pot synthesis of poly(methacrylic acid)-poly(2-(methacryloyloxy)ethyl trimethylammonium chloride) (PMAA-PMETAC) diblock copolymer

The large-scale protocol for the synthesis of a $PMAA_{67}$-$PMETAC_{120}$ zwitterionic diblock copolymer was conducted as follows. MAA (6.00 g, 69.6 mmol) and CPDB (257 mg, 1.16 mmol) were stirred thoroughly to ensure solvation of CPDB at 60% w/w solids. ACVA (65.1 mg, 232 mmol) and deionised water (4.2 g) were added to a 100 ml two-necked round-bottomed flask. This aqueous solution was then purged for 30 min with nitrogen and heated up to 70 °C. In a second vial, deionised water (31.6 g) was degassed and then added to the reaction solution after 45 min to reduce the increasing viscosity of the polymerizing solution (targeting 15% w/w solids). After 3 h, the MAA polymerisation had reached more than 99% conversion (as determined by ^{1}H NMR spectroscopy). In a separate vial, METAC (14.4 g, 69.7 mmol), ACVA (125 mg, 0.387 mmol) and deionised water (79.0 g, targeting 20% w/w solids) were purged with nitrogen for 30 min. This degassed aqueous solution was added under a nitrogen atmosphere and the second-stage polymerisation was allowed to continue for 6 h at 70 °C. A final METAC conversion of 99% was achieved as determined by ^{1}H NMR spectroscopy, yielding a viscous reddish-pink solution. Derivatisation of these copolymers is described in Chapter 4, see Section 4.2.

Synthesis of poly(2-(dimethylamino)ethyl methacrylate) (PDMA) macro-CTA

The synthesis details for this macro-CTA are described in Chapter 4, see Section 4.2.

Large scale synthesis of poly(2-(dimethylamino)ethyl methacrylate)-poly(methacrylic acid)- *stat*-(benzyl methacrylate) (PDMA-P(MAA-*stat*-BzMA) copolymer

The 100 g scale protocol for the synthesis of the $PDMA_{50}−P(MAA_{0.8}- \textit{stat}-BzMA_{0.2})_{100}$ diblock copolymer was as follows: $PDMA_{50}$ macro-CTA (6.98 g, 0.851 mmol), MAA monomer (5.86 g, 0.068 mol), BzMA (3.00 g, 0.251 mmol), ACVA (59.6 mg, 0.213 mmol; CTA/initiator molar ratio = 4.0), and deionised water (90.36 g, 10% w/w) were weighed into a 25 mL round-bottom flask and the pH of the reaction solution was adjusted to pH 2.5. The reaction solution was then purged with nitrogen for 30 min and subsequently placed in a 70 °C oil bath for 16 h. A final conversion of more than 99% was achieved as determined by ^{1}H NMR spectroscopy.

Exhaustive methylation protocol

This derivatisation protocol is described in Chapter 4, see Section 4.2.

Gel Permeation Chromatography (GPC)

This analytical protocol is described in Chapter 4, see Section 4.2.

Preparation of trident vial dispersions

A typical trident vial dispersion was made up as follows. The desired pigment (1.00 g) was added to an empty 14 mm trident vial. To obtain a copolymer concentration of 20% based on pigment mass when using a polymer dispersion synthesised at 20% solids, quantities used were as follows. Copolymer dispersion (1.00 g) and water (8.00 g) along with glass beads (3.50 g) were added in that order. The resulting vials were hand-shaken, then fastened to a mechanical shaker to be shook more vigorously for 16 h at 20 °C prior to analysis by LUMiSizer, rheometer, dynamic light scattering, aqueous electrophoresis and/or TEM.

Dynamic Light Scattering

Dilute (0.10% w/w) aqueous copolymer dispersions were analysed at 25 °C using a Malvern NanoZS instrument. Scattered light was detected at 173° and hydrodynamic diameters were calculated using the Stokes-Einstein equation, which assumes dilute non-interacting spheres. Data were averaged over three consecutive measurements comprising eleven runs per measurement.

Aqueous Electrophoresis

Zeta potentials were calculated from electrophoretic mobilities using a Malvern NanoZS instrument. Measurements (averaged over 20 runs) were made as a function of pH on dilute dispersions (0.05-0.10% w/w) in deionised water in the presence of 1 mM KCl background salt. In each case, the solution pH was gradually lowered by adding 0.1 M HCl.

Transmission electron microscopy

Copper/palladium grids were surface-coated in-house to produce a thin film of amorphous carbon before being plasma glow-discharged for 40 seconds to produce a hydrophilic surface. A 1 µL droplet of a 0.1% w/w aqueous copolymer dispersion (solution pH adjusted using either 0.1 M HCl or 0.1 M NaOH) was placed onto a grid for 45 seconds, then stained using a 0.75% w/v aqueous solution of uranyl formate for 45 seconds. Excess stain was removed by careful blotting and the grid was then dried using a vacuum hose. TEM images were recorded using a Philips CM100 instrument operating at 100 kV and equipped with a Gatan 1k CCCD camera. ImageJ software was used to calculate mean diameters and standard deviations from TEM images (at least 100 nanoparticles were analysed per sample).

Analytical Centrifugation using the LUMiSizer instrument

Copolymer-dispersed pigment dispersions were assessed using a LUMiSizer® analytical photocentrifuge (LUM GmbH, Berlin, Germany) at 25 °C. Measurements were conducted on

aqueous pigment dispersions directly from trident vials at 4,000 rpm using 2 mm path length polyamide cells. The LUMiSizer® employs STEP™ Technology (Space- and Time-resolved Extinction Profiles) to measure the intensity of transmitted light as a function of time and position over the entire cell length simultaneously. The progression of these transmission profiles contains information on the rate of sedimentation. Given knowledge of the particle density, this enables assessment of the particle size distribution and hence the degree of dispersion.

Viscosity measurements

An AR-G2 rheometer equipped with a variable temperature Peltier plate and a 40 mm 2° steel cone was used for all experiments. Viscosity was measured as a function of shear rate between 0.1 and 1000 s^{-1}. Angular frequency sweeps were conducted at 25 °C using a constant percentage strain of 1.0%.

5.3 Results and Discussion

5.3.1 Characterisation of Zwitterionic Pigment Dispersants
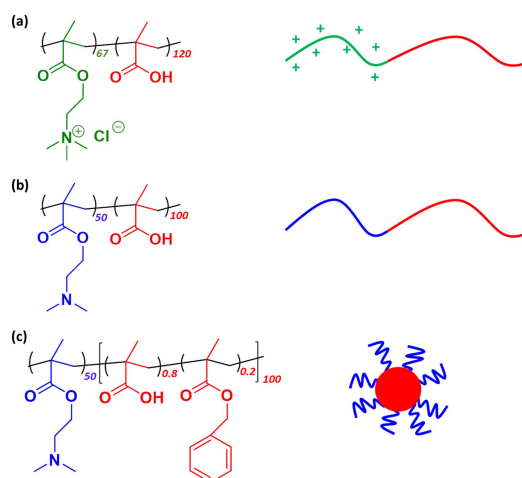
Figure 5.1 Representative molecular structures of the three copolymer dispersants used in this Chapter. **(a)** poly(2-(methacryloyloxy)ethyl trimethylammonium chloride)-poly(methacrylic acid) [PMETAC$_{67}$-PMAA$_{120}$], **(b)** poly(2-dimethylaminoethyl methacrylate)-poly(methacrylic acid) [PDMA$_{50}$-PMAA$_{100}$], **(c)** poly(2-dimethylaminoethyl methacrylate)-poly((methacrylic acid)-*stat*-(benzyl methacrylate)) [PDMA$_{50}$-(PMAA$_{0.8}$-*stat*-PBzMA$_{0.2}$)$_{100}$]

As discussed in Chapter 4, zwitterionic diblock copolymers can be readily synthesised in high yield using either RAFT aqueous solution polymerisation or RAFT aqueous dispersion polymerisation, depending on the aqueous (in)solubility of the second block. The three zwitterionic diblock copolymer structures shown in **Figure 5.1** represent the dispersants studied in this Chapter. These dispersants were chosen because there is literature precedent for their effectiveness as pigment dispersants. Small-scale screening tests indicated some degree of efficacy for these specific block compositions. The first dispersant is poly(2-(methacryloyloxy)ethyl trimethylammonium chloride)-poly(methacrylic acid) [$PMAA_{67}$-$PMETAC_{120}$] (**Figure 5.1a**), which can be synthesised *via* an aqueous one-pot RAFT protocol, as discussed in Chapter 4. This zwitterionic diblock copolymer comprises an acidic anionic block, which is highly hydrophilic in its anionic deprotonated form above pH 6 but becomes weakly hydrophobic and water-insoluble when fully protonated at low pH. On the other hand, the cationic block PMETAC possesses quaternary ammonium groups that remain cationic across the entire pH range.
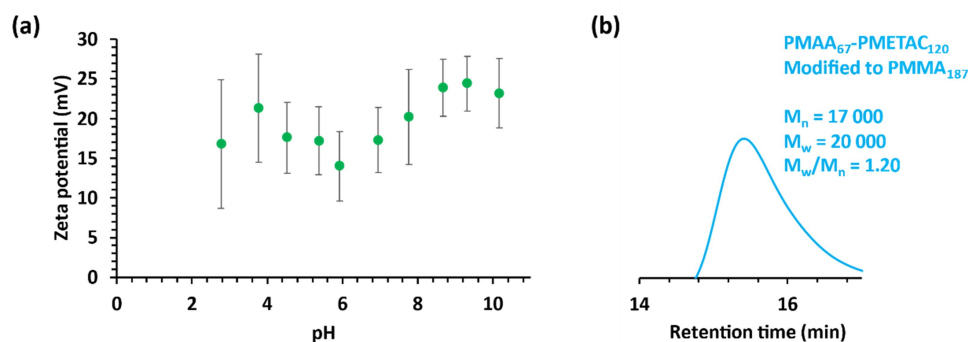
Figure 5.2 (a) Zeta potential vs. pH curve recorded for a $PMAA_{67}$-$PMETAC_{120}$ diblock copolymer in 1 mM aqueous KCl, confirming its cationic character across the whole pH range. **(b)** THF GPC showing molecular weight data obtained for the derivatised $PMAA_{67}$-$PMETAC_{120}$ diblock copolymer following its forced ester hydrolysis and exhaustive methylation to produce $PMMA_{187}$.

Figure 5.2a shows its zeta potential vs pH curve, which confirms that this diblock remains cationic between pH 2 and pH 11, as discussed in Chapter 4. Chemical derivatisation was

required to dissolve this copolymer in a suitable solvent for GPC analysis. Firstly, the PMETAC chains were subjected to forced ester hydrolysis at 120 °C for 6 h in ethylene glycol in the presence of 3 M KOH. ^{1}H NMR studies confirmed that all the methacrylic ester bonds had been cleaved, thus converting the $PMAA_{67}$-$PMETAC_{120}$ diblock copolymer chains into $PMAA_{187}$ homopolymer (**Figure 5.3**). This intermediate was then subjected to exhaustive methylation using trimethylsilyldiazomethane to produce $PMMA_{187}$ homopolymer, which was amenable to GPC analysis using THF eluent. The GPC data indicated an M_n of 17,000 and a dispersity of 1.20 (**Figure 5.2b**), suggesting that the original $PMAA_{67}$-$PMETAC_{120}$ diblock copolymer had a narrow MWD.
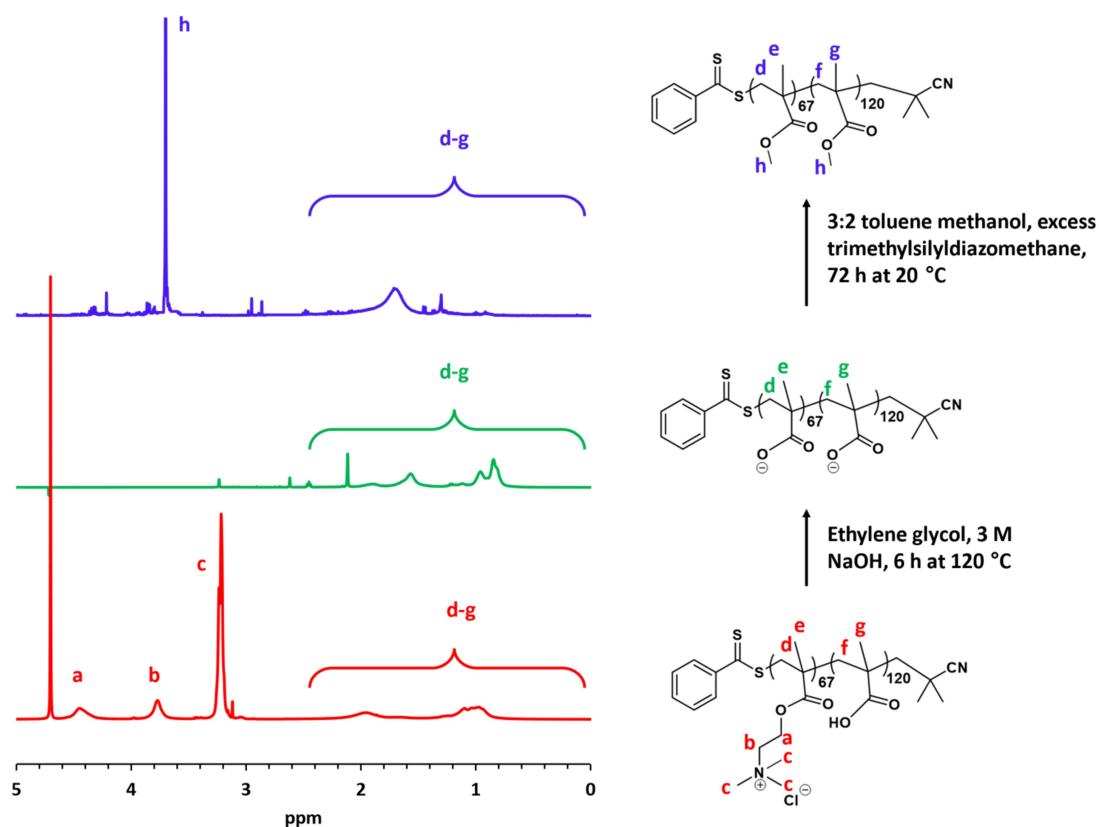
Figure 5.3 ^{1}H NMR spectrum recorded for a $PMAA_{67}$-$PMETAC_{120}$ diblock copolymer as synthesised in D_2O (**red spectrum**), the same sample following forced hydrolysis of its ester groups using 3 M NaOH at 120 °C to afford $PMAA_{187}$ homopolymer (**green spectrum**) and the final $PMMA_{187}$ homopolymer in $CDCl_3$ following exhaustive methylation of $PMAA_{187}$ using excess trimethylsilyldiazomethane (**blue spectrum**).
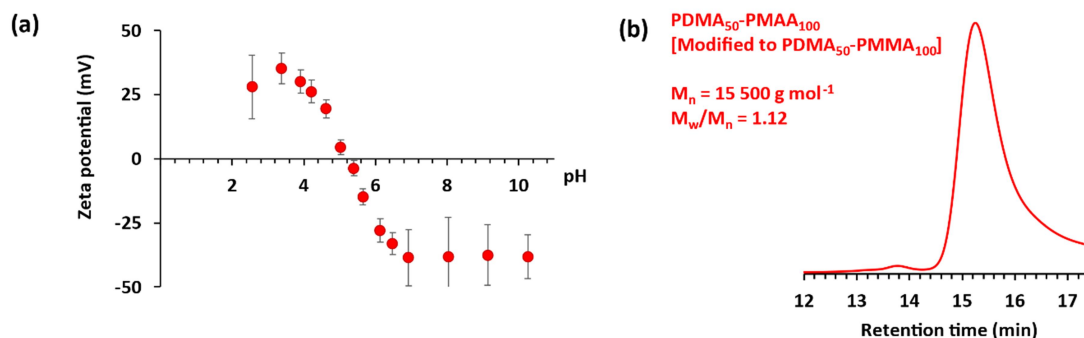
Figure 5.4 (a) Zeta potential vs. pH curve recorded for a $PDMA_{50}$-$PMAA_{100}$ diblock copolymer in 1 mM aqueous KCl illustrating its zwitterionic character (IEP at pH ~ 5.1). **(b)** DMF GPC data for $PDMA_{50}$-$PMAA_{100}$ diblock copolymer following its exhaustive methylation to afford $PDMA_{50}$-$PMMA_{100}$.

The second zwitterionic diblock copolymer studied in this Chapter is poly(2-(dimethylamino)ethyl methacrylate)-poly(methacrylic acid) [$PDMA_{50}$-$PMAA_{100}$] (**Figure 5.1b**). This putative dispersant is characterised by aqueous electrophoresis and GPC analysis, see **Figure 5.4**. It has an IEP at approximately pH 5.1, around which it forms a macroscopic precipitation. At this pH, the tertiary amine groups on the PDMA block are partially protonated while the methacrylic acid groups on the PMAA block are partially ionised, which leads to electrical neutrality for this particular diblock composition. This diblock copolymer was also prepared in high yield using a wholly aqueous one-pot protocol. Exhaustive methylation of the PMAA block afforded a $PDMA_{50}$-$PMMA_{100}$ diblock copolymer, which enabled GPC analysis using DMF eluent. This selective derivatisation approach indicated a relatively narrow dispersity of 1.12, indicating that good control over the copolymer MWD was achieved during the original RAFT synthesis.
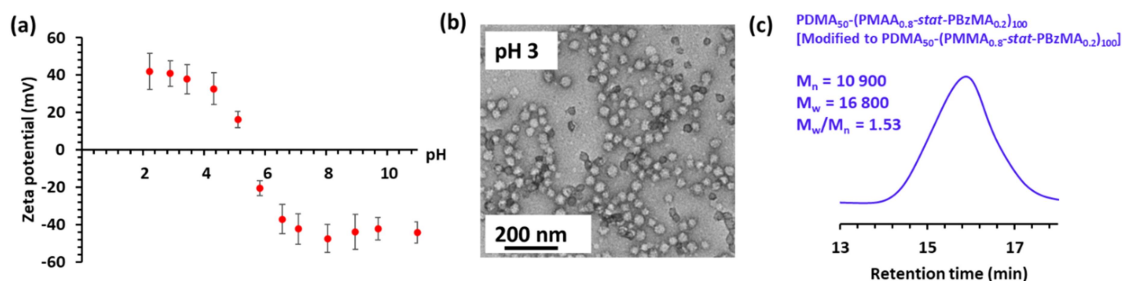
Figure 5.5 (a) Zeta potential vs. pH curve recorded for a zwitterionic $PDMA_{50}$-$(PMAA_{0.8}$-*stat*-$PBzMA_{0.2})_{100}$ diblock copolymer in 1 mM aqueous KCl (IEP is pH ~ 5.7); **(b)** representative TEM image obtained for a 0.1% w/w aqueous dispersion of $PDMA_{50}$-$(PMAA_{0.8}$-*stat*-$PBzMA_{0.2})_{100}$, which indicates the presence of well-defined spherical nanoparticles when dried at pH 3; (c) THF GPC trace recorded for $PDMA_{50}$-$(PMMA_{0.8}$-*stat*-$PBzMA_{0.2})_{100}$ following exhaustive selective methylation of the MAA residues in $PDMA_{50}$-$(PMAA_{0.8}$-*stat*-$PBzMA_{0.2})_{100}$.

The third dispersant studied herein is poly(2-(dimethylamino)ethyl methacrylate)-poly(methacrylic acid-*stat*-benzyl methacrylate) or $PDMA_{50}$-$(PMAA_{0.8}$-*stat*-$PBzMA_{0.2})_{100}$ (**Figure 5.1c**). Following the approach reported by Canning *et al.*,[15] 20 mol% of BzMA was statistically polymerised with MAA to confer additional hydrophobic character on the second block. Although initial screening studies suggested that introducing BzMA comonomer reduced dispersant efficacy in organic pigments (as briefly discussed in Chapter 3), it was hypothesised that such hydrophobic aromatic groups might enable stronger adsorption to the surface of the pigment particles to be achieved at an optimum solution pH for inorganic pigments. The aqueous electrophoresis data obtained for this zwitterionic diblock copolymer are shown in **Figure 5.5a**. As expected, cationic nanoparticles with poly(methacrylic acid-*stat*-benzyl methacrylate) cores are formed at low pH and anionic PDMA-core nanoparticles are produced at high pH, with an IEP at approximately 5.7. This is slightly higher than that observed for $PDMA_{50}$-$PMAA_{100}$ owing to the subtle difference in diblock copolymer composition (i.e. replacement of 20% of the ionisable MAA residues by non-ionic BzMA residues).

The BzMA comonomer should aid the formation of well-defined spherical nanoparticles at low pH, where the MAA residues are fully protonated. In contrast, the BzMA groups are expected to be located within the highly anionic coronal stabiliser block at high pH, as confirmed by ^{1}H NMR in D_2O (**Figure 5.6**).[15]
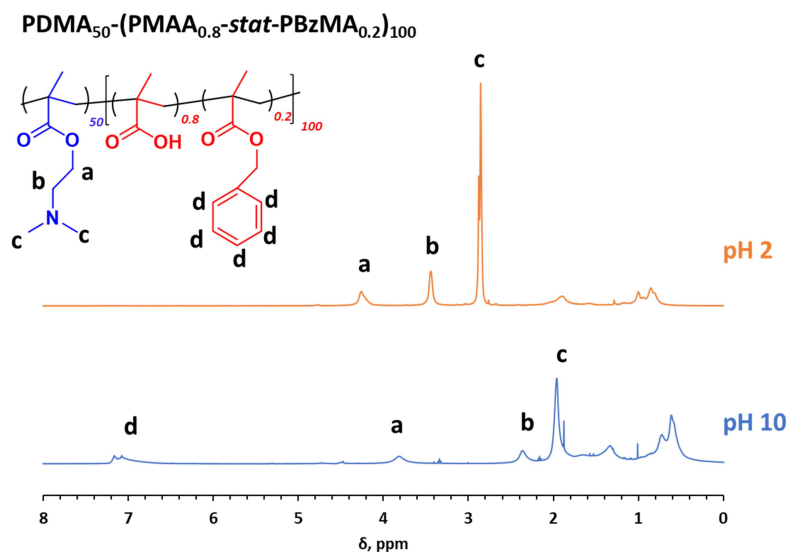
Figure 5.6 ^{1}H NMR spectroscopy of PDMA$_{50}$-(PMAA$_{0.8}$-*stat*-PBzMA$_{0.2}$)$_{100}$ copolymer in D_2O at pH (pD) 2 (orange/top) and 10 (blue/bottom).

5.3.2 Dispersion of Titania (R-960) Pigment Particles

The first inorganic pigment to be discussed is Titania R-960, used as supplied by Lubrizol. This pigment is well-known to be readily dispersed in water. Commercial titania formulations only require using 2% of Lubrizol's proprietary dispersant per unit mass of pigment.
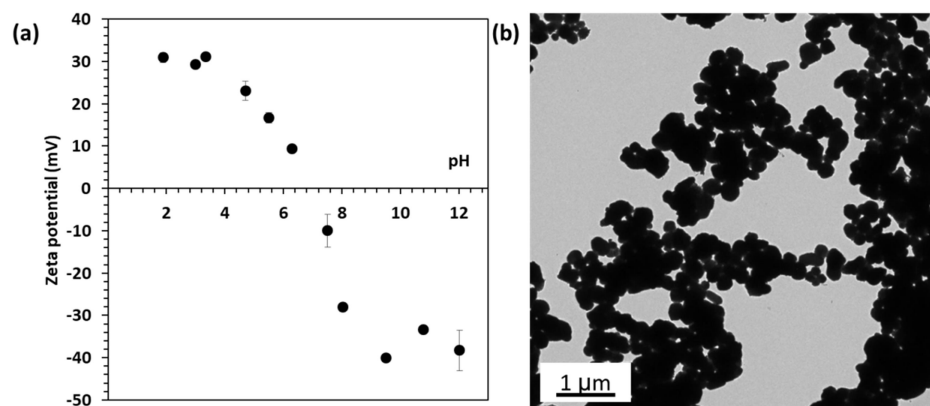
Figure 5.7 (a) Zeta potential vs. pH curve recorded for a 0.1% w/w aqueous dispersion of titania particles in the presence of 1mM KCl indicating an IEP at approximately pH 7.0. **(b)** Representative TEM image recorded after drying the same aqueous titania dispersion.

The aqueous electrophoresis data (**Figure 5.7a**) indicate that this pigment has an isoelectric point at approximately pH 7.0. Nevertheless, the titania particles appeared to be colloidally stable at all solution pH values. This is most likely owing to the surface modification of this pigment: alumina and amorphous silica make up 3.3% and 5.5% of the total mass of titania R-960, respectively.[26] The TEM image (**Figure 5.7b**) was recorded after drying a 0.1% w/w aqueous dispersion of titania particles. This pigment appears to have a relatively broad particle size distribution. The specific surface area, as determined by BET measurements, is 16.3 m^2 g^{-1}, which is comparable to that for other surface-treated titania pigments.[27] Given a pigment density of 4.09 g cm^{-3} (as measured by helium pycnometry), and assuming zero porosity, this suggests a primary grain diameter of approximately 90 nm (as calculated using **Equation 3.1**). However, a number-average particle diameter of 242 ± 54 nm is observed by TEM. Therefore, this suggests that the titania pigment is present in the form of aggregates consisting of 2-3 primary particles. Analytical centrifugation studies using the LUMiSizer instrument indicates a weight-average diameter of 212 ± 72 nm, while DLS reports a z-average diameter of 360 nm (polydispersity = 0.20). The latter particle size data suggest that these particles have a reasonably high degree of dispersion in aqueous media even in the

absence of any copolymer dispersant. Although the number-average TEM diameter is closer to the intensity-average DLS diameter than the weight-average LUMiSizer diameter, the LUMiSizer value is more likely to be closer to the true value, as it is taking an average of the largest number of particles. Although over 100 pigment particles were counted, due to their relatively large size compared to the TEM grid, a representative sample is difficult to obtain.

In initial screening experiments, an arbitrary copolymer concentration was used for a 10% pigment dispersion. $PDMA_{50}$-$PMAA_{100}$ produced the highest degree of pigment dispersion, with the DLS diameter being reduced to 320 nm prior to any optimisation of dispersant concentration or solution pH. $PMAA_{67}$-$PMETAC_{120}$ diblock copolymer resulted in a similar DLS diameter of 364 nm. In contrast, other dispersants exhibiting no zwitterionic character (such as $PMAA_{50}$-$PHPMA_{100}$) led to DLS diameters of more than 400 nm.
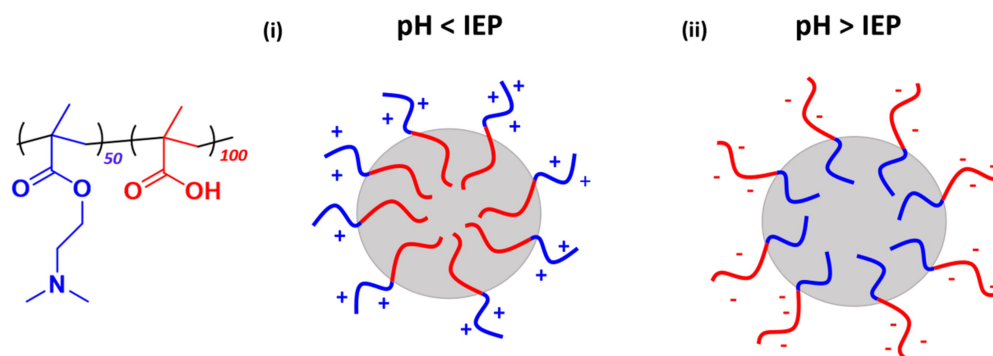
Scheme 5.1 Schematic representation of $PDMA_{50}$-$PMAA_{100}$ dispersing titania (i) below its IEP, where the red PMAA block is neutral and anchored to the particle surface, with charged, soluble blue PDMA providing stabilisation, and (ii) the same copolymer dispersing titania above its IEP where the blue PDMA block is neutral and anchoring to the surface, while the red anionic PMAA is charged and providing stabilisation.

$PDMA_{50}$-$PMAA_{100}$ was further evaluated to identify its optimum dosage when preparing a 10% w/w aqueous titania dispersion (**Figure 5.8**). The z-average diameter of these pigment particles was determined by DLS for a range of dispersant concentrations. A minimum was

observed at a copolymer concentration of 20% per unit mass of pigment, corresponding to

0.20 g copolymer per gram of pigment.
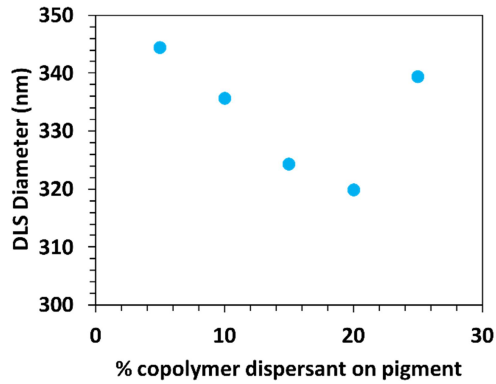
Figure 5.8 Dosage ladder constructed for a series of aqueous titania dispersions prepared using PDMA$_{50}$-PMAA$_{100}$ by determining the DLS diameter against copolymer dispersant concentration (expressed per unit mass of pigment). The minimum diameter observed at 20% corresponds to the optimal copolymer loading.
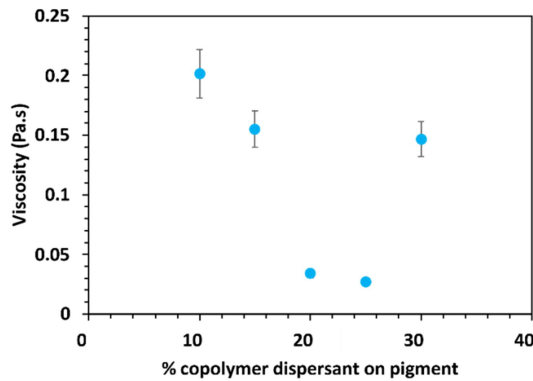
Figure 5.9 Dosage ladder constructed for a series of aqueous titania dispersions prepared using PDMA$_{50}$-PMAA$_{100}$ by determining the dispersion viscosity against copolymer dispersant concentration (expressed per unit mass of pigment). A minimum in dispersion viscosity at 37 s^{-1} is observed at 20-25% copolymer, which corresponds to the optimal concentration.

Dispersant performance can also be assessed by viscosity measurements: a minimum in dispersion viscosity at a fixed pigment concentration is known as the 'surfactant demand' of the pigment.[28] This is where the particles are assumed to be fully dispersed. Excess surfactant – or, in this case, copolymer dispersant - can cause depletion flocculation, which increases the dispersion viscosity.[28] This is because the dispersant is located in the continuous phase, as

well as adsorbed at the surface of the pigment particles.[29] On the other hand, adding too little

dispersant leads to bridging flocculation because the particles are not sufficiently coated

(submonolayer coverage). **Figure 5.9** shows that there is a minimum in dispersion viscosity

at 20-25% copolymer per unit mass of pigment. These observations are consistent with the

DLS data. In subsequent experiments, 20% copolymer dispersant per unit mass of pigment

was selected.

The next step was to study the effect of varying the dispersion pH on the degree of pigment

dispersion. Aqueous electrophoresis data were obtained for titania alone, the copolymer alone

and the copolymer-dispersed titania particles (**Figure 5.10**). The electrophoretic footprint for

the latter system more closely resembles that of the copolymer alone than that of the naked

titania particles. This is consistent with the copolymer forming an adsorbed monolayer at the

surface of the titania particles, thus conferring electrosteric stabilisation.
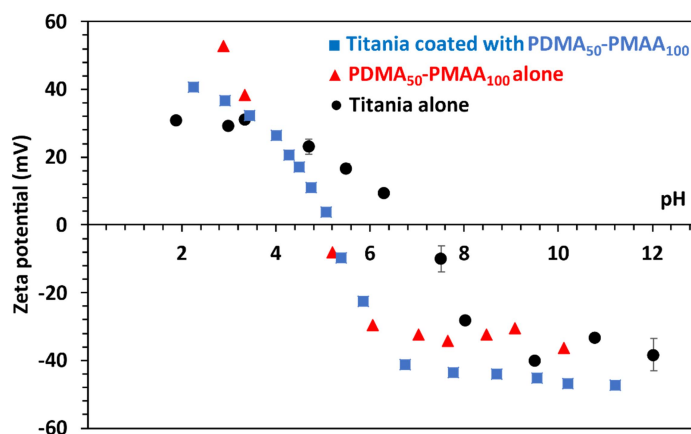
Figure 5.10 Zeta potential vs. pH curve constructed for a 0.1 w/w aqueous dispersion of titania alone (**black circles**), the zwitterionic $PDMA_{50}$-$PMAA_{100}$ diblock copolymer alone (**red triangles**) and titania particles dispersed using the $PDMA_{50}$-$PMAA_{100}$ copolymer (**blue squares**).

According to Lubrizol,[17] the minimum acceptable DLS diameter for this type of dispersant

test should be less than 400 nm. This assumes that grinding does not reduce the mean grain

size of the pigment.
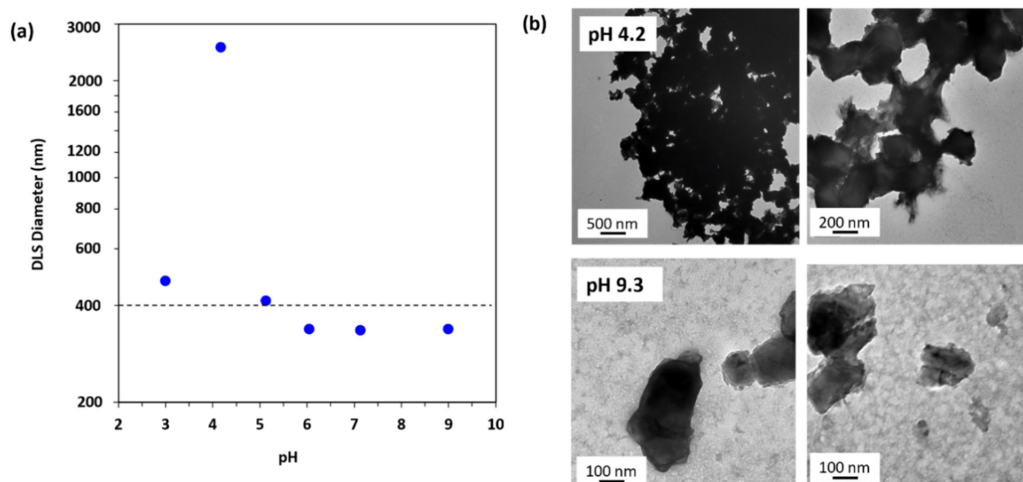
Figure 5.11 (a) pH dependence for the DLS diameter of a titania dispersion prepared using a zwitterionic $PDMA_{50}$-$PMAA_{100}$ diblock copolymer dispersant. The dashed line indicates the minimum acceptable z-average diameter for this type of test, with only those dispersions prepared above pH 6 falling below this line. **(b)** Representative TEM images recorded for dilute titania dispersions dried at pH 3.0 (relatively low degree of dispersion) and pH 8.3 (relatively high degree of dispersion).

The effect of varying the dispersion pH on the z-average particle diameter is shown in **Figure 5.11**. The apparent particle size below pH 6 is relatively large, which suggests flocculation. This is consistent with the TEM image recorded for a dilute dispersion dried at pH 4.2, which reveals aggregates of particles (**Figure 5.11b**). In contrast, the titania particles are relatively well-dispersed above pH 6, with TEM studies of a dilute dispersion dried at pH 9.3 indicating the presence of mainly primary particles, rather than aggregates. However, it is emphasised that such studies may be prone to drying artefacts. Nonetheless, LUMiSizer studies confirm that the smallest particle size distribution can be obtained at pH 9.3.

These findings suggest that the PDMA block is a more effective anchor block for titania, with the anionic PMAA chains acting as a stabiliser block. This is not unexpected: there is good literature precedent to suggest that polyamines adsorb onto titania.[3,30,31] Below pH 6, the PDMA chains have a relatively high degree of protonation and hence are more hydrophilic/cationic; under such conditions they adsorb more weakly onto titania particles.[32]

Moreover, the degree of ionisation of the PMAA chains is reduced at low pH, so such blocks have less anionic character to stabilise the pigment dispersion. At pH 8.3, the PDMA block is weakly hydrophobic[33] and thus adsorbs more strongly onto the surface of titania particles.[32]

The second dispersant examined for the titania particles was PDMA$_{50}$-(PMAA$_{0.8}$-*stat*-PBzMA$_{0.2}$)$_{100}$. A dosage ladder was constructed at pH 8 to establish the relationship between dispersion viscosity and copolymer concentration (**Figure 5.12**). This indicated that a minimum dispersion viscosity is obtained when using 20% copolymer per unit mass of pigment. The expected stabilisation mechanism is depicted in **Scheme 5.2**.
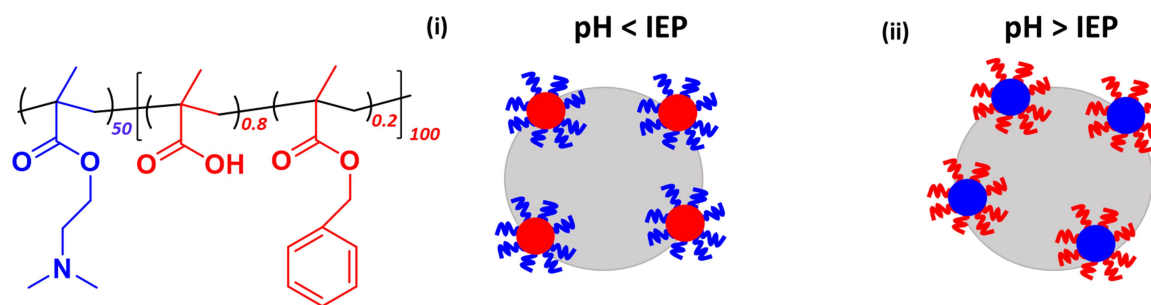
Scheme 5.2 Schematic representation of PDMA$_{50}$-(PMAA$_{0.8}$-*stat*-PBzMA$_{0.2}$)$_{100}$ nanoparticles dispersing titania (i) below its IEP, where the red PMAA-*stat*-PBzMA block forms the hydrophobic core of the copolymer nanoparticle and soluble blue PDMA is providing stabilisation, and (ii) the same copolymer nanoparticles dispersing titania above its IEP where the blue PDMA block forms the core of the nanoparticles, while the red anionic PMAA-*stat*-PBzMA is charged and in solution.
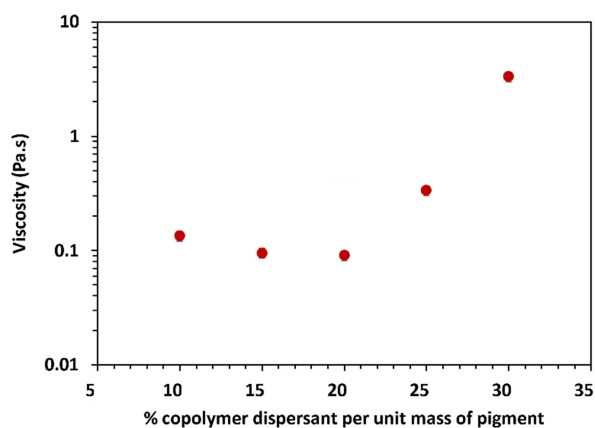
Figure 5.12 Dosage ladder constructed at pH 8 for a series of titania dispersions stabilised using various concentrations of PDMA$_{50}$-(PMAA$_{0.8}$-*stat*-PBzMA$_{0.2}$)$_{100}$ to determine the minimum dispersion viscosity. A viscosity minimum is obtained when using 20% copolymer per unit mass of pigment, which corresponds to the optimal concentration.

Owing to the particulate nature of these zwitterionic diblock copolymer nanoparticles, DLS analysis indicated bimodal particle size distributions (**Figure 5.13).** This was not ideal, as this led to average results which were not representative of the real particle size distribution (**Figure 5.13b**).
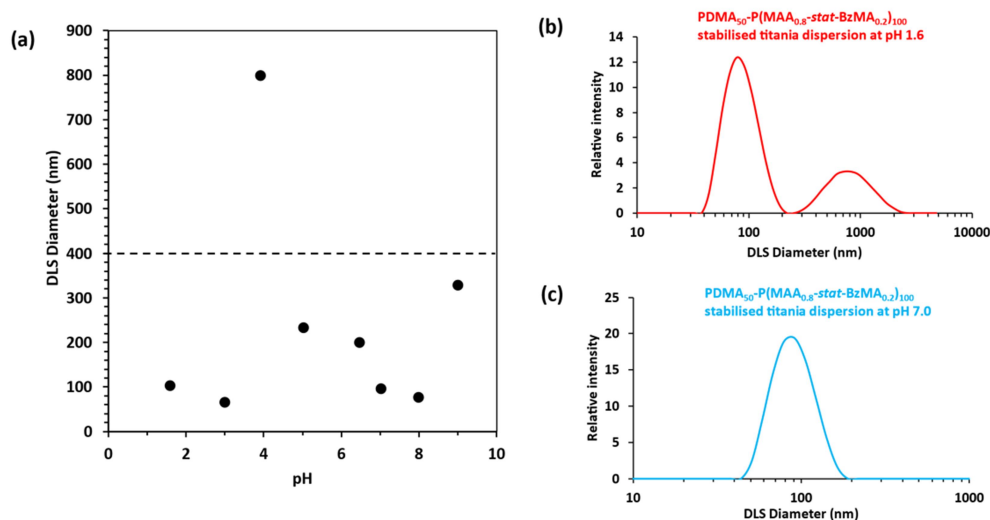
Figure 5.13 (a) DLS diameter vs. dispersion pH obtained for dilute titania dispersions prepared using the $PDMA_{50}$-$P(MAA_{0.8}$-*stat*-$BzMA_{0.2})_{100}$ dispersant; **(b)** DLS true particle size distribution of selected dispersion at pH 1.6 illustrating bimodal nature **(c)** DLS true particle size distribution of selected dispersion at pH 7.0 illustrating unimodal nature.

The DLS particle size distribution observed at pH 1.6 shown in **Figure 5.13b** is dominated by a large population of particles of less than 100 nm. This population most likely corresponds to diblock copolymer nanoparticles comprising P(MAA-*stat*-BzMA) cores. These particles exhibit a z-average diameter of approximately 70 nm when diluted in deionised water. The second population at approximately 900 nm suggests the formation of colloidal aggregates of titania particles. The unimodal peak in **Figure 5.13c** also appears to be too small to correspond to titania particles, however it could be DLS reporting an average of well-stabilised titania and excess copolymer nanoparticles, since there does not seem to be a population of large, aggregated species. Zeta potential vs pH curves were obtained for the titania particles alone, the zwitterionic diblock copolymer nanoparticles alone and the titania

particles dispersed with the aid of the copolymer (**Figure 5.14).** Although these three curves are quite similar, it is clear that the curve obtained for the nanoparticles alone more closely resembles that for the titania particles prepared in the presence of this copolymer. In particular, the IEP observed for the titania particles alone is at approximately pH 7, whereas the IEP for the other two samples is shifted to below pH 6. Moreover, the latter two samples exhibit significantly higher cationic zeta potentials at pH 2-3. These findings are consistent with adsorption of the copolymer nanoparticles at the surface of the titania particles.
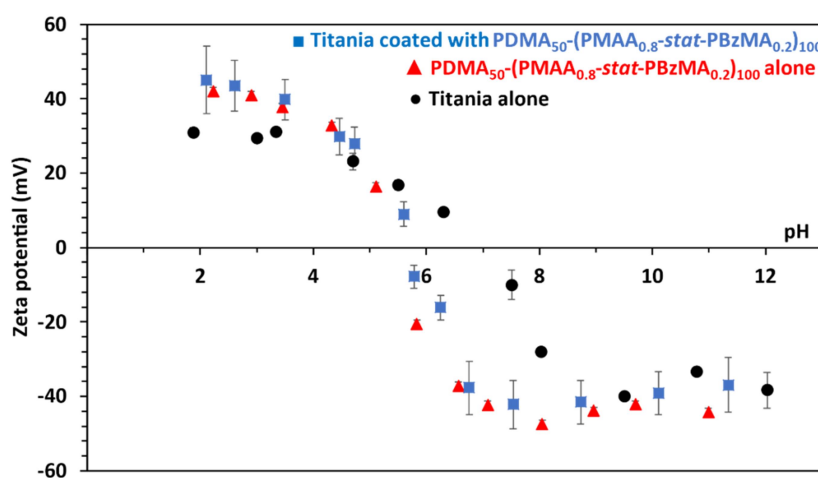
Figure 5.14 Zeta potential vs. pH curves obtained for 0.1% w/w aqueous dispersions of titania alone (**black circles**), $PDMA_{50}$-$P(MAA_{0.8}$-*stat*-$BzMA_{0.2})_{100}$ copolymer alone (**red triangles**) and titania dispersed using the $PDMA_{50}$-$P(MAA_{0.8}$-*stat*-$BzMA_{0.2})_{100}$ copolymer (**blue squares**).

TEM studies confirm the presence of many non-adsorbed copolymer nanoparticles in the background of dilute titania dispersions after drying at pH 3.0 (**Figure 5.15a**). This zwitterionic diblock copolymer forms stable spherical nanoparticles at this pH with the neutral hydrophobic P(MAA-*stat*-BzMA) chains being located within the nanoparticle cores. Although the titania particles seem to be coated with the copolymer nanoparticles, TEM analysis suggests that floccs are nevertheless formed, indicating that this particular dispersant does not perform effectively in acidic solution.
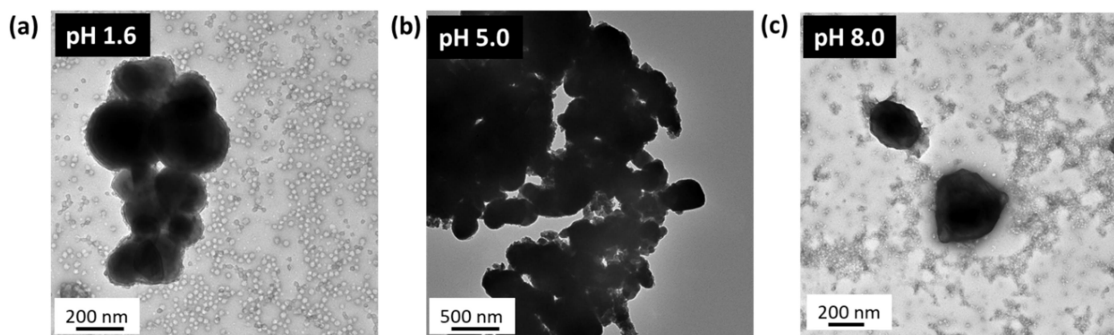
Figure 5.15 TEM images recorded for titania dispersions prepared using the $PDMA_{50}$-$P(MAA_{0.8}$-*stat*-$BzMA_{0.2})_{100}$ copolymer nanoparticles as a dispersant at **(a)** pH 1.6, **(b)** pH 5.0 and **(c)** pH 8.0.

The zwitterionic nanoparticles undergo macroscopic precipitation as they approach their isoelectric point at approximately pH 5.0. Thus, it is not surprising that TEM analysis indicates strong aggregation of the titania particles under these conditions (**Figure 5.15b**). Curiously, the corresponding apparent DLS particle diameter is relatively low (**Figure 5.13a**). However, this must be an artefact because visual inspection of this dispersion confirms its colloidal instability. Given the relatively high density of the titania particles, it seems likely that the relatively large aggregates undergo sedimentation on the timescale of the DLS measurements, which would make this technique insensitive to their presence. At pH 8.0, the titania particles appear to be both coated and stabilised by the copolymer nanoparticles as judged by TEM analysis (**Figure 5.15c**). This interpretation is consistent with the aqueous electrophoresis data, and this enhanced colloidal stability at pH 8.0 is supported by the DLS data (**Figure 5.13a**).

Above pH 7, the anionic $P(MAA_{0.80}$-*stat*-$BzMA_{0.20})$ block acts as an electrosteric stabiliser while the weakly hydrophobic neutral PDMA acts as an anchor block. Perhaps not surprisingly, the copolymerised hydrophobic BzMA units do not offer any useful performance advantage under such conditions. The particle size distribution of the titania dispersion becomes slightly narrower at lower pH. Here the copolymer dispersant offers no

performance advantage because it has no affinity for the titania surface: the surface-treated pigment particles are simply self-stabilised under such conditions.

5.3.3 Dispersion of Transparent Yellow Iron Oxide (Lanox 8916)

The second pigment investigated in this Chapter is a transparent yellow iron oxide, Lanox 8916. This pigment has a characteristic anisotropic 'needle-like' or 'rice grain' morphology as a result of its α-FeOOH goethite structure (**Figure 5.16b**).[21] According to the pigment manufacturer, the BET specific surface area is 108-120 m^2 g^{-1}. The density was measured to be 4.21 g cm^{-3} by helium pycnometry. Assuming these particles are non-porous, this indicates a primary grain diameter of around 12-13 nm. TEM studies confirm that this pigment has a distinctive 'rice grain' morphology. This should be borne in mind when interpreting DLS data because this particle sizing technique reports a sphere-equivalent hydrodynamic diameter.
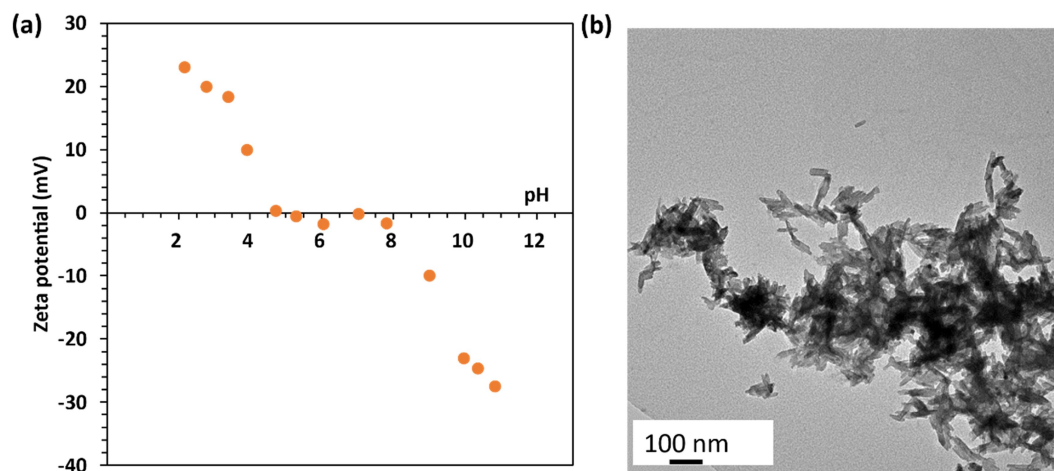
Figure 5.16 (a) Zeta potential vs. pH curve obtained for a 0.1% w/w aqueous dispersion of transparent yellow iron oxide (Lanox 8916) nanoparticles in the presence of 1 mM KCl, showing an IEP at approximately pH 7.0; **(b)** representative TEM image recorded for a dried 0.1% w/w aqueous dispersion of transparent yellow iron oxide nanoparticles.

As expected, this pigment is unstable with respect to aggregation at around its IEP. However, it can be dispersed in the form of micron-sized aggregates below pH 5 and above pH 9, exhibiting maximum zeta potentials of approximately +25 mV and -28 mV respectively. DLS measures a hydrodynamic diameter of 921 nm at pH 9.5, and 2.11 μm at pH 3.6.

The first dispersant examined for dispersion of this pigment was $PMAA_{67}$-$PMETAC_{120}$ (**Figure 5.1a),** which gave promising results in initial small-scale screening experiments. Initially, a dosage ladder was conducted using DLS to determine the optimum copolymer concentration required for this pigment (**Figure 5.17**). Surprisingly, no minimum size was observed for this system: the apparent particle z-average particle diameter remained more or less constant at around 200 nm above a copolymer concentration of 20% per unit mass of pigment. In contrast, a well-defined local minimum in dispersion viscosity was observed at a copolymer concentration of 20% per unit mass of pigment (**Figure 5.18**). Nevertheless, these two techniques indicate essentially the same optimum copolymer concentration per unit mass of pigment is required for this transparent yellow iron oxide pigment.
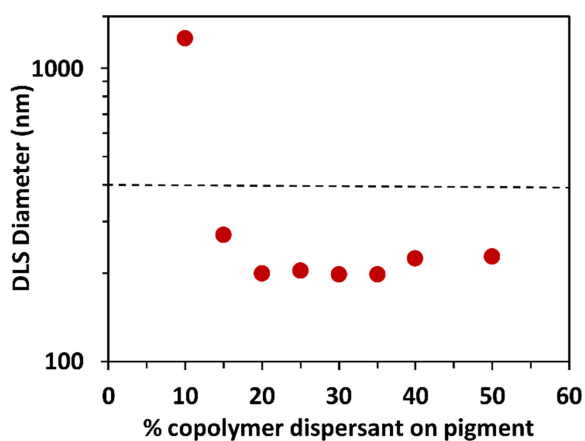
Figure 5.17 Dosage ladder obtained by DLS studies of dilute aqueous dispersions of yellow iron oxide particles prepared using various concentrations of $PMAA_{67}$-$PMETAC_{120}$ dispersant.
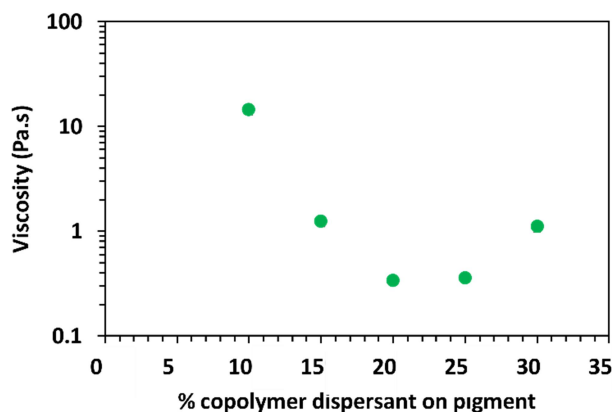
Figure 5.18 Dosage ladder obtained by dispersion viscosity measurements for an aqueous dispersion of transparent yellow iron oxide nanoparticles prepared using the PMAA$_{67}$-PMETAC$_{120}$ dispersant.

The aqueous electrophoresis data obtained for the copolymer alone and the naked pigment particles are very different. Thus, zeta potential measurements should provide a good indication of the pH-dependent affinity of the dispersant for the pigment particles. According to **Figure 5.19**, the copolymer-coated particles exhibit higher zeta potentials between pH 2 and pH 7 than either the pigment particles alone or the cationic copolymer. This suggests that the weakly hydrophobic (pH 2) or weakly anionic (pH 3-7) PMAA block could be acting as the anchor block while the permanently cationic PMETAC block acts as a stabiliser block under these conditions. The zeta potential for these coated pigment particles is higher than that for the copolymer nanoparticles alone because the anionic PMAA chains partially offset the cationic character of the PMETAC block in the latter case, whereas the PMAA chains interact with the cationic pigment surface in the former case. However, the pigment particles acquire anionic character above pH 9, suggesting that in situ desorption of the copolymer nanoparticles occurs under such conditions. This is not particularly surprising, because mutual electrostatic repulsion between the highly anionic PMAA block and the anionic pigment surface is expected to occur in alkaline solution. This is depicted in **Scheme 5.3**.
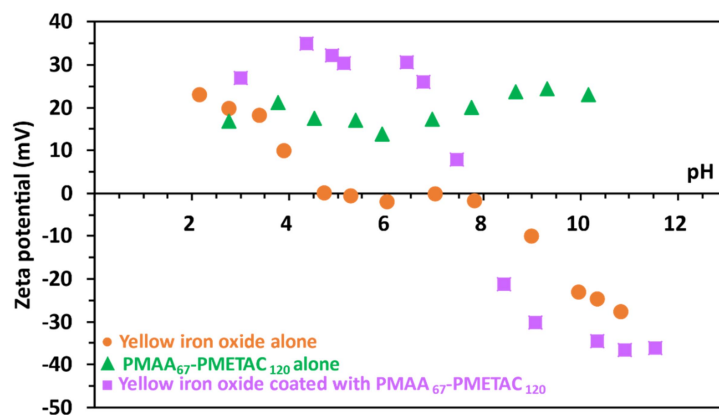
Figure 5.19 Zeta potential vs. pH curves obtained for 0.1% w/w dispersions of transparent yellow iron oxide nanoparticles alone (**orange circles**), the PMAA$_{67}$-PMETAC$_{120}$ copolymer alone (**green triangles**) and the transparent yellow iron oxide nanoparticles dispersed in the presence of PMAA$_{67}$-PMETAC$_{120}$ (using 20% copolymer per unit mass of pigment) (**purple squares**).
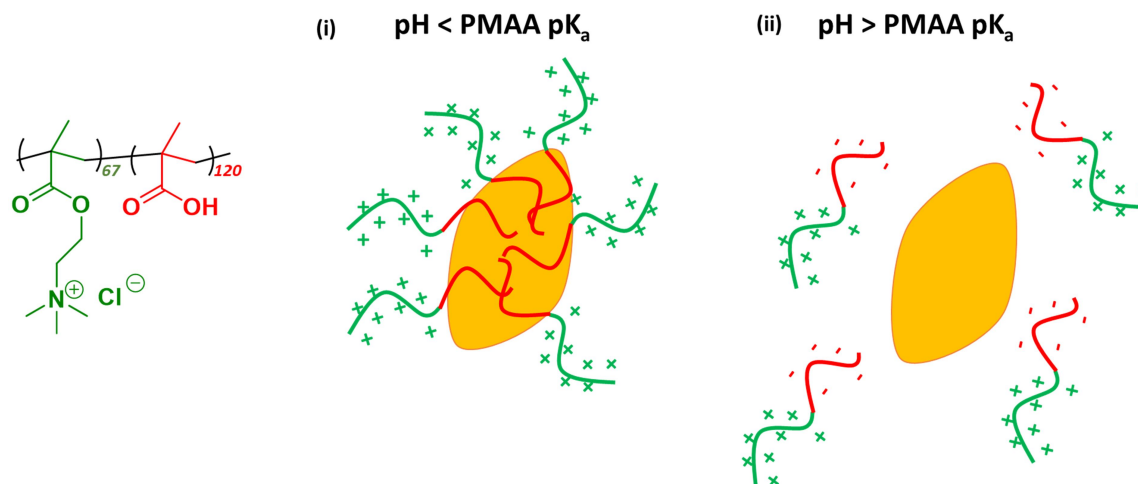
Scheme 5.3 Schematic representation of PMAA$_{67}$-PMETAC$_{120}$ dispersing transparent yellow iron oxide (i) below the pK$_a$ of PMAA. where the red PMAA block is neutral and anchored to the particle surface, with charged, soluble green PMETAC providing stabilisation, and (ii) the same copolymer with transparent yellow iron oxide where the red PMAA block is now charged and anionic, so neither block can provide stabilisation, leading to pigment flocculation.

This system was further investigated by analytical centrifugation (**Figure 5.20a**). The weight-average particle diameter was determined between pH 2.5 and pH 11.6. According to Lubrizol, the minimum acceptable particle diameter for this particular inorganic pigment is

approximately 400 nm (as indicated by the horizontal dashed line shown in **Figure 5.20a)**, so the optimal pH range for the PMAA$_{67}$-PMETAC$_{120}$ dispersant appears to lie between pH 2.5 and pH 4.0. This can be explained by the zwitterionic character of this copolymer: the PMETAC block remains cationic across the entire pH range; in principle, it can always act as the stabiliser block. However, the PMAA block is only weakly hydrophobic in its neutral form at low pH. It can act as an effective anchor block under such conditions, enabling a relatively high degree of dispersion to be achieved for this pigment. However, as the PMAA becomes ionised and acquires anionic character above pH 4, it can no longer act as an effective anchor block and the copolymer chains begin to desorb from the pigment surface. This leads to flocculated pigment dispersions with an apparent particle size approaching ~ 1 µm (**Figure 5.20a)**.
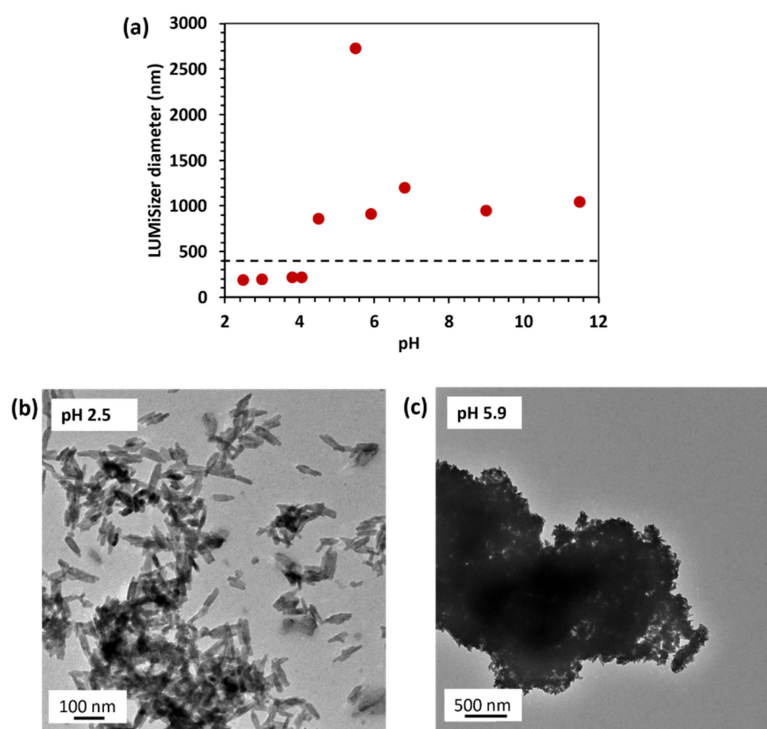
Figure 5.20 (a) LUMiSizer diameter vs. pH measurements of transparent yellow iron oxide dispersed with PMAA$_{67}$-PMETAC$_{120}$ between pH 2 and 12; **(b)** representative TEM image of yellow iron oxide particles well dispersed at pH 2.5; **(c)** representative TEM image of poorly dispersed (aggregated) yellow iron oxide particles at pH 5.9.

This interpretation is consistent with TEM studies of such pigment dispersions (**Figure 5.20b**). At pH 2.5, the copolymer-coated pigment particles are well-dispersed, which is consistent with good colloidal stability and a relatively small apparent particle size. In contrast, highly flocculated pigment particles are observed at pH 5.9 (**Figure 5.20c**), which is consistent with the much higher apparent particle diameter indicated by analytical centrifugation under such conditions.

This zwitterionic diblock copolymer was then used at its optimum concentration and dispersion pH for direct comparison against three alternative dispersants. These are a proprietary commercial dispersant used by Lubrizol for this pigment (employed at 25% copolymer per unit mass of pigment), and $PDMA_{50}$-$PMAA_{100}$ (employed at 20% copolymer per unit mass of pigment, as determined by viscosity measurements in **Figure 5.21**). A control experiment was also performed using an aqueous dispersion of flocculated transparent yellow iron oxide particles prepared in the absence of any copolymer dispersant, which exhibited an apparent particle diameter of 1.23 μm. The smallest apparent z-average particle diameter of 125 nm was obtained when using the commercial dispersant (**Figure 5.21**; pink curve). This is well below the minimum acceptable particle diameter of 400 nm required for such pigment dispersions. However, close inspection of this particle size distribution revealed the presence of relatively large micron-sized aggregates. The $PMAA_{67}$-$PMETAC_{120}$ –stabilised pigment particles exhibit a narrower particle size distribution but the apparent z-average particle diameter is somewhat higher at 205 nm, indicating a lower degree of dispersion. Interestingly, this dispersion also contained a minor population of micron-sized aggregates. In contrast, the particle size distribution recorded for the pigment dispersion prepared using the $PDMA_{50}$-$PMAA_{100}$ copolymer contained no evidence for any micron-sized aggregates. In this case, the apparent z-average particle diameter was 180 nm. Given that this zwitterionic diblock copolymer is employed at a significantly lower copolymer

concentration per unit mass of pigment, it seems that its dispersant performance in this particular case is at least comparable to that of Lubrizol's proprietary commercial dispersant.
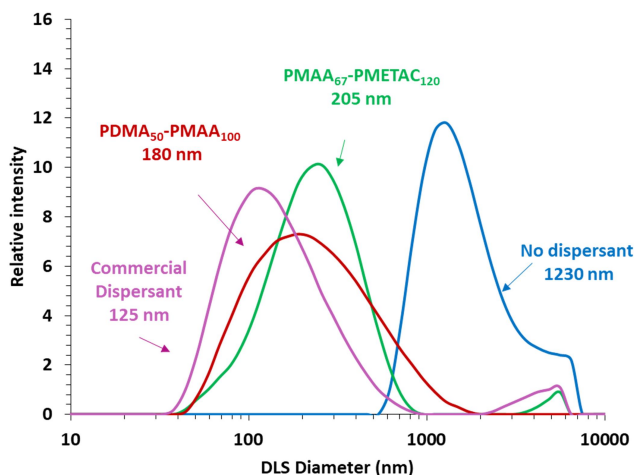

Figure 5.21 DLS intensity-average particle size distributions and corresponding z-average diameters obtained for dilute aqueous dispersions of transparent yellow iron oxide nanoparticles prepared using the following copolymers: the current best-performing commercial dispersant for this pigment employed at 25% copolymer per unit mass of pigment and pH 3(**pink curve**), $PDMA_{57}$-$PMAA_{132}$ employed at 20% copolymer per unit mass of pigment and pH 3 (**red curve**), $PMAA_{67}$-$PMETAC_{120}$ employed at 20% copolymer per unit mass of pigment and pH 3 (**green curve**) and a control experiment performed in the absence of any dispersant (**blue curve**).

Given the success of the $PDMA_{50}$-$PMAA_{100}$ diblock copolymer as a dispersant for transparent yellow iron oxide, this and two other zwitterionic diblock copolymers ($PDMA_{50}$-$PMAA_{50}$ and $PDMA_{100}$-$PMAA_{50}$) were also examined to assess the effect of varying the block composition on the degree of dispersion. Details of their syntheses can be found in Chapter 4. Each of these three copolymers were evaluated above and below their individual IEPs., and provide stabilisation as depicted in **Scheme 5.4**.
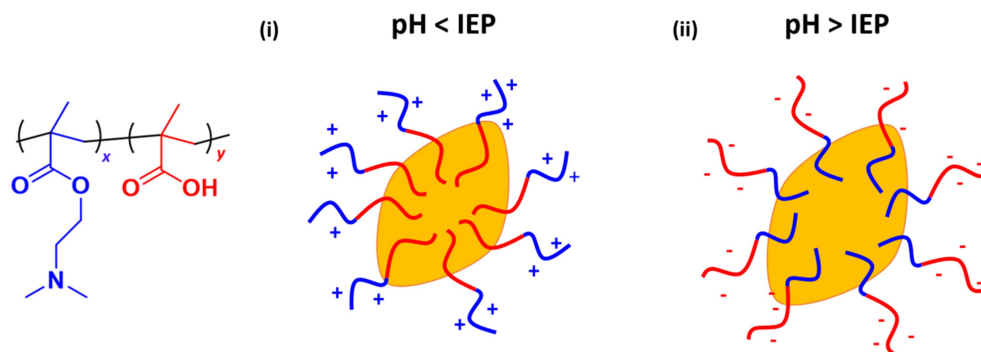
Scheme 5.4 Schematic representation of PDMA$_x$-PMAA$_y$ dispersing transparent yellow iron oxide (i) below its IEP, where the red PMAA block is neutral and anchored to the particle surface, with charged, soluble blue PDMA providing stabilisation, and (ii) the same copolymer dispersing titania above its IEP where the blue PDMA block is neutral and anchoring to the surface, while the red anionic PMAA is charged and providing stabilisation.
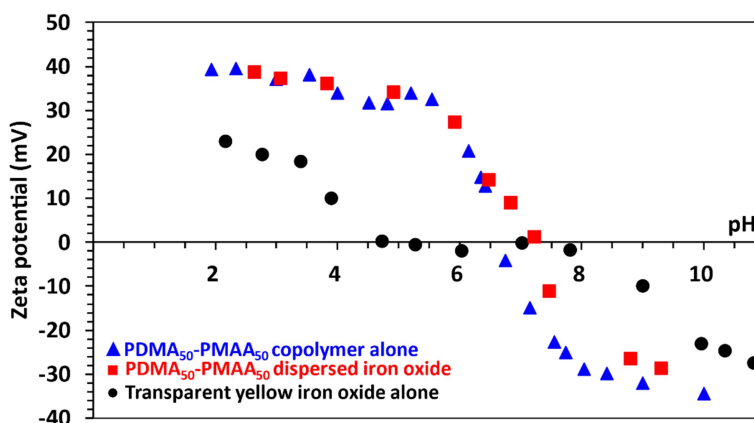

Figure 5.22 Zeta potential vs. pH curve obtained for 0.1% w/w aqueous dispersions of PDMA$_{50}$-PMAA$_{50}$ copolymer alone (**blue triangles**), transparent yellow iron oxide particles alone (**black circles**), and the same pigment particles dispersed in the presence of PDMA$_{50}$-PMAA$_{50}$ (**red squares**).

Firstly, the PDMA$_{50}$-PMAA$_{50}$ diblock copolymer was assessed. Aqueous electrophoresis data are shown in **Figure 5.22** for the PDMA$_{50}$-PMAA$_{50}$ copolymer alone (**blue triangles**), transparent yellow iron oxide particles alone (**black circles**), and the same pigment particles dispersed in the presence of PDMA$_{50}$-PMAA$_{50}$ (**red squares**). These results suggest that the pigment particles remain coated with copolymer over a wide pH range, because this zeta potential vs. pH curve is very similar to that of the copolymer alone.

PDMA$_{50}$-PMAA$_{50}$ was used as a dispersant at pH 8.5 and pH 4.0, which correspond to either side of its IEP (around pH 6.7). At a solution pH of 8.5, the PDMA block is deprotonated and hence has neutral character, while the PMAA block is ionised and so acquires anionic character. In principle, the latter block should act as a steric stabiliser, while the neutral PDMA chains adsorb onto the surface of the pigment particles.

DLS studies of the aqueous copolymer/pigment dispersions suggest that this copolymer acts as a good dispersant at pH 8.5, with an optimum loading of approximately 25% copolymer with respect to mass of pigment being observed (**Figure 5.23**). Moreover, the sphere-equivalent diameter of 118 nm for the pigment particles is well below the minimum threshold of 400 nm, indicating a sufficiently high degree of dispersion. Using these data, an upper limit adsorbed amount of approximately 2.9 mg m^{-2} can be calculated for the copolymer chains on the pigment particles, which is a physically realistic value.
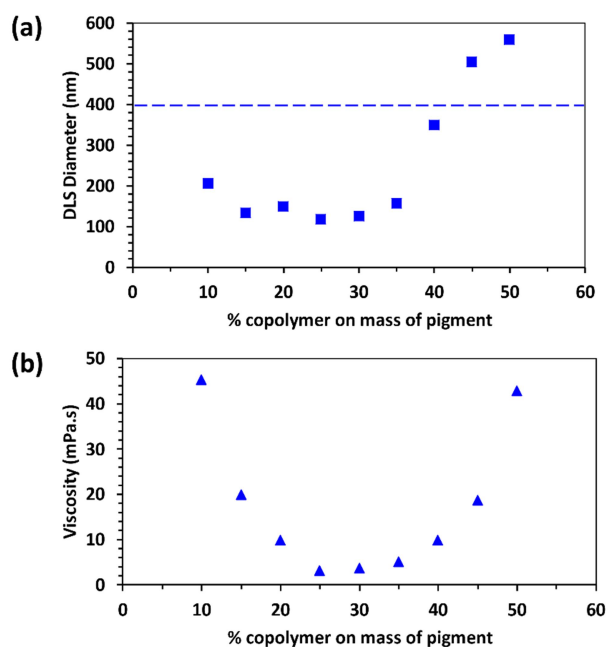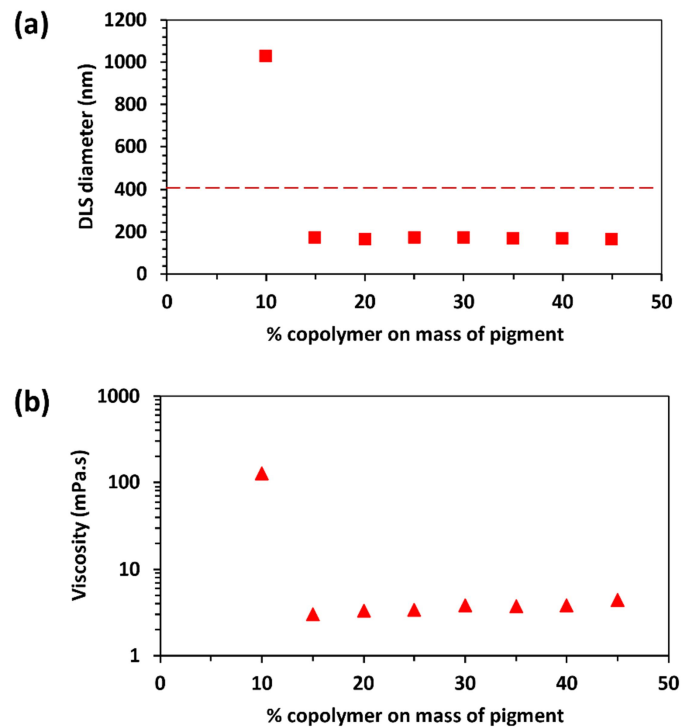

Figure 5.23 (a) DLS studies of 0.1% w/w aqueous dispersions of transparent yellow iron oxide pigment particles prepared using various amounts of PDMA$_{50}$-PMAA$_{50}$ diblock copolymer relative to the mass of pigment at pH 8.5. (b) Corresponding viscosity data obtained for the same aqueous pigment dispersions.

The sphere-equivalent DLS diameter is 206 nm when using 10% copolymer based on the mass of pigment, which is still well below the minimum acceptable diameter. However, this dispersion is relatively viscous (**Figure 5.23b**), which indicates an unstable dispersion. This is confirmed by TEM studies, which indicate the presence of large flocs (see **Figure 5.24a**). This suggests bridging flocculation owing to insufficient dispersant. In contrast, the pigment particles are well dispersed when the mass of copolymer relative to pigment is increased to 25% (see **Figure 5.24b**), with both DLS and viscosity data suggesting an optimum degree of dispersion under such conditions. However, using 50% copolymer based on pigment leads to the formation of relatively large aggregates (see **Figure 5.24c**). In this case, it is likely that free, non-adsorbed copolymer chains lead to a depletion flocculation mechanism. [34,35] This is consistent with the relatively large apparent particle diameter reported by DLS and a correspondingly high dispersion viscosity (45 mPa.s).
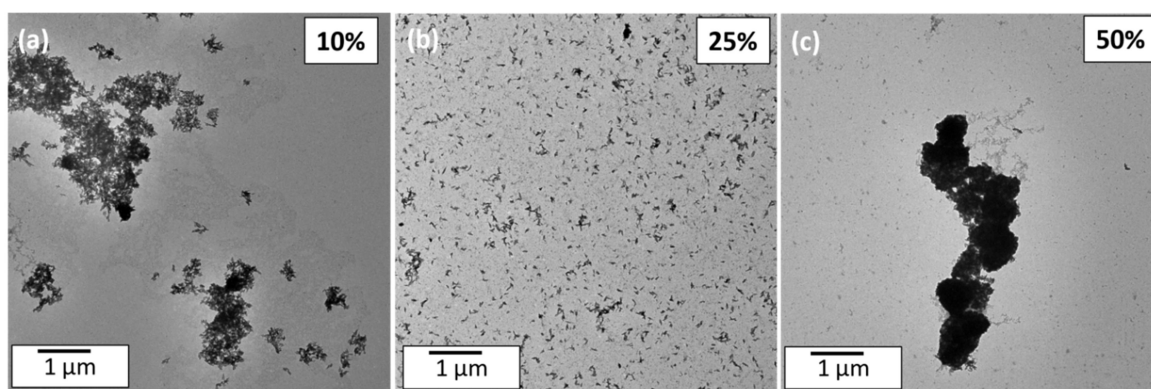
Figure 5.24 Representative TEM images recorded for dried 0.1% w/w aqueous dispersions of 'rice grain' shaped transparent yellow iron oxide particles at pH 8.5 using varying amounts of $PDMA_{50}$-$PMAA_{50}$ with respect to pigment mass: **(a)** 10% copolymer, **(b)** 25% copolymer (which corresponds to the optimum concentration for a high degree of dispersion), **(c)** 50% copolymer.

Similar pigment dispersion experiments were also performed at pH 4.0, which is below the copolymer IEP. Under these conditions, the PMAA block is in its neutral form, whereas the PDMA block is protonated and hence acquires cationic character. In this case, the cationic

block most likely acts as the steric stabiliser, while the PMAA block adsorbs at the surface of the pigment particles.

DLS and viscosity measurements suggest that this dispersant is effective over a wider range of copolymer concentration at pH 4.0, with any copolymer concentration above 15% based on the mass of pigment resulting in a stable dispersion (**Figure 5.25**). The minimum dispersion viscosity is 3.3 mPa.s, which is comparable to the minimum value of 3.2 mPa.s observed at pH 8.5. However, DLS studies indicate an apparent minimum diameter of 165 nm, which is somewhat larger than that achieved at pH 8.5.

Figure 5.25 (a) DLS studies of 0.1% w/w aqueous dispersions of transparent yellow iron oxide pigment particles prepared using various amounts of PDMA$_{50}$-PMAA$_{50}$ diblock copolymer relative to the mass of pigment at pH 4.0. **(b)** Corresponding viscosity data obtained for the same aqueous pigment dispersions.

TEM studies confirm the presence of flocs when using 10% copolymer at pH 4.0, suggesting a bridging flocculation mechanism (**Figure 5.26a**). However, TEM images recorded when

using either 15% or 25% copolymer relative to pigment mass (**Figures 5.26b** and **5.26c**) suggest that a high degree of dispersion is achieved under these conditions.
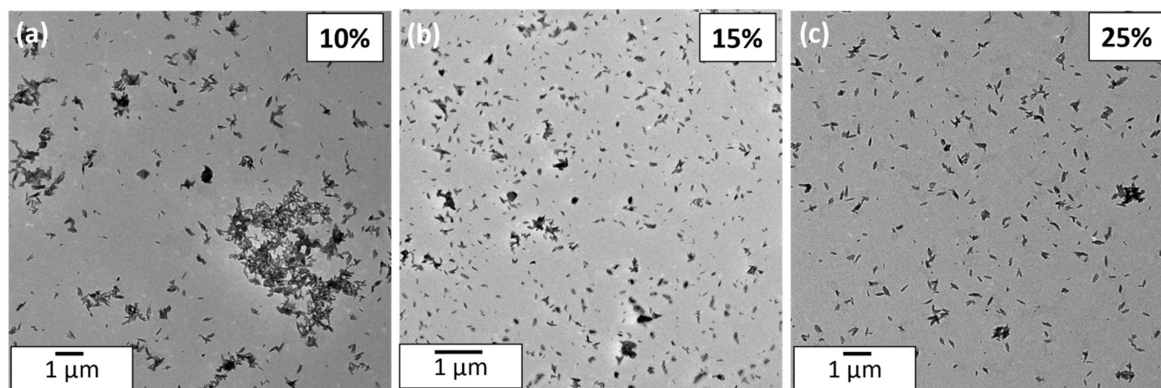

Figure 5.26 Representative TEM images recorded for dried 0.1% w/w aqueous dispersions of 'rice grain' shaped transparent yellow iron oxide particles at pH 4.0 using varying amounts of PDMA$_{50}$-PMAA$_{50}$ with respect to pigment mass: **(a)** 10% copolymer, **(b)** 15% copolymer, which corresponds to the optimum concentration for a high degree of dispersion and **(c)** 25% copolymer.

Two other zwitterionic diblock copolymers were also assessed as putative dispersants for the transparent yellow iron oxide pigment. Again, the dispersion pH was selected to be either above or below the IEP of the copolymer in question (see **Table 5.1**).

The minimum particle size that could be reached for a PDMA$_{50}$-PMAA$_{100}$ dispersant above the copolymer IEP at pH 7.5 was 369 nm at 25% copolymer (**Figure 5.27**), which is only just below the minimum acceptable diameter. TEM confirms a relatively coarse dispersion (see **Figure 5.27c**). However, this copolymer can act as an effective copolymer dispersant below its IEP, with a relatively low apparent pigment particle diameter of 201 nm being achieved under these conditions (**Figure 5.28**). This suggests that the neutral PMAA$_{100}$ block acts as a good anchor. The TEM image in **Figure 5.28c** confirms that a relatively high degree of dispersion can be achieved in this case.
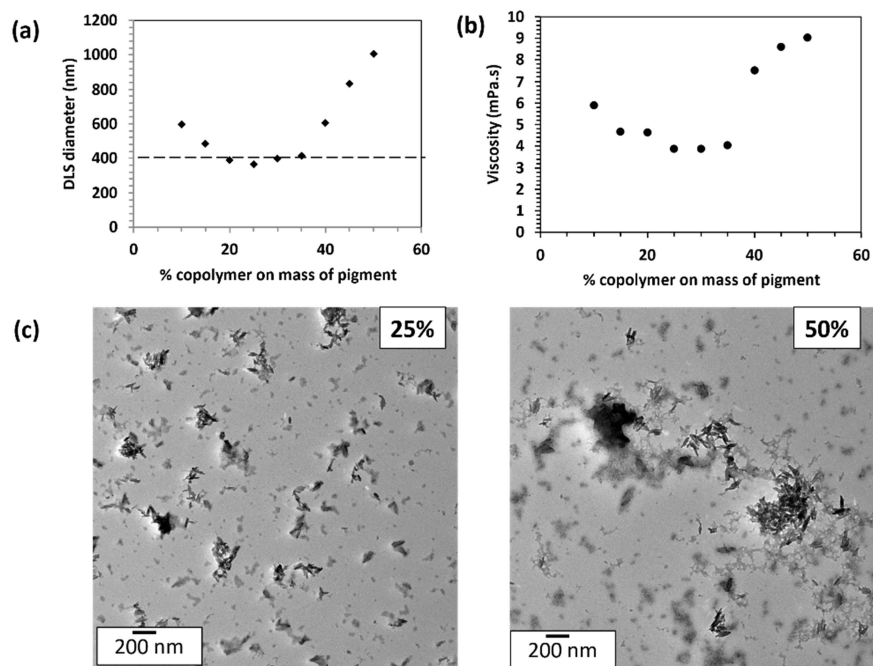
Figure 5.27 Dispersion of transparent yellow iron oxide pigment particles using PDMA$_{50}$-PMAA$_{100}$ at pH 7.5, above its IEP: **(a)** variation in DLS diameter with copolymer concentration, **(b)** variation in dispersion viscosity with copolymer concentration, **(c)** TEM images recorded at 25% and 50% copolymer with respect to pigment mass.
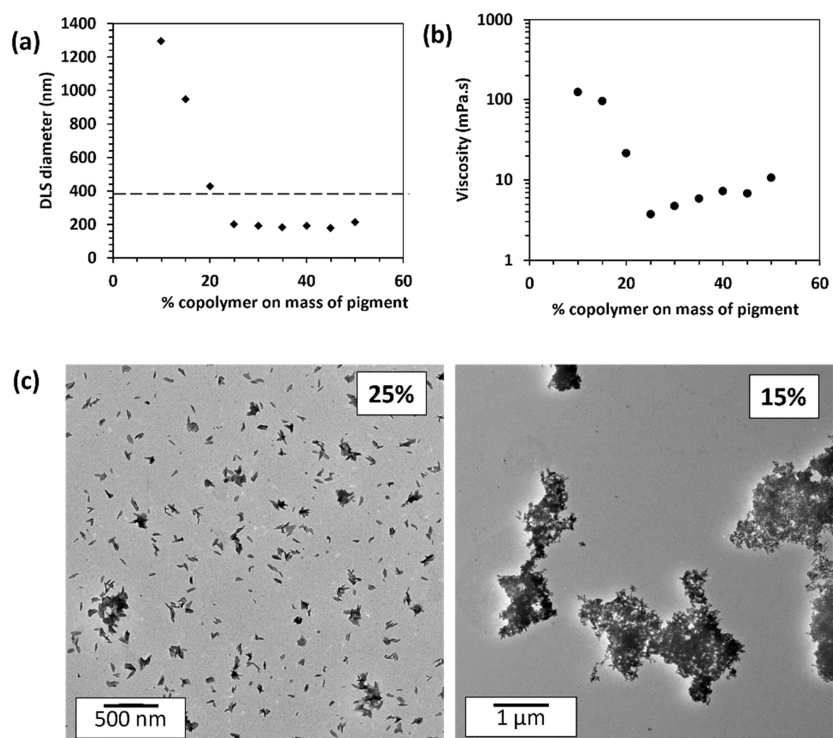

Figure 5.28 Dispersion of transparent yellow iron oxide with PDMA$_{50}$-PMAA$_{100}$ at pH 3.5, below its IEP: **(a)** variation in DLS diameter with copolymer concentration, **(b)** variation in dispersion viscosity with copolymer concentration, **(c)** TEM images recorded at 25% and 15% copolymer with respect to pigment mass.

Similarly, using a PDMA$_{100}$-PMAA$_{50}$ copolymer produced a reasonably high degree of dispersion at pH 10.5 (**Figure 5.29**), with a minimum pigment size of 305 nm obtained at 20% copolymer based on the mass of pigment.
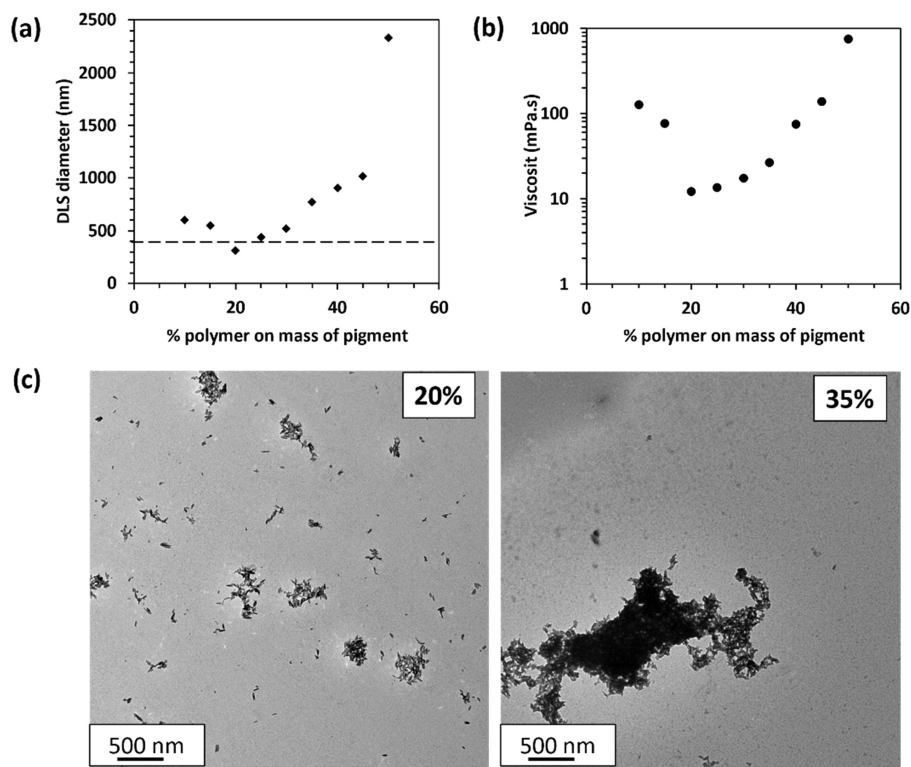

Figure 5.29 Dispersion of transparent yellow iron oxide pigment particles using PDMA$_{100}$-PMAA$_{50}$ at pH 10.5, above its IEP: (a) variation in DLS diameter with copolymer concentration, (b) variation in dispersion viscosity with copolymer concentration, (c) TEM images recorded at 20% and 35% copolymer with respect to pigment mass.

Only a very poor degree of dispersion could be achieved at pH 5.0 (**Figure 5.30**), where the apparent particle size exceeds the minimum requirement of 400 nm.
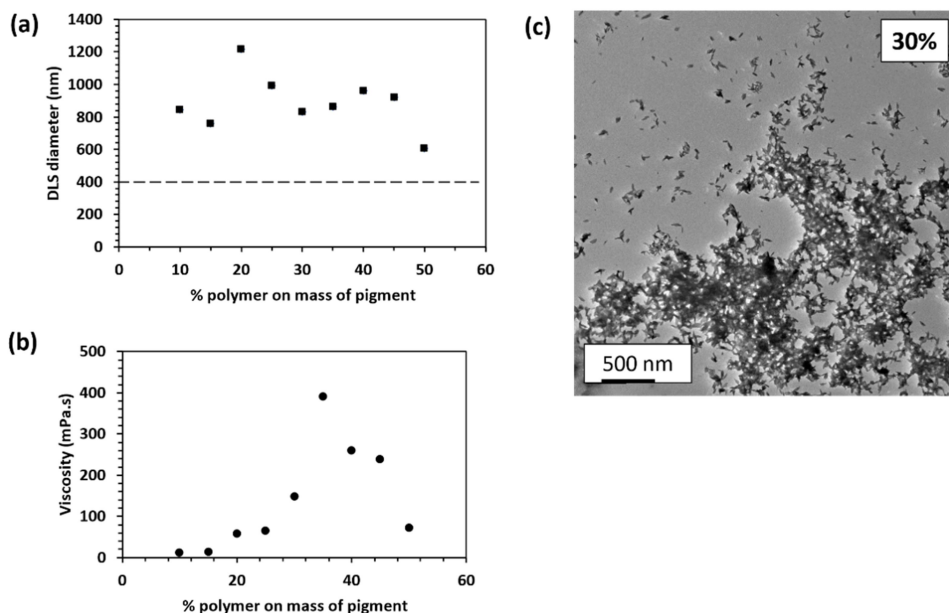
Figure 5.30 Dispersion of transparent yellow iron oxide pigment particles using PDMA$_{100}$-PMAA$_{50}$ at pH 5.0, which is below its IEP: **(a)** variation in DLS diameter with copolymer concentration, **(b)** variation in dispersion viscosity with copolymer concentration, **(c)** TEM image recorded at 30% copolymer with respect to pigment.

A comparison between these three PDMA$_x$-PMAA$_y$ diblock copolymers as dispersants for the transparent yellow iron oxide pigment is made in **Table 5.1**.

Table 5.1 Summary of the optimal concentration, minimum apparent pigment diameter and dispersion viscosity of aqueous dispersions of transparent yellow iron oxide particles prepared using three different PDMA$_x$-PMAA$_y$ diblock copolymers at a solution pH either above or below their IEP.

Copolymer	pH	Optimal concentration	Minimum pigment size at optimal [copolymer] (nm)	Minimum dispersion viscosity at optimal [copolymer] (mPa.s)
PDMA$_{49}$-PMAA$_{100}$	7.5	25%	369	3.88
	3.5	25%	201	3.75
PDMA$_{50}$-PMAA$_{50}$	8.5	25%	118	3.21
	4.0	20%	165	3.30
PDMA$_{100}$-PMAA$_{50}$	10.5	20%	305	12.03
	5.0	-	(606)	(13.2)

These results highlight the importance of optimizing both the zwitterionic diblock copolymer composition and also the dispersion pH to achieve the highest possible degree of pigment dispersion. In particular, the PDMA$_{50}$-PMAA$_{50}$ copolymer seems to be a particularly

promising dispersant for transparent yellow iron oxide particles, since it led to the smallest apparent particle diameter and lowest dispersion viscosity. Moreover, a high pH is normally required for pigment dispersion when formulating aqueous inkjet inks, making this copolymer well-suited for potential industrial use. Further studies would be necessary to deduce why these smaller, symmetrical blocks work so well as dispersants, and if time allowed would also be tested with titania.

The $PDMA_{50}$-$P(MAA_{0.80}$-$stat$-$BzMA_{0.20})_{100}$ copolymer was also evaluated as a dispersant for transparent yellow iron oxide (**Figure 5.1c**). Again, a dosage ladder was constructed to identify an optimum copolymer concentration of 20% per unit mass of pigment via dispersion viscosity measurements (**Figure 5.31**).
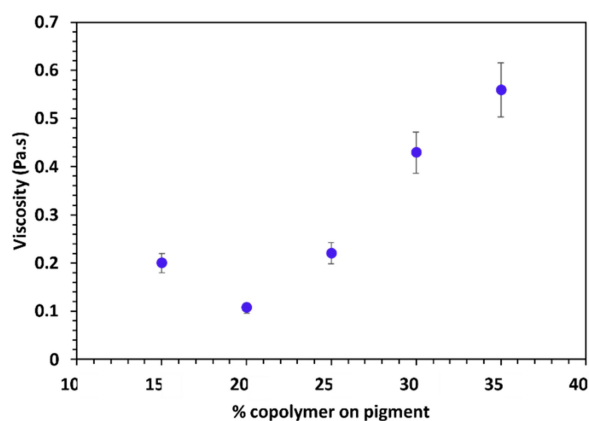

Figure 5.31 Dosage ladder constructed via dispersion viscosity measurements for transparent yellow iron oxide dispersions prepared using $PDMA_{50}$-$P(MAA_{0.80}$-$stat$-$BzMA_{0.20})_{100}$. A minimum in dispersion viscosity is observed at 20% copolymer per unit mass of pigment.
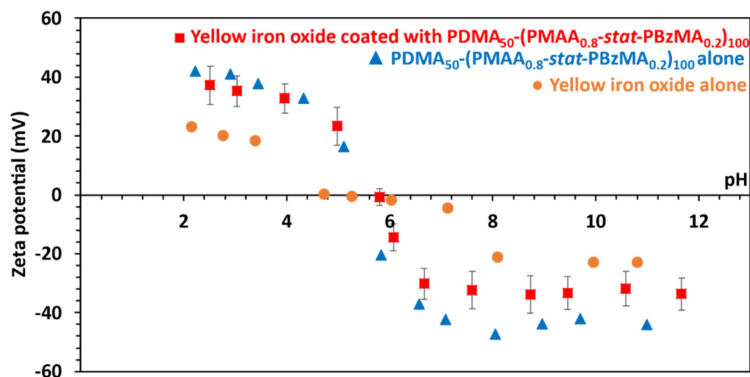
Figure 5.32 Zeta potential vs. pH curves obtained for 0.1% w/w aqueous dispersions of transparent yellow iron oxide particles alone (**yellow circles**), $PDMA_{50}$-$P(MAA_{0.80}$-$stat$-$BzMA_{0.20})_{100}$ copolymer alone (**blue triangles**) and transparent yellow iron oxide particles dispersed with the aid of $PDMA_{50}$-$P(MAA_{0.80}$-$stat$-$BzMA_{0.20})_{100}$ copolymer (**red squares**).

Accordingly, $PDMA_{50}$-$P(MAA_{0.80}$-$stat$-$BzMA_{0.20})_{100}$ was evaluated as a dispersant at this copolymer concentration. Zeta potential vs. pH curves were determined for 0.1% w/w aqueous dispersions of $PDMA_{50}$-$P(MAA_{0.80}$-$stat$-$BzMA_{0.20})_{100}$ copolymer alone, transparent yellow iron oxide particles alone, and the same pigment particles dispersed with the aid of $PDMA_{50}$-$P(MAA_{0.80}$-$stat$-$BzMA_{0.20})_{100}$ copolymer (**Figure 5.32**). Below the IEP (i.e., pH 2-5), the copolymer-coated pigment particles exhibited comparable cationic character to that of the copolymer alone. However, above the IEP (i.e., pH 7-11), the copolymer nanoparticles proved to be more anionic than the copolymer-coated pigment particles (**Figure 5.32**).
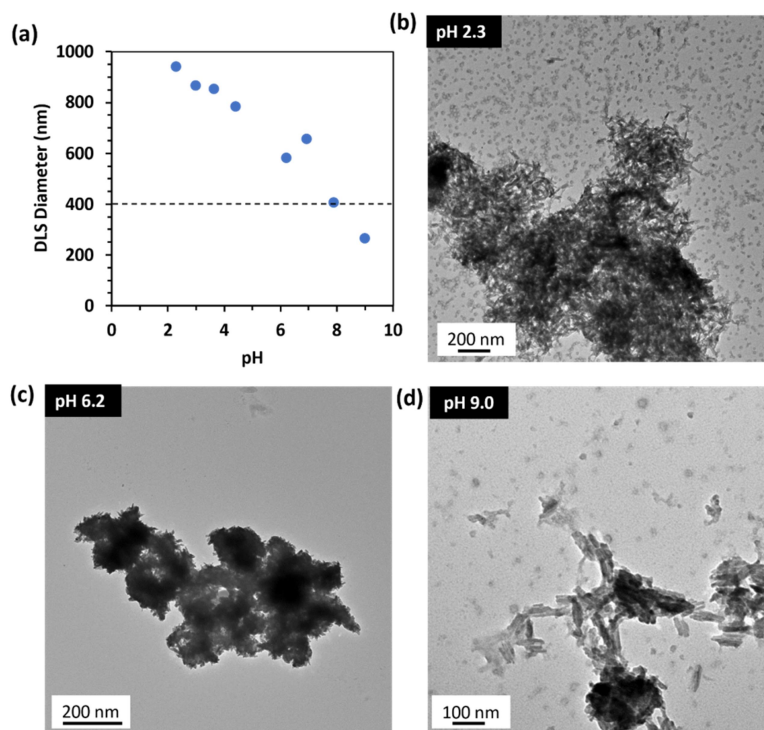
Figure 5.33 (a) Effect of varying the dispersion pH on the apparent z-average particle diameter reported by DLS for transparent yellow iron oxide particles dispersed using $PDMA_{50}$-$P(MAA_{0.80}$-*stat*-$BzMA_{0.20})_{100}$ copolymer between pH 2 and pH 9. Representative TEM images recorded for: **(b)** poorly-dispersed yellow iron oxide particles at pH 2.3; **(c)** poorly-dispersed yellow iron oxide particles at pH 6.2; **(d)** fairly well-dispersed yellow iron oxide particles at pH 9.0.

For the titania pigment discussed earlier, the $PDMA_{50}$-$P(MAA_{0.80}$-*stat*-$BzMA_{0.20})_{100}$

copolymer exhibited poor dispersant performance at low pH but functioned better at high pH,

where the DMA block is present in its weakly hydrophobic neutral form. This also appears to

be the case for the transparent yellow iron oxide pigment. When formulated at low pH, such

dispersions are poorly dispersed with relatively large apparent particle diameters indicated by

DLS studies (**Figure 5.33a**). This interpretation is consistent with the TEM image shown in

Figure 5.33b, which reveals a large number of non-adsorbed nanoparticles in the

background. Given that this dispersion was prepared at the optimum copolymer

concentration, this suggests that the copolymer is not strongly adsorbed at the pigment

surface. As expected, macroscopic precipitation is observed at the IEP (**Figure 5.33c**). There

are no nanoparticles visible in the background, suggesting that heteroflocculation of the

copolymer and pigment particles occurs under such conditions. The minimum acceptable diameter of 400 nm cannot be achieved for the yellow iron oxide pigment until the dispersion pH exceeds pH 8 (**Figure 5.33a**). The TEM image shown in **Figure 5.33d** was recorded for a dispersion dried at pH 9. Under such conditions, the weakly hydrophobic PDMA block can adsorb at the pigment surface, with the anionic $P(MAA_{0.80}\text{-}stat\text{-}BzMA_{0.20})_{100}$ chains acting as the steric stabiliser block.

5.4 Conclusions

Zwitterionic diblock copolymers (readily synthesised via RAFT aqueous solution polymerisation as discussed in Chapter 4) can be effective dispersants for both titanium dioxide and transparent yellow iron oxide pigments. At high pH, the weakly hydrophobic PDMA chains appear to be a good anchor block adsorption onto both titania and iron oxide particles. At low pH (approximately below pH 4), neutral PMAA chains can also serve as an effective anchor block for the same two pigments. Perhaps surprisingly, this does not appear to be the case if 20 mol% BzMA is statistically copolymerised with MAA. Similarly, PMAA-PMETAC diblock copolymers proved to be ineffective dispersants when examined over a wide range of dispersion pH, most likely owing to in situ desorption of the copolymer chains from the surface of the pigment particles.

In the case of the titania pigment, the dispersant dosage required for good colloidal stability (20% per unit mass of pigment) is much higher than that for commercial dispersants (2% per unit mass of pigment). Thus, zwitterionic diblock copolymers are highly unlikely to be commercially viable for this pigment. Nevertheless, the experimental data still provide valuable insights regarding the mechanism of pigment dispersion for these dispersants.

In the case of the transparent yellow iron oxide pigment, zwitterionic diblock copolymers appear to offer genuine application potential. Very promising results were obtained in terms of both the relatively high degree of dispersion (minimum apparent particle size) and viscosity reduction. Moreover, a dispersant concentration of only 20% was required, as opposed to 25% for the current best commercial dispersant. Given the wholly aqueous, atom-efficient one-pot synthetic protocol developed in this Thesis, zwitterionic PDMA-PMAA diblock copolymers may prove to be commercially attractive new dispersants for transparent yellow iron oxide.

5.5 References

1. Höfer, R. & Bigorra, J. Green chemistry - A sustainable solution for industrial specialties applications. *Green Chem.* **9**, 203–212 (2007).

2. Farrokhpay, S. A review of polymeric dispersant stabilisation of titania pigment. *Adv. Colloid Interface Sci.* **151**, 24–32 (2009).

3. Creutz, S., Jérôme, R., Kaptijn, G. M. P., Van Der Werf, A. W. & Akkerman, J. M. Design of polymeric dispersants for waterborne coatings. *J. Coatings Technol.* **70**, 41–46 (1998).

4. Creutz, S. & Jérôme, R. Effectiveness of poly(vinylpyridine) block copolymers as stabilizers of aqueous titanium dioxide dispersions of a high solid content. *Langmuir* **15**, 7145–7156 (1999).

5. Creutz, S. & Jérôme, R. Effectiveness of block copolymers as stabilizers for aqueous titanium dioxide dispersions of a high solid content. *Prog. Org. Coatings* **40**, 21–29 (2000).

6. Hoogeveen, N. G., Cohen Stuart, M. A. & Fleer, G. J. Polyelectrolyte adsorption on oxides. I. Kinetics and adsorbed amounts. *J. Colloid Interface Sci.* **182**, 133–145 (1996).

7. Luckham, P. F., Bailey, A. I., Miano, F. & Tadros, T. F. Effectiveness of Surfactants as Steric Stabilizers. in *Surfactant Adsorption and Surface Solubilization* **615**, 166–182 (ACS Symposium Series, 1996).

8. Fritz, G., Schädler, V., Willenbacher, N. & Wagner, N. J. Electrosteric stabilization of colloidal dispersions. *Langmuir* **18**, 6381–6390 (2002).

9. Pan, K., Chen, H., Baek, S. J. & Zhong, Q. Self-assembled curcumin-soluble soybean polysaccharide nanoparticles: Physicochemical properties and in vitro anti-proliferation activity against cancer cells. *Food Chem.* **246**, 82–89 (2018).

10. Yamamoto, S., Watler, P. K., Feng, D. & Kaltenbrunner, O. Characterization of unstable ion-exchange chromatographic separation of proteins. *J. Chromatogr. A* **852**, 37–41 (1999).

11. Szilágyi, I., Rosická, D., Hierrezuelo, J. & Borkovec, M. Charging and stability of anionic latex particles in the presence of linear poly(ethylene imine). *J. Colloid Interface Sci.* **360**, 580–585 (2011).

12. Trulsson, M., Forsman, J., Åkesson, T. & Jönsson, B. Simulations of latex particles immersed in dendrimer solutions. *Langmuir* **25**, 6106–6112 (2009).

13. Wang, W. *et al.* Improving Loading Amount and Performance of Quantum Dot-Sensitized Solar Cells through Metal Salt Solutions Treatment on Photoanode. *ACS Appl. Mater. Interfaces* **8**, 31006–31015 (2016).

14. Kosmulski, M., Maczka, E. & Rosenholm, J. B. Isoelectric points of metal oxides at high ionic strengths. *J. Phys. Chem. B* **106**, 2918–2921 (2002).

15. Canning, S. L., Neal, T. J. & Armes, S. P. PH-Responsive Schizophrenic Diblock Copolymers Prepared by Polymerization-Induced Self-Assembly. *Macromolecules* **50**, 6108–6116 (2017).

16. Jin, G. W. *et al.* Formation of polyion complex micelles with tunable isoelectric points based on zwitterionic block copolymers. *Macromol. Res.* **20**, 1249–1256 (2012).

17. Coulbeck, E. personal communication. (2020).

18. Schonbrun, Z. The Quest for the Next Billion-Dollar Color. *Bloomberg L.P.* 1–17 (2018).

19. Braun, J. H. Titanium dioxide - A review. *Journal of Coatings Technology* **69**, 59–72 (1997).

20. Morris, G. E., Skinner, W. A., Self, P. G. & Smart, R. S. C. Surface chemistry and rheological behaviour of titania pigment suspensions. *Colloids Surfaces A Physicochem. Eng. Asp.* **155**, 27–41 (1999).

21. Liang, C. *et al.* The effect of acrylamides copolymers on the stability and rheological properties of yellow iron oxide dispersion. *Colloids Surfaces A Physicochem. Eng. Asp.* **513**, 136–145 (2017).

22. Xu, C. yang, Deng, K. ying, Li, J. yu & Xu, R. kou. Impact of environmental conditions on aggregation kinetics of hematite and goethite nanoparticles. *J. Nanoparticle Res.* **17**, 1–13 (2015).

23. Vogel, M., Kleinsteinberg, F. & Milanovic, N. Dispersant technology for red and yellow iron oxides: A new additive technology for waterborne iron oxide pigment concentrates. *PCI-Paint and Coatings Industry* **2016**, (2016).

24. Fujitani, T. Stability of pigment and resin dispersions in waterborne paint. *Prog. Org. Coatings* **29**, 97–105 (1996).

25. Penfold, N. J. W., Whatley, J. R. & Armes, S. P. Thermoreversible Block Copolymer Worm Gels Using Binary Mixtures of PEG Stabilizer Blocks. *Macromolecules* **52**, 1653–1662 (2019).

26. *Ti Pure R960 Titanium Dioxide Product Information*. (2017).

27. Day, R. E. The characterisation of the surface of titanium dioxide pigments. *Prog. Org. Coatings* **2**, 269–288 (1974).

28. Kissa, E. *Dispersions: Characterization, Testing, and Measurement - Erik Kissa - Google Books*. (Marcel Dekker Inc., 1999).

29. Kostansek, E. Controlling particle dispersion in latex paints containing associative thickeners.

J. Coatings Technol. Res. **4**, 375–388 (2007).

30. Farrokhpay, S., Morris, G. E., Fornasiero, D. & Self, P. Effects of chemical functional groups on the polymer adsorption behavior onto titania pigment particles. *J. Colloid Interface Sci.* **274**, 33–40 (2004).

31. Farrokhpay, S., Morris, G. E., Fornasiero, D. & Self, P. Stabilisation of titania pigment particles with anionic polymeric dispersants. *Powder Technol.* **202**, 143–150 (2010).

32. Hoogeveen, N. G., Stuart, M. A. C. & Fleer, G. J. Adsorption of charged block copolymers with two adsorbing blocks. *Faraday Discuss.* **98**, 161–172 (1994).

33. Dupin, D., Armes, S. P., Connan, C., Reeve, P. & Baxter, S. M. How does the nature of the steric stabilizer affect the pickering emulsifier performance of lightly cross-linked, acid-swellable poly(2-vinylpyridine) latexes? *Langmuir* **23**, 6903–6910 (2007).

34. Snowden, M. J., Clegg, S. M., Williams, P. A. & Robb, I. D. Flocculation of silica particles by adsorbing and non-adsorbing polymers. *J. Chem. Soc. Faraday Trans.* **87**, 2201–2207 (1991).

35. Snowden, M. J., Williams, P. A., Garvey, M. J. & Robb, I. D. Phase separation of concentrated aqueous silica dispersions in the presence of nonadsorbed polyelectrolytes. *J. Colloid Interface Sci.* **166**, 160–167 (1994).

Chapter 6

PISA synthesis and aqueous solution properties of schizophrenic PDEA-PCEA diblock copolymer nanoparticles and their use as aqueous dispersants for titania

6.1 Introduction

The micellar self-assembly of block copolymers in solution has been studied for more than fifty years.[1,2] In 1998, the first example of an AB diblock copolymer that could form either A-core or B-core micelles in aqueous media was reported by Bütün et al.[3,4] for PMEMA-PDEA diblock copolymers synthesised via group transfer polymerisation (GTP), which is a type of anionic polymerisation developed for (meth)acrylic monomers (**Scheme 6.1**).
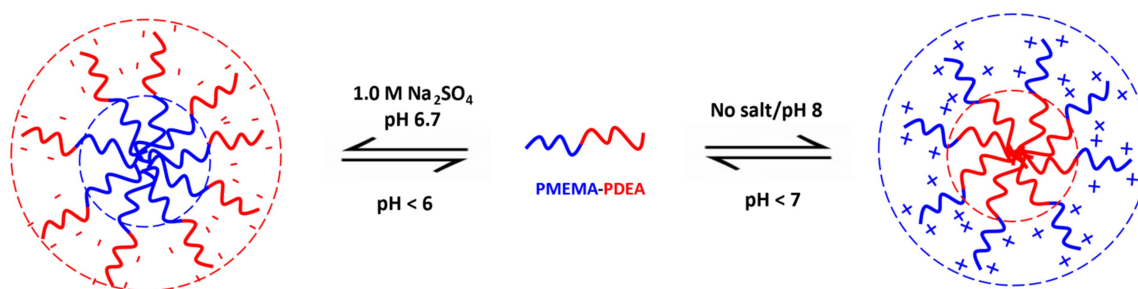
Scheme 6.1 Schematic representation of the formation of micelles and so-called 'reverse micelles' for a **PMEMA**-**PDEA** diblock copolymer in aqueous solution at 20 °C. Reproduced from Ref. 4.

In 2001, Armes and co-workers reported that PPO-PDEA diblock copolymers could form two types of micelles by adjusting the solution pH and temperature but neither micellar state was stable at ambient temperature.[5] The phrase 'schizophrenic' was coined to describe this new class of diblock copolymers.[6] In 2002, Laschewsky et al.[7] prepared the first (meth)acrylamide example of a doubly-thermoresponsive schizophrenic diblock copolymer via RAFT solution polymerisation. However, such copolymers had relatively broad MWDs and were contaminated with homopolymer. Also in 2002, Weaver et al.[8] reported a doubly-thermoresponsive schizophrenic methacrylate-based diblock copolymer with a relatively narrow MWD by GTP. Of particular relevance to this Thesis Chapter, Liu et al.[9] designed a zwitterionic poly(4-vinyl benzoic acid)-poly(2-(diethylamino)ethyl methacrylate) (PVBA-PDEA) diblock copolymer that underwent spontaneous self-assembly in aqueous solution

simply by adjusting the solution pH at room temperature (**Scheme 6.2**).
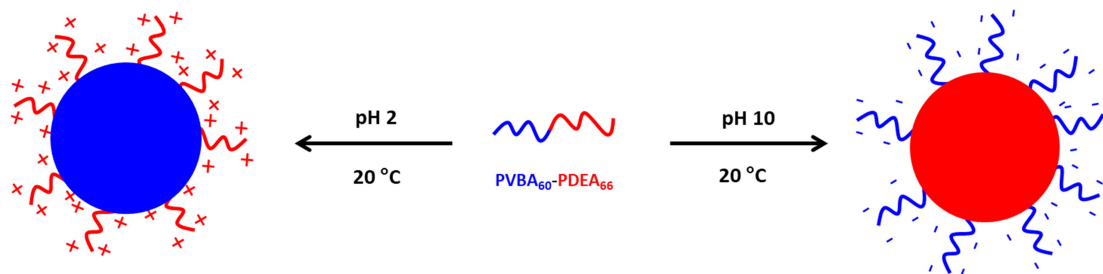
Scheme 6.2 Schematic representation of a poly(4-vinyl benzoic acid)-poly(2-(diethylamino)ethyl methacrylate) (PVBA-PDEA) diblock copolymer and its pH-responsive 'schizophrenic' micellization behaviour in aqueous solution. Reproduced from ref. 9.

Unlike the previously reported PDMA-PMAA zwitterionic diblock copolymers,[10–13] both the weakly acidic PVBA block and the weakly basic PDEA block were sufficiently hydrophobic in their neutral forms to produce well-defined PVBA-core or PDEA-core micelles at either low pH or high pH, respectively.[9]

Over the past decade or so, PISA has become widely recognised as a powerful technique for the synthesis of a wide range of functional block copolymer nano-objects.[14–16] Most pertinently, Canning *et al*. reported the aqueous PISA synthesis of zwitterionic diblock copolymers *directly* in the form of sterically-stabilised nanoparticles (**Figure 6.1**).[17]
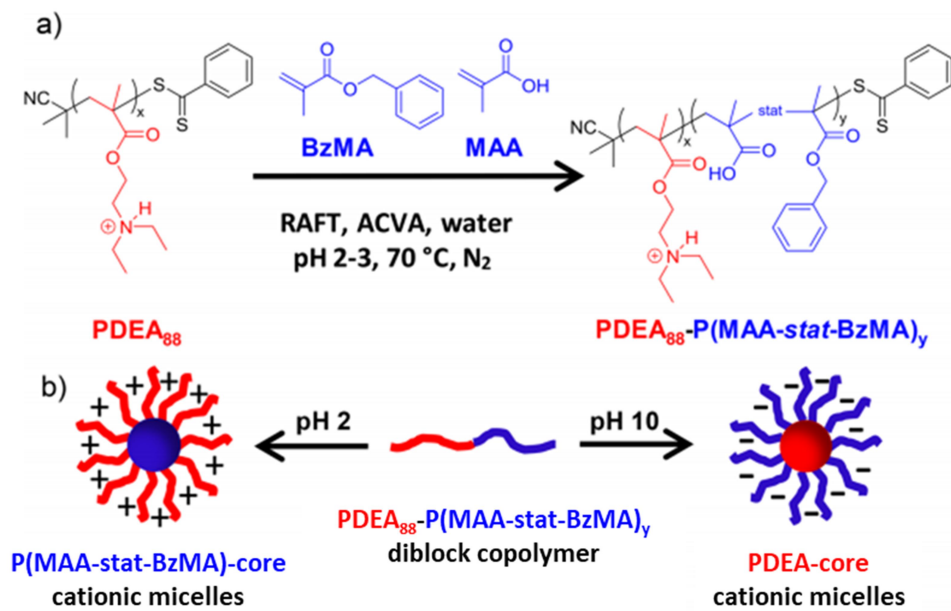
Figure 6.1 (a) Schematic representation of the RAFT aqueous emulsion copolymerisation of methacrylic acid and benzyl methacrylate using a protonated PDEA$_{88}$ precursor. (b) Schizophrenic micellization behaviour exhibited by PDEA$_{88}$-P(MAA-*stat*-BzMA)$_y$ diblock copolymers in aqueous solution. Reproduced from reference 17.

Various experimental techniques were employed to verify the schizophrenic behaviour of this new zwitterionic diblock copolymer system. ^{1}H NMR spectroscopy studies confirmed that the polyacid block became desolvated at low pH, while the polybase block became desolvated at high pH. These observations were consistent with TEM, DLS and aqueous electrophoresis observations, which indicated the formation of cationic and anionic spherical nanoparticles, respectively.[18] Interestingly, suitable rhodamine- and fluorescein-based comonomers were statistically copolymerised into the polybase and polyacid blocks respectively in order to produce 'self-reporting' pH-responsive nanoparticles.[18] However, Canning *et al.* always prepared their PDEA precursor using an organic solvent (THF)[18] and the feasibility of developing a wholly aqueous one-pot formulation was not explored.

More recently, schizophrenic diblock copolymer nanoparticles have been evaluated as stimulus-responsive Pickering emulsifiers. For example, Ranka *et al.*[19] utilised a doubly-

thermoresponsive schizophrenic diblock copolymer to form stable emulsions at elevated temperature, with macroscopic phase separation occurring on cooling to ambient temperature. In principle, such schizophrenic nanoparticles may find applications in diverse fields such as enhanced oil recovery,[20,21] catalysis, or possibly in the field of pigment dispersion.

In this Chapter, the synthesis of doubly pH-responsive PDEA-PCEA diblock copolymers directly in the form of sterically-stabilised nanoparticles is achieved using an aqueous PISA formulation. The schizophrenic behaviour of such nanoparticles is characterised and their potential use as a putative universal dispersant for aqueous titania dispersions is briefly assessed.

6.2 Experimental

Materials

4-Cyano-4-(2-phenylethanesulfanylthiocarbonyl)sulfanylpentanoic acid) (PETTC) was synthesised as previously reported.[22] 2-(Diethylamino)ethyl methacrylate (DEA), 2-carboxyethyl acrylate (CEA) and trimethylsilyldiazomethane (supplied as a 2.0 M solution in diethyl ether) were purchased from Sigma-Aldrich (Dorset, UK) and were used as received. 2,2'-Azobis(2-(2-imidazolin-2-yl)propane) dihydrochloride (VA-044) was purchased from Wako Pure Chemical Industries (Japan). 4,4′-Azobis(4-cyanovaleric acid) (ACVA; 98%) was purchased from Alfa Aesar (Heysham, UK) and was used as received. CD_3OD and CD_2Cl_2 were purchased from Goss Scientific Instruments Ltd (Cheshire, UK). $CDCl_3$, D_2O, sodium deuteroxide (NaOD) and deuterium chloride (DCl) were purchased from Sigma-Aldrich (Dorset, UK). All other solvents were purchased from Fisher Scientific (Loughborough, UK) and were used as received. Deionised water was used for all experiments and the solution pH

was adjusted using either HCl or NaOH. Inkjet-grade Titania R-960 pigment particles were kindly supplied by Lubrizol (Blackley, Manchester).

One pot synthesis of poly[(2-diethylamino)ethyl methacrylate)-poly(2-carboxyethyl acrylate) (PDEA-PCEA) diblock copolymer

A typical protocol for the one-pot wholly aqueous synthesis of a PDEA-PCEA zwitterionic diblock copolymer was conducted as follows. DEA (2.00 g, 10.8 mmol), PETTC (0.0547 g, 0.161 mmol; target DP = 67), VA-044 (17.2 mg, 0.053 mmol; PETTC/VA-044 molar ratio = 3) and deionised water (3.11 g) were added to a 100 ml two-necked round-bottomed flask and the mixture was stirred thoroughly to afford an aqueous solution. 36% HCl (0.92 g, 10.8 mmol) was used to deprotonate the DEA. This 40% w/w aqueous solution was then purged for 30 min with nitrogen and heated up to 44 °C. After 4 h, the DEA polymerisation had reached more than 99% conversion as determined by ^{1}H NMR spectroscopy. In a separate vial, CEA (3.11 g, 21.6 mmol; target DP = 134), VA-044 (17.3 mg, 0.054 mmol; PETTC/VA-044 molar ratio = 3) and deionised water (17.6 g, target solids concentration = 20% w/w) were purged with nitrogen for 30 min. This degassed aqueous solution was added under a nitrogen atmosphere and the second-stage polymerisation was allowed to continue for 16 h at 44 °C. This one-pot protocol yielded a yellow dispersion of PCEA-core diblock copolymer nanoparticles, with a final CEA conversion of 99% being indicated by ^{1}H NMR spectroscopy.

Dynamic light scattering

Dilute (0.10% w/w) aqueous copolymer dispersions were analysed at 25 °C using a Malvern NanoZS instrument. Scattered light was detected at 173° and hydrodynamic diameters were calculated using the Stokes-Einstein equation, which assumes dilute non-interacting spheres.

Data were averaged over three consecutive measurements comprising eleven runs per measurement.

Aqueous electrophoresis

Zeta potentials were calculated from electrophoretic mobilities using a Malvern NanoZS instrument. Measurements (averaged over 20 runs) were made as a function of pH on dilute dispersions (0.05-0.10% w/w) in deionised water in the presence of 1 mM KCl background salt. In each case, the solution pH was gradually lowered by adding 0.1 M HCl.

Transmission electron microscopy

Copper/palladium grids were surface-coated in-house to produce a thin film of amorphous carbon before being plasma glow-discharged for 40 seconds to produce a hydrophilic surface. Typically, a 1 μL droplet of a 0.1% w/w aqueous copolymer dispersion (solution pH adjusted using either 0.1 M HCl or 0.1 M NaOH) was placed onto a TEM grid for 45 seconds, then stained using a 0.75% w/v aqueous solution of either phosphotungstic acid or uranyl formate for 45 seconds. Excess stain was removed by careful blotting and each grid was then dried using a vacuum hose. TEM images were recorded using a Philips CM100 instrument operating at 100 kV and equipped with a Gatan 1k CCCD camera. ImageJ software was used to calculate mean diameters and standard deviations from TEM images (at least 100 nanoparticles were analysed per sample).

Methylation protocol for GPC analysis

Prior to GPC analysis, PDEA-PCEA diblock copolymers were derivatised by selective methylation of the carboxylic acid groups in the PCEA block. Accordingly, excess trimethylsilyldiazomethane was added dropwise to a solution of copolymer (40 mg) in 3:2 toluene/methanol solution (10 mL), until the yellow colour persisted. This reaction solution was stirred for up to 72 h at room temperature until all solvent had evaporated. The mean

degree of methylation was determined by ^{1}H NMR spectroscopy by comparing the integrated methoxy proton signal of the methylated PCEA block at 3.7 ppm to that of the oxymethylene protons of the PCEA block at 4.3 ppm.

Gel permeation chromatography (GPC)

THF GPC was used to assess copolymer molecular weight distributions. The GPC set-up consisted of an Agilent 1260 Infinity II GPC/SEC system operating at 30 °C equipped with an autosampler and two 5 µM Mixed-C columns connected to a refractive index detector. The mobile phase was HPLC-grade THF at a flow rate of 1.0 mL min^{-1}. Molecular weights were calculated using a series of near-monodisperse PMMA calibration standards. All copolymers were modified by selective methylation prior to GPC analysis to ensure their solubility in THF.

Preparation of Titania dispersions

Titania R960 pigment (0.40 g) was added to a 5 mL vial. To prepare a dispersion at 15% copolymer based on mass of pigment, 0.30 g of a 20 w/w% copolymer dispersion was added, and the dispersion volume was made up to 4 mL using deionised water. The pH was adjusted using 0.1 M HCl or 0.1 M NaOH and the resulting dispersions were placed on a roller mixer operating at 120 rpm for at least 24 h prior to analysis.

Analytical Centrifugation

Weight-average diameters were determined for copolymer-stabilised pigment dispersions using a LUMiSizer® analytical photocentrifuge (LUM GmbH, Berlin, Germany) at 25 °C. Measurements were conducted on 0.5% w/w aqueous pigment dispersions at 1350 rpm using 2.0 mm pathlength polyamide cells. The LUMiSizer® employs STEP™ Technology (Space- and Time-resolved Extinction Profiles) that enables the intensity of transmitted light to be measured as a function of time and position simultaneously over the entire cell length. The

progression of these transmission profiles contains information on the rate of sedimentation and, given knowledge of the pigment particle density (4.09 g cm^{-3}), enables assessment of the particle size distribution.

Viscosity measurements

An AR-G2 rheometer equipped with a variable temperature Peltier plate and a 40 mm 2° steel cone was used for all experiments. Titania dispersions had a pigment concentration of 10% w/w in all cases, with varying copolymer dispersant concentration. After equilibration at 25 °C, the dispersion viscosity was measured as a function of shear rate between 0.1 and 1000 s^{-1}. Angular frequency sweeps were conducted at 25 °C using a constant strain amplitude of 1.0%. Viscosity values are calculated from the measured shear stress at a shear rate of 37 s^{-1}.

6.3 Results and Discussion

6.3.1 Synthesis and characterisation of PDEA-PCEA diblock copolymer nanoparticles

The synthesis of PDEA$_x$-PCEA$_y$ diblock copolymers was initially explored using a two-stage protocol. More specifically, the RAFT solution polymerisation of DEA was conducted in THF, followed by the RAFT polymerisation of CEA in aqueous solution. Subsequently, a wholly aqueous, one-pot protocol was developed (see **Scheme 6.3**). This involved conducting the initial DEA polymerisation at pH 2, whereby the PETTC is solubilised in DEA monomer prior to addition of water (and the resulting PDEA chains are molecularly dissolved in their fully protonated form) and the subsequent CEA polymerisation is performed at the same pH. Given that the CEA monomer is fully soluble in the acidic reaction solution and the growing PCEA chains become insoluble under such conditions, this PISA formulation is an interesting new example of a RAFT aqueous dispersion polymerisation.[23]

It is emphasised that the aqueous PISA synthesis of such PDEA-PCEA diblock copolymers must be performed by polymerising the methacrylic DEA monomer first. If the acrylic CEA monomer were to be polymerised first instead, only very poor blocking efficiencies would be achieved owing to the inefficient cross-over when switching from acrylic to methacrylic monomers.[24]
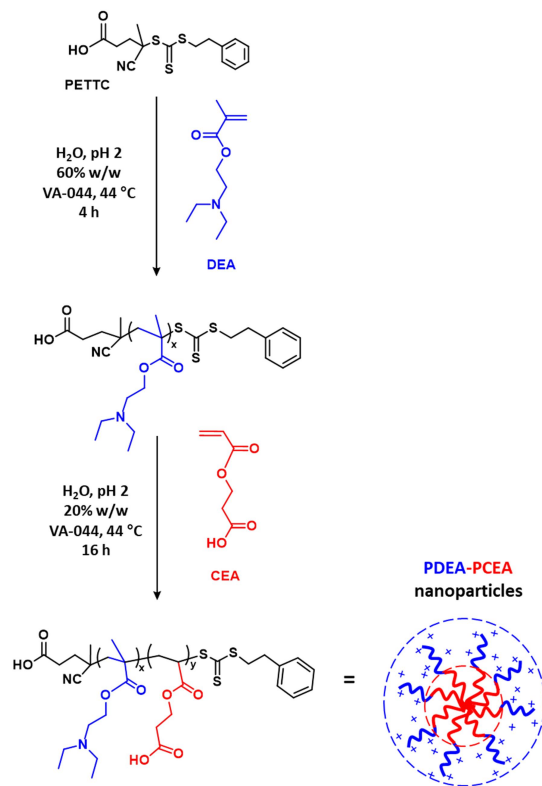
Scheme 6.3 Wholly aqueous one-pot synthesis of PDEA-PCEA diblock copolymer nanoparticles via (i) RAFT aqueous solution polymerisation of DEA at low pH followed by (ii) the RAFT aqueous dispersion polymerisation of CEA to form cationic PCEA-core nanoparticles at low pH *via* PISA.
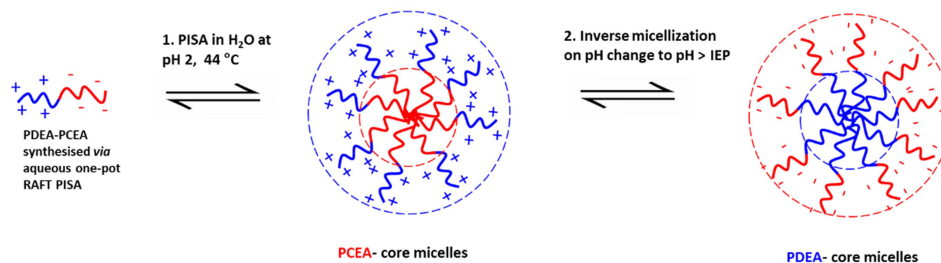
Scheme 6.4 Schematic cartoon depicting the schizophrenic behaviour exhibited by PDEA-PCEA diblock copolymers, which can form cationic PCEA-core micelles at low pH and anionic PDEA-core micelles at high pH. At intermediate solution pH, macroscopic precipitation at the isoelectric point is observed.

^{1}H NMR spectroscopy studies confirmed that high monomer conversions were achieved for each block (the CEA monomer was only added after achieving at least 99% DEA conversion). Exhaustive selective methylation of the carboxylic acid residues in the PCEA block was required prior to THF GPC analysis (**Figure 6.2**).
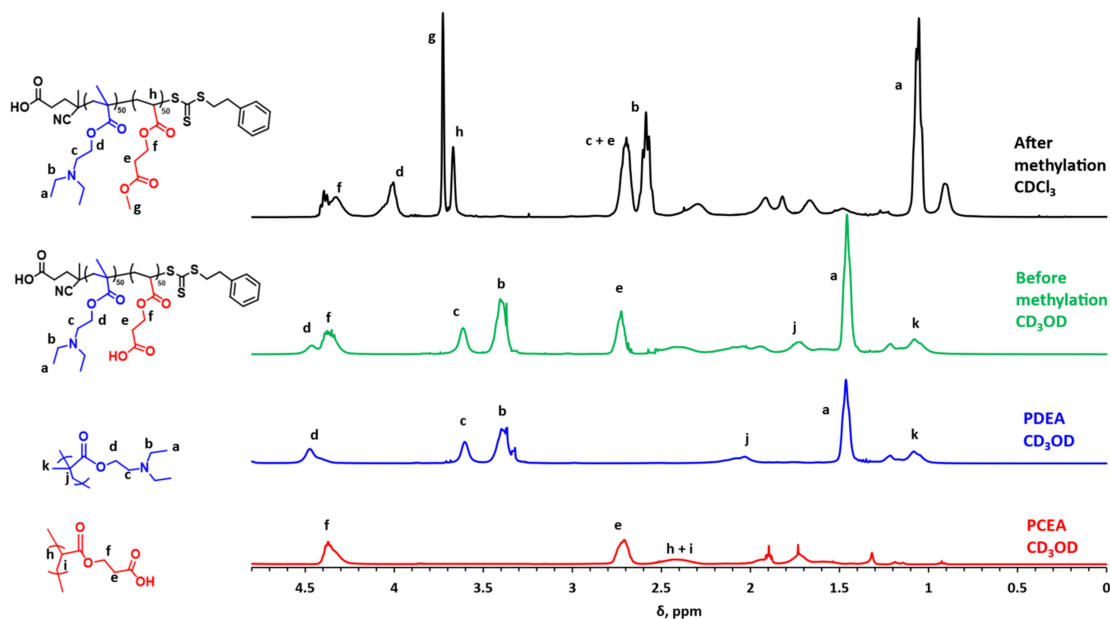

Figure 6.2 Representative ^{1}H NMR spectra recorded for a PDEA$_{50}$-PCEA$_{50}$ diblock copolymer before (green spectrum recorded in CD$_3$OD) and after (black spectrum recorded in CDCl$_3$) exhaustive methylation of its pendent carboxylic acid groups to afford the corresponding methyl ester. Spectra for PDEA and PCEA homopolymers are also included to aid spectral assignments.

This technique indicated a systematic increase in M$_n$ and relatively low dispersities (M$_w$/M$_n$ $\leq$ 1.33) when targeting higher PCEA DPs using a PDEA precursor with a fixed DP of 67, which suggests reasonably good RAFT control. These NMR and GPC data are summarised in **Table 6.1**.

Table 6.1 Summary of comonomer conversions by ^{1}H NMR spectroscopy and molecular weight data by THF GPC for a series of PDEA$_x$-PCEA$_y$ diblock copolymers prepared using a wholly aqueous one-pot protocol based on the RAFT aqueous solution polymerisation of DEA followed by the RAFT aqueous dispersion polymerisation of CEA (after exhaustive selective methylation of the carboxylic acid residues in the PCEA block).

Diblock copolymer composition	^{1}H NMR conversion (%)	THF GPC (following exhaustive methylation)		
		M_n (g mol^{-1})	M_w (g mol^{-1})	M_w/M_n
PDEA$_{67}$-PCEA$_{30}$	98	10 200	13 600	1.33
PDEA$_{67}$-PCEA$_{67}$	98	15 300	19 100	1.25
PDEA$_{67}$-PCEA$_{100}$	96	24 000	27 100	1.13
PDEA$_{67}$-PCEA$_{134}$	99	29 200	34 000	1.17
PDEA$_{67}$-PCEA$_{160}$	99	35 000	39 000	1.12
PDEA$_{67}$-PCEA$_{200}$	99	42 100	48 200	1.14
PDEA$_{100}$-PCEA$_{50}$	99	15 500	20 000	1.29
PDEA$_{50}$-PCEA$_{50}$	99	12 400	15 800	1.27

According to **Figure 6.3,** blocking efficiencies were reasonably high, particularly given that the structure of the trithiocarbonate RAFT agent is optimised for the polymerisation of methacrylic monomers, rather than acrylic monomers. Although some contamination by the PDEA precursor is evident, this problem is minimised by using the wholly aqueous one-pot protocol and is estimated to be no more than 13% in the worst-case scenario (see red trace for PDEA$_{67}$-PCEA$_{134}$ shown in **Figure 6.3**).
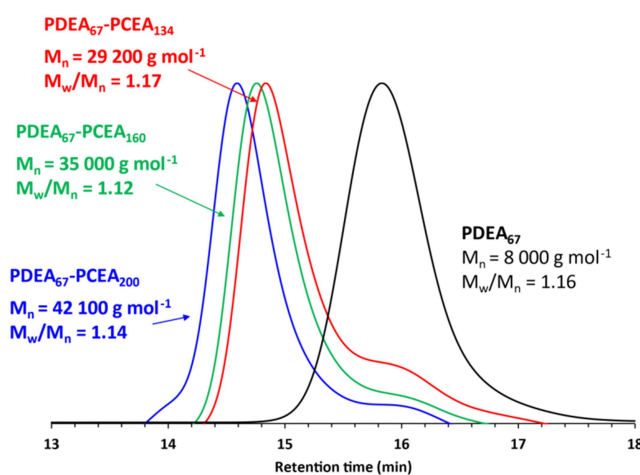

Figure 6.3 THF GPC curves recorded for three PDEA$_{67}$-PCEA$_x$ diblock copolymers and the corresponding PDEA$_{67}$ precursor following exhaustive methylation using trimethylsilyldiazomethane. These data indicate that relatively high blocking efficiencies can be obtained using a convenient wholly aqueous one-pot formulation.

The 'schizophrenic nature' of this type of pH-responsive diblock copolymer means that PDEA-core micelles are expected at high pH and PCEA-core micelles should be formed at low pH. Accordingly, ^{1}H NMR spectroscopy studies were conducted to provide evidence for these two types of micelles. Thus PDEA$_{67}$-PCEA$_{67}$ was dispersed in D$_2$O at 1.0% w/w (**Figure 6.4**). The pH (strictly, pD) was then adjusted as required using either NaOD or DCl. At pH 9, the ionised PCEA block is highly anionic and acts as the steric stabiliser, while the neutral PDEA block is hydrophobic and therefore water-insoluble, so it forms the micelle cores. Thus, only the proton signals at positions *f, e, j* and *i* assigned to the PCEA block can

be observed by ^{1}H NMR spectroscopy (purple spectrum). In contrast, the PCEA block is present in its neutral, hydrophobic form at pH 2, while the PDEA block is highly cationic under such conditions owing to protonation of its pendent tertiary amine groups. Thus cationic PCEA-core micelles are formed under such conditions. In this case, we can observe ^{1}H NMR signals assigned to the PDEA block (*d, c, b, a, h* and *g*; see red spectrum). However, there is also an unexpected signal at 2.75 ppm, which is attributed to the *e* protons on the PCEA block. For this particular diblock copolymer composition, an IEP is observed at pH 5 and the copolymer forms a macroscopic precipitate at this pH. Thus, barely any copolymer signals are detected under such conditions (green spectrum).
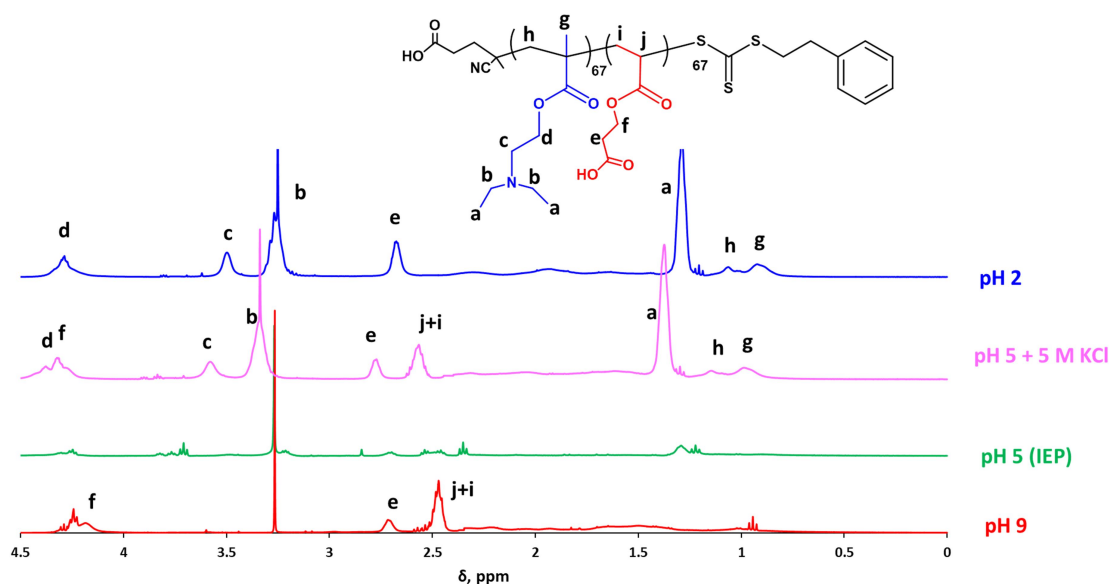
Figure 6.4 ^{1}H NMR spectra recorded for a 1.0% w/w dispersion of PDEA$_{67}$-PCEA$_{67}$ diblock copolymer in D$_2$O/NaOD at pH 9 (purple spectrum), in D$_2$O at pH 5, which corresponds to the isoelectric point of the polymer (green spectrum), in D$_2$O at pH 5 in the presence of 5 M KCl, which is added to suppress the IEP (blue spectrum), and in D$_2$O/DCl at pH 2 (red spectrum). The chemical structure that is shown depicts this diblock copolymer in its neutral state; in practice, the PDEA block becomes protonated at low pH while the PCEA block becomes ionised at high pH.

However, as discussed in Chapter 4, the macroscopic precipitation of zwitterionic diblock copolymers at their IEP can be suppressed by addition of sufficient salt because this screens the electrostatic attractive forces between the anionic and cationic blocks. Thus, addition of 5

M KCl to D_2O enabled all the proton signals expected for each block to be observed (blue trace). However, the presence of this salt causes a subtle shift in the position of each proton signal.

Figure 6.5 shows the zeta potential vs. pH curves recorded for four $PDEA_{67}$-$PCEA_x$ diblock copolymers, where x ranges from 30 (**Figure 6.5a**) to 200 (**Figure 6.5d**). As expected, adjusting the DP of the PCEA block leads to a systematic shift in the IEP from pH 8.1 for $PDEA_{67}$-$PCEA_{30}$ to pH 3.6 for either $PDEA_{67}$-$PCEA_{134}$ or $PDEA_{67}$-$PCEA_{200}$.
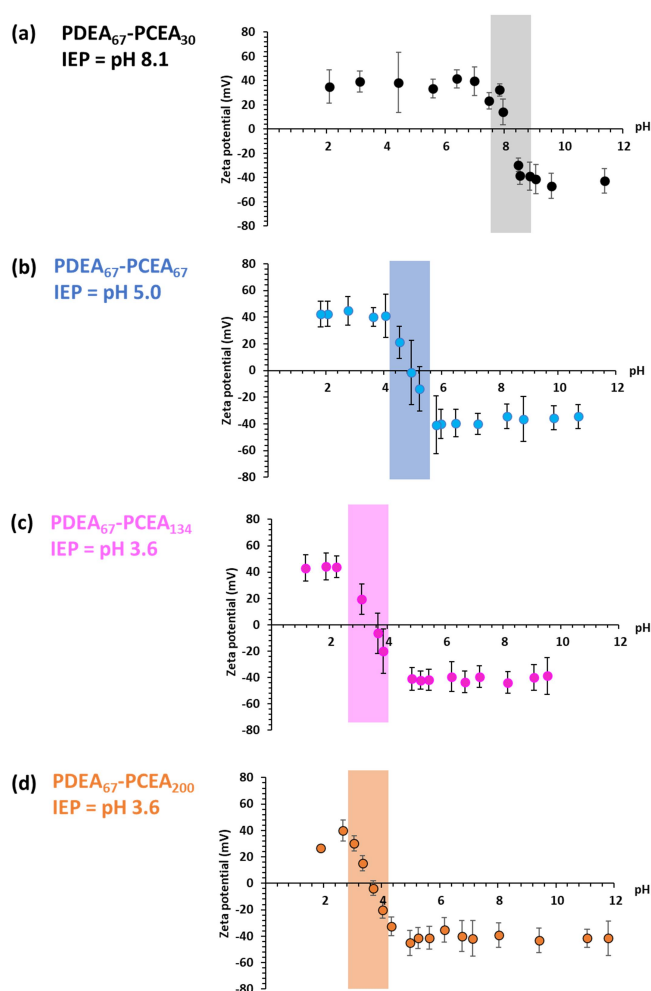
Figure 6.5 Zeta potential vs. pH curves obtained for four $PDEA_{67}$-$PCEA_x$ zwitterionic diblock copolymers where **(a)** x = 30, **(b)** x = 67, **(c)** x = 134 or **(d)** x = 200. Clearly, the isoelectric point (IEP) observed for each copolymer can be systematically reduced from 8.1 to 3.6 on increasing the DP of the PCEA block.

The RAFT aqueous dispersion polymerisation of CEA results in the direct formation of cationic PCEA-core nanoparticles at low pH, as judged by DLS and TEM studies (see, for example, the $PDEA_{67}-PCEA_{134}$ nanoparticles formed at pH 2 in **Figure 6.6)**. The number-average diameter of the nanoparticle cores estimated by digital image analysis of such TEM images is 24 ± 5 nm. The hydrodynamic diameter for these spherical nanoparticles recorded at the same pH is 28 nm. Given that DLS reports a z-average diameter, this technique inevitably oversizes relative to TEM for any size distribution of finite width. Moreover, TEM only reveals the nanoparticle cores and is insensitive to the steric stabiliser layer. Thus such data constitute reasonably good agreement. At pH 10, the spheres appear to be somewhat less well-defined but can be nevertheless visualised with the aid of a phosphotungstic acid stain. In this case, the number-average TEM diameter is 26 ± 5 nm. Again, DLS studies indicate a slightly higher hydrodynamic diameter of 32 nm.
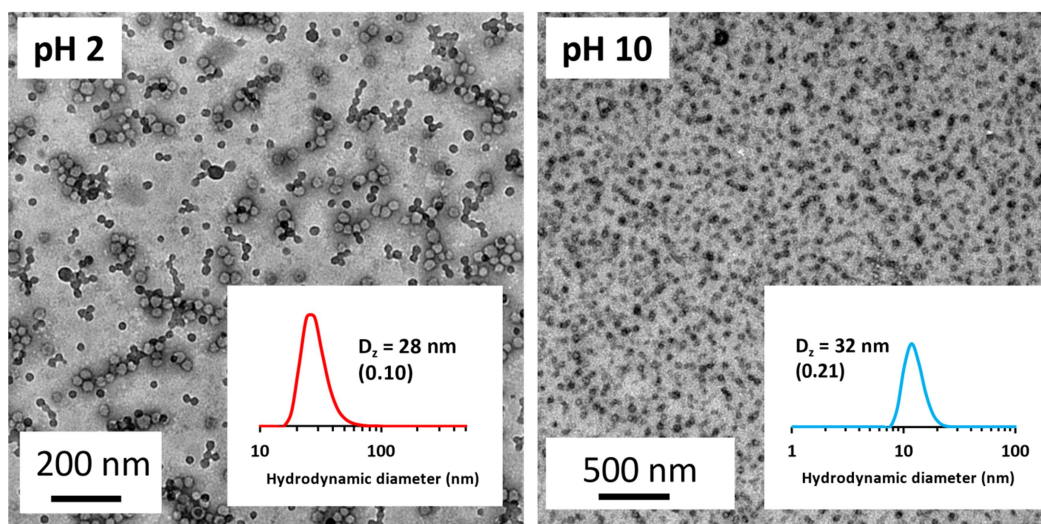

Figure 6.6 Representative TEM and DLS data obtained for $PDEA_{67}-PCEA_{134}$ nanoparticles at pH 2 (synthesis pH) and at pH 10, confirming the presence of cationic PCEA-core micelles and anionic PDEA-core micelles respectively.

The two types of nanoparticles formed by $PDEA_{67}$-$PCEA_{200}$ above and below its IEP were also investigated (**Figure 6.7**). Relatively large, polydisperse spheres are formed at pH 2 with TEM studies indicating a number-average diameter of 97 ± 51 nm. This is consistent with the z-average diameter of 117 nm (polydispersity = 0.09) reported by DLS. Further studies would be required to examine whether this diblock copolymer can form higher-order morphologies such as vesicles. At pH 10, the number-average diameter estimated by TEM is 15 ± 4 nm while the corresponding DLS diameter is 30 nm. Given the asymmetry of this diblock copolymer and bearing in mind well-established theories of block copolymer self-assembly,[25] it is reasonable to expect that the PCEA-core nanoparticles should be significantly larger than the PDEA-core nanoparticles. However, this was not the case for the $PDEA_{67}$-$PCEA_{134}$ nanoparticles. It is possible that the precise reaction pH has a large effect on the nanoparticles synthesised, further studies into this are needed.
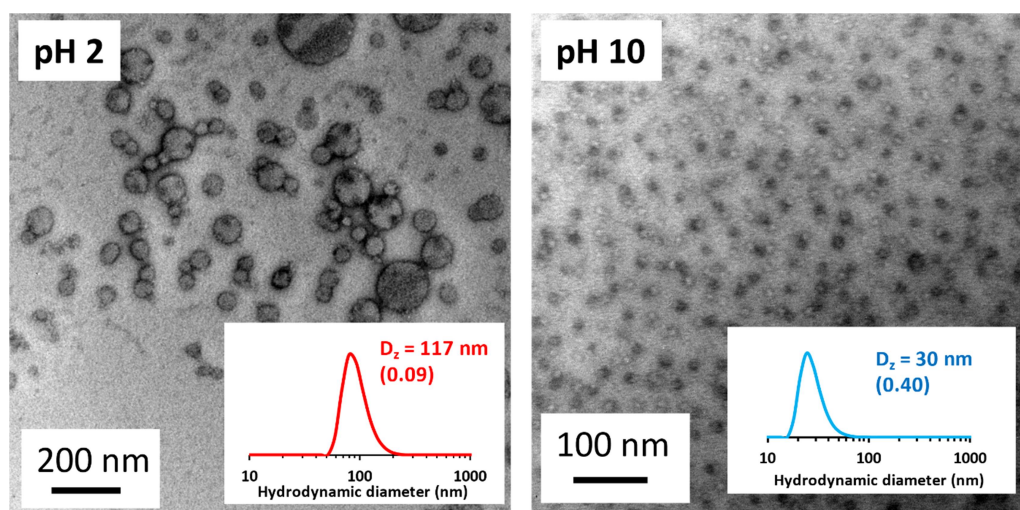

Figure 6.7 Representative TEM and DLS data obtained for $PDEA_{67}$-$PCEA_{200}$ nanoparticles at pH 2 (synthesis pH) and at pH 10, confirming the presence of cationic PCEA-core micelles and anionic PDEA-core micelles respectively.

The next two diblock copolymer compositions are characterised prior to their evaluation as pigment dispersants for Titania R-960, which is a pigment that was discussed in Chapter 5.

The first copolymer is PDEA$_{100}$-PCEA$_{50}$ (**Figure 6.8**). At pH 2, this copolymer forms PCEA-core nanoparticles with a number-average diameter of 50 ± 22 nm as estimated by TEM, though a DP of 50 for the PCEA resulted in less well-defined spherical particles, making this estimation difficult. The corresponding z-average diameter determined by DLS is 70 nm, albeit with a very high polydispersity index, suggesting the presence of different size populations. At pH 10, TEM studies indicate the presence of relatively uniform PDEA-core nanoparticles with a number-average diameter of 25 ± 6 nm, and a corresponding z-average diameter of 53 nm reported by DLS.
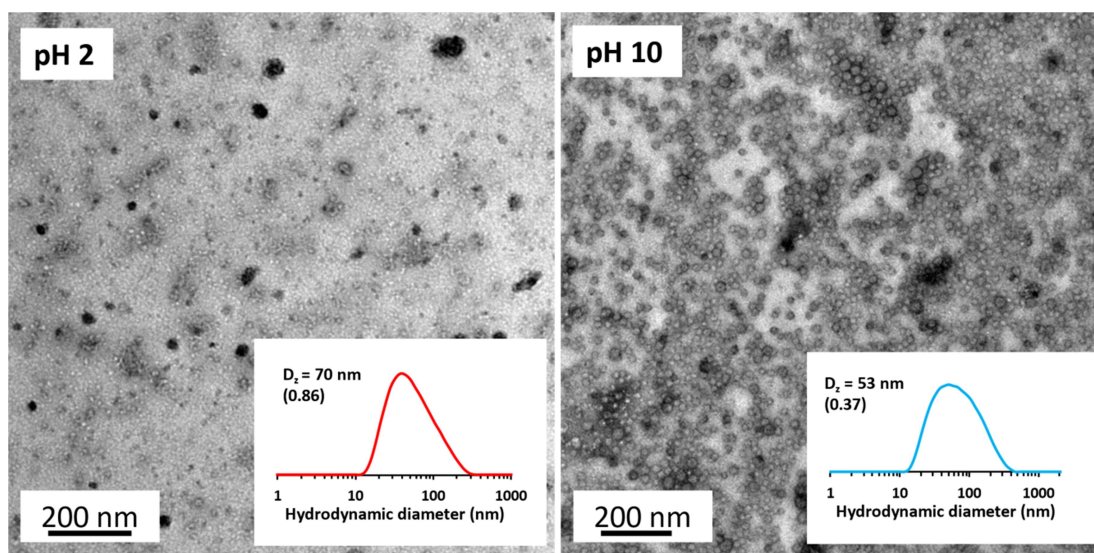

Figure 6.8 Representative TEM and DLS data obtained for the PDEA$_{100}$-PCEA$_{50}$ diblock copolymer at pH 2 (synthesis pH) and at pH 10, confirming the presence of cationic PCEA-core micelles and anionic PDEA-core nanoparticles, respectively.

In the case of the PDEA$_{50}$-PCEA$_{50}$ diblock copolymer at pH 2, TEM reveals the presence of nanoparticles with a number-average diameter of 24 ± 6 nm, which appear to be aggregated and not particularly spherical. DLS studies indicate a z-average diameter of 27 nm. In contrast, relatively well-defined (albeit polydisperse) anionic PDEA-core spheres with a number-average diameter of 23 ± 9 nm are indicated by TEM studies conducted after drying

at pH 10, with DLS studies indicating a corresponding z-average diameter of 26 nm (**Figure 6.9**).
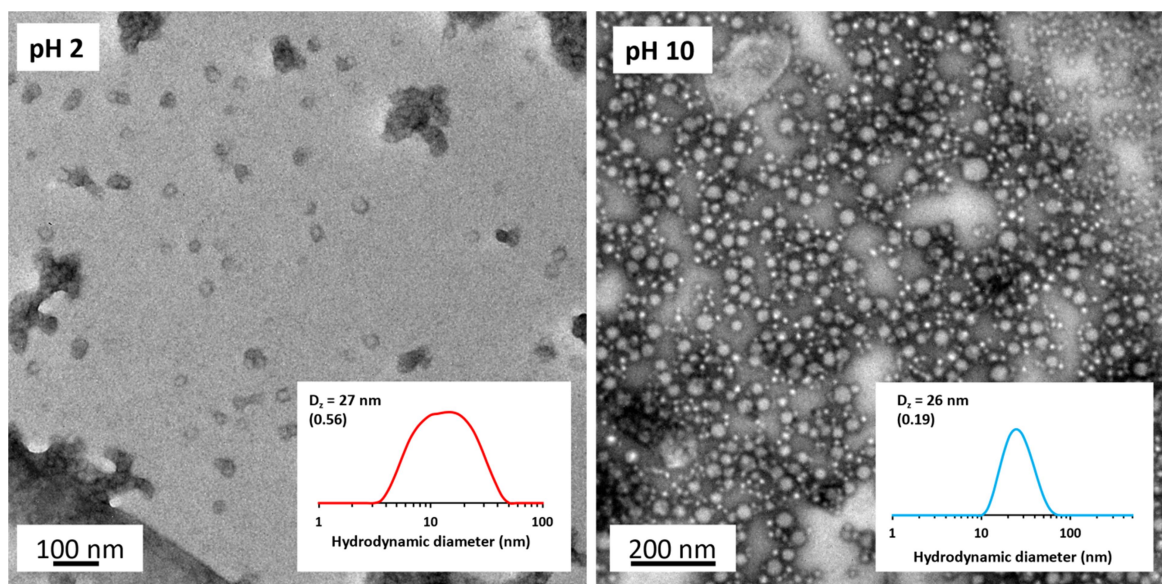

Figure 6.9 Representative TEM and DLS data obtained for the PDEA$_{50}$-PCEA$_{50}$ diblock copolymer at pH 2 (synthesis pH) and at pH 10, confirming the presence of cationic PCEA-core micelles and anionic PDEA-core nanoparticles, respectively.

6.3.2 Dispersion of Titania R-960 pigment particles using PDEA$_x$-PCEA$_y$ diblock copolymer nanoparticles

To assess the efficacy of these diblock copolymer nanoparticles as putative dispersants, they were evaluated for the dispersion of Titania R-960 pigment particles in aqueous solution. As discussed in Chapter 5, this pigment has a specific surface area of 16.3 m^2 g^{-1} and a solid-state density of 4.09 g cm^{-3}, enabling an apparent primary grain diameter of 90 nm to be calculated. However, a number-average particle diameter of 242 ± 54 nm is indicated by TEM, which is close to the mean reported particle diameter of 300 nm.[26] Analytical centrifugation studies indicate a weight-average diameter of 212 ± 72 nm, while DLS reports a z-average diameter of 360 nm (polydispersity = 0.20). These pigment particles have been surface-modified to improve their dispersibility in aqueous media: alumina and amorphous

silica make up 3.3% and 5.5% of the total pigment mass, respectively.[27] Evidence for the presence of this surface layer can be obtained by TEM (**Figure 6.10**).
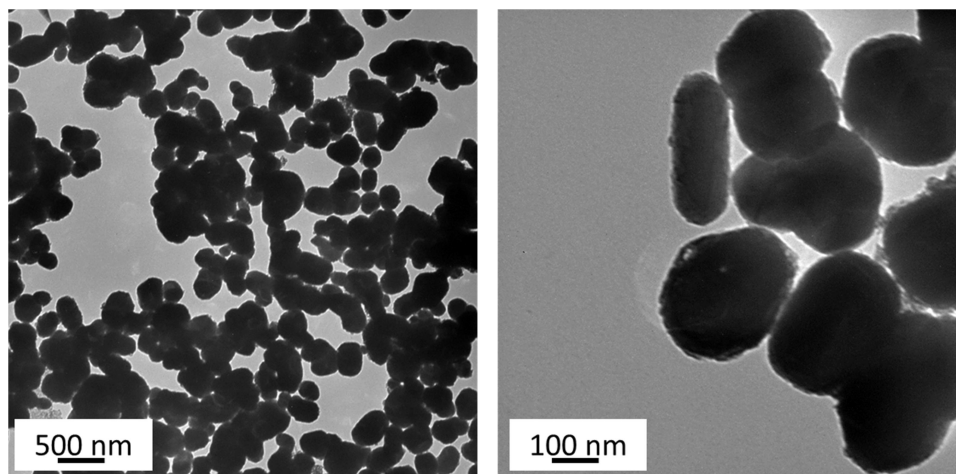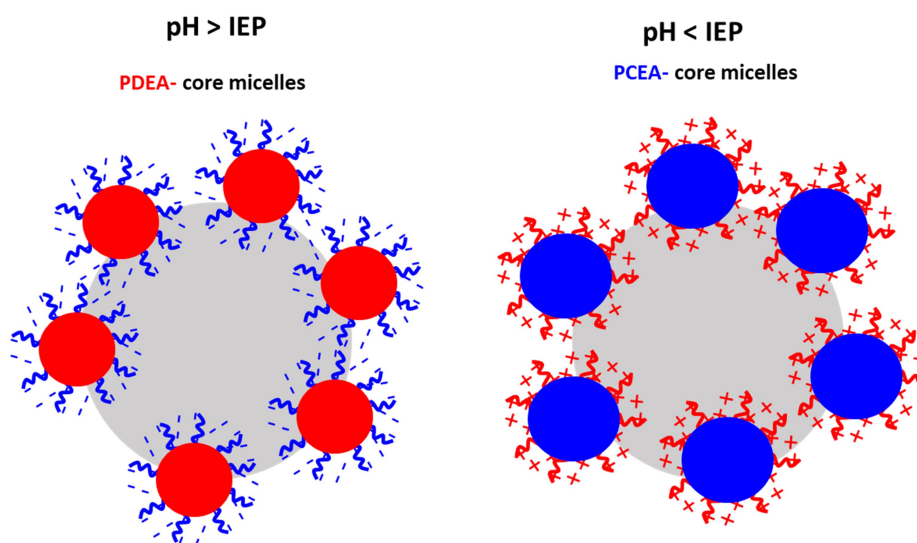

Figure 6.10 Representative TEM images for bare titania pigment particles recorded at low (left) and high (right) magnification. A surface layer of alumina is clearly visible for such particles, which makes the subsequent detection of adsorbed copolymer nanoparticles somewhat problematic.

Scheme 6.5 Cartoon representation of mechanism of aqueous dispersion using $PDEA_x$-$PCEA_y$ as stabilisers for titania pigment. PDEA-core particles will be formed in dispersion below the IEP, and PCEA-core micelles will form above it. In each case the neutral (core-forming) block is likely to anchor to the pigment surface and may involve micelle deformation.

Two diblock copolymers were investigated: $PDEA_{100}$-$PCEA_{50}$ and $PDEA_{50}$-$PCEA_{50}$. This pair enabled the effect of varying the PDEA block DP and the nanoparticle diameter to be examined. Based on previous experiments, it was anticipated that varying the PDEA block DP should influence the degree of pigment dispersion because the titania particles are expected to have greater affinity for the cationic PDEA block than the anionic PCEA block.[28]

Firstly, aqueous electrophoresis measurements were performed on titania particles alone, $PDEA_{100}$-$PCEA_{50}$ diblock copolymer nanoparticles and titania dispersions prepared using the same copolymer (**Figure 6.10**).
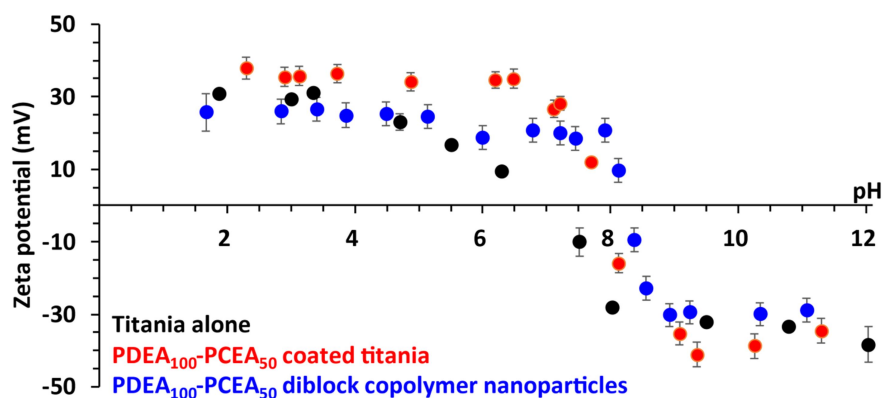

Figure 6.10 Zeta potential vs. pH curves recorded for 0.1% w/w aqueous dispersions of $PDEA_{100}$-$PCEA_{50}$ diblock copolymer nanoparticles alone (**blue**), titania particles alone (**black**), and the same pigment particles dispersed in the presence of $PDEA_{100}$-$PCEA_{50}$ nanoparticles (**red**).
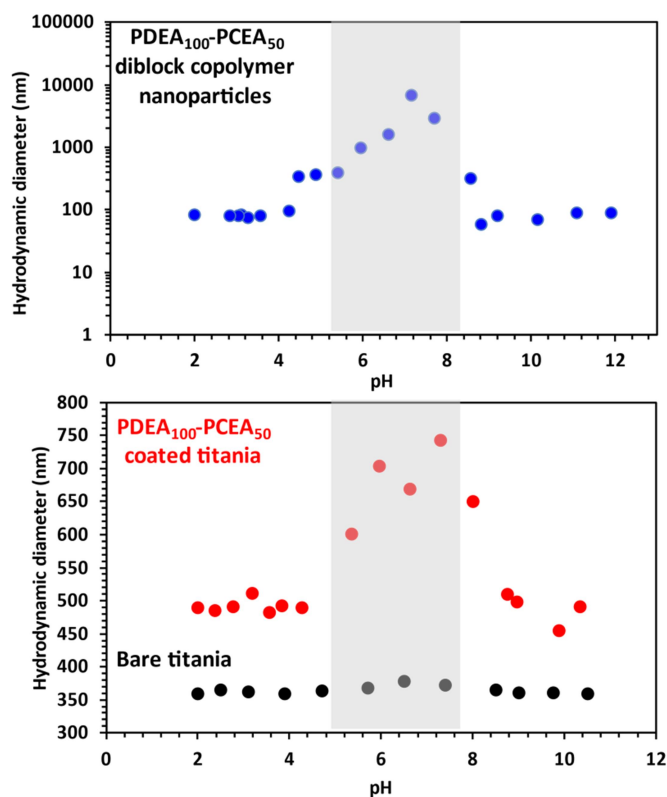
Figure 6.11 DLS hydrodynamic diameter vs pH data recorded for aqueous dispersions of PDEA$_{100}$-PCEA$_{50}$ diblock copolymer nanoparticles alone (**top, blue**) and titania pigment particles dispersed in the presence of these nanoparticles (**bottom, red**). The highlighted regions indicate the pH window corresponding to macroscopic precipitation for each system. These data suggest that the titania particles are coated with an adsorbed layer of the nanoparticles.

The copolymer-coated titania particles exhibit a similar IEP (pH 7.9) to that of the diblock copolymer nanoparticles alone (pH 8.2). In contrast, the titania particles have an IEP at approximately pH 7.0. This suggests that the copolymer nanoparticles adsorb onto the surface of the titania particles and hence modify their electrophoretic footprint.[29] The effect of varying the dispersion pH was also investigated (**Figure 6.11**). In the absence of any dispersant, titania particles have a constant particle diameter (approx. 360 nm) with varying solution pH, due to the polar groups on the pigment surface maintaining their colloidal stability, even around the pigment IEP. As discussed previously, PDEA$_x$-PCEA$_y$ diblock copolymers undergo macroscopic precipitation at around their IEP. A similar colloidal instability region is also observed for the pigment dispersion: the apparent size of both the

copolymer nanoparticles and the copolymer-dispersed pigment increases significantly within this pH range, with the latter particles sedimenting rapidly under such conditions. Thus, such titania dispersions are only colloidally stable either below approximately pH 5 or above pH 9.

The effect of varying the copolymer concentration during the preparation of such titania dispersions was assessed using four techniques: DLS, TEM, analytical centrifugation (LUMiSizer instrument) and dispersion viscosity (**Figures 6.12** and **6.13**). At pH 10, the $PDEA_{100}$ block forms the hydrophobic core, and the $PCEA_{50}$ block acts as an anionic stabiliser. The hydrodynamic z-average diameter reported by DLS for such nanoparticles at this pH is 53 nm while bare titania particles exhibit a z-average diameter of 360 nm. The minimum z-average diameter obtained for the nanoparticle-coated titania particles at pH 10 is 433 nm (**Figure 6.12a**). Allowing for some deformation of the sterically-stabilised nanoparticles during their adsorption at the pigment surface,[30] this particle size seems to be physically reasonable.

The optimum copolymer concentration required for the minimum LUMiSizer diameter (**Figure 6.12b**) is consistent with that indicated by DLS. The former technique reports a much smaller apparent minimum diameter of 111 nm, which is physically unrealistic. However, this value assumes that the effective particle density is equal to that of the pure titania particles (4.09 g cm^{-3}) and it is well-documented that analytical centrifugation can be rather sensitive to this input parameter.[31] Clearly, nanoparticle-coated titania particles will exhibit a lower effective density than that of the titania particles alone.[30] Although the actual effective density is unknown, this does not prevent the use of analytical centrifugation as a relative technique to assess the optimum copolymer concentration required to achieve monolayer coverage of the titania particles by the nanoparticles. Finally, the dispersion viscosity data set (**Figure 6.12c**) indicates that the optimum copolymer concentration per unit mass of pigment is approximately 15%, which is consistent with that suggested by the two

particle sizing techniques. The viscosity is a measurement of the shear stress at a shear rate of

37 s^{-1}, an industry standard parameter relevant to inkjet applications.
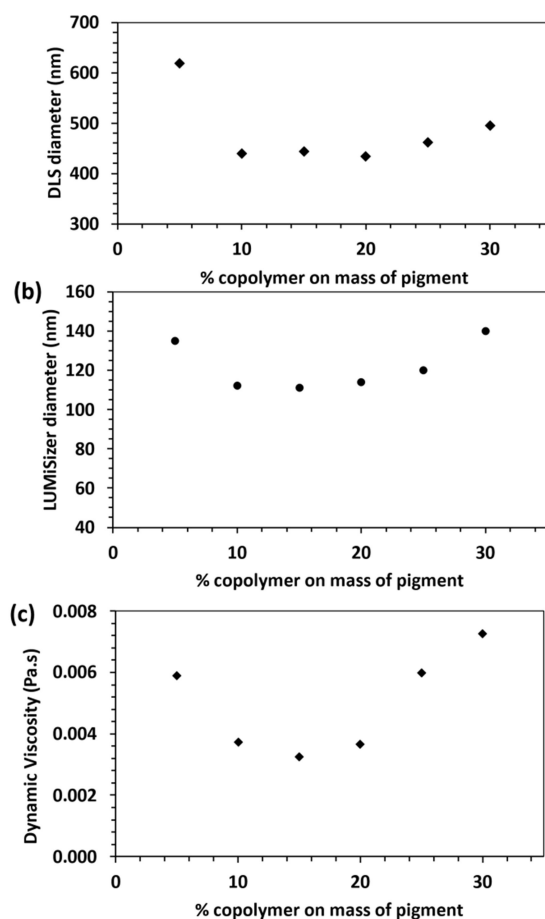

Figure 6.12 Effect of varying the copolymer concentration on the degree of dispersion of titania R-960 pigment particles in the presence of anionic PDEA$_{100}$-PCEA$_{50}$ nanoparticles at pH 10: (a) DLS z-average diameter determined for 10% w/w titania dispersions diluted to 0.10% w/w, (b) LUMiSizer mean diameter determined for 10% w/w titania dispersions diluted to 0.50% w/w, and (c) dispersion viscosity determined for 10 % w/w titania dispersions at a shear rate of 37 s^{-1}. These data suggest an optimum concentration of around 10-15% copolymer per unit mass of pigment.

TEM studies were also performed on each dispersion. For PDEA$_{100}$-PCEA$_{50}$-coated titania

dispersions prepared at pH 10, TEM studies were conducted at 5, 10 and 15% copolymer per

unit mass of pigment (**Figure 6.13)**. At 15% copolymer, well-dispersed particles are observed

but there seems to be a large excess of non-adsorbed copolymer nanoparticles. Although this

copolymer concentration produces the smallest apparent particle size and minimum viscosity,

further optimisation is required to identify the optimum copolymer concentration that corresponds to monolayer coverage (i.e. no excess non-adsorbed nanoparticles).
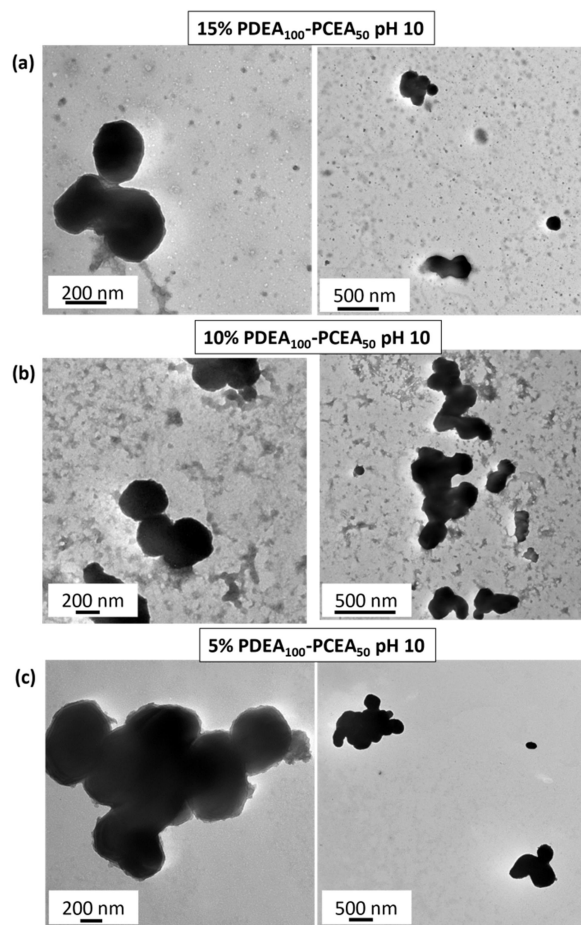

Figure 6.13 Representative TEM images recorded for titania dispersions prepared in the presence of either (a) 15%, (b) 10% or (c) 5% $PDEA_{100}$-$PCEA_{50}$ nanoparticles at pH 10 (i.e. above the copolymer IEP) after dilution to 0.1% w/w prior to drying on a carbon-coated grid.

At 10% copolymer, less copolymer was expected to be present in the aqueous continuous phase (**Figure 6.13b**). However, there still appears to be a significant proportion of copolymer nanoparticles that are not adsorbed at the pigment surface. At 5% copolymer, the titania particles are weakly flocculated. Far fewer copolymer nanoparticles are visible in the background under these conditions. However, close inspection provides no evidence for nanoparticle adsorption at the surface of the titania pigment particles. This suggests that the

copolymer nanoparticles may provide a colloid stability mechanism that does not involve their adsorption. It is also possible that this excess background copolymer is just an artefact of the dilution or drying process, observed by TEM. The neat dispersion could involve adsorption of copolymer nanoparticles onto the titania surface.

The same copolymer was used to disperse titania particles at pH 3. Thus the $PCEA_{50}$ block is now in its neutral hydrophobic form and hence forms the nanoparticle core, whereas the protonated cationic $PDEA_{100}$ acts as the steric stabiliser. Such nanoparticles have a hydrodynamic z-average diameter of approximately 70 nm as judged by DLS.
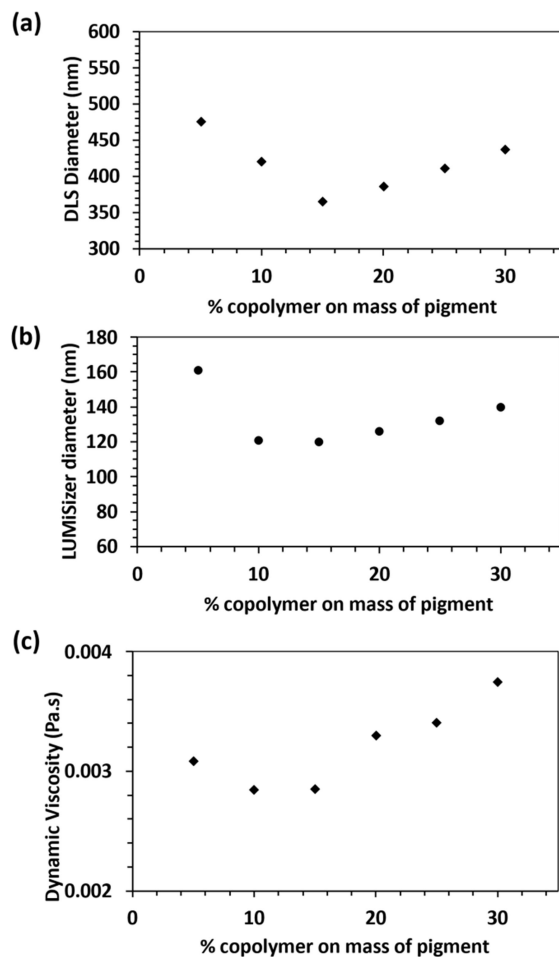

Figure 6.14 Effect of varying the copolymer concentration on the degree of dispersion of titania R-960 pigment particles in the presence of anionic $PDEA_{100}$-$PCEA_{50}$ nanoparticles at pH 3: (a) DLS z-average diameter determined for 10% w/w titania dispersions diluted to 0.10% w/w, (b) LUMiSizer mean diameter determined for 10% w/w titania dispersions diluted to 0.50% w/w, and (c) dispersion viscosity determined for 10 % w/w titania dispersions. These data suggest an optimum concentration of around 10-15% copolymer per unit mass of pigment.

DLS reports that a minimum particle size of 365 nm could be obtained at 15% copolymer (**Figure 6.14a**), which could indicate that some particle size reduction has taken place. It could also suggest that the dispersion is unstable to dilution, as this is very similar to the primary size of these titania particles alone. However, a lower minimum viscosity is obtained (2.85 mPa.s at pH 3, and 3.25 mPa.s at pH 10), indicating that the copolymer is acting as an effective dispersant at this concentration (**Figure 6.14b**). Although the LUMiSizer diameter does not reflect this lower particle size, it does indicate a minimum in at 15% copolymer (**Figure 6.14c**).
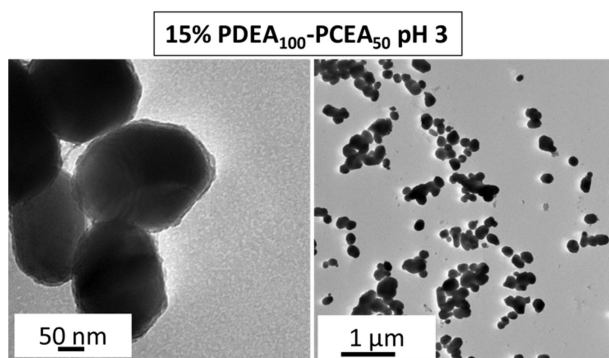

Figure 6.15 Representative TEM images recorded for titania dispersions prepared in the presence of either (a) 15% $PDEA_{100}$-$PCEA_{50}$ nanoparticles at pH 3 (i.e. below the copolymer IEP) after dilution to 0.1% w/w prior to drying on a carbon-coated grid.

TEM studies conducted at pH 3 suggest that a relatively high degree of dispersion can be achieved at 15% copolymer (**Figure 6.15**). However, a higher magnification image does not confirm the presence of surface-adsorbed nanoparticles as the coated titania particles do not differ visually from the original uncoated titania pigment (**Figure 6.10**). Other literature studies of polymer adsorption onto the surface of titania suggest that similar TEM images confirm the presence of a surface layer (see Figure 4 in Reference 32),[32] however it was decided that the same conclusion could not be made for the titania particles in this chapter, as they have too similar an appearance to the bare titania particles.

The efficacy of $PDEA_{50}$-$PCEA_{50}$ as a dispersant for this titania pigment was also investigated. This diblock copolymer exhibits an IEP at pH 5.1 (**Figure 6.16**). The IEP of the nanoparticle-coated titania particles is around pH 5.7, which is intermediate between that of the nanoparticles alone and the bare titania pigment particles (IEP at pH 7.0). Thus the aqueous electrophoresis data are consistent with nanoparticle adsorption at the surface of the titania. One reason that this is not closer to the IEP of the polymer particles alone could be due to submonolayer coverage of the pigment particles by the polymer particles.
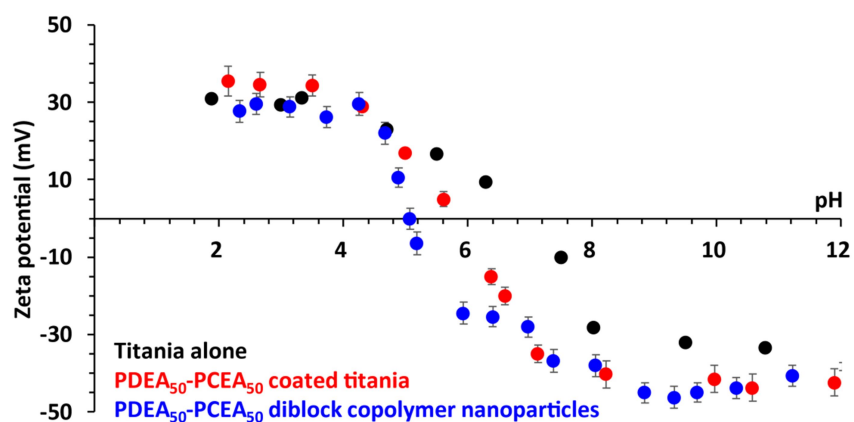

Figure 6.16 Zeta potential vs. pH curves recorded for 0.1% w/w aqueous dispersions of $PDEA_{50}$-$PCEA_{50}$ diblock copolymer nanoparticles alone (**blue**), titania particles alone (**black**), and the same pigment particles dispersed in the presence of $PDEA_{50}$-$PCEA_{50}$ nanoparticles (**red**).
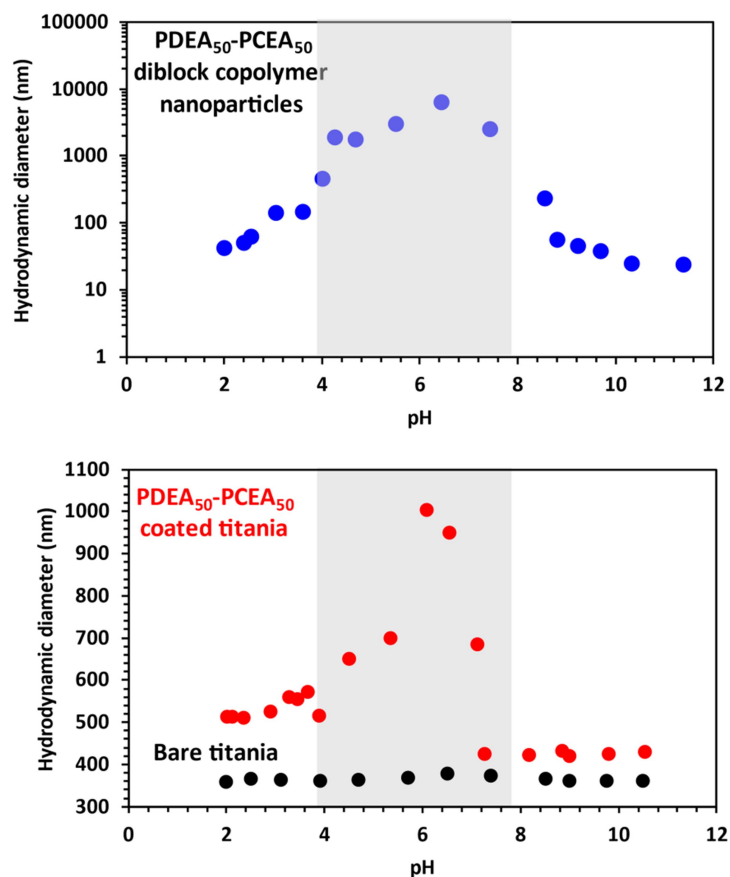
Figure 6.17 DLS hydrodynamic diameter vs pH data recorded for aqueous dispersions of PDEA$_{50}$-PCEA$_{50}$ diblock copolymer nanoparticles alone (**top, blue**) and titania pigment particles dispersed in the presence of PDEA$_{50}$-PCEA$_{50}$ (**bottom, red**). Highlighted regions show that the macroscopic precipitation zone observed for the copolymer corresponds to the colloidal instability observed for the pigment dispersion.

The effect of varying the dispersion pH was evaluated by DLS (**Figure 6.17**). Like the first

copolymer dispersant, the colloidal instability zone observed for this diblock copolymer lies

within the same pH window as that found for the copolymer-stabilised titania particles. This

behaviour is significantly different from the pH dependent behaviour of the titania pigment

alone, confirming that adsorption has occurred. In this case, PDEA$_{50}$-PCEA$_{50}$ forms a

macroscopic precipitate over a wider pH range (pH 4-8). Therefore, only titania dispersions

either above or below these pH values can be considered to be colloidally stable.

These nanoparticle-stabilised titania dispersions were again assessed above and below their

IEP to see how each type of nanoparticle performed as a dispersant. At pH 3, the PCEA$_{50}$

block is hydrophobic and forms the nanoparticle core, leaving the cationic PDEA$_{50}$ block to

act as the steric stabiliser. DLS studies indicate a z-average diameter of 27 nm for such
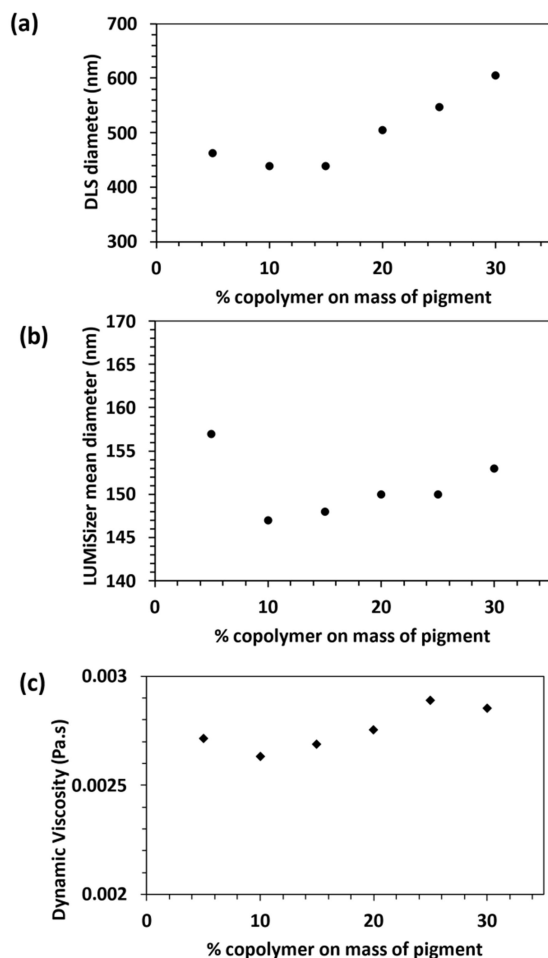
nanoparticles.

Figure 6.18 Effect of varying the copolymer concentration on the degree of dispersion of titania R-960 pigment particles in the presence of anionic PDEA$_{50}$-PCEA$_{50}$ nanoparticles at pH 3: (a) DLS z-average diameter determined for 10% w/w titania dispersions diluted to 0.10% w/w, (b) LUMiSizer mean diameter determined for 10% w/w titania dispersions diluted to 0.50% w/w, and (c) dispersion viscosity determined for 10 % w/w titania dispersions. These data suggest an optimum concentration of around 10-15% copolymer per unit mass of pigment.

DLS studies report a minimum pigment diameter of 438 nm at 10-15% copolymer (**Figure**

6.18a). This is somewhat higher than that achieved for the PDEA$_{100}$-PCEA$_{50}$ dispersant,

which suggests that PDEA$_{50}$-PCEA$_{50}$ is a less effective dispersant. On the other hand, the

minimum viscosity observed at 10% copolymer is 2.65 mPa.s, which is the lowest obtained

in such experiments (**Figure 6.18c**). Analytical centrifugation studies also indicate that a minimum apparent particle diameter is achieved at 10% copolymer, which is consistent with the DLS data (**Figure 6.18b**).
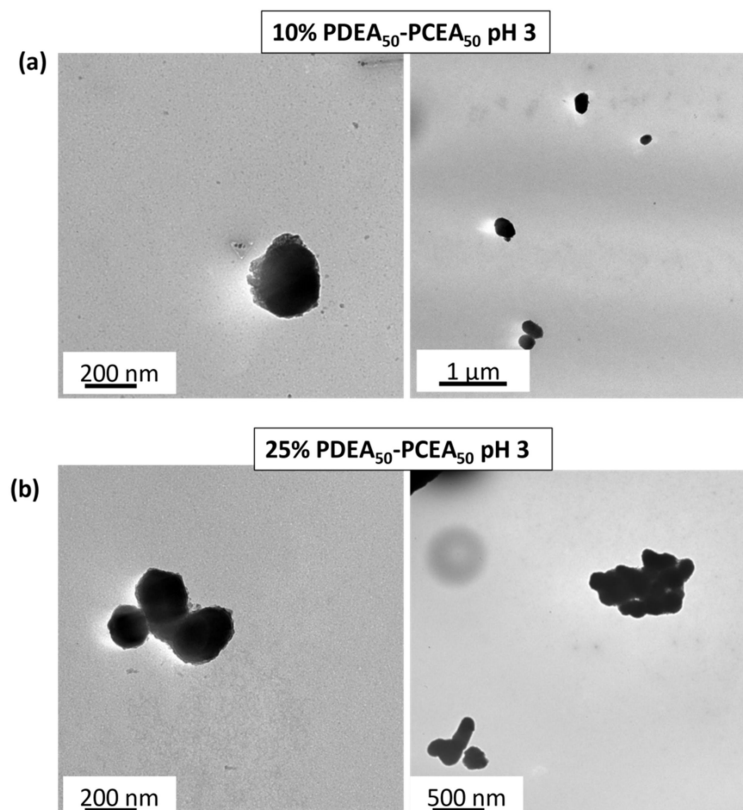

Figure 6.19 Representative TEM images recorded for titania dispersions prepared in the presence of either (a) 10% or (b) 25% $PDEA_{50}$-$PCEA_{50}$ nanoparticles at pH 3 (i.e. below the copolymer IEP) after dilution to 0.1% w/w prior to drying on a carbon-coated grid.

$PDEA_{50}$-$PCEA_{50}$ stabilised titania dispersions proved to be rather more difficult to image by TEM. Nevertheless, a relatively high degree of dispersion seems to be achieved at 10% copolymer while there is some evidence for aggregated pigment particles at 25% copolymer (**Figure 6.19**). Again, this suggests that a depletion flocculation mechanism may be operating, but in this case the excess copolymer nanoparticles are difficult to image with either a uranyl formate stain or a phosphotungstic acid stain.
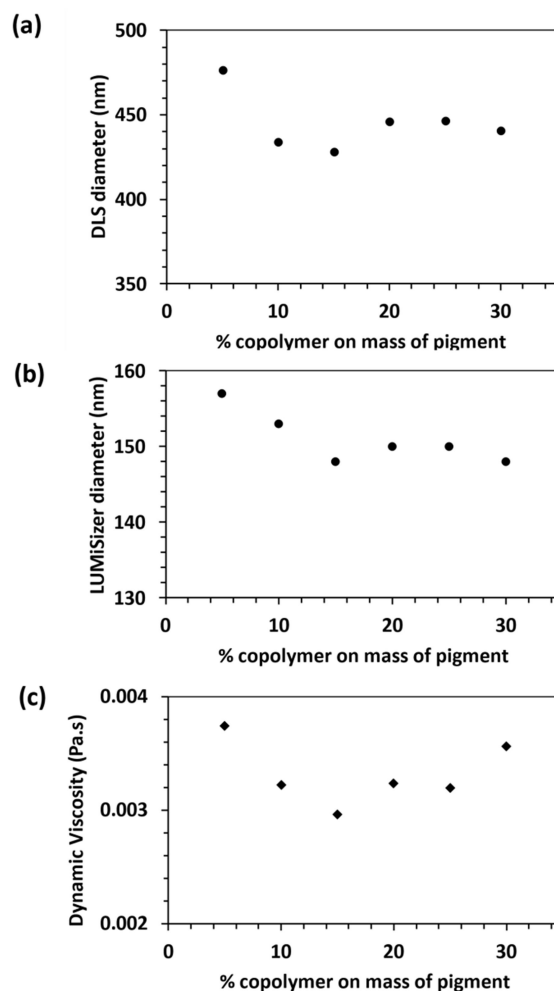
Figure 6.20 Effect of varying the copolymer concentration on the degree of dispersion of titania R-960 pigment particles in the presence of anionic $PDEA_{50}$-$PCEA_{50}$ nanoparticles at pH 10: (a) DLS z-average diameter determined for 10% w/w titania dispersions diluted to 0.10% w/w, (b) LUMiSizer mean diameter determined for 10% w/w titania dispersions diluted to 0.50% w/w, and (c) dispersion viscosity determined for 10 % w/w titania dispersions. These data suggest an optimum concentration of around 15% copolymer per unit mass of pigment.

Finally, this $PDEA_{50}$-$PCEA_{50}$ diblock copolymer was assessed as a pigment dispersant at pH 10. Under such alkaline conditions, the $PDEA_{50}$ block forms the nanoparticle cores and the $PCEA_{50}$ block acts as the anionic steric stabiliser, with DLS studies indicating a z-average diameter of 26 nm. In this case, a minimum apparent pigment diameter of 428 nm (**Figure 6.20**) is observed at 15% copolymer dispersant. Minima in the dispersion viscosity and the apparent diameter reported by analytical centrifugation are also achieved at the same copolymer concentration (**Figures 6.20c and 6.20b**). Moreover, the minimum viscosity is

2.97 mPa.s, which is lower than that achieved using the $PDEA_{100}$-$PCEA_{50}$ dispersant at pH 10. Given the relatively low dispersion viscosities at both pH 3 and pH 10, these preliminary low-energy mixing data suggest that $PDEA_{50}$-$PCEA_{50}$ is perhaps a more effective dispersant for the titania pigment. Furthermore, effective dispersion can be achieved at lower copolymer concentrations.
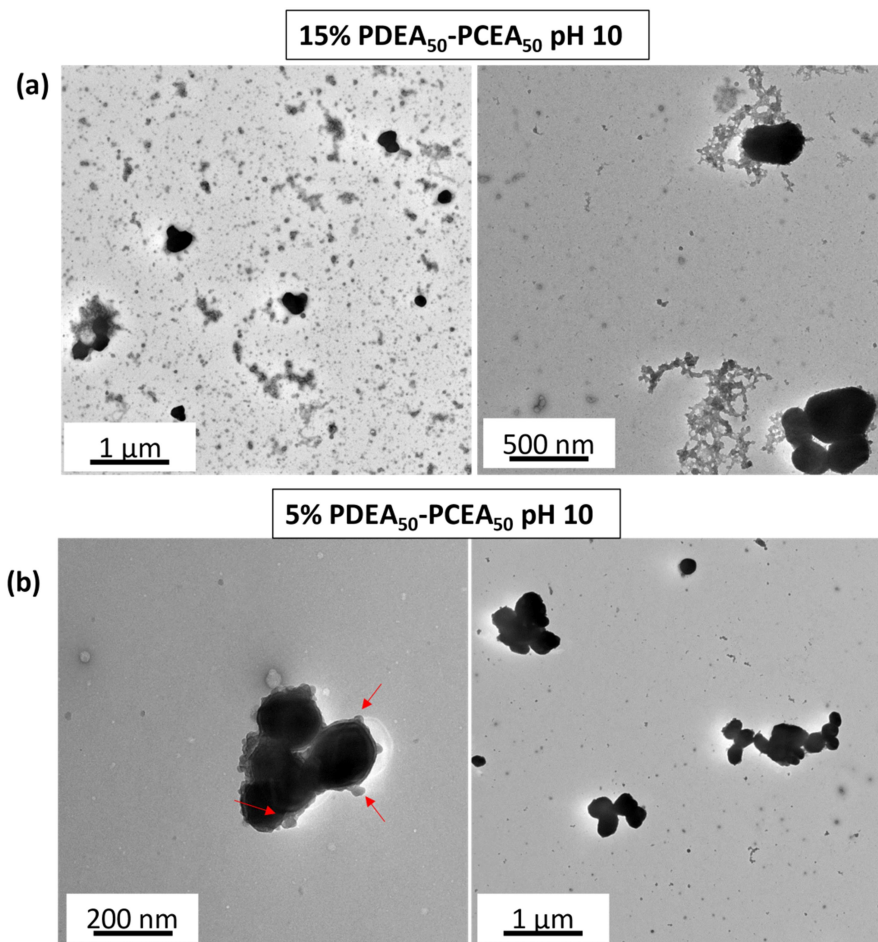
Figure 6.21 Representative TEM images recorded for titania dispersions prepared in the presence of either (a) 15% or (b) 5% $PDEA_{50}$-$PCEA_{50}$ nanoparticles at pH 10 (i.e. below the copolymer IEP) after dilution to 0.1% w/w prior to drying on a carbon-coated grid. Red arrows indicate possible nanoparticle adsorption onto titania surface.

However, TEM studies indicate that there are excess non-adsorbed nanoparticles present at 15% copolymer (**Figure 6.21a**). In principle, this may indicate a depletion stabilisation mechanism, but further work would be required to examine this hypothesis. Interestingly,

TEM images recorded at 5% copolymer (**Figure 6.21b**) provide evidence for the adsorption of nanoparticles onto the surface of the pigment particles., Surprisingly, excess non-adsorbed nanoparticles can be detected in the background even at this relatively low concentration.

6.4 Conclusions

A series of well-defined $PDEA_x$-$PCEA_y$ diblock copolymers has been efficiently prepared via a highly convenient one-pot formulation based on (i) RAFT aqueous solution polymerisation of DEA at low pH followed by (ii) RAFT aqueous dispersion polymerisation of CEA. THF GPC studies of selectively methylated diblock copolymers indicate a systematic increase in copolymer M_n when targeting longer PCEA blocks using a PDEA precursor with a fixed DP of 67. Moreover, M_w/M_n values remain below 1.33, indicating reasonably good RAFT control. A range of diblock compositions have been studied in aqueous solution and their so-called 'schizophrenic' pH-responsive self-assembly behaviour has been verified by TEM, DLS, ^{1}H NMR spectroscopy and aqueous electrophoresis measurements. $PDEA_{100}$-$PCEA_{50}$ and $PDEA_{50}$-$PCEA_{50}$ nanoparticles were also briefly evaluated as copolymer dispersants for titania particles above and below the IEP of this white pigment. DLS, TEM, aqueous electrophoresis, analytical centrifugation and viscosity measurements at varying copolymer concentrations suggest that these nanoparticles may be able to adsorb onto the pigment surface and confer some degree of colloidal stabilisation at approximately 10-15% copolymer per unit mass of pigment.

6.5 References

1.   Newman, S. Note on colloidal dispersions from block copolymers. *J. Appl. Polym. Sci.* **6**, S15–S16 (1962).

2.   Krause, S. Dilute Solution Properties of a Styrene-Methyl Methacrylate Block Copolymer. *J.*

Phys. Chem. **68**, 1948–1955 (1964).

3. Bütün, V., Billingham, N. C. & Armes, S. P. Unusual aggregation behavior of a novel tertiary amine methacrylate- based diblock copolymer: Formation of Micelles and reverse Micelles in aqueous solution. *J. Am. Chem. Soc.* **120**, 11818–11819 (1998).

4. Bütün, V. *et al.* Remarkable `Flip-flop' self-assembly of a diblock copolymer in aqueous solution. *Macromolecules* **34**, 1503–1511 (2001).

5. Liu, S., Billingham, N. C. & Armes, S. P. A Schizophrenic Water-Soluble Diblock Copolymer. *Angew. Chemie* **113**, 2390–2393 (2001).

6. Bütün, V. *et al.* A brief review of 'schizophrenic' block copolymers. *React. Funct. Polym.* **66**, 157–165 (2006).

7. Arotçaréna, M., Heise, B., Ishaya, S. & Laschewsky, A. Switching the inside and the outside of aggregates of water-soluble block copolymers with double thermoresponsivity. *J. Am. Chem. Soc.* **124**, 3787–3793 (2002).

8. Weaver, J. V. M., Armes, S. P. & Bütün, V. Synthesis and aqueous solution properties of a well-defined thermo-responsive schizophrenic diblock copolymer. *Chem. Commun.* **2**, 2122–2123 (2002).

9. Liu, S. & Armes, S. P. Polymeric surfactants for the new millennium: A pH-responsive, zwitterionic, schizophrenic diblock copolymer. *Angew. Chemie* **41**, 1413–1416 (2002).

10. Gohy, J. F. *et al.* Aggregates formed by amphoteric diblock copolymers in water. *Macromolecules* **33**, 6378–6387 (2000).

11. Chen, W. Y. h., Chen, K. H., Chen, H. & Ruaan, R. C. Effect of block size and sequence on the micellization, hydrophobicity, and surface adsorption of ABC triblock methacrylic polyampholytes by isothermal titration calorimetry. *J. Chinese Inst. Chem. Eng.* **33**, 599–608 (2002).

12. Lowe, A. B., Billingham, N. C. & Armes, S. P. Synthesis and characterization of zwitterionic block copolymers. *Macromolecules* **31**, 5991–5998 (1998).

13. Creutz, S., Jérôme, R., Kaptijn, G. M. P., Van Der Werf, A. W. & Akkerman, J. M. Design of polymeric dispersants for waterborne coatings. *J. Coatings Technol.* **70**, 41–46 (1998).

14. Canning, S. L., Smith, G. N. & Armes, S. P. A Critical Appraisal of RAFT-Mediated Polymerization-Induced Self-Assembly. *Macromolecules* **49**, 1985–2001 (2016).

15. Tan, J., Sun, H., Yu, M., Sumerlin, B. S. & Zhang, L. Photo-PISA: Shedding Light on Polymerization-Induced Self-Assembly. *ACS Macro Lett.* **4**, 1249–1253 (2015).

16. Blackman, L. D., Doncom, K. E. B., Gibson, M. I. & O'Reilly, R. K. Comparison of photo- and thermally initiated polymerization-induced self-assembly: A lack of end group fidelity drives the formation of higher order morphologies. *Polym. Chem.* **8**, 2860–2871 (2017).

17. Canning, S. L., Neal, T. J. & Armes, S. P. pH-Responsive Schizophrenic Diblock Copolymers Prepared by Polymerization-Induced Self-Assembly. *Macromolecules* **50**, 6108–6116 (2017).

18. Bütün, V., Vamvakaki, M., Billingham, N. C. & Armes, S. P. Synthesis and aqueous solution properties of novel neutral/acidic block copolymers. *Polymer* **41**, 3173–3182 (2000).

19. Ranka, M., Katepalli, H., Blankschtein, D. & Hatton, T. A. Schizophrenic Diblock-Copolymer-Functionalized Nanoparticles as Temperature-Responsive Pickering Emulsifiers.

Langmuir **33**, 13326–13331 (2017).

20. Laschewsky, A. Structures and Synthesis of Zwitterionic Polymers. *Polymers (Basel).* **6**, 1544–1601 (2014).

21. Liu, H. *et al.* Zwitterionic copolymer-based and hydrogen bonding-strengthened self-healing hydrogel. *RSC Adv.* **5**, 33083–33088 (2015).

22. Penfold, N. J. W., Whatley, J. R. & Armes, S. P. Thermoreversible Block Copolymer Worm Gels Using Binary Mixtures of PEG Stabilizer Blocks. *Macromolecules* **52**, 1653–1662 (2019).

23. Warren, N. J. & Armes, S. P. Polymerization-induced self-assembly of block copolymer nano-objects via RAFT aqueous dispersion polymerization. *J. Am. Chem. Soc.* **136**, 10174–10185 (2014).

24. Keddie, D. J. A guide to the synthesis of block copolymers using reversible-addition fragmentation chain transfer (RAFT) polymerization. *Chem. Soc. Rev.* **43**, 496–505 (2014).

25. Mai, Y. & Eisenberg, A. Self-assembly of block copolymers. *Chem. Soc. Rev* **41**, 5969–5985 (2012).

26. Smith, G. A., Zulli, A. L., Grieser, M. D. & Counts, M. C. Dispersion of titanium dioxide pigments by alkyl polyglycoside surfactants in aqueous solution. *Colloids Surfaces A Physicochem. Eng. Asp.* **88**, 67–73 (1994).

27. *Ti Pure R960 Titanium Dioxide Product Information*. (2017).

28. Creutz, S. & Jérôme, R. Effectiveness of block copolymers as stabilizers for aqueous titanium dioxide dispersions of a high solid content. *Prog. Org. Coatings* **40**, 21–29 (2000).

29. North, S. M. & Armes, S. P. Aqueous one-pot synthesis of well-defined zwitterionic diblock copolymers by RAFT polymerization: an efficient and environmentally friendly route to a useful dispersant for aqueous pigments. *Green Chem.* (2021). doi:10.1039/d0gc04271d

30. North, S. M. *et al.* Adsorption of Small Cationic Nanoparticles onto Large Anionic Particles from Aqueous Solution: A Model System for Understanding Pigment Dispersion and the Problem of Effective Particle Density. *Langmuir* **33**, 1275–1284 (2017).

31. Growney, D. J. *et al.* Determination of Effective Particle Density for Sterically Stabilized Carbon Black Particles: Effect of Diblock Copolymer Stabilizer Composition. *Langmuir* **31**, 8764–8773 (2015).

32. Rong, Y., Chen, H. Z., Li, H. Y. & Wang, M. Encapsulation of titanium dioxide particles by polystyrene via radical polymerization. *Colloids Surfaces A Physicochem. Eng. Asp.* **253**, 193–197 (2005).

Chapter 7

Conclusions and Outlook

7.1 Conclusions & Outlook

The invention and use of pseudo-living radical polymerisation techniques over the last twenty years has greatly increased the number of possibilities to synthesise new polymers.[1–3] In particular, the synthesis of amphiphilic macromolecules with controlled polymer architectures, which are capable of stimuli-induced self-assembly in aqueous media, or at interfaces, have a wide range of potential applications.[4]

In this thesis, the synthesis of novel aqueous dispersants for carbon black, titania and transparent yellow iron oxide, and their dispersant effectiveness are reported. The synthesis of these dispersants directly in water is desirable for the inkjet industry, due to the relative cost and environmental impact. One of the fundamental questions poised at the start of this project was whether a diblock copolymer nanoparticle could act as a better dispersant than an amphiphilic single chain. The benefit of a single chain is that a greater number of chemically adsorbing groups can reach the surface of the pigment particle, however a diblock copolymer nanoparticle has the potential to adsorb as a spherical micelle, increasing the overall size of dispersed pigment, reducing its overall density and increasing buoyancy.

Chapter 2 focuses on the synthesis and aqueous solution behaviour of novel PMAA-PHPMA diblock copolymer nanoparticles, *via* RAFT aqueous dispersion polymerisation at pH 5.5.[5] The precise composition $PMAA_{50}$-$PHPMA_{235}$ was investigated in close detail. As synthesised, these particles are large and polydisperse, resulting in a turbid dispersion, due to the ionisation state of the PMAA block. If the pH is increased, the PMAA becomes highly anionic, leading to the formation of thermoresponsive nanoparticles. They dissolve to form chains at 5 °C, aggregate to form spheres between 10 – 35 °C, and form anisotropic worm-like particles at 50 °C. It was discovered in Chapter 3 that a similar diblock composition could work well as a pigment dispersant for carbon black. The hydrophobic PHPMA block can act as a good anchoring block onto the carbon black surface, with soluble PMAA acting

as an electrosteric stabiliser. The thermoresponsive nature of these particles means that the dispersing ability of molecularly dissolved chains can be directly compared to that of self-assembled nanoparticles, simply by adjusting the dispersion temperature. It was found that PMAA-PHPMA at lower temperatures could act as a more effective dispersant for carbon black. This is likely to be due to the greater surface area that molecularly dissolved chains can cover of the pigment surface, and individual PMAA chains can remain in solution, stabilising the dispersion by charge and steric repulsion. The fact that PHPMA has sparing water solubility allows it to have a more dynamic nature than other more hydrophobic core-forming blocks (such as benzyl methacrylate), which cannot reversibly form micelles. The high molecular weight (or aggregation number) of these nanoparticles compared to classic surfactant dispersants is beneficial for later in the industrial dispersion process, as mechanical milling creates more pigment surface area. Nanoparticles will act as so-called 'reservoirs' to provide more dispersant, this will prevent flocculation occurring in the milling process, where pigment is broken down into finer particle sizes, thus requiring more dispersant. Furthermore, PMAA-PHPMA shows greater long-term stability when compared to the non-ionic commercial dispersant. To extend this work, compositions which are not sufficiently long to produce micelles (i.e. below the critical length for self-assembly) could be investigated. This could be done by synthesising PMAA-PHPMA diblock copolymers with much longer PMAA blocks. Literature, and screening studies for the zwitterionic diblocks showed that the anchoring block should be shorter than the stabilising block. This could provide even more insight into the differences between nanoparticle and dissolved chain dispersants.

In Chapter 4, a novel method to synthesise zwitterionic diblock copolymers *via* a wholly aqueous, one-pot RAFT synthesis is reported.[6] Many different diblock compositions are investigated, and their syntheses can be categorised by aqueous solution, dispersion or emulsion polymerisation. Compositions that proceed *via* RAFT aqueous solution

polymerisation were necessarily carried out at a pH whereby both blocks are water-soluble due to the pK_a of the cationic block. Zwitterionic copolymers with PCEA as the second block are synthesised *via* RAFT aqueous dispersion polymerisation. This is because the second step is done in water at pH 1.5, where the acidic PCEA is non-ionised and fully protonated, therefore becomes hydrophobic as the polymerisation proceeds. Zwitterionic diblock copolymers which have a second block comprising PDEA or PDPA are synthesised *via* RAFT emulsion polymerisation at pH 8.5, where the monomer and growing polymer chain is insoluble. Finally, one-pot, wholly aqueous synthesis for PMAA-PMETAC, PDMA-PMAA and PMAA-PDMA *via* RAFT aqueous solution polymerisation is developed. These syntheses allow direct polymerisation into water, with no need for modification, reducing the number of steps, and ultimately allowing a more sustainable synthetic process. Furthermore, zwitterionic copolymers have interesting pH-responsive behaviour. They exhibit an IEP at the point where cationic and anionic charge become equal, resulting in a macroscopic precipitation. It is shown that this can be utilised for the facile solvent-free separation of polymers from small molecules following end-group removal with hydrazine.

A number of these zwitterionic diblock copolymers were investigated as dispersants for inorganic pigments in Chapter 5. They were found to effectively disperse titania and transparent yellow iron oxide. Each of their pH-dependent behaviours had significant influence on the optimal pH for each dispersion and made them interesting systems to deduce methods of adsorption. PDMA in its more hydrophobic form (above pH ∼ 7) acts as a good anchoring block, and at this pH, PMAA is fully ionised, allowing it to act as a good stabilising block. PMAA was also able to act as a good anchoring block at low pH, where the PMAA is unionised and protonated, making it more hydrophobic and have a greater affinity for the pigment surface. In this case, PDMA is ionised and more water-soluble, allowing it to take the role of stabiliser. As many common commercial dispersants contain aromatic groups,

the statistical addition of 20 mol% benzyl methacrylate to the acidic block was investigated, however this resulted in poorer dispersion: at low pH, the hydrophobic PMAA is kinetically trapped within a nanoparticle, so it cannot anchor to the pigment surface. Asymmetric $PMAA_{67}$-$PMETAC_{120}$ was interesting, as the composition chosen did not exhibit an IEP, since the longer PMETAC is permanently cationic, so the charges can never match each other or cause precipitation. This allowed an investigation of the effect of having no hydrophobic anchoring block. It was found that effective pigment dispersion could only occur at low pH, where the PMAA block is hydrophobic. This proves the necessity for a block that has affinity for the hydrophobic pigment surface, because if both blocks are in their ionised state, neither can act as an anchoring block, resulting in flocculation. This IEP effect could be further investigated for PMAA-rich PMAA-PMETAC diblock copolymers, which do exhibit an IEP. Although it would be hypothesised that at high pH this diblock would not have an anchoring block available, the overall anionic charge of the diblock may influence the mechanism of pigment dispersion.

These zwitterionic polymers show promising results in reduction of particle size and viscosity for both inorganic pigments. For the transparent yellow iron oxide, which is industry-known as a difficult to disperse pigment, a zwitterionic dispersant is only required at 20% AOP, where the industry-used dispersants are used at 25%. Coupled with the wholly aqueous, one-pot synthesis, these could provide a more sustainable route to using aqueous pigment dispersants.

Finally in Chapter 6, a zwitterionic diblock copolymer which undergoes micellar inversion to give sterically-stabilised, kinetically frozen nanoparticles above and below its IEP, PDEA-PCEA, was investigated. A one-pot, wholly aqueous protocol for its synthesis has also been developed. These nanoparticles were found to provide some degree of stabilisation to titania pigment particles, and their zwitterionic nature means that they can be directly compared to

the PDMA-PMAA chains also used to disperse titania in Chapter 5. Although preliminary studies suggest that these nanoparticles can behave as effective dispersants, preliminary studies suggest that the PCEA-core nanoparticles formed at pH 3 are more effective than PDEA-core nanoparticles at pH 10. Since it is known that polyaminated blocks have a high affinity for titania surface, this could suggest that the lower aqueous solubility of PDEA compared to PDMA is hindering the dispersing ability of these nanoparticles. When PDEA is a stabiliser block, it is on the outside of the nanoparticles and can provide some degree of electrosteric stabilisation, with the PCEA residing in the core. At pH 10, the PDEA provides no stabilisation as it is insoluble and has no access to the pigment surface. It appears that PCEA can still provide some degree of stabilisation, however these results do not appear to be as effective as PDMA-PMAA dissolved chain dispersants. The lower particle sizes achieved with chains validates the fact that diblock copolymer chains can more efficiently disperse pigments than adsorbed nanoparticles. Nonetheless, different PDEA-PCEA compositions could be explored, and the effect of the nanoparticle IEP on the pH dependent dispersion behaviour could be studied more closely. A nanoparticle with a lower IEP than the pigment could impart greater stabilisation at the high pH values required for industrial pigment dispersion.

Overall, a greater understanding of aqueous diblock copolymer pigment dispersants, and their methods of adsorption, has been achieved. Novel compositions which incorporate polyelectrolytic blocks to confer electrosteric stabilisation have been discovered. The necessity of having two distinct blocks, of which one is freely able to anchor to the pigment and one can stabilise the particle by protruding into solution has been made apparent. Micelles where the anchoring block is not able to reach the pigment surface, or where the anchoring block is not sufficiently hydrophobic, cannot disperse pigments efficiently. Zwitterionic copolymers in particular have the ability to stabilise a wide range of pigments,

and the inception of a more environmentally-friendly approach to their synthesis is a positive

step forward for industrial synthesis of these so-called 'universal' dispersants.

7.2 References

1. Matyjaszewski, K. Atom Transfer Radical Polymerization (ATRP): Current status and future perspectives. *Macromolecules* **45**, 4015–4039 (2012).

2. Nicolas, J. *et al.* Nitroxide-mediated polymerization. *Prog. Polym. Sci.* **38**, 63–235 (2013).

3. Moad, G., Rizzardo, E. & Thang, S. H. Living radical polymerization by the RAFT process A second update. *Aust. J. Chem.* **62**, 1402–1472 (2009).

4. McCormick, C. L. & Lowe, A. B. Aqueous RAFT polymerization: Recent developments in synthesis of functional water-soluble (Co)polymers with controlled structures. *Acc. Chem. Res.* **37**, 312–325 (2004).

5. North, S. M. & Armes, S. P. Aqueous solution behavior of stimulus-responsive poly(methacrylic acid)-poly(2-hydroxypropyl methacrylate) diblock copolymer nanoparticles. *Polym. Chem.* **11**, 2147–2156 (2020).

6. North, S. M. & Armes, S. P. Aqueous one-pot synthesis of well-defined zwitterionic diblock copolymers by RAFT polymerization: an efficient and environmentally friendly route to a useful dispersant for aqueous pigments. *Green Chem.* (2021). doi:10.1039/d0gc04271d